Functional Characterization of MEL-28/ELYS

Georgina Gómez Saldivar

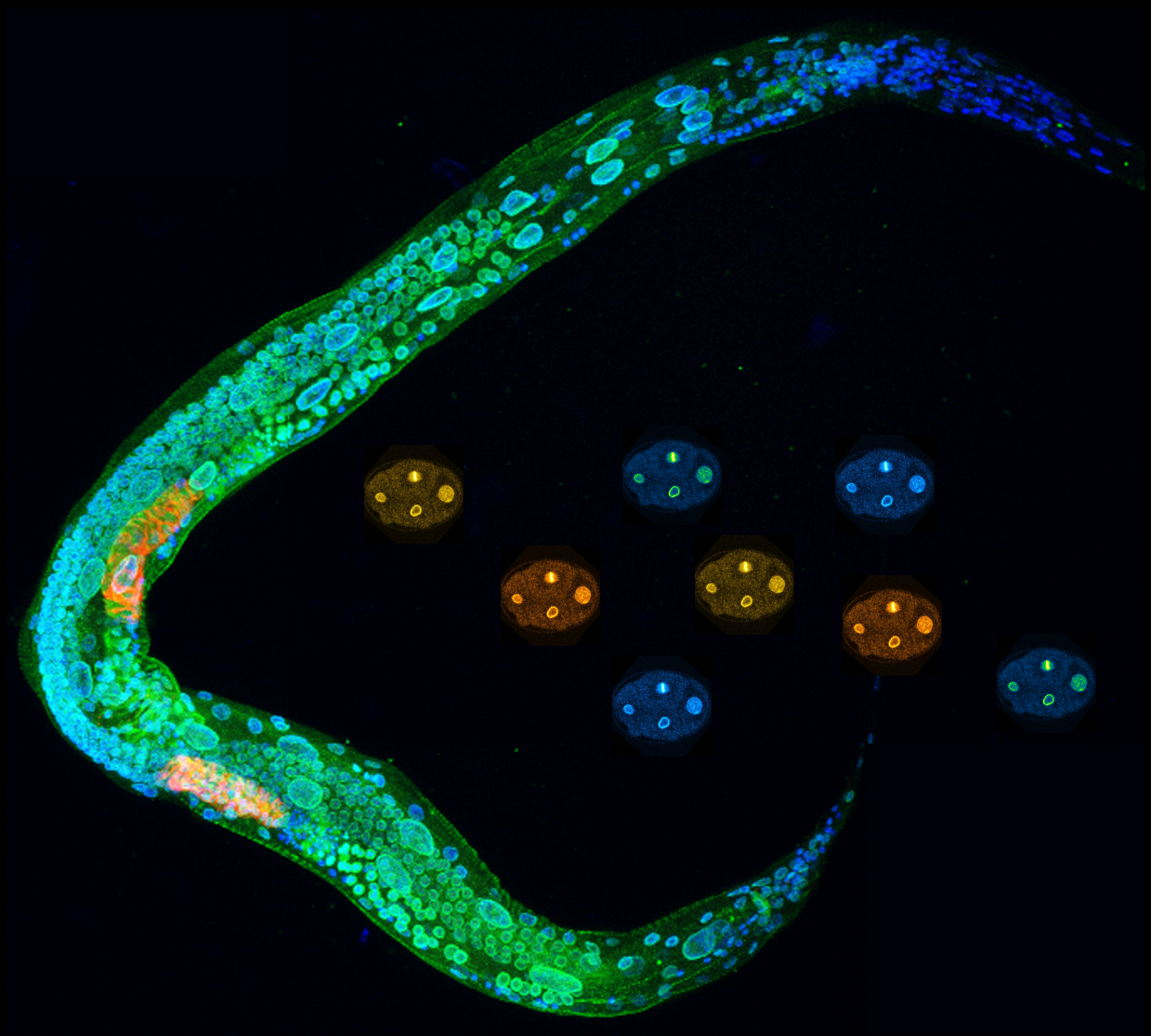

Doctoral Thesis
2017

Centro
Andaluz
de Biología
del Desarrollo

FUNCTIONAL CHARACTERIZATION

OF MEL-28/ELYS

BY

GEORGINA GÓMEZ SALDIVAR

DISSERTATION

Submitted in fulfillment of the requirements for the degree of Doctor of Philosophy in Biotechnology, Engineering and Chemical Technology in the Pablo de Olavide University.

Seville, Spain

Andalusian Centre for Developmental Biology

May 26, 2017.

FUNCTIONAL CHARACTERIZATION

OF MEL-28/ELYS

Approved by:

Dr. Peter Askjaer, Advisor.
Andalusian Centre for Developmental Biology.
Pablo Olavide University

Dr. Manuel Jésus Muñoz Ruíz.
Department of Molecular Biology and Biochemical Engineering.
Pablo Olavide University

PhD. Candidate. Georgina Gómez Saldivar
Andalusian Centre for Developmental Biology.
Pablo Olavide University

Date Approved: May 26, 2017.

It always seems impossible

until it is done

-Nelson Mandela

A mis padres y hermanas

Table of contents

List of Abbreviations

˚C	degrees Celsius
aa	Amino Acid
APC	Anaphase Promoting Complex
ASE	Autosomal Signal Element
AT-hook	AT-rich DNA
Cdk	Cyclin-dependent kinases
ChIP	Chromatin Immunoprecipitation
CPC	Chromosome Passenger Complex
CTCF	CCCTC- binding Factor
DamID	DNA adenine methyltransferase IDentification
DC	Dosage Compensation
DCC	Dosage Compensation Complex
DIC	Differential Interference Contrast
DNC	Dorsal Nerve Cord
EAD	Emerin Association Domain
TEM	transmission Electron Microscopy
ER	Endoplasmic Reticulum
ELYS	Embryonic Large molecule derived from Yolk Sac
FDR	False Discovery Rate
FG	Phenylalanine-Glycine
FG-Nup	FG-Nucleoporin
FISH	Fluorescence In Situ Hybridization

FLP	Flipase
FRAP	Fluorescence Recovery After Photobleaching
gDNA	Genomic DNA
GFP	Green Florescent Protein
GRS	Gene Recruitment Sequences
GVB	Germline Vesicle Breakdown
H2A/H3	Histone 2A/Histone H3
HDAC	Histone Deacetylase
HGPS	Hutchinson-Gilford Progeria Syndrome
h	hour
HS	Heat Shock
HSAS	Heat shock Associated Site
HSE	Heat Shock Elements
INM	Inner Nuclear Membrane
IQR	Interquartile Range
Kap	Karyopherin
kDa	Kilodalton
KDE	Kernel Density Estimation
LAD	Lamina Associated Domain
LINC	LInker of Nucleoskeleton and Cytoskeleton complex
Log2	Logarithm base 2
l2m	loop2 point mutation
Megator	Mtor
MEL-28	Maternal-effect Embryonic-Lethal mutation 28

MEX	Motif Enriched on the X
min	minutes
mRNA	messenger RNA
MSP	Major Sperm Protein
NAD	Nucleoli Association Domain
NAR	Nucleoporin-Associated Regions
NE	Nuclear Envelope
NEBD	Nuclear Envelope Break-Down
NES	Nuclear Export Signal
NET	Nuclear Envelope Transmembrane protein
NL	Nuclear Lamina
NLS	Nuclear Localization Signal
NP	Nuclear Pore
NPC	Nuclear Pore Complex
NPP	Nuclear Pore Protein
NTR	Nuclear Transport Receptor
Nup	Nucleoporin
ONM	Outer Nuclear Membrane
ORF	Open Reading Frame
PLK-1	Polo-Like Kinase
POI	Protein Of Interest
POL	Polymerase
PRC1	Polycomb-Repressive Complex 1
PP1	Protein Phosphatases 1

PY-NLS	Proline-Tyrosine-rich NLS
RANBP1	RAN-Binding Protein 1
RANGAP	RAN GTPase-Activating Protein
rex	recruitment sites on the X
RG-NLS	Arginine-Glycine-rich NLS
RNAi	RNA interference
RNA-seq	RNA-sequencing
sdc	sex determination and dosage compensation
SE	Super Enhancer
snoRNA	small nucleolar RNA
STAT5	Signal Transducer and Activator of Transcription 5
TAD	Topological Association Domain
tRNA	transfer RNA
TSA	Trichostatin A
TSS	Transcription Start Sites
VNC	Ventral Nerve Cord
XSE	X Signal Element
YFP	Yellow Fluorescent Protein

Abstract

The nuclear envelope (NE) is a hallmark of eukaryotic cells. The NE encloses the nuclear genome and separates it from the cytoplasm allowing to the cell a high level of organization and regulation of transcription and translation. The NE is formed by four major components: the inner nuclear membrane (INM), the outer nuclear membrane (ONM), the nuclear lamina (NL) and the nuclear pore complexes (NPCs; Hetzer, 2010).

Transport of macromolecules between the nucleus and the cytoplasm is regulated by NPCs, which are constituted of 30 different nucleoporins (Nups). Nups can be classified into three general classes. The first class is formed by approximately 15 Nups rich in phenylalanine-glycine (FG) repeats and that constitute peripheral and transport channel components of the NPC. The second class is composed by the transmembrane Nups NDC1, POM121, GP210 and POM33/TMEM33 (Chadrin et al., 2010). And, the third class denotes the structural scaffold of the NPC, including the Nup MEL-28/ELYS and the complexes NUP107-160 and NUP205-188-93 (Rabut, Doye, & Ellenberg, 2004). The association of Nups with chromatin is one of the initial steps in nuclear reorganization, suggesting that they could have a role in the chromatin organization through mitosis and, consequently, in the propagation of epigenetic memory.

This Thesis is focused on a conserved Nup known as MEL-28 in *Caenorhabditis elegans* and ELYS in vertebrates. MEL-28/ELYS plays a critical role in post-mitotic NPC reassembly through recruitment of the NUP107-160 complex and is required for correct segregation of mitotic chromosomes (Fernandez & Piano, 2006; Franz et al., 2007; Galy, Askjaer, Franz, López-Iglesias, & Mattaj, 2006a).

MEL-28 has a dynamic behavior: it localizes to NPCs and chromatin during interphase and shuttles to spindle microtubules and kinetochores during cell division. Several studies done in *C. elegans* and HeLa cells have reported that mutations or knockdown of MEL-28/ELYS produces defects in NE morphology and in NPC assembly as well as defects in chromatin segregation, mitotic spindle assembly and nucleocytoplasmic transport (Fernandez & Piano, 2006; Galy, Askjaer, Franz, López-Iglesias, et al., 2006a; Beth A Rasala, Orjalo, Shen, Briggs, & Forbes, 2006). However, it is unknown how MEL-28 localization and activity is regulated.

The general objective of my Ph.D. project is the analysis of chromatin organization through identification of chromatin domains bound by MEL-28. For this purpose, we evaluate the function of MEL-28/ELYS according to its location, either when located in NPC or in the nucleoplasm using *C. elegans* as model organism.

The results of this thesis are present in chapters IV and V; besides, in chapter III (Materials and Methods), we describe the DamID-seq workflow from sample preparation to bioinformatics analysis, which was published in the book "The Nuclear Envelope: Methods and Protocols", chapter name: **"DamID Analysis of Nuclear Organization in *Caenorhabditis elegans*"**, (Gómez-Saldivar, Meister, & Askjaer, 2016). DamID is based on the in vivo expression of a chromatin-associated protein of interest fused to the *Escherichia coli* DNA adenine methyltransferase, which produces unique identification tags at binding site in the genome (Van Steensel & Henikoff, 2000). This marking is simple, highly specific and can be mapped by sensitive enzymatic and next generation sequencing (NGS) approaches.

In chapter IV: **"Identification of Conserved MEL-28/ELYS Domains with Essential Roles in Nuclear Assembly and Chromosome Segregation",** (Gómez-Saldivar, Fernandez, et al., 2016), we present a systematic, functional and structural analysis of MEL-28 in *C. elegans* early development and human ELYS in cultured cells. In collaboration with Dr. Anita Fernandez from Fairfield University (USA), Dr. Yasushi Hiraoka and Dr. Tokuko Haraguchi from Graduate School of Frontier Biosciences, Osaka University (Japan), we have generated and examined the expression and localization of full-length and almost 50 different MEL-28/ELYS truncations that lack different domains and fused these to GFP to track their localization by confocal microscopy.

We have identified functional domains responsible for NPC and kinetochore localization, chromatin binding, mitotic spindle matrix association and chromosome segregation. Surprisingly, we found that perturbations to MEL-28's conserved AT-hook and loop2 domains do not affect MEL-28 localization although they disrupt MEL-28 function and delay cell cycle progression. Specifically, deletion of the AT-hook domain from MEL- 28 activates the ATR DNA damage checkpoint. Our analyses also uncover a novel meiotic role of MEL-28, intervening in the proper development of anaphase I and II. Together, these results show that MEL-28 has conserved structural domains that are essential for its fundamental roles in NPC assembly and chromosome segregation during meiosis and mitosis.

In chapter V: **"Characterization of genome-nucleoporin interaction in *Caenorhabditis elegans"*** (manuscript in preparation), we propose the DamID technique as an attractive method to globally characterize chromatin organization in *C. elegans*. In this part of our research, we have used DamID-array and DamID-sequencing to identify the chromatin regions with which MEL-28 associates. Interestingly, MEL-28 is enriched at transcribed genes and correlates positively with active histone marks (H3K4me3 and H3K36me3), suggesting that it may be involved in regulation of gene expression.

In addition, we have performed DamID with two MEL-28 fragments that are unable to bind to NPCs, which were characterized in chapter IV. In general, the binding profile of MEL-28 fragments is very similar to the full-length protein, suggesting that MEL-28-chromatin interaction is placed mostly in the nucleoplasm and not in the nuclear periphery.

Besides, we compared the MEL-28 chromatin profile with the profile of another Nup, NPP-22/NDC1, which is permanently anchored to the nuclear pore complex. Surprisingly, despite its location this protein interacts with the genome in a very similar percentage than the mobile Nup MEL-28; although we saw a wide reduction of interaction with the sex chromosome. Likewise, we found that the chromatin association profile of NPP-22 was more similar to the profile of the nuclear lamina protein LMN-1 (González-Aguilera et al., 2014) than to MEL-28's profile, suggesting that individual Nups interact with specific chromatin domains.

Interestingly, GO-term analysis reveals that MEL-28-associated genes are related to embryonic, larval and reproductive development, as well as with mitotic processes. This suggests that MEL-28 has postembryonic functions that have not yet been studied. On the other hand, genes placed in the DNA interaction domains of NPP-22 and LMN-1, are involved with processes more typical from the NE, such as signaling pathways, sensorial perception, metabolism, and innate immune response.

Finally, in the appendix I, we attach the article: **"Differential spatial and structural organization of the X chromosome underlies dosage compensation in *C. elegans*",** (Sharma et al., 2014), a research work done in collaboration with Dr. Peter Meister from University of Bern (Switzerland). There, we performed MEL-28 DamID in males and hermaphrodites, and this study revealed new information about the mechanism of dosage compensation. Dosage compensation is a genetic regulatory mechanism, which operates to equalize expression of genes that are present on the X chromosome, and thus ensure that these genes are expressed equally in the two sexes. In *C. elegans*, dosage compensation is

achieved by two-fold down-regulation of gene expression from both X chromosomes in hermaphrodites. We found that in males, the single X chromosome interacts with NPC proteins, while in hermaphrodites; the dosage compensation complex impairs this interaction altering X chromosome localization, and probably its transcription.

Resumen

La envoltura nuclear (NE, por sus siglas en inglés) es una característica identificativa y única de las células eucariotas. La NE confina el genoma nuclear y lo separa del citoplasma, permitiendo a la célula un alto nivel de organización en la regulación de la transcripción y la traducción. La NE está formado por cuatro componentes principales: la membrana nuclear interna (INM, por sus siglas en inglés), la membrana nuclear externa (ONM, por sus siglas en inglés), la lámina nuclear y los complejos de poro nuclear (NPC, por sus siglas en inglés; Hetzer 2010).

El transporte de macromoléculas entre el núcleo y el citoplasma es regulado por los NPCs, que están constituidos por aproximadamente 30 diferentes proteínas llamadas nucleoporinas, (Nups). Las Nups pueden clasificarse en tres grupos principales. El primer grupo está formada por aproximadamente 15 Nups enriquecidas con la secuencia repetida fenilalanina-glicina (FG) y constituyen los componentes periféricos del canal de transporte del NPC. El segundo grupo está compuesto por las Nups trans-membranales NDC1, POM121, GP210 y POM33/TMEM33 (Chadrin et al., 2010). Finalmente, el tercer grupo lo constituye el andamiaje estructural del NPC, incluyendo a la Nup MEL-28/ELYS y a los complejos NUP107-160 y NUP205-188-93 (Rabut et al. 2004). La asociación de Nups con la cromatina es uno de los pasos iniciales en la reorganización nuclear, sugiriendo que podría tener un papel en la organización de la cromatina a través de la mitosis y, por consiguiente, en la propagación de la memoria epigenética.

Esta tesis se centra en el estudio de una Nup altamente conservada, conocida como MEL-28 en *Caenorhabditis elegans* y ELYS en vertebrados. MEL-28/ELYS desempeña un papel crítico en el ensamblaje post-mitóticos de los NPCs a través del reclutamiento del complejo NUP107-160, y es necesario para la correcta segregación de los cromosomas mitóticos (Fernandez & Piano 2006; Galy et al. 2006; Franz et al. 2007).

MEL-28 tiene un comportamiento dinámico: se localiza en los NPCs y en la cromatina durante la interfase, posteriormente se traslada a los microtúbulos del huso mitótico y a los cinetocores durante la división celular. Varios estudios realizados en *C. elegans* y células HeLa han reportado que las mutaciones en MEL-28/ELYS producen defectos en la morfología de la NE y el ensamblaje del NPC, así como defectos en la segregación de la cromatina, el ensamblaje del huso mitótico y el transporte núcleocitoplasma (Rasala et al.

2006; Galy et al. 2006; Fernandez & Piano 2006). Sin embargo, aún se desconoce el mecanismo con el cual MEL-28 regula su localización y actividad.

El objetivo general de mi doctorado es el análisis de la organización de la cromatina a través de la identificación de los dominios de unión de MEL-28 al ADN. Para ello, evaluamos la función de MEL-28/ELYS en dependencia a su ubicación, ya sea cuando se encuentra en el NPC o en el nucleoplasma, utilizando *C. elegans* como organismo modelo.

Los resultados de esta tesis se presentan en los capítulos IV y V; adicionalmente en el capítulo III (Materiales y métodos) se muestra el protocolo, paso a paso, de la técnica DamID-seq, desde la preparación de muestras hasta su análisis bioinformático, el cual fue publicado en el libro "The Nuclear Envelope: Methods and Protocols", con el nombre "**DamID Analysis of Nuclear Organization in *Caenorhabditis elegans***", (Georgina. Gómez-Saldivar et al. 2016). El método de DamID (van Steensel & Henikoff 2000), se basa en la expresión *in-vivo* de la proteína de interés fusionada a la proteína ADN adenina metiltransferasa (Dam, por sus siglas en inglés) de *Escherichia coli*. Cuando dicha proteína de fusión se asociada a la cromatina, produce una etiqueta de identificación única en el sitio de unión en el ADN. Esta marca es simple, altamente específica y puede ser mapeada a través del genoma por medio de reacciones enzimáticas que producen fragmentos metilados del genoma que posteriormente son analizados con métodos de secuenciación de nueva generación (NGS por sus siglas en inglés).

En el capitulo IV: **"Identification of Conserved MEL-28/ELYS Domains with Essential Roles in Nuclear Assembly and Chromosome Segregation",** (Georgina Gómez- Saldivar et al. 2016), presentamos los resultados obtenidos del objetivo 1; para ello, realizamos un análisis sistemático, estructural y funcional de las proteínas MEL-28 y ELYS; dicho análisis fue desarrollado en embriones de *C. elegans* en estadio de desarrollo temprano y en cultivos celulares, respectivamente. En colaboración con la Dra. Anita Fernandez de la Universidad de Fairfield (Estados Unidos de América), Y de los Doctores Yasushi Hiraoka y Tokuko Haraguchi, de la Escuela de Postgrado en Biociencias de la Universidad de Osaka (Japón), hemos generado y examinó la expresión y localización de la proteína MEL-28/ELYS de longitud completa, así como de casi 50 fragmentos diferentes que carecen de diversos dominios o regiones. Estas proteínas fueron fusionadas a la proteína verde fluorescente (GFP, por sus siglas en inglés) para rastrear su localización por microscopia confocal.

En este trabajo hemos identificado los dominios funcionales responsables de la localización de MEL-28 en el NPC y el cinetocoro, la unión a la cromatina, la asociación a la matriz del huso mitótico y la segregación cromosómica. Sorprendentemente, encontramos que cualquier menor perturbaciones de las regiones estructurales de MEL-28/ELYS afecta su correcta dinámica y localización. Sin embargo, la supresión o mutación del dominio funcional de unión al ADN denominado AT-hook, o del dominio estructural llamado loop-2, no perturba a la localización de MEL-28 aunque afecta su función, produce defectos durante meiosis y retrasar la progresión del ciclo celular. Concretamente, la supresión del dominio AT-hook activa el punto de control de daño al ADN. Nuestro análisis también evidenció una nueva función de MEL-28 en la Meiosis, interviniendo en el correcto desarrollo de la anafase I y II. En conclusión estos resultados muestran que MEL-28 ha conservado los dominios estructurales que son esenciales para sus roles en el ensamble del NPC y la segregación de los cromosomas durante la meiosis y la mitosis.

En este capitulo V: **"Characterization of genome-nucleoporin interaction in *Caenorhabditis elegans*"**, (manuscrito en preparación), mostramos los resultados obtenidos de los objetivos 2 y 3; y proponemos la técnica de DamID como un atractivo y poderoso método para caracterizar globalmente la organización de la cromatina en *C. elegans*. En esta parte de la investigación utilizamos las técnicas de DamID-microarreglo y DamID-seq para identificar las regiones de la cromatina con que MEL-28 interactúa. Interesantemente, los dominios de asociación de MEL-28 (MAD; por sus siglas en ingles, MEL-28 association domains) están enriquecido en genes transcritos y correlacionan positivamente con las marcas de histonas H3K4Me3 y H3K36Me3, encontradas en eucromatina transcripcionalmente activa; lo cual nos sugiere que puede estar implicado en la regulación de la expresión génica.

Además, hemos realizado el análisis de DamID con dos fragmentos de MEL-28 que son incapaces de unirse al NPC, los cuales fueron caracterizados en el capitulo IV. En general, el perfil de unión a la cromatina de estos fragmentos es muy similar a la proteína MEL-28 de longitud completa, sugiriendo que el sitio de interacción de MEL-28 con la cromatina se sitúa principalmente en el nucleoplasma y no en la periferia nuclear.

Adicionalmente, hemos comparado el perfil de unión a la cromatina de MEL-28, con el perfil de la Nup NPP-22/NDC1, la cual está permanentemente anclada a los NPCs. Sorprendentemente, a pesar de su localización esta proteína interacciona con el genoma en un porcentaje muy similar que la nucleoporina móvil MEL-28; Aunque vimos una amplia reducción de interacción con el cromosoma sexual. Así mismo, encontramos que el perfil de

asociación a la cromatina de NPP- 22 era más similar al perfil de la proteína de la lámina nuclear LMN-1 (González- Aguilera et al. 2014), que al perfil de MEL-28, sugiriendo que cada Nups puede interactuar individualmente con diferentes dominios de la cromatina.

Interesantemente, el análisis de ontología de Genes (GO; por sus siglas en inglés), reveló que los genes asociados a MEL-28 están relacionados con el desarrollo embrionario, larval y reproductivo, así como con procesos mitóticos. Lo anterior sugiere que MEL-28 tiene funciones post-embrionarias que aún no han sido estudiadas. Por otro lado, los genes localizados en los dominios de interacción con el ADN de NPP-22 y LMN-1, estuvieron relacionados con procesos más característicos de la NE, como por ejemplo: vías de señalización, percepción sensorias, metabolismo y respuesta inmune innata.

Finalmente, en el apéndice I adjuntamos el artículo: **"Differential spatial and structural organization of the X chromosome underlies dosage compensation in *C. elegans*",** (Sharma et al. 2014), Investigación realizada en colaboración con el Dr. Peter Meister de la Universidad de Berna (Suiza), realizamos DamID análisis de la proteína MEL-28 en machos y hermafroditas del gusano *C. elegans*. Este estudio reveló novedosa información sobre el mecanismo de compensación de la dosis génica. La compensación de la dosis genética es un mecanismo regulador que opera para igualar la expresión de los genes que están presentes en el cromosoma X, asegurando así, que estos genes se expresan en un cantidad equivalente en los dos sexos. En *C. elegans*, la compensación de dosis se logra por una regulación negativa de la expresión génica en las hermafroditas, que disminuye dos veces la transcripción de los genes presente en ambos cromosomas X. Interesantemente, encontramos que en los machos, el cromosoma X interactúa con proteínas del NPC, mientras que en hermafroditas, el complejo de compensación de la dosificación (DCC, por sus siglas en inglés) inhibe esta interacción alterando la localización del cromosoma X, y probablemente su nivel de transcripción.

Chapter I

Introduction

Role of Nuclear Envelope Proteins in Eukaryotes

One of the major events in the biological evolution was the appearance of an endomembrane system that enabled cellular compartmentalization, especially the nucleus, giving rise to the lineage Eukaryota. The nucleus contains the genome, which is structured and organized to safeguards the integrity of genes and guarantee cell function by regulating gene expression. The principal structure forming the cell nucleus is the nuclear envelope (NE) (For review see (Devos, Gräf, & Field, 2014)).

During evolution, the NE emerged from the prokaryotic plasma membrane. Moreover, NE-associated structures, e.g., nuclear pore complexes (NPCs), the nuclear lamina (NL), NE transmembrane proteins (NETs) and proteins forming the linker of nucleoskeleton and cytoskeleton (LINC) complex, have evolved to perform other special functions such as organization of the chromatin within the three-dimensional space of the nucleus (for review see (BLOBEL, 2010)).

Therefore a hallmark of eukaryotic cells is the NE, a highly organized system of double-layered membrane perforated by nuclear pores (NPs), that encloses the genetic material, keeping it separated from the cytoplasm (Martin W. Hetzer, 2010). The NE forms a physical barrier that blocks the accessibility of cytoplasmic proteins to DNA, and allows a selective export of newly synthesized mRNA from the nucleus to the cytoplasm, achieving a novel spatial and temporal regulation of transcription and translation specific to eukaryotic cells. This bi-directional traffic is made through the NPCs.

Despite the traditional view of NE functions is focusing on its role in the separation of the nuclear genome from cytoplasmic components, supporting the shape of the nucleus and coordinate nucleocytoplasmic transport, over the last two decades, several studies have provided a new insight of its role in the distribution and organization of the genome and, in consequence, NE and NPC might directly regulate gene expression through the positioning of genes and chromosomes within the nucleus (for review see (Fraser, Williamson, Bickmore, & Dostie, 2015; Zuleger, Robson, & Schirmer, 2011). Besides, the NE and NPC also participate in mitosis and transcriptional control.

It has been reported that mutations in certain NE-proteins, such as lamins and inner nuclear membrane protein emerin, produce a series of diseases called envelopathies or laminopathies (for review see (Dobrzynska, Gonzalo, Shanahan, & Askjaer, 2016)) (Figure 1.1).

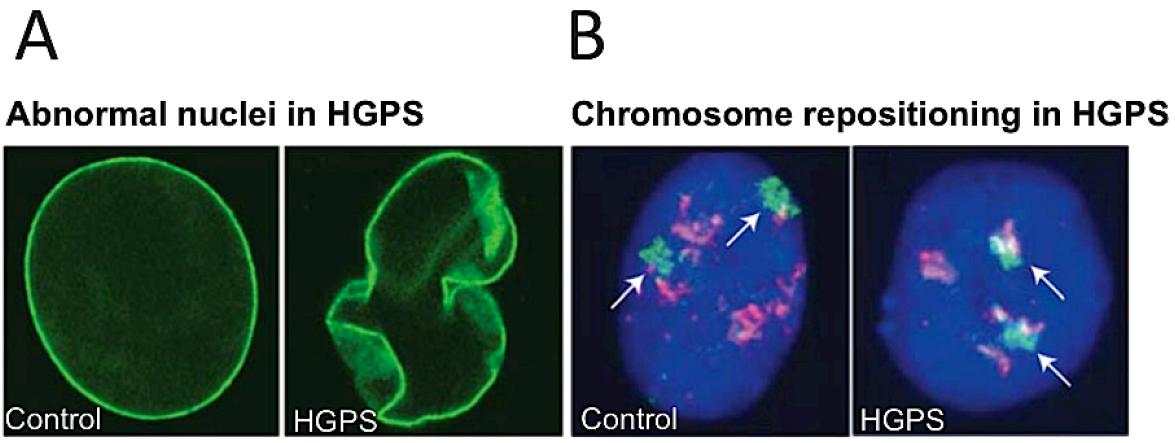

Figure 1.1. Nuclear organization defects in laminopathies. (A) Abnormal nuclear shape in Hutchinson-Gilford Progeria Syndrome (HGPS), caused by mutation in *LMNA* gene. Healthy individuals show a regular nuclei shape (Control), contrasting with nuclei from patients show an abnormal morphology (HGPS). (B) Chromosome repositioning in HGPS. Interior repositioning of human chromosome 13 (green, arrows) in HGPS fibroblast cell line (right), in comparison to a control cell line (left). Proliferation marker pKi-67 (red). Adapted from (Ferrai, de Castro, Lavitas, Chotalia, & Pombo, 2010).

Importantly, nuclear organization and gene positioning are critical during development. Meister and collaborators have reported that in *C. elegans* embryos developmental promoters expressed in transgene arrays, remain attached to the periphery in undifferentiated cells, but upon activation arrays shift inside of the nuclei in respective tissues (Meister, Towbin, Pike, Ponti, & Gasser, 2010). This shift of position is in accord with the nuclear organization model, where nuclear periphery represents an environment with silent chromatin anchored at the NL, whereas the active chromatin localizes in the center of the nuclei (Ikegami, Egelhofer, Strome, & Lieb, 2010; Towbin et al., 2012). However, active domains can also locate close to NPC by transcription-dependent mechanisms (Ikegami & Lieb, 2013; Rohner et al., 2013).

Besides, recently the NE has been implicated to play a function in the mechanism of dosage compensation (DC) in *C. elegans*. In appendix I of this thesis, we show a work done in collaboration with Dr. Peter Meister group where we evaluate the role of NE in X chromosome positioning during DC (Sharma et al., 2014). In *C. elegans*, DC is achieved by two-fold down-regulation of gene expression from both X chromosomes in hermaphrodites. We found that in males, the single X chromosome interacts with a conserved nucleoporin (Nup) called MEL-28, potentially at NPC; while in hermaphrodites, the DC complex (DCC)

impairs this interaction altering X chromosome localization, and probably its transcription. Consistent with this, knocking down DCC subunits in hermaphrodites, produces peripheral (re-)positioning of the X chromosome.

The Nup MEL-28, called ELYS in vertebrates, has a dynamic behavior. During interphase, MEL-28 localizes to NPCs and chromatin, later on, relocalizes to condensed chromosomes during prophase and shuttles to spindle microtubules and kinetochores during cell division (Fernandez & Piano, 2006; Galy, Askjaer, Franz, López-Iglesias, et al., 2006a). MEL-28/ELYS plays a critical role in post-mitotic NPC reassembly through recruitment of the Nup107-160 complex and is required for correct segregation of mitotic chromosomes (Franz et al., 2007). In chapter IV, using *C. elegans* as a model organism, we explored which regions of MEL-28 are required for its different localizations and functions; and we identified functional domains responsible for NPC and kinetochore localization, chromatin binding, mitotic spindle matrix association and chromosome segregation. Interestingly, we found a novel role of MEL-28 during meiotic chromosome segregation.

In the following sections we will detail some of the biological processes that we described in the thesis in which we find a novel participation of MEL-28 protein, but first a brief outline of *C. elegans* as organism model will serve to introduce the processes.

Caenorhabditis elegans as Model Organism

A Brief History of *Caenorhabditis elegans* Research

Nowadays, the nematode *Caenorhabditis elegans* is extensively investigated in over a thousand laboratories worldwide. The interesting history of the introduction of *C. elegans* as a model organism started with Dr. Ellsworth C. Dougherty. One of his significant contributions to science was his recognition of the value of rhabditid nematodes, expressly *Caenorhabditis* spp. (Ferris & Hieb, 2015), as biological models for studies of many fields of biology such neurobiology, genetics, and molecular biology.

Dougherty was one of the first to detect the potential use of rhabditid nematodes in genetics research. In 1948, he published a letter (Dougherty & Calhoun, 1948) summarizing some of

the main features of rhabditid nematodes, i.e. their small size, short life cycle, easy cultivation on nutrient agar, utilization of bacteria as a food resource. Besides, he highlighted some its advantages for genetic research, for example: a) these nematodes have low chromosomes number making it easy for manipulation, detection, and study of mutations; b) its invariable number of somatic cells (around one thousand) enabling determination of mutations effects at cellular level; c) the organism shows different sex patterns and its sex-determination is produced by an unusual regulation of X-chromosome behaviour in meiosis; d) It is possible to study physiological mutant by culturing in chemically defined media.

However, probably one of the most famous moments in the history of *C. elegans* occurred in June of 1963, when Dr. Sydney Brenner wrote in a letter to Max Perutz, the director of the Laboratory of Molecular Biology in Cambridge, UK, his concern to extend molecular biology to other more biological fields:

"Nearly all the classical problems of molecular biology have either been solved or will be solved in the next decade ... the future of molecular biology lies in the extension of research to other areas of biology, notably development and the nervous system".

In this letter, Brenner proposed the nematode *Caenorhabditis briggsae* as a good system to approach these problems (Ankeny, 2001). Subsequently, in October of 1963, Brenner requested to Dougherty a culture of *C. elegans*. The culture of the Bristol strain was designated N2 (N from "Nematode"; N1 was not a *Caenorhabditis* and later was identified *as Mesodiplogaster lheritieri*); Brenner received a culture of the Bristol strain of *C. elegans* from Dougherty. Between the reasons for the switch of specie have been speculated that *C. elegans* is more photogenic and has better growth rate (Ferris & Hieb, 2015). Finally *C. elegans* genetics started formally in October of 1967 with the generation of the two firsts mutants using ethyl methanesulphonate mutagenesis (Brenner, 2009).

Caenorhabditis elegans Basics

C. elegans is a tiny, free-living soil nematode present worldwide. Newly hatched larvae are 0.25 mm long whereas adults are ~1 mm long. Using a stereoscope, it is possible to observe worms while they move, eat, develop, mate, and lay eggs on Petri dishes seeded with *Escherichia coli* bacteria as a food source. The compound microscope allows observation at much finer resolution, reaching single-cell level. Since *C. elegans* is

transparent, individual cells and subcellular compartments are easily visualized using differential interference contrast (DIC) optics.

C. elegans exists in two sexes: self-fertilizing hermaphrodites and males (Figure 1.2). Both sexes are diploid for the five autosomal chromosomes (I-V) and the number of X chromosomes determines the sex: hermaphrodites have two whereas males have a single X chromosome (Cline & Meyer, 1996). Adult males are thinner than hermaphrodites. Males appear at a frequency of 0.1-0.2% by spontaneous non-disjunction of the X chromosome during meiosis in the hermaphrodite germline but this frequency can be increased up to 50% through mating. Self-fertilization of the hermaphrodite follows the standard Mendelian rules of segregation, then homozygous worms generate isogenic progeny (Brenner, 1974). Mating with males allows the movement of mutations between strains and the mapping of alleles.

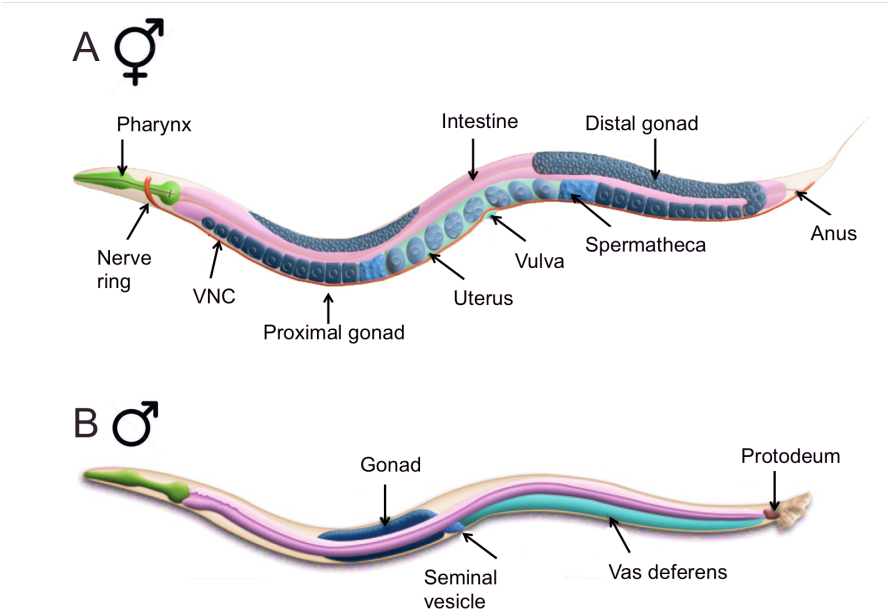

Figure 1.2 *Caenorhabditis elegans* anatomy. Schematic drawing of major anatomical features of a hermaphrodite (A) and male (B) viewed laterally. VNC: Ventral nerve cord. Adapted from WormAtlas.

Because *C. elegans* has an invariant number of somatic cells (959 hermaphrodites and 1031 in males), researchers have been able to track the fate of every cell lineage (Sulston & Horvitz, 1977; Sulston, Schierenberg, White, & Thomson, 1983). Another convenience of the anatomy of the worm is that despite its morphological simplicity, *C. elegans* has fully defined systems. The nematode body is composed by two concentric tubes separated from each other by the pseudocoelomic space (Figure 1.3). The outer tube (body wall) consists of

cuticle, hypodermis, excretory system, neurons and muscles; whereas the inner tube is formed by the pharynx, intestine and, in the adult, the gonads. In the following sections, we will focus on developmental processes that take place in the gonad and reproductive system.

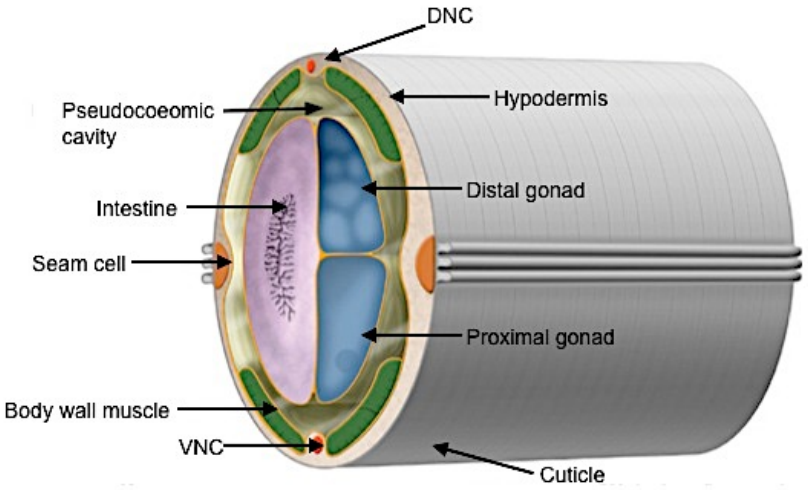

Figure 1.3. Cross-section through the posterior region of the *C. elegans* hermaphrodite. Schematic drawing showing the four muscle quadrants surrounded by the hypodermis and cuticle with the intestine and gonad enclosed within the pseudocoelomic cavity. DNC: Dorsal nerve cord; VNC: Ventral nerve cord. Adapted from WormAtlas.

Moreover, *C. elegans* was the first multicellular organism with a complete genome sequence, allowing efficient forward and reverse genetics to identify many key genes in developmental and cell biological processes. Approximately 60–80% of human genes have an ortholog in the *C. elegans* genome, and 40% of genes known to be associated with human diseases have clear orthologs in the *C. elegans* genome (Corsi, Wightman, & Chalfie, 2015). Therefore, several discoveries in *C. elegans* have applicability in the study of human health and disease.

In addition to its easy and low maintenance expenses, several other features greatly facilitate the experimental use of *C. elegans* in the laboratory. First, animal populations can be long-term cryopreserved and revived when needed. Second, animals can be grown at temperatures ranging from 12ºC to 25ºC. Growth at different temperatures makes it possible to control the rate of development and use of temperature-sensitive mutants. Shorter incubation to higher temperatures (from 30ºC to 34ºC) is possible for stress response

experiments and to increase production of males. Third, animals can be synchronised by treating gravid adults with bleach and isolating eggs, which are resistant to bleach treatment. Fourth, gene knockdown is achieved through the usage of RNA interference (RNAi). Actually, Dr. Andrew Fire and Dr. Craig C. Mello received the 2006 Nobel price in physiology or medicine for establishing RNAi technique in *C. elegans*. Fifth, transparency enables performance of studies in living animals utilizing fluorescent protein reporters. This, in part thanks to the work done by Dr. Martin Chalfie with the green fluorescent protein (GFP) in *C. elegans*, which earned him the Nobel Prize in Chemistry in 2008. Transparency also allows using of optogenetic tools. Finally, the open attitude to share information, techniques, supplies, etc. in the community of *C. elegans* researchers has been central to the success of *C. elegans* research. Reviews on many topics of *C. elegans* biology are provided as Open Access in WormBook (www.wormbook.org), WormAtlas (www.wormatlas.org) and Wormbase (www.wormbase.org).

Life Cycle

In addition to the many advantages of *C. elegans* mentioned above, its quick generation time is a quality that facilitates many experiments in the laboratory. *C. elegans* has a short life cycle, its development from egg to egg-laying adult takes 3 days at 22ºC (Figure 1.4) under standard conditions. *C. elegans* is most commonly found in the wild as dauer larvae. The dauer state is a non-aging stage that provides protection against environmental stresses and ends when the animal experiences favorable conditions and develops into an L4 larva, to later become an adult. During adulthood, a self-fertilizing hermaphrodite produces around 300 eggs. *C. elegans* embryogenesis takes approximately 16 hours (h) at 20ºC and it is roughly divided into two stages: proliferation and organogenesis. Proliferation stage is further subdivided into two phases: The first phase (0 to 150 minutes; min) spans the time between zygote formation to generation of embryonic founder cells (AB, E, MS, C, D and germline P4), which takes place within in the uterus, and the embryo is laid outside when it reaches approximately 30-cell stage (as gastrula). The second phase (150 to 350 min) covers the most of the cell divisions and gastrulation (Bucher & Seydoux, 1994). Now, the embryo is a spheroid of cells organized into three germ layers, ectoderm that forms hypodermis and neurons, mesoderm that generates pharynx and muscle, and endoderm that produces the germline and intestine. In organogenesis (5.5-6 h to 12-14 h) the embryo elongates threefold and takes form as a larva with fully differentiated tissues and organs (Altun & Hall, 2016). In favorable conditions, after hatching the animal begins to eat and develop through four larval stages (L1–L4). Each stage ends with a period of inactivity

named lethargus, which concludes with the molting of the old cuticle. Approximately 12 h after the L4 molt, adult hermaphrodites begin producing progeny for a period of 2–3 days starting the cycle again. In the lab, the dauer stage can be induced at the end of L2 stage with the absence of food or in the crowded conditions.

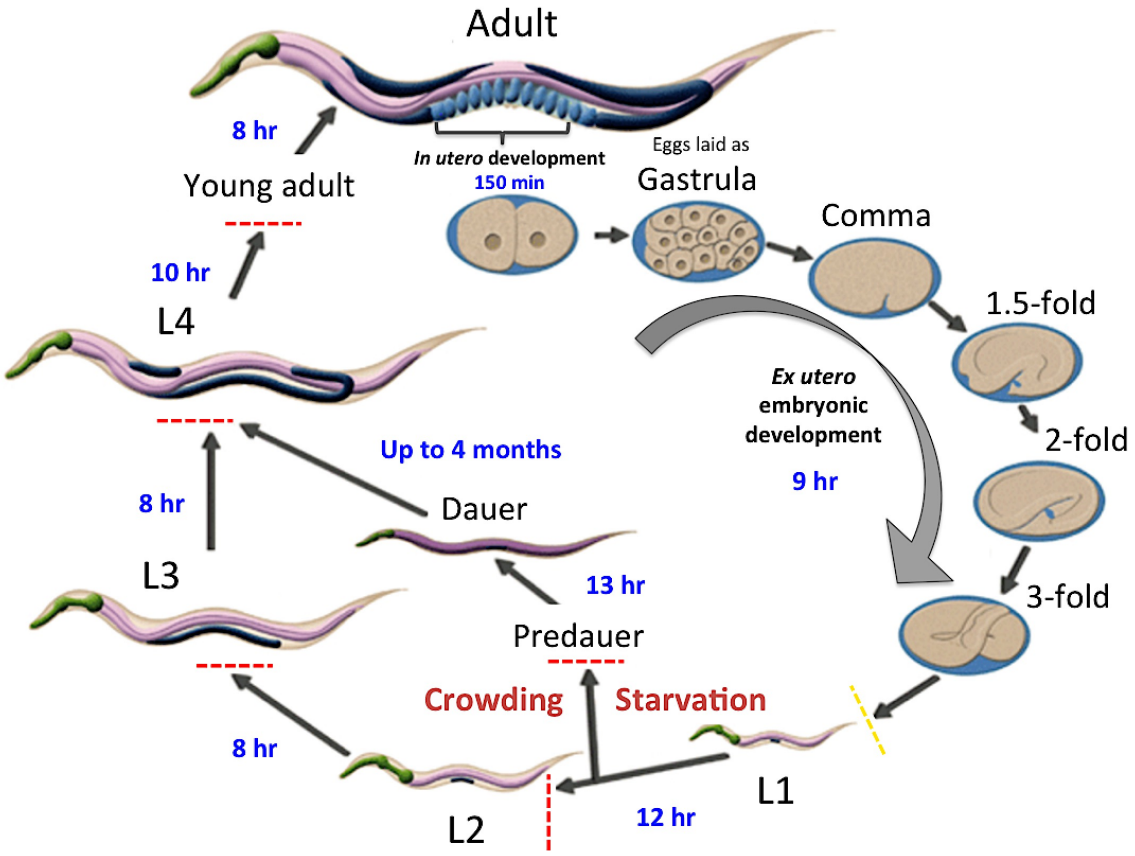

Figure 1.4. Life cycle of *C. elegans* at 22˚C. The time the animal spends at a certain stage is shown in blue. 0 min is fertilization. Eggs are laid outside at about 150 min post fertilization during the gastrula. The red and yellow dashed lines indicate the larval molt and hatching time respectively. Adapted from WormAtlas.

Caenorhabditis elegans Sex Determination and Dosage Compensation

The X:A Ratio Determines both Sex and Dosage Compensation

Sexual fate in *C. elegans* is determined genetically by X-to-autosome (or X:A) chromosomes

ratio (Cline & Meyer, 1996) (Figure 1.4). Specific genes present on the X chromosome, called X-signal elements (XSEs), act in a collective dose-dependent mode to repress levels of the developmental switch gene *xol-1*. Contrarily, a set of genes on the autosomes (ASEs, autosomal signal elements) code for proteins that activate *xol-1* (for review see, (Meyer, 2005)). Compared to XO embryos, an XX embryo has twice as many XSEs, which reduces *xol-1* expression by ~10-fold (Rhind, Miller, Kopczynski, & Meyer, 1995). Then, during development males (XO) show high levels of XOL-1, whereas hermaphrodites (XX) show low levels. XOL-1 guaranties the proper sexual differentiation and male viability, also allows the expression of the gene *her-1* promoting male development (Zarkower, 2006). The final effector of XOL-1 is TRA-1, which controls all aspects of somatic sexual differentiation. In hermaphrodites TRA-1 activity leads to a female somatic fate and oogenesis, blocking spermatogenesis. In males, TRA-1 is inactive, inducing male fate and spermatogenesis (Cline & Meyer, 1996).

Moreover, XOL-1 levels determine the activation state of the dosage compensation (DC) mechanism (Luz et al., 2003). Then, DC responds to the X:A ratio similarly (Figure 1.4). The DC mechanism works only in hermaphrodite where it decreases the level of gene expression in both X chromosomes by 50% to equalize X-linked transcript levels between the sexes (for review see (Sevinç Ercan, 2015; Meyer, 2005))

The link in the role of X:A ratio in both processes it is due to a set of genes called *sdc* genes (sex determination and dosage compensation). *sdc* genes were discovered in a screening that reduced the viability of XX but not XO. Curiously, the few XX animals that survive had a dumpy phenotype (for review see, (Meyer, 2005)). These set of eight genes are *sdc-1, sdc-2, sdc-3, dpy-21, dpy-26, dpy-27, dpy-28, and dpy-30*. Today it is known that these proteins, along with MIX-1 and CAPG-1, form the dosage compensation complex (DCC). Although sex determination and dosage compensation follow a common step of regulation, distinct genetic pathways control them.

Dosage Compensation Complex

Biochemical and genetic analysis of the DCC revealed that the complex consists of two subparts. The SDC subcomplex is formed by SDC-1, SDC-2, SDC-3, DPY-21 and DPY-30 proteins. Five additional proteins, DPY-26, DPY-27, DPY-28, MIX-1, and CAPG-1, conform the second subcomplex called DPY/condensin-like complex or condensin I^{DC} because of its

homology with the conserved condensin complex required for mitotic and meiotic chromosome segregation and compaction (Hagstrom & Meyer, 2003; Lucchesi, Kelly, & Panning, 2005). SDC-2 is the only protein that can localize to X independently from all other DCC proteins, implying that SDC-2 is crucial for X chromosome recognition and gives chromosome specificity to DC (Dawes et al., 1999). Moreover, SDC-2 is only expressed in XX embryos, therefore SDC-2 is responsible for giving the sex-specificity to the DCC (Nusbaum & Meyer, 1989)

Interestingly, the DCC is regulated by the developmental switch that coordinates sex determination in males, *xol-1*, which represses the expression of *sdc-2*, thereby preventing DCC from assembling on the single male X (L. M. Miller, Plenefisch, Casson, & Meyer, 1988) (Figure 1.5 in the top). In hermaphrodites, *sdc-2* is active and together with *dpy-30* activates *sdc-3*. These three proteins recruit the rest of the DCC (for review see (Meyer, 2005)). SDC-3 works as a scaffold for the assembly of the DCC in the X chromosome reducing its expression 2-fold. In addition, SDC-3 binds to *her-1* locus on chromosome V and downregulates its expression 20-fold (Figure 1.5 in the bottom), promoting hermaphrodite development (Davis & Meyer, 1996). The difference in the level of repression mediated by SDC-3 may be due to the components that form the repressor complex. For example, one of the components of the complex that binds to the X chromosome is DPY-21, which is absent in the complex that binds to *her-1* locus.(Yonker & Meyer, 2003).

To achieve dosage compensation, DCC must identify X chromosomes from autosomes. The X chromosome presents a DNA sequence, which is recognized by DCC as a recruitment site for later *cis*-spread to secondary sites onto the X chromosome to accomplish chromosome-wide gene repression (Györgyi Csankovszki, McDonel, & Meyer, 2004; Sevinç Ercan, Dick, & Lieb, 2009). These sites were designated as recruitment sites on the X (rex sites) (Sevinc Ercan et al., 2007). Until today, 38 rex sites have been experimentally demonstrated but is predicted that along the length of its 17.5 Mb, the X chromosome has around 200 rex sites, which are enriched with a 12-bp DNA sequence called motif enriched on the X (MEX) (Jans et al., 2009). The MEX motif is involved in recruiting the DCC to rex sites. However, is still unknown which proteins of the DCC associate with the MEX motif.

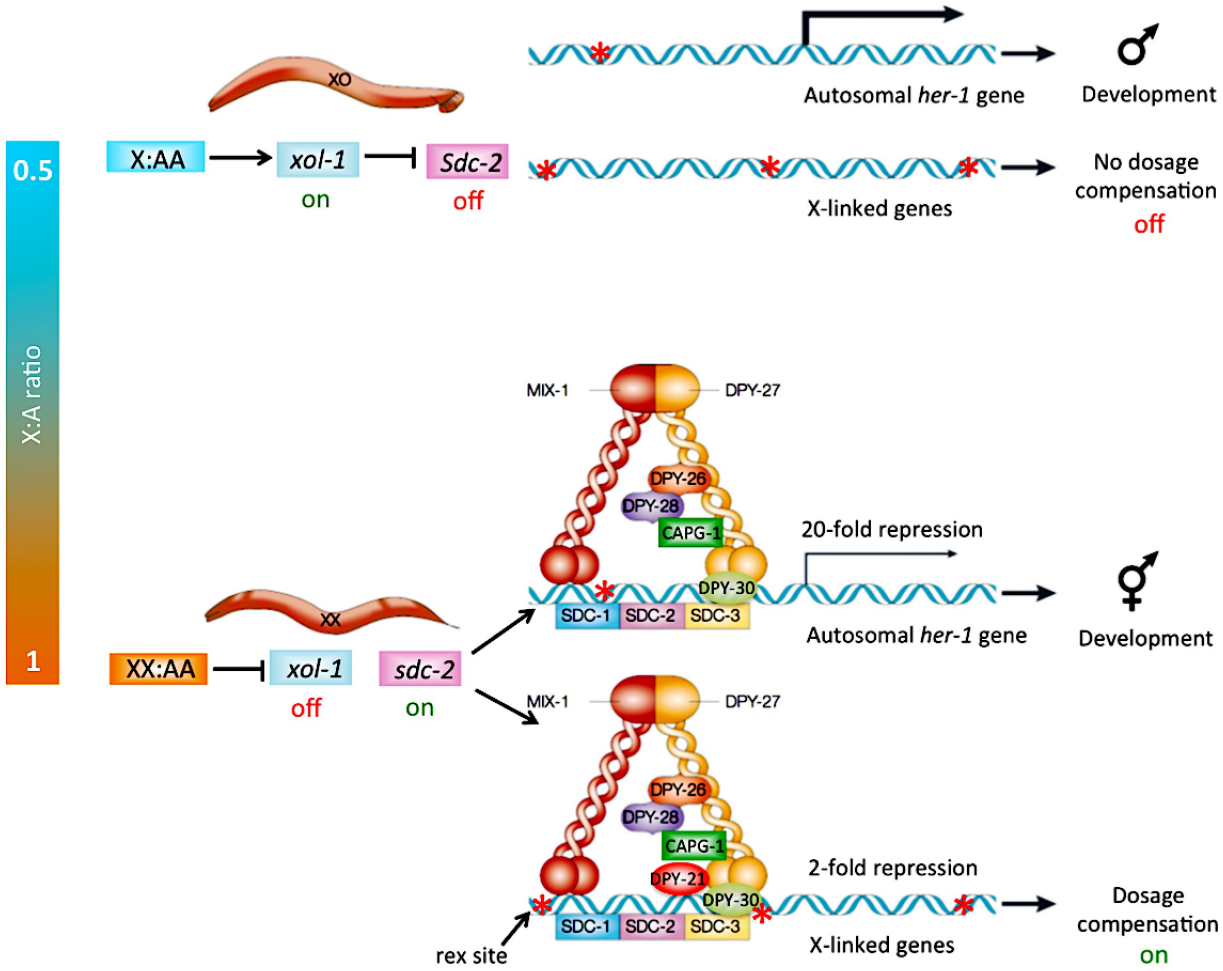

Figure 1.5. Dosage compensation in *C. elegans*. A regulatory pathway regulates both dosage compensation (DC) and sex determination in response to the main sex determination signal: the X:A chromosomes ratio. In the top, low ratios (for example, 1X:2A = 0.5) activate the master switch gene *xol-1*, which represses *sdc-2* allowing male sexual development and inhibition of DC. In the bottom, high ratios (for example, 2X:2A = 1) silence *xol-1*, promoting hermaphrodite sexual development and the assembly of a dosage compensation complex (DCC) onto rex sites (recruitment sites on the X; red asterisk) along X chromosomes to produce the reduction in gene expression by 2-fold. Moreover, SDC-2 acts with SDC-3 recruiting the DCC machinery (with exception of DPY-21) to induce hermaphrodite development by repression of the expression level of the autosomal male-fate-promoting gene *her-1* by ~20-fold. Adapted from (Hagstrom & Meyer, 2003).

The *Caenorhabditis elegans* Gonad: A Transparent Tube for Cell and Developmental Biology

C. elegans adults present several anatomical differences between sexes, e.g. number of (somatic) gonads, secondary sexual structures, and body size (Figure 1.2). Males have a

single U-shaped gonad arm, whereas hermaphrodites have two mirror-image U-shaped gonads. Development of the germline in both sexes is regulated by intercellular signaling. The hermaphrodites are females that produce sperm for a short and precise time early in gametogenesis and then produce exclusively oocytes as adults. In contrast, males produce only sperm and can mate with hermaphrodites to produce cross progeny. Here, I have focused on describing the development in the self-fertile hermaphrodite.

The distal region of the hermaphroditic gonad is a syncytium of partially enclosed nuclei that share a common maternal cytoplasm (Lints & Hall, 2016). Germ cells proliferate near the distal tip cell and enter the meiotic pathway as they progress proximally (Figure 1.6). In the transition zone region germ cells pass from mitotic cell cycle into meiosis and initiate meiotic recombination. At the time that germline nuclei pass through the loop region they exit pachytene, become completely enclosed by a plasma membrane, and line up in the proximal gonad arm. Germ cell apoptosis, a feature of oogenesis, take place in adult hermaphrodites next to the gonad loop region. Oocytes develop in association with proximal gonadal sheath cells, which through a sperm-sensing mechanism regulate oocyte meiotic maturation and ovulation, ensuring that oocyte production and growth occur only when sperm are present (J McCarter, Bartlett, Dang, & Schedl, 1997; Yamamoto, Kosinski, & Greenstein, 2006). The developing oocytes enter diplotene, which is characterized by chromatin condensation. From this stage, bivalents (pairs of homologous of chromosomes attached by chiasmata) become visible as six separate chromatin structures. In diakinesis, these six bivalents are easily visualized within the nucleus (for review see Hillers, Jantsch, Martinez-Perez, & Yanowitz, 2015).

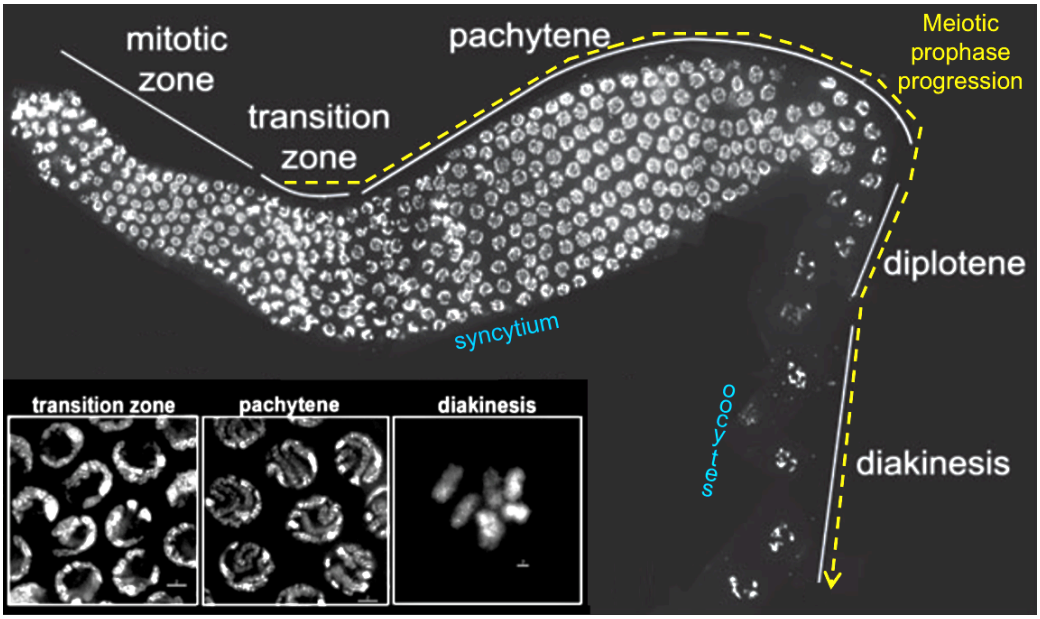

Figure 1.6. The *C. elegans* hermaphrodite germ line contains a complete time course of meiotic prophase. Projection of three-dimensionally data stacks of a dissected hermaphrodite germ line stained with DAPI to visualize chromatin. Progression from the distal to the proximal end is depicted from left to right. Stages of meiotic prophase and magnification of representative nuclei are shown below the germ line. Adapted from (Lui & Colaiácovo, 2013).

In the absence of sperm, oocytes arrest in diakinesis (prophase of meiosis I) (James McCarter, Bartlett, Dang, & Schedl, 1999). When sperm are present, meiotic maturation begins in an assembly-line fashion where the oldest oocyte is adjacent to the spermatheca (often referred to as the –1 oocyte; Figure 1.7). Sperm releases the major sperm protein (MSP) signal which is sensed through an oocyte MSP/EPH receptor to trigger meiotic maturation (M. A. Miller, Ruest, Kosinski, Hanks, & Greenstein, 2003). Meiotic maturation includes all physiological changes required for the oocyte just before zygote formation and is essential for achieving meiosis and a prerequisite for successful fertilization (for review see Greenstein, 2005; Robertson, Lin, Robertson, Lin, & Lin, 2013; Yamamoto, Kosinski, & Greenstein, 2006). During meiotic maturation, the oocyte passes from diakinesis to metaphase of meiosis I and is accompanied by nuclear envelope breakdown (NEBD), rearrangement of the cortical cytoskeleton, and meiotic spindle assembly. Every ~23 min the oldest oocyte undergoes NEBD, also called germinal vesicle breakdown (GVBD) (James McCarter et al., 1999), and squeezes into the spermatheca at ovulation, where it is fertilized. Next, the fertilized zygote enters the uterus where it synthesizes a chitinous multilayered eggshell and completes meiosis I and II, generating the oocyte pronucleus and two polar bodies. The resulting one cell embryo (E1) subsequently undergoes several rounds of mitotic cell division. Therefore, fertilization it has three main roles: to complete the meiotic divisions, block to polyspermy, and activation of the embryonic program.

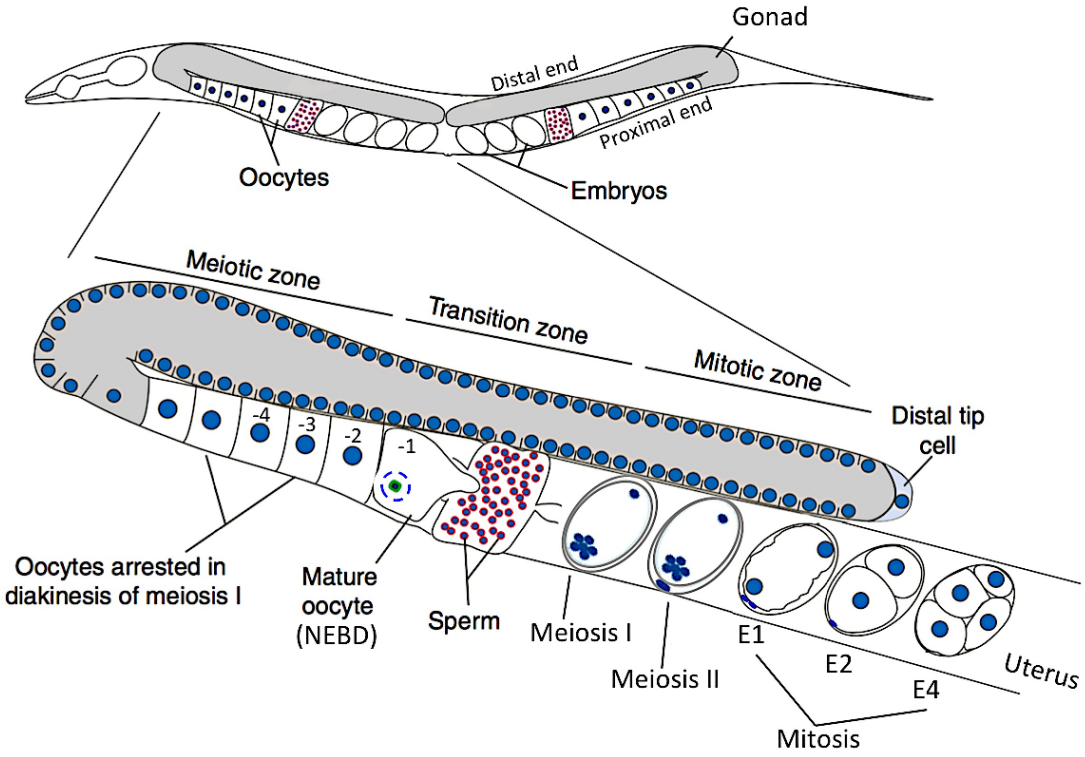

Figure 1.7. Oogenesis and early embryogenesis in *C. elegans*. Zoom in of one gonad arm from adult hermaphrodite. Germ cell nuclei (in blue), undergo mitotic divisions in the distal end, they migrate to the proximal end, enter meiosis and are enclosed into oocytes. Meiotic maturation takes place in an assembly line fashion (the most proximal and mature oocyte is referred to as –1). The mature oocyte suffers NEBD and enters the spermatheca, is fertilized and exits as zygote into the uterus. The fertilized zygote forms an eggshell and finishes meiosis I and II creating the oocyte pronucleus and two polar bodies. The one cell embryo (E1) undergoes the firsts mitotic divisions in the uterus to develop into two and four cell embryo (E2 and E4, respectively). Adapted from (Bowerman & Kurz, 2006).

In summary, the stereotypical architecture and reproducible cell divisions of the *C. elegans* gonad, oocyte and early embryo offer an attractive model system. Moreover, the high efficiency of RNAi-mediated gene knockdown facilitates quantitative analysis of the loss-of-function phenotypes. The reproducibility of protein depletion is caused by the syncytial architecture of the gonad since dsRNA is introduced in the continual maternal cytoplasm and later packaged into oocytes. Furthermore, *C. elegans* exhibits easily tractable phenotypes, e.g. defects in meiotic prophase I events result in increased chromosome non-disjunction, generating aneuploid gametes that produce embryonic lethality phenotype or high incidence of males (Lui & Colaiácovo, 2013).

Finally, transparency it is once again an indisputable advantage which converts the germ line in a visible gradient of development; we have the possibility to film the meiotic cycle in around 35 - 45 min from NEBD through pronucleus formation using an anesthetized worm (H. Yang, McNally, & McNally, 2003). The *C. elegans* embryo is also transparent and can live and develop outside of the hermaphrodite making possible the direct observations of embryogenesis, which is performed in an invariant pattern and timing. An example is the difference in cell cycle timing in two-cell embryo (E2) when the larger anterior blastomere AB divides ~2 min earlier than the smaller posterior blastomere P1 (Tavernier, Labbé, & Pintard, 2015). Moreover, thanks to many investigations using time-lapse microscopy (Bucher & Seydoux, 1994; Cheeseman et al., 2004; Hird & White, 1993; Labbé, McCarthy, & Goldstein, 2004; Maddox, Portier, Desai, & Oegema, 2006; James McCarter et al., 1999) we have a well defined timeline of landmark morphological events during oocyte and embryo development (Figure 1.8), which allows us to measure any parameter of interest (i.e. the intensity of a GFP fusion protein, the nuclear size, the number of polar bodies, etc.) as function of time according to a specific temporal landmark (i.e. NEBD, anaphase onset, or the initiation of furrow ingression, etc.). In the next section, we will examine in detail aspects of the dynamics of meiotic division and early embryogenesis.

A

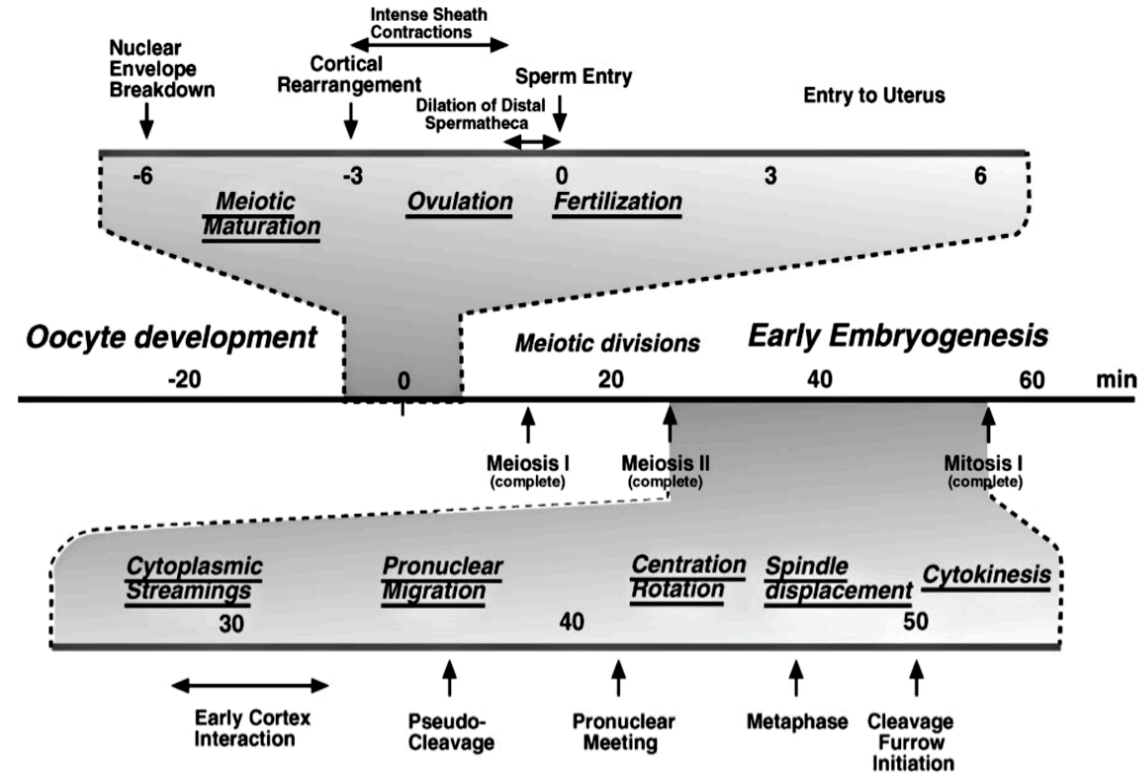

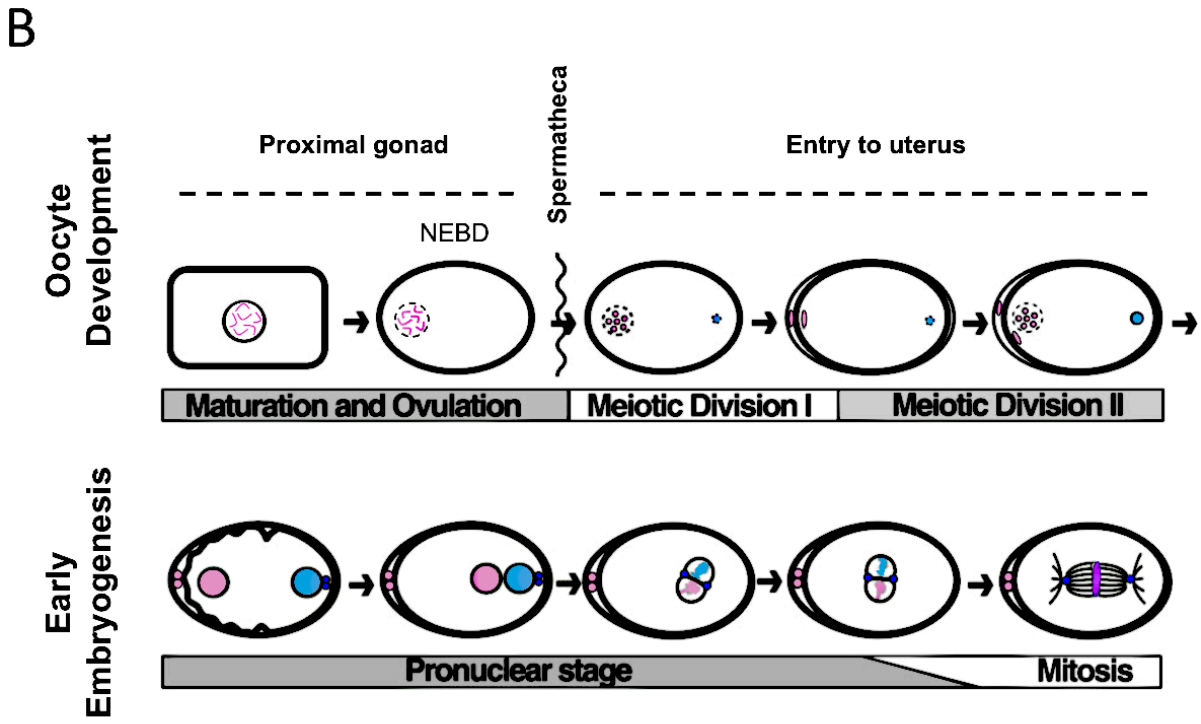

Figure 1.8. Timeline of the landmark morphological events during early development. (A) Timing of events during oogenesis, meiosis, and early embryogenesis (at ~22ºC). The end of ovulation is defined as 0 min and coincides closely with fertilization. In the top, oogenesis, oocyte maturation, and ovulation are shown with an extended time scale. In the bottom, the first mitotic division is extended. Time is in minutes. (B) Schematic drawing of meiotic divisions and early embryogenesis. In the top, oocyte meiotic maturation involves nuclear envelope breakdown (NEBD) and cortical rearrangement. The oocyte (in pink) is fertilized in the spermatheca. The condensed sperm chromatin is shown in the posterior (in blue) of the embryo. In the bottom, pronuclei form, meet in the posterior, and fuse as they enter mitotic phase. A pair of centrioles (small circles in dark blue) enters the egg with the sperm during fertilization (shown until embryogenesis). Adapted from (Furuta et al., 2000; Schneider & Bowerman, 2003)

Female Meiosis in *C. elegans*

In this section, we will center on the meiosis in *C. elegans* hermaphrodite since they are generating both sperm and oocytes.

In preparation for meiosis I, during meiotic prophase, homologous chromosomes pair and synapse, generating a configuration that supports the formation of crossover recombination events, which is crucial for the formation of chiasmata. These crossovers, in conjunction with sister chromatid cohesion, produce bivalents where the connected homologs are oriented away from each other; this promotes bipolar attachment of homologs to the meiosis I spindle. During meiosis I, homologous chromosomes segregate away from each to opposite poles at anaphase I. Later, half of the genome is ejected into a small non-developing cell

called the first polar body. In the other hand during meiosis II, which is similar to mitosis, sister chromatids segregate to opposite poles of the spindle and again half of the remaining genome is ejected into a second polar body. These meiotic divisions are mediated by asymmetric spindle positioning which are attached by one pole to the oocyte cortex at anaphase facilitating the extrusion of polar bodies. The precise segregation of chromosomes at each cycle of meiotic cell division is required for the formation of cells carrying a correct number of chromosomes and defects in these processes lead to aneuploidy. Therefore, given its importance, there are several mechanisms to guarantee the proper chromosome segregation, as illustrated by meiosis I, where homologous chromosomes must pair, align, and form physical connections prior to the first meiotic division. During fertilization, several key processes support the normal progression of meiosis I and II. I mention below some of the most important processes and components of meiotic divisions in *C. elegans,* emphasizing the mechanisms of the meiotic division that are fundamentally different from those of the mitotic division (Figure 1.9).

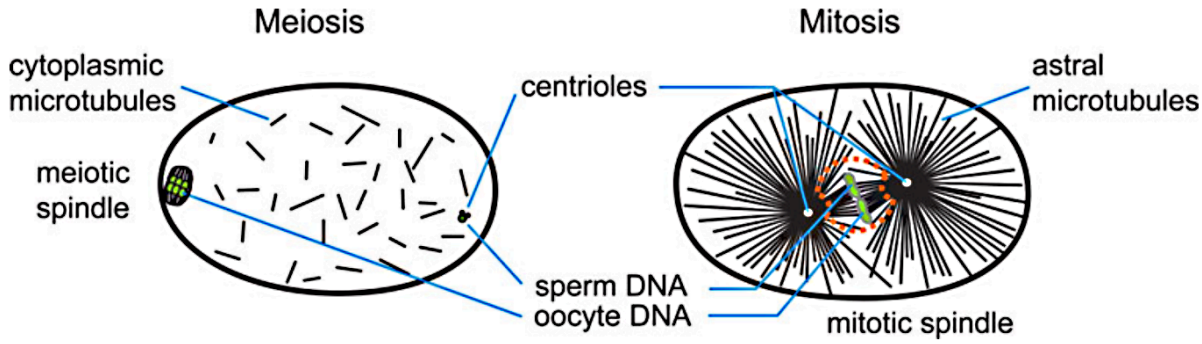

Figure 1.9. Schematic comparison of meiotic and mitotic division in the early *C. elegans* embryo. The fertilized oocyte assembles two consecutive acentrosomal meiotic spindles, which are relatively small (~3-4 µm) at metaphase and show a cortical positioning (left). In contrast, the centrosome-based mitotic spindle of the one-cell embryo is large (~14 µm) at metaphase and has prominent spindle poles with a profusion of astral microtubules (right). Chromatin is shown in green. The nuclear envelope (orange dashed line) persists in the early stages of mitotic spindle assembly, but disappears by anaphase. Adapted from (Müller-Reichert, Greenan, O 'toole, & Srayko, 2010)

Asymmetric Division of Oocytes

During oogenesis, two meiotic divisions generate a single daughter, which becomes an egg and two polar bodies, which not participate in reproduction. The asymmetric meiotic divisions maintain the size and cytoplasmic contents of the oocyte for the fertilized zygote.

For successful asymmetric division, the spindle must remain positioned near the cell cortex with a perpendicular orientation.

Several studies on asymmetric divisions have been done using the first mitotic division of the early *C. elegans* embryo, identifying important roles of PAR proteins and centrosomes (for review see (Pierre Gönczy, 2008; Labbé et al., 2004; Rose & Gönczy, 2014; Tavernier et al., 2015). However, during oogenesis there is no presence of centrosomes, therefore, other structures or mechanisms must be involved in meiotic spindle orientation and positioning.

Cortical Positioning of Female Meiotic Spindles

In many species, the oocyte nucleus translocate from a central location to a predetermined spot on the cortex during the maturation process (for review see Fabritius, Ellefson, & McNally, 2011). In *C. elegans* after NEBD, the meiotic spindle displays further translocation to the cortex, this nuclear migration results in the spindle assembling close to the cortex (Figure 1.10). This translocation is dependent on the microtubule motor, kinesin-1, and its binding partner KCA-1 (H. Yang, Mains, & McNally, 2005). In embryos with depletion of kinesin-1– or KCA-1, the spindles assemble far from the cortex and persist there during metaphase. During metaphase I, the spindles maintain a constant length of approximately 8 μm, with a parallel orientation at the cortex for an average of 7 min after ovulation. Then the anaphase-promoting complex (APC) initiates a series of events, where meiotic spindles shorten to only 5 μm (Crowder et al., 2015; K. L. McNally & McNally, 2005; H. Yang et al., 2003). Later, subsequent rotation of the spindle results in an orientation perpendicular to the cortex. In anaphase I chromosome separation initiates and the spindle elongates simultaneously with the generation and ingression of the polar body contractile ring, which results in the extrusion of chromosomes into a polar body. This cycle happens again during meiosis II (H. Yang et al., 2003). The perpendicular orientation with one spindle pole attached to the cortex at anaphase is extremely conserved across animal phyla and presumably facilitates the expulsion of half the chromosomes into a polar body.

This asymmetric meiotic spindle positioning in the cortex presents several advantages: maximizes the volume of a single egg, avoiding interference with the meiotic spindle by the sperm aster; maintains predetermined embryonic polarity gradients; and provides the possibility to correct trisomy by preferentially elimination of the extra chromosome into a polar body (Cortes, McNally, Mains, & McNally, 2015).

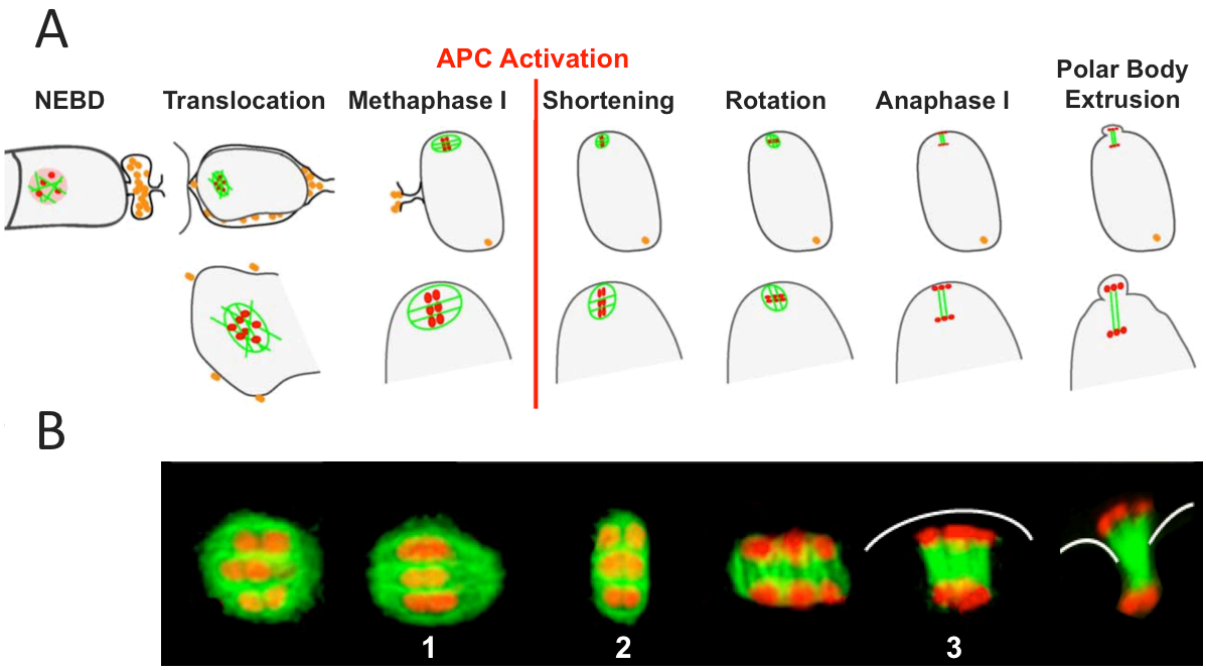

Figure 1.10. Different steps of chromosome segregation during meiosis I in the *C. elegans* oocyte. (A) Drawing of meiosis I. Microtubules (green), chromosomes (red), and sperm (orange) are illustrated. The meiotic spindle is assembled a short distance from the cortex after nuclear envelope breakdown (NEBD), then after fertilization, it translocates to a parallel orientation. The metaphase meiotic spindle persists at a constant 8 um length and parallel position until activation of the anaphase-promoting complex (APC). Once APC is activated, the meiotic spindle shortens and rotates 90º to a perpendicular position. Later, during early anaphase, the meiotic spindle continues to shorten in its pole-to-pole axis, then elongates producing the extrusion of the first polar body. Time of activation of APC is indicated by a red line. (B) High magnification montage of meiotic spindle positioning in the oocyte. (1) a microtubule-based spindle (GFP::tubulin, green) assembles during meiotic division and promotes chromosome (mCherry::histone, red) alignment on a metaphase plate. (2) Spindle poles then shorten around chromosomes. (3) Finally, in anaphase, microtubules concentrate between the separating chromosomes and 'push' them toward the two future daughter cells. The embryo cortex is outlined in white lines for clarity. Adapted from (Fabritius et al., 2011).

Acentrosomal Spindle Assembly

Most animal cells need centrosomes to nucleate microtubules when building the bipolar spindle apparatus. However, the assembly of the female meiotic spindle in several organisms is independent of centrosomes (for review see (Müller-Reichert et al., 2010; Ohkura, 2016)).

In *C. elegans*, centrioles disappear during oocyte maturation. Although the mechanism is unclear, the cyclin-dependent kinase inhibitor *cki-2* gene (negatively regulator of cyclin E-Cdk1 complex) has been implicated in centriole elimination (Kim & Roy, 2006). As a result of the elimination of centrioles from the cytoplasm, oocytes need to use non-centrosomal mechanisms to build a bipolar spindle for the two consecutive meiotic divisions. One key feature of acentrosomal spindle assembly is that chromatin, rather than centrosomes, promote the formation of microtubules.

In *C. elegans* the MEI-1/MEI-2-katanin complex is required specifically for the assembly of the acentrosomal female meiotic spindles. Katanin is an AAA-ATPase critical for the generation of microtubules near meiotic chromatin (K. McNally et al., 2014; M Srayko, Buster, Bazirgan, McNally, & Mains, 2000; H. Yang et al., 2003). Katanin severs microtubules along their length and *C. elegans* mutants lacking katanin have fewer but longer microtubules in the meiotic spindle: although microtubules assemble around meiotic chromatin, they fail to assemble a bipolar spindle (M Srayko et al., 2000; Martin Srayko et al., 2006). In consequence, polar bodies are often not generated due to the failure to segregate chromosomes, and those that do form are usually very large. Thus severing apparently supports microtubule assembly, and possibly also promotes the use of tiled, discontinuous microtubules in oocyte spindles. However, why oocyte meiotic spindles should be composed of short, discontinuous microtubules is unknown (Figure 1.9 and 1.3).

Chromosome Segregation Mechanisms

One of the main structures responsible for chromosome segregation during cell division is the centromere, which acts as a chromosomal site of kinetochore association, connecting chromosomes to spindle microtubules (for review see (Kitagawa, 2009). Most eukaryotes present monocentric chromosomes, where kinetochore proteins assemble at a single point per chromosome. In monocentric species, the cohesion of sister chromatids must be released in two steps during meiosis, to support the co-orientation of chromosomes and their segregation (Figure 1.11A). First, during anaphase of meiosis I, releasing the chiasmata and cohesion along the chromosome arms allows homologous chromosomes to segregate to opposite poles, while sister chromatids migrate together to the same pole (mono-orientation) due to the cohesion of sister centromeres/kinetochores in a side-by-side geometry. Second, during anaphase of meiosis II, the centromeric cohesion of sister

chromatids is released allowing a segregation similar to mitosis with sister centromeres/kinetochores migrating to opposite poles (bi-orientation) in a back-to-back geometry. This allows amphitelic attachment, through the capture of sister kinetochores by microtubules emanating from opposite poles (Petronczki et al., 2003).

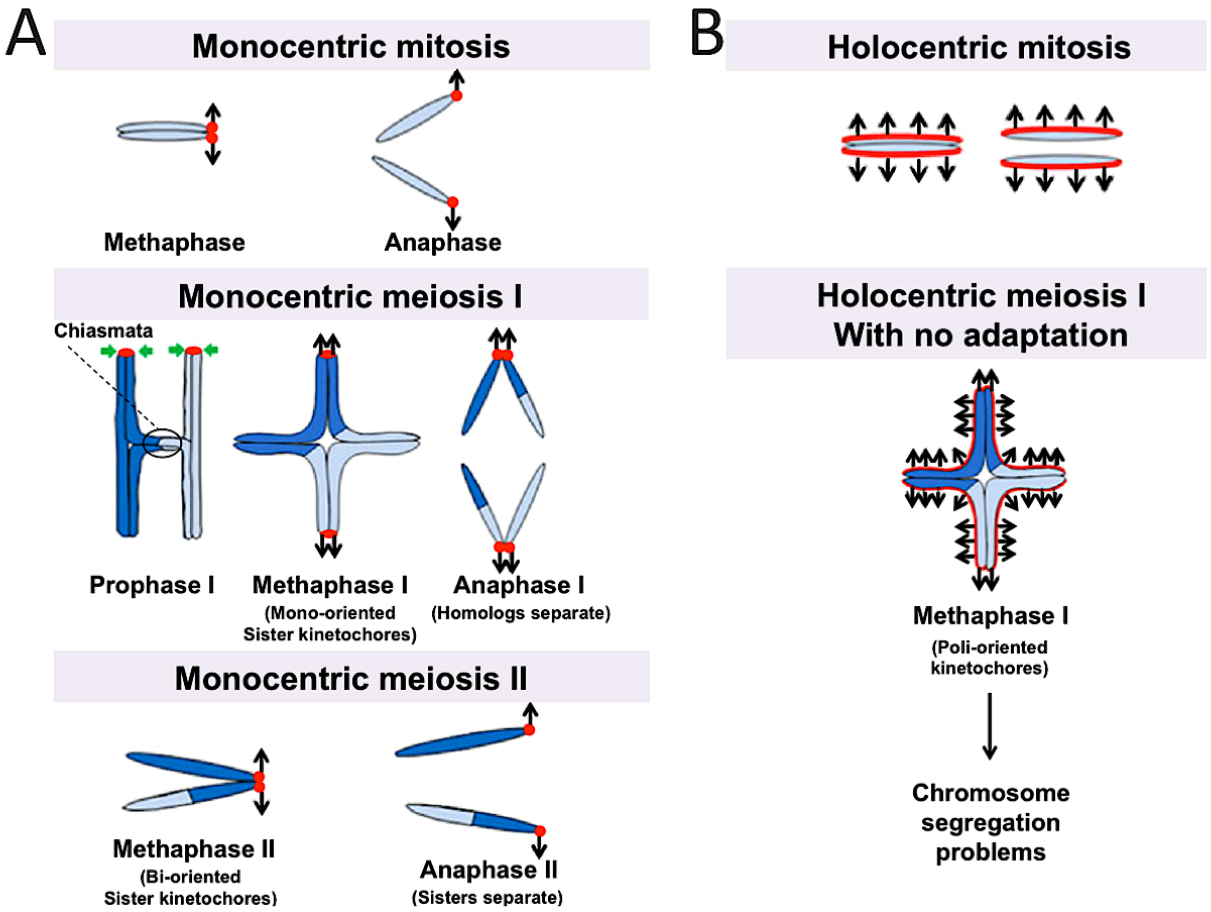

Figure 1.11. Mitosis and meiosis with monocentric and holocentric chromosomes. (A) Monocentric cell division. In mitosis, sister kinetochores of monocentric chromosomes face opposite spindle poles, leading the separation of sister chromatids in anaphase. In meiosis I, sister kinetochores are fused and face in the same direction, leading homologous chromosome separation in anaphase I. In meiosis II, similar to mitosis, the sister kinetochores face in opposite directions in metaphase, and sister chromatids separate in anaphase II. (B) Holocentric cell divisions. In mitosis, kinetochores are distributed along the length of the holocentric chromosomes, which connect to the spindle in their entire length. In anaphase, kinetochore plate allows the spindle-attachment sites face in opposite directions and sister chromatids separate. In meiosis I, if there is no adaptation of chromosome structure or attachment surface position, attachment sites can face in all directions, producing problems in chromosome segregation. Adapted from (Melters, Paliulis, Korf, & Chan, 2012).

C. elegans presents holocentric chromosomes where kinetochore proteins can bind along the entire length of the chromosomes. This extended centromere structure introduces a problem during meiosis I because sister holocentromeres are not co-oriented and bivalents can attach to the spindles randomly (Figure 1.11B). Interestingly, to deal with this condition, holocentric chromosomes have developed different strategies to allow accurate meiotic segregation (for review see (Marques & Pedrosa-Harand, 2016; Melters et al., 2012). In *C. elegans*, chromosomes adapted to meiosis by losing their holocentric behavior and adopting a monocentric mode (Figure 1.12) (For review see (Melters et al., 2012).

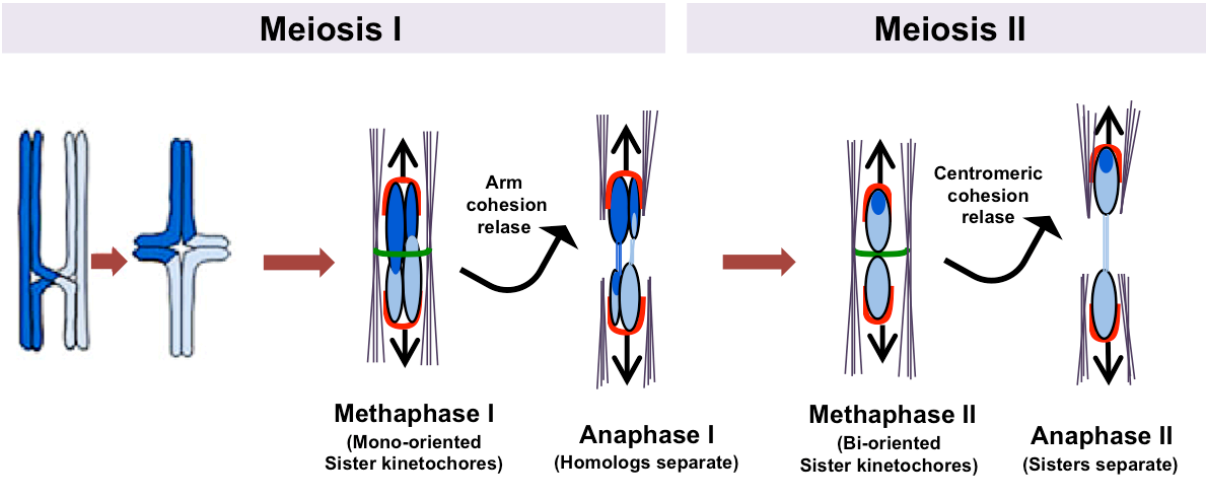

Figure 1.12. *C. elegans* oocyte adaptation to the problem of holocentric chromosomes in meiosis. During meiosis I, sisters become paired by cohesin, and DNA exchange between homologs takes place. The kinetochore forms a cup-like structure and spindles form a sheet around the bivalents. Unlike in mitosis, sister kinetochores attach to the spindle in monopolar fashion whereas attachment of the homolog kinetochores is bipolar. Following resolution of crossovers and cohesin disassembly along the arms (but not at centromeres), the homologs segregate. During meiosis II, sister kinetochores bi-orient on the spindle, and cohesin removal at the centromeres triggers their segregation. Adapted from (Melters et al., 2012).

Transmission electron microscopy (EM) of *C. elegans* mitotic chromosomes showed the formation of a trilaminar kinetochore plate, which is not visible during meiosis (D G Albertson & Thomson, 1982; Donna G Albertson, Rose, & Villeneuve, 1997). Instead, holocentric kinetochores adopt a structure that encloses the long arms of bivalents in meiosis (Figure 1.13). *C. elegans* bivalents have a single asymmetrically positioned chiasma. Therefore, they take a cruciform form in late prophase I similar to monocentric chromosomes at the same stage. Before NEBD of meiosis I, bivalents condense very tightly and takes the capsule shape. Later, immediately before oocyte meiotic segregation, kinetochore proteins

CENP-C, KNL-1, BUB-1, NDC-80, Nuf2, and MIS-12 are recruited and form a cup around each end of the bivalent via a mechanism that is independent of CENP-A (Dumont, Oegema, & Desai, 2010; Monen, Maddox, Hyndman, Oegema, & Desai, 2005). Next, each end of the bivalent faces a spindle pole and moves toward that pole in anaphase. Surprisingly, the segregation of homologs involves a mechanism of chromosome remodelling independent of the inner kinetochore components HCP-3/CeCENP-A and HCP-4/CeCENP-C (Dumont et al., 2010; Howe, McDonald, Albertson, & Meyer, 2001; Monen et al., 2005).

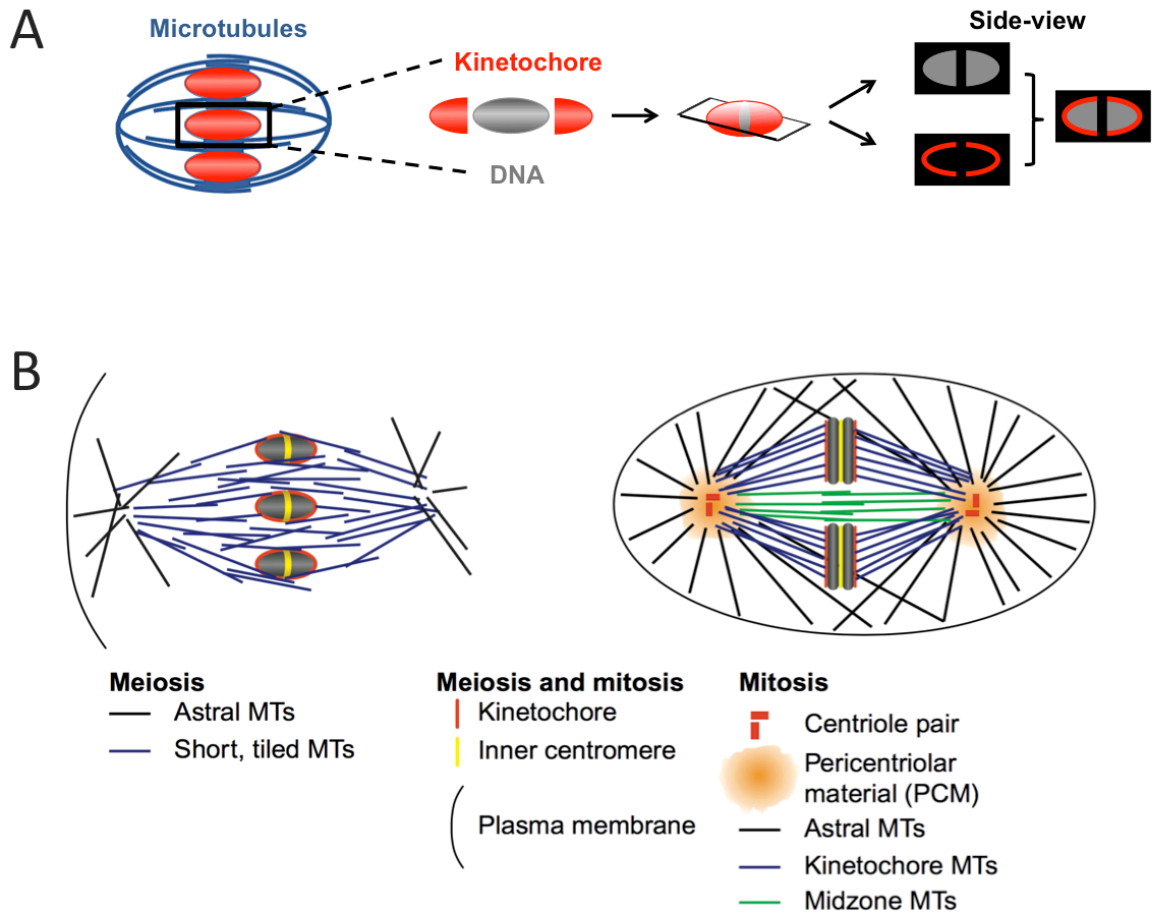

Figure 1.13. Cartoons of kinetochore and spindle structure during meiosis and mitosis in *C. elegans*. (A) Schematic representation of cup-shaped meiotic kinetochores. (B) During meiosis (left), centrioles are degraded prior to assembly of the oocyte meiotic spindle. Short, often tiled, microtubules form near chromosomes and ultimately coalesce into a bipolar structure. During mitosis (right), inner and outer kinetochores (red) form a trilaminar kinetochore plate along the chromosomes (gray). A long, radial microtubule arrays are nucleated in the pericentriolar material surrounding the centrioles. Microtubules (blue) from each spindle pole are captured by kinetochores. Antiparallel microtubules (green) become packaged together in the midzone, a process that stabilizes mitotic spindle structure. These kinetochore/microtubule attachments align each chromosome on the metaphase plate. Adapted from (Severson, von Dassow, & Bowerman, 2016).

Interestingly, the outer-kinetochore protein, HIM-10 was first identified as a protein needed for proper meiotic chromosome segregation (Hodgkin, Horvitz, & Brenner, 1979). Thus, HIM-10/CeNUF-2 and other conserved outer kinetochore components may form the meiotic kinetochores that assemble on the surface of chromosomes responsible for guiding the chromosomes on the spindle axis via attachment of a few microtubules to the ends of the bivalents (Dumont et al., 2010; Monen et al., 2005).

Early Embryogenesis in *C. elegans*

Timeline of Morphological Events During the First Mitotic Division

During fertilization, a mature oocyte enters the spermatheca and encounters a sperm cell; typically the sperm enters on the opposite side relative to the oocyte nucleus. In addition to providing DNA, the sperm entry makes several essential contributions to the embryo (for review see (Riddle, Blumenthal, Meyer, & Priess, 1997)). (1) Activation of the oocyte to begin embryogenesis, (2) The sperm contributes with a pair of centrioles to the new embryo, which recruits pericentriolar material and acquires the ability to nucleate microtubules (3) The site of sperm entry designates the future posterior side of the embryo. Once meiosis is complete, the haploid oocyte and sperm-derived pronuclei increase in size and are easily visible by DIC microscopy. The two sperm-derived centrioles separate and form two centrosomes, which are positioned on opposite sides of the paternal pronucleus (Cowan & Hyman, 2004).

During mitotic prophase, the male and female pronuclei migrate towards each other, coinciding with the condensation of chromosomes. Pronuclear migration consists of the movement of the oocyte pronucleus towards the sperm pronucleus and movement of the sperm pronucleus away from the cortex towards the embryo center. Initially, the oocyte pronucleus moves ~ 12 µm towards the posterior at a slow rate. Later on, the oocyte pronucleus accelerates, moving an additional 10 µm at ~5-10 times its initial rate (D G Albertson, 1984). The sperm pronucleus begins its migration later than the female pronucleus and travels at a slow rate till it meets with it near the embryo center (~7 µm). Once the pronuclei meet, the nuclear-centrosome complex moves to the center of the

embryo and rotates to align with the anterior-posterior axis of the embryo (D G Albertson, 1984). This coincides with the pronuclei NEBD (Lee, Gruenbaum, Spann, Liu, & Wilson, 2000). Next, condensed chromosomes congress to and distribute over the metaphase plate to align (Oegema, Desai, Rybina, Kirkham, & Hyman, 2001). The sister chromatids then separate, decondense, and cytokinesis partitions the two segregated DNA masses into daughter cells (Figure 1.14).

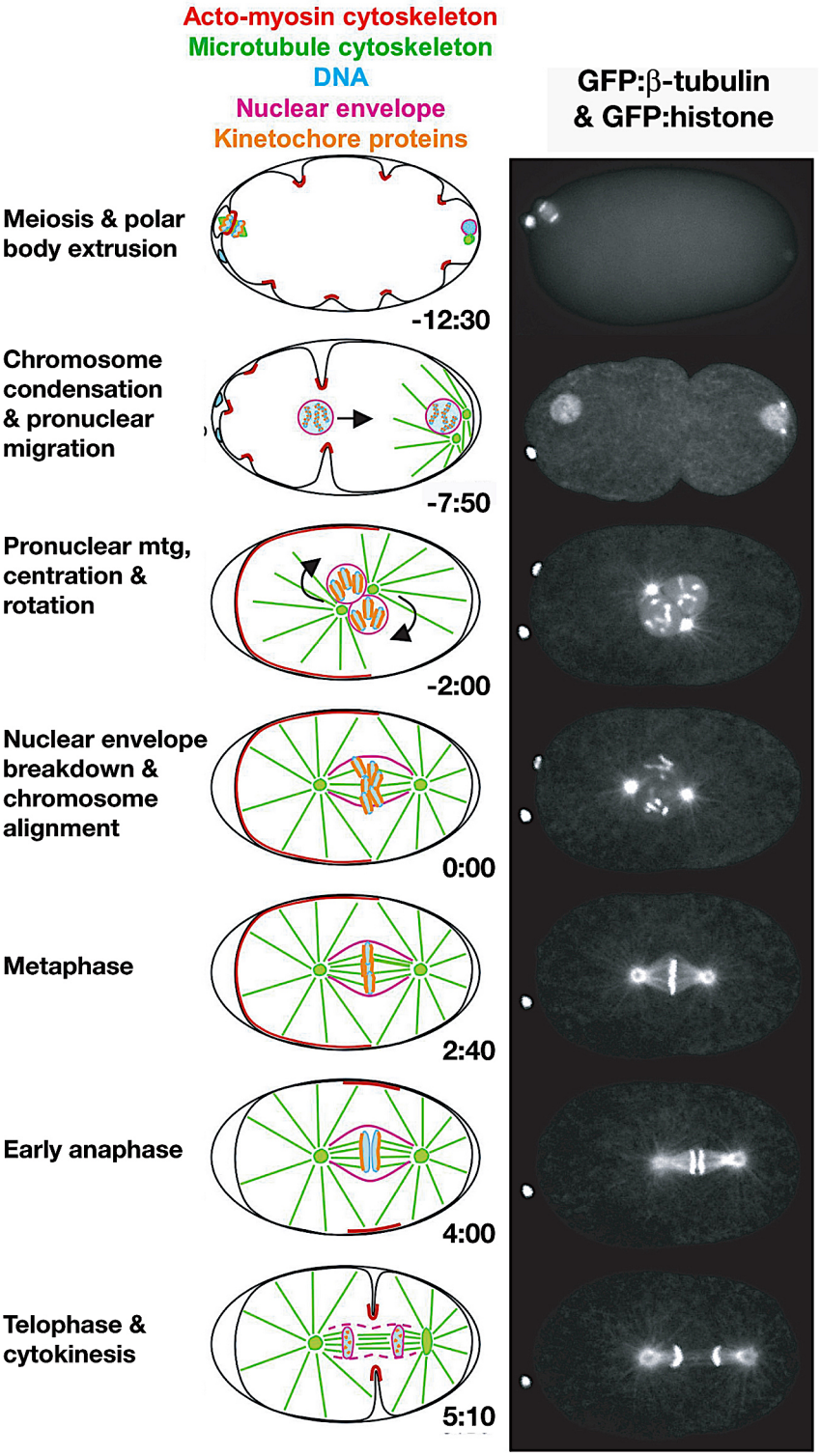

Figure 1.14. Timeline of morphological events during the first division of *C. elegans* embryo. The left column shows schematics drawing of major features of the first division. Time is indicated relative to nuclear envelope breakdown (min:sec). In the right column simultaneously visualize the microtubule cytoskeleton (GFP::β-tubulin) and DNA (GFP::histone). Adapted from (Oegema & Hyman, 2006).

Structure of Mitotic Chromosomes

Cohesin is a protein complex that coordinates the separation of sister chromatids during cell division. Cohesin is loaded onto chromosomes and hold sister chromatids together after DNA replication until anaphase when removal of cohesin drives the separation of sister chromatids. The formation of the cohesin complex is required for generating appropriate tension at kinetochores, which captures centrosomal microtubules. The cohesin complex is formed by a heterodimer of the SMC proteins SMC1 and SMC3, and the non-SMC subunits RAD21/SCC1 and SCC3 (Michaelis, Ciosk, & Nasmyth, 1997). Cohesin components play crucial roles in determining the timing of anaphase onset. At the metaphase-anaphase transition, RAD21/SCC1 is cleaved by the endopeptidase separase (Uhlmann, Lottspeich, & Nasmyth, 1999). Separase is bound and inactivated by the anaphase inhibitor securin, which is degraded via ubiquitination by the anaphase-promoting complex also called cyclosome (APC/C) as soon as chromosome alignment is complete. Then, separase is active to cleave cohesin, leading to sister chromatid separation, thereby initiating anaphase (for review see (Hagstrom & Meyer, 2003). In *C. elegans*, depletion of cohesin complex components affects proper mitotic chromosome segregation and the pairing of homologous chromosomes during meiosis (Pasierbek et al., 2003).

Chromosome condensation is a key event that occurs at the beginning of mitosis. Condensation shortens chromosomes to facilitate proper sister chromatid separation. The condensin protein complexes have crucial roles in the formation, compaction, and segregation of mitotic and meiotic chromosomes (Hagstrom, Holmes, Cozzarelli, & Meyer, 2002; Hudson, Marshall, & Earnshaw, 2009). *C. elegans* contains three condensin complexes, condensin I, II, and I^{DC}. Whereas condensin I and II bind to all chromosomes, condensin I^{DC} only associates with X chromosomes in hermaphrodites, showing important functions in the dosage compensation of X-chromosome in the hermaphrodite (Gyorgyi Csankovszki et al., 2009). Condensin I and II contribute differently to chromosome segregation. Whereas condensins of many organisms associate with the central

chromosome axis, *C. elegans* condensin localizes to holokinetochores during mitosis (Hagstrom et al., 2002). Condensin II concentrates on chromosomes during prophase when condensation initiates while condensin I seems to stabilize chromosome rigidity (Hirota, Gerlich, Koch, Ellenberg, & Peters, 2004; Maddox et al., 2006). Despite depletion of each complex individually produces distinct chromosome morphology defects, both complexes are required for the proper sister-chromatid segregation (Hagstrom et al., 2002). In embryos with condensin depletion, chromosome condensation is delayed. However, DNA compaction is completed (Maddox et al., 2006), indicating the existence of condensin-independent mechanisms that can compact mitotic chromatin.

Similar to condensins, the chromosomal passenger complex (CPC, formed by the aurora B kinase AIR-2, BIR-1, ICP-1, and CSC-1) is recruited to mitotic chromosomes and is required for their proper segregation (Kitagawa, 2009; Oegema et al., 2001). The CPC plays important roles in chromosome structure and has key functions correcting aberrant kinetochore-microtubule attachments during meiosis and mitosis (Collette, Petty, Golenberg, Bembenek, & Csankovszki, 2011; Dumont, 2015; Rogers, Bishop, Waddle, Schumacher, & Lin, 2002).

Kinetochore Assembly

As we mentioned above, eukaryotes can be divided into two groups, monocentrics and holocentrics (Figure 1.15A), based on the architecture of their mitotic chromosomes. *C. elegans* has emerged as an important model system for studying holocentric chromosome architecture. Moreover, several studies have reported that the molecular composition of kinetochores in *C. elegans* and monocentric organisms are very similar (for review see (Oegema & Hyman, 2006)). In both monocentric and holocentric organisms, mitotic kinetochores assemble on the specialized centromeric chromatin characterized by the presence of nucleosomes containing the histone H3 variant CENP-A/HCP-3 (Buchwitz, Ahmad, Moore, Roth, & Henikoff, 1999).

CENP-A/HCP-3 associates with chromosomes throughout the cell cycle and is the first kinetochore component that localizes to *C. elegans* holocentric chromosomes. Depletion of CENP-A/HCP-3 leads to “kinetochore-null” phenotype, in which defective kinetochores fail to interact with spindle microtubules, producing abnormal chromosome distribution over the spindle equator and segregation (Oegema et al., 2001). Four kinetochore proteins have

been identified whose depletion produces a kinetochore-null defect: CENP-A/HCP-3, CENP-C/HCP-4, KNL-3 and KNL-1 (Figure 1.15D), which can be located in a linear assembly hierarchy (Figure 1.15B) with CENP-A/HCP-3 at the top (Cheeseman, Chappie, Wilson-Kubalek, & Desai, 2006; Desai et al., 2003; Oegema et al., 2001). Depletion of the rest of kinetochore proteins results in less severe chromosome segregation defects (Howe et al., 2001; Oegema & Hyman, 2006).

The mitotic kinetochore complex is assembled in hierarchy mode (Figure 1.15B). The subsequent protein downstream of CENP-A/HCP-3 is CENP-C/HCP- 4. In addition to its role in directing kinetochore assembly, CENP-C/HCP-4 has also been implicated in sister kinetochore resolution (Moore & Roth, 2001), the process by which the kinetochores on the two sister chromatids resolve from one another, to position them on opposite sides of the mitotic chromosome.

Similar to kinetochore-localized proteins, the chromokinesin KLP-19, which localizes to the chromatin between the diffuse kinetochores, is also crucial for chromosome segregation. Interactions between KLP-19 and spindle microtubules are proposed to generate a pushing force that rotates chromosomes to orient the sister kinetochores to face opposite spindle poles (Powers et al., 2004). This mechanism reduces the risk that a single kinetochore will become incorrectly attached to microtubules coming from both spindle poles.

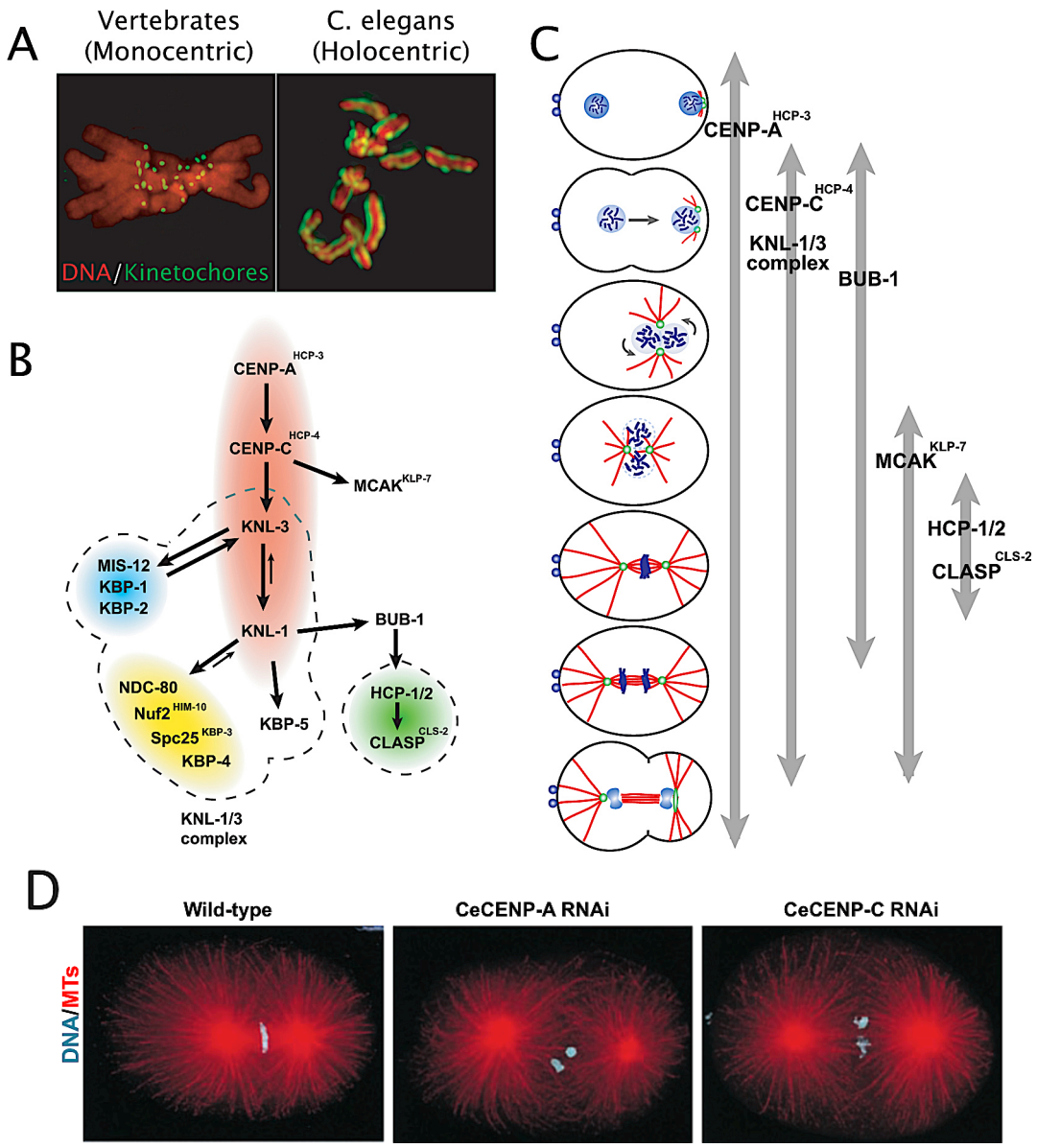

Figure 1.15. Mitotic kinetochores in the *C. elegans* embryo. (A) Comparison of kinetochores in monocentric chromosomes (in vertebrates), and holocentric chromosomes (in *C. elegans*). (B) Schematic drawing of the hierarchy for mitotic kinetochore assembly. Dotted lines are drawn around groups of proteins that co-purify in immunoprecipitations from *C. elegans* embryonic extracts. The colored ovals indicate groups of proteins whose individual depletions result in a similar phenotype. Red: "Kinetochore Null"/KNL proteins. Blue: "MIS" proteins whose depletion leads to relatively subtle chromosome segregation defects. Yellow: "NDC" proteins whose depletion results in intermediately severe chromosome alignment and segregation defects, relative to the KNL and MIS classes. In NDC embryos, attachments that can sustain tension fail to form, leading to premature spindle poles separation. Green: HCP/CLASP proteins, whose depletion causes sister chromatids to co-segregate to the same spindle pole. (C) Schematic illustrating of the temporal localization of kinetochore proteins during the first mitotic division. (D) *C. elegans* embryos fixed and stained to visualize DNA (cyan), MTs (red), CeCENP-A, and CeCENP-C during metaphase. Embryos CeCENP-A–, or CeCENP- C–depleted show kinetochore-null phenotype. Adapted from (Oegema et al., 2001; Oegema & Hyman, 2006).

Centrosome-based Spindle Assembly and Chromosome Segregation

At the end of meiosis, the centrosomes start to nucleate microtubules in preparation for mitosis. Simultaneously to NEBD, centrosomal proteins enter the nuclear space and start to interact with mitotic chromosomes. Approximately 2.5 minutes after NEBD (Figure 1.14), spindle assembly is completed, just before the onset of anaphase (for review see (Oegema & Hyman, 2006).

In C. elegans, mitotic spindles consist principally of microtubules connecting centrosomes to kinetochores. The mechanism of spindle assembly in *C. elegans* employs centrosomal microtubule asters to reinforce spindle bipolarity and position the spindle within the cell (for review see (Gadde & Heald, 2004)), which form a large metaphase mitotic spindle of approximately 14 µm, with prominent spindle poles and a profusion of astral microtubules in the one-cell embryo (figures 1.9 and 1.13) (D G Albertson, 1984). Functional centrosomes and kinetochores are essential for proper spindle assembly. A stable mitotic spindle requires kinetochores that can produce stable bipolar microtubule attachments. In the absence of functional kinetochores, the two spindle poles are abruptly pulled apart at onset of cortical pulling forces (Oegema et al., 2001).

Several proteins have been identified that play key roles in spindle assembly in mitosis and most of them locate to the centrosome or the spindle microtubules (for review see (Kitagawa, 2009)). Among the main regulators of mitotic spindle assembly are the Aurora kinases. Metazoans have two different Aurora kinases, Aurora A and Aurora B, called AIR-1 and AIR-2, respectively, in *C. elegans* (Schumacher, Ashcroft, Donovan, & Golden, 1998; Schumacher, Golden, & Donovan, 1998). Aurora B kinase is port of the chromosomal passenger complex and is associated with kinetochores until anaphase. In other hand, Aurora A kinase locates to the centrosome and spindle microtubules, and plays three major roles in *C. elegans*: (1) centrosome maturation and microtubule nucleation (Schumacher, Ashcroft, et al., 1998), (2) bipolar spindle formation and stability of spindle microtubules (Ozlü et al., 2005), and (3) NE breakdown (Portier et al., 2007).

Chromosome segregation typically consists of two steps during anaphase. The first step consists in the movement of chromosomes towards the spindle poles. Later in the second step, spindle poles separate from each other with the chromosomes in tow, generating the largest part of chromosome movement in *C. elegans* (Oegema et al., 2001). This movement

derives from a combination of pulling forces from the cortex that separates centrosomal microtubule asters, and pushing forces from the central spindle that separates chromosomes. Both forces act on the centrosomal microtubule asters allowing their segregation. The central spindle is considered to limit the rate of pole separation (P Gönczy, Grill, Stelzer, Kirkham, & Hyman, 2001). However, in *C. elegans* embryos with disruption of G protein signalling, which mediates cortical pulling forces, spindles still elongate but at a slower rate (Colombo et al., 2003), suggesting that other spindle intrinsic forces contribute to spindle elongation during anaphase.

The Nuclear Envelope

The NE is contiguous with the endoplasmic reticulum (ER), and is formed by three main components: the outer and inner nuclear membranes (ONM and INM, respectively), the nuclear pore complex (NPC) and the nuclear lamina (NL; Figure 1.16). The dynamics of NE disassembly and reassembly during the first mitotic division has been extensively studied in embryos of *C. elegans* and others organisms (for review see (Gorjánácz, Jaedicke, & Mattaj, 2007; Schellhaus, De Magistris, & Antonin, 2015; Schooley, Vollmer, & Antonin, 2012).

Outer Nuclear Membrane and Inner Nuclear Membrane

The INM and ONM are separate by the nuclear lumen, which is continuous with the ER lumen. In contrast, both membranes are connected at sites where NPC are inserted. The ONM contains many NETs that connect to the cytoskeleton. The INM encloses the nuclear interior and contains a unique group of proteins, including LEM-domain proteins, which provide anchors to the nuclear lamina and chromosomes. The two LEM-domain proteins most studied in *C. elegans* are LEM-2, also called Ce-MAN1, and EMR-1, also called Ce-EMERIN (González-Aguilera et al., 2014; Ikegami et al., 2010; Lee et al., 2000; Margalit, Segura-Totten, Gruenbaum, & Wilson, 2005). Both proteins can interact with the chromatin-binding protein BAF-1 through their LEM domain and with the nuclear lamina component LMN-1. Moreover, it has been proposed that those interaction can mediates their association with chromatin (Margalit et al., 2005).

Currently, a large number of INM proteins have been identified and characterized, and interestingly many of these proteins show tissue-specific expression ((Chen, Huber, Guan,

Bubeck, & Gerace, 2006; Dauer & Worman, 2009; Morales-Martínez, Dobrzynska, & Askjaer, 2015; Schirmer, Florens, Guan, Yates, & Gerace, 2003), suggesting a heterogeneity of the NE composition in different cell types, being a possible explanation of why some diseases associated with these proteins, as envelopathies or laminopathies, show tissue-specific phenotypes ((Dauer & Worman, 2009; Gomez-Cavazos & Hetzer, 2012).

Nuclear Lamina

The NL is a filamentous meshwork formed by specialized intermediate filament proteins called lamins. In metazoans, there are two types of lamins: B- type lamins, which is found in all cell types; and A-type lamins, which is found only in differentiated cells (For review see (E. Lund & Collas, 2013). In *C. elegans* a single lamin protein is encoded by the *lmn-1* gene, and is homologous to lamin B (J. Liu et al., 2000), but it probably performs functions of both lamin A and lamin B. Lamin filaments together with Lamin-associated proteins are known to provide structural support to the nucleus and to assist as a scaffold for spatial genome organization (Dittmer & Misteli, 2011). Several studies have shown that Lamin proteins participate in tethering of heterochromatic and developmentally silenced domains to the nuclear periphery (Guelen et al., 2008; Ikegami et al., 2010; Daan Peric-Hupkes et al., 2010; Vogel, Peric-Hupkes, & van Steensel, 2007). Moreover, they can interact with multiple proteins affecting chromatin organization and dynamics, i.e., transcription factors and chromatin remodelers (Ho & Lammerding, 2012). In human, genome-lamina interactions are present through more than 1,300 chromatin domains, called lamina associated domains (LADs), with a range size of 0.1–10 Mb and enriched of genes with lower expression levels. Moreover LADs are enriched in repressive histone marks, H3K27me3 (tri-methylation of lysine 27 on histone 3) and H3K9me2 (dimethylation of lysine 9 on his- tone 3), but are depleted of the active histone mark H3K4me2 (Ferrai et al., 2010; González-Aguilera et al., 2014; Guelen et al., 2008; E. G. Lund, Duband-Goulet, Oldenburg, Buendia, & Collas, 2015). Interestingly, in *C. elegans* has been reported down-regulation and mutations of *lmn-1* produce severe defects in nuclear morphology and mislocalization of many NE proteins (J. Liu et al., 2000; Mattout et al., 2011).

Nuclear Pore Complex

NPCs are aqueous transport channels that mediate the bidirectional exchange of macromolecules between the nucleus and cytoplasm. The NPC is a large ~100-MDa structure formed by an evolutionarily conserved set of multiple copies of ~30 different Nups (NPPs in *C. elegans*), organized in octagonal rotational symmetry around the central transport channel (For review see (Cohen-Fix & Askjaer, 2017).

Based on their approximate localization within the NPC, the Nups can be classified into six categories: (1) transmembrane Nups which link the NPC to the NE, (2) Nups from the inner ring (adaptor), (3) Nups from the outer (cytoplasmic and nucleoplasmic) ring, (4) central channel Nups, (5) nuclear basket Nups, and (6) cytoplasmic filament Nups (Figure 1.16B; for review see (Hoelz, Debler, & Blobel, 2011))

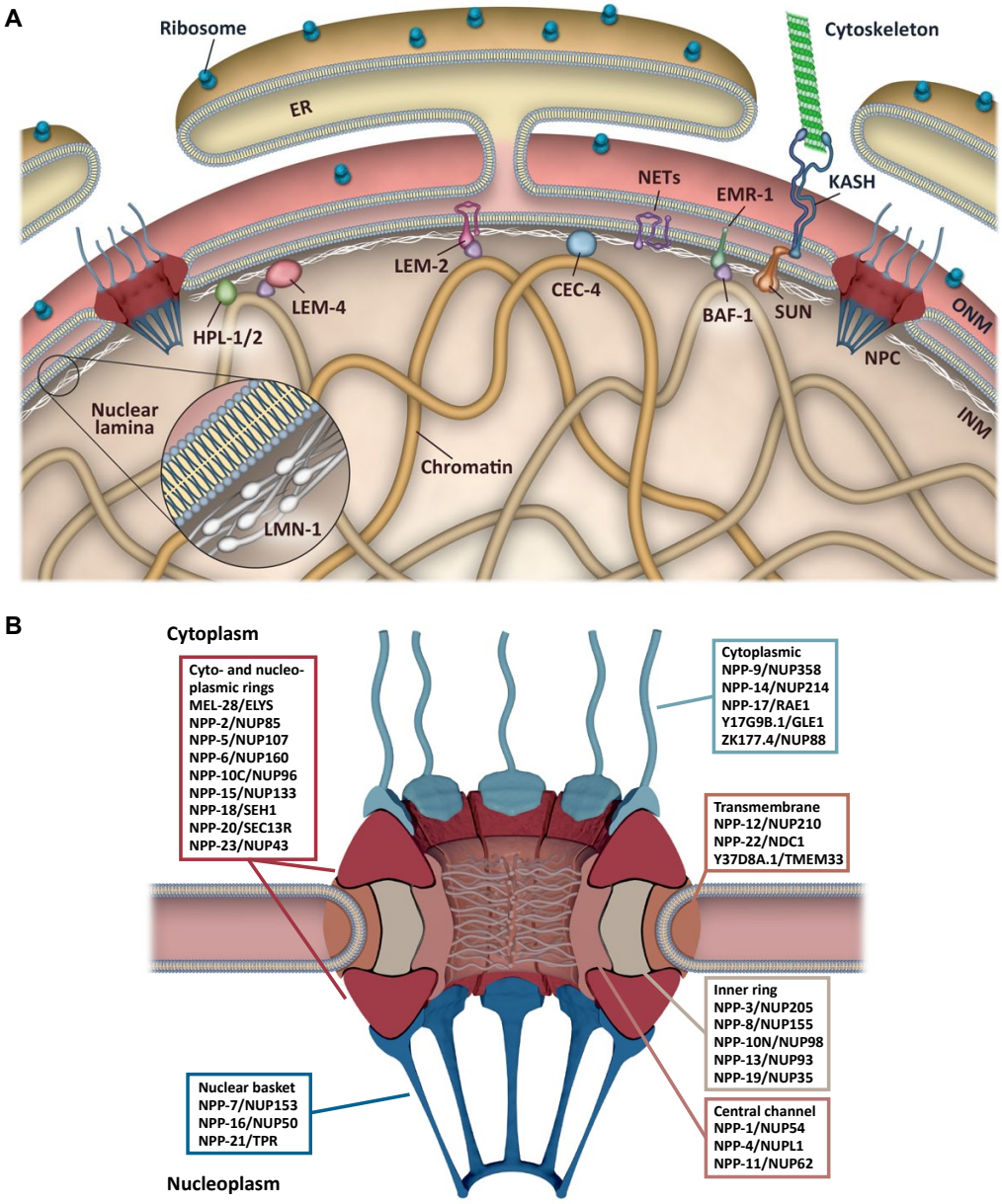

Figure 1.16. The nuclear envelope in *C. elegans*. (A) The NE is formed by three major components: the ONM and INM, the nuclear lamina, and NPCs. The ONM is continuous with the ER and many macromolecules such as ribosomes are associated. In contrast, the INM is rich in several NETs, such as EMR-1 and LEM-2, which both bind the chromatin factor BAF-1. Other proteins found at the INM are CEC-4, HPL-1/2, and LEM-4. In the nuclear lumen connection between SUN-domain proteins and KASH-domain proteins (from the cytoskeleton) are established. (B) NPCs are formed by ~30 Nups (NPP). Many Nups form stable NPC subcomplexes, such as the NPP-5/NUP107 and NPP-13/NUP93 complexes that form the outer and inner rings, respectively. Transmembrane Nups are implicated in connecting the NPC with the NE. Nups from central channel, peripheral cytoplasmic filaments, and nuclear basket are responsible for translocation of substrates through the NPCs. Adapted from Cohen-Fix & Askjaer 2016.

NPCs have traditionally been considered as structures with regular composition. However, new evidence suggests that the protein composition of NPCs varies among cell types and tissues (for review see (Maya Capelson & Hetzer, 2009; Raices & D'Angelo, 2012). For example, mutations in various Nups result in tissue-specific diseases (Table 1.1).

Table 1.1. Tissue-specific expression and developmental functions of metazoan Nups

NUP	Organism	*C. elegans*	Tissue-specific expression and/or developmental defect
NUP45	*Mus musculus*, *Rattus norvegicus*	NPP-4	Variable expression levels in different mouse and rat cell lines relative to other NUPs
NUP50	*Rattus norvegicus*	NPP-16	Highly expressed in the testis, variable expression in other cells and tissues
NUP62	*Homo sapiens*	NPP-11	Homozygous missense mutation causes recessive infantile bilateral striatal necrosis
NUP88	*Drosophila melanogaster*	ZK177.4	Expressed in imaginal discs of larvae, central nervous system and trache, functions in innate immunity
NUP96	*Mus musculus*	NPP-10C	Functions in immunity, involved in the interferon response
NUP98	*Caenorhabditis elegans*	NPP-10N	Mutation affects germline P-granules function and integrity
NUP98	*Danio rerio*	NPP-10N	Knockdown affects brain vasculogenesis and shows defective myeloid development
NUP98 NUP96	*Drosophila melanogaster*	NPP-10N NPP-10C	Functions in gametogenesis
NUP133	*Mus musculus*	NPP-15	Involved in neural stem and progenitor cell differentiation
NUP154	*Drosophila melanogaster*	NPP-8	Functions in male and female gametogenesis
NUP155	*Homo sapiens, Mus musculus*	NPP-8	Mutations cause atrial fibrillation and early sudden cardiac death
NUP210 (also known as GP210)	*Mus musculus*	NPP-12	Cell-type specific expression during mouse organogenesis, functions in myogenic and neuronal differentiation
NUP358	*Homo sapiens*	NPP-9	Heterozygous missense mutation causes infection triggered acute necrotizing encephalopathy
Aladin	*Homo sapiens*	–	Various mutations cause triple A syndrome
ELYS	*Danio rerio*	MEL-28	Functions in progenitor cell proliferation in intestinal and retinal epithelium
SEH1	*Drosophila melanogaster*	NPP-18	Functions in oogenesis

Adapted from (Raices & D'Angelo, 2012).

This unexpected NPC heterogeneity suggests that cells use a combination of different Nups to assemble NPCs with specialized functions, and/or Nups can perform functions beyond the NPC structure, possible as regulators of gene expression (discussed below; for review see (Pascual-Garcia & Capelson, 2014; Strambio-De-Castillia, Niepel, & Rout, 2010), Celia_chapter).

Nuclear Envelope Dynamics

In contrast to *C. elegans* somatic cells, early embryonic cells are in constant division, and thus the nuclear morphology is exceptionally dynamic (Figure 1.17). During interphase, the nuclei grow increasing its size, whereas when cells enter mitosis, the NE has to break down to allow the mitotic machinery, i.e. centrosome-nucleated microtubules, to access chromosomes. Once chromosome segregation is completed the NE must reassemble and expand to reach the normal size in the two new daughter cells. Several studies have reported that depletion or mutations of NE proteins not only produce nuclear structure defects but also defects in other processes of cell division, such as chromosome condensation and chromosome segregation (Gómez-Saldivar et al., et al., 2000; Margalit, Segura-Totten, Gruenbaum, & Wilson, 2005; Ródenas, Klerkx, Ayuso 2016; Lee, Audhya, & Askjaer, 2009), suggesting an intrinsic interplay between the NE and mitosis.

In *C. elegans*, as mitosis starts, during prophase, chromatin must separate from the NE, and the lamina and NPCs must disassemble. Several Nups are released from the NPC forming stables Nup-subcomplexes, most of them are dispersed into the cytoplasm, excluding the transmembrane Nups, which together with other NE proteins are associated with the ER. Interestingly, some of the Nups distributed within the mitotic cytoplasm have an active mitotic function (for review see (Chatel & Fahrenkrog, 2011)). Moreover, some INMs holding Ce-emerin and Ce-MAN-1 persist intact and surround the mitotic spindle during metaphase, then are disassembling entirely during mid-anaphase (Figure 1.15) (Lee et al., 2000). Finally, the formation of new NE around the segregated chromatin is detected around 1 minute after anaphase onset (for review see (Oegema & Hyman, 2006)). In the next section, I will describe the basis of NE and NPC disassembly and reassembly, with a special mention of the role of some Nups on the process.

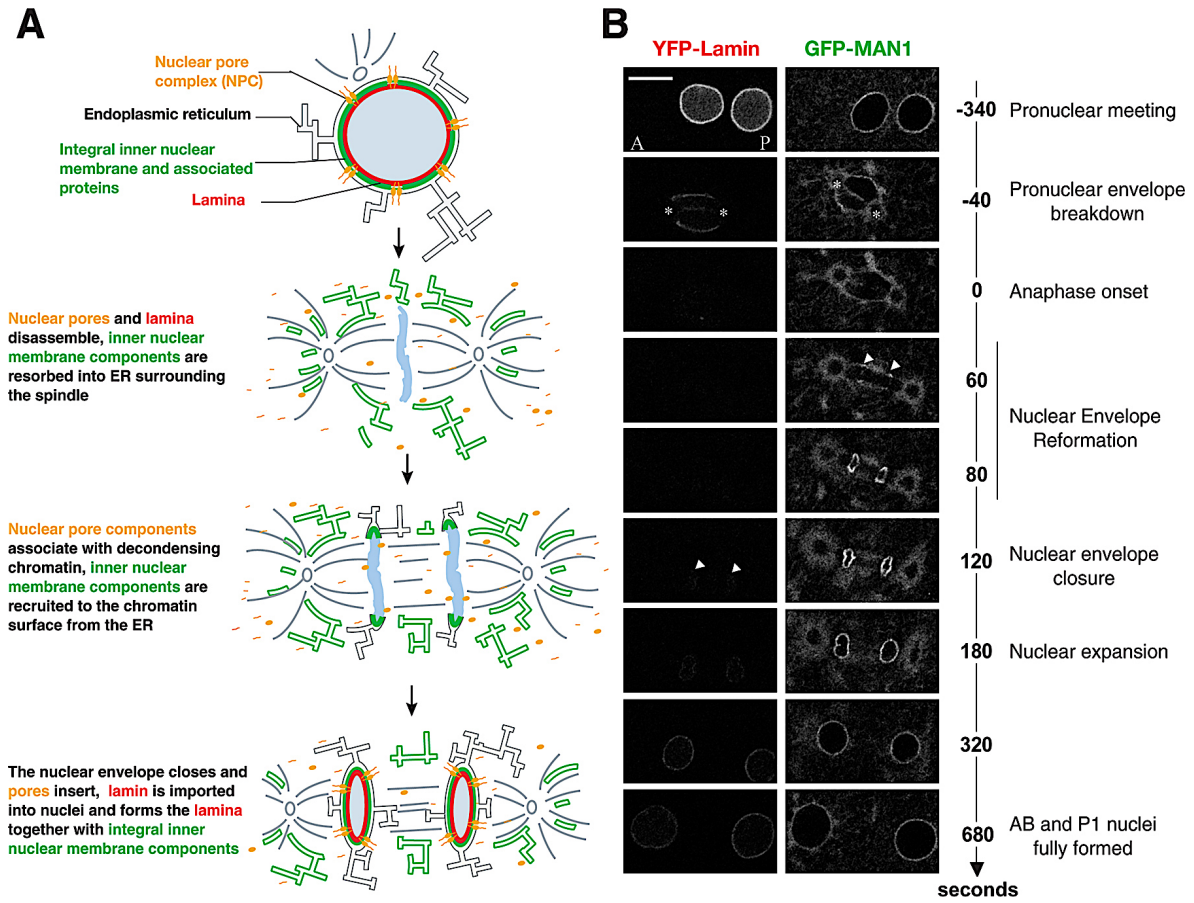

Figure 1.17. Nuclear envelope dynamics in the *C. elegans* embryo. (A) Schematics drawing of nuclear envelope breakdown and reassembly. (B) Still images of the first mitotic division of embryos expressing YFP::Lamin (left column) and GFP::MAN1 (right column). Times are relative to first metaphase to anaphase transition (sec). Arrowheads indicate the reappearance of GFP::MAN1 around the chromatin at t=60 sec and YFP::Lamin at t=120 sec. White stars indicate the positions of the centrosomes. Scale bar = 10μm. Adapted from (Oegema & Hyman, 2006).

Nuclear Envelope Breakdown

A difference to mammalian cells where NE is completely disassembled in prometaphase, in *C. elegans* early embryo, NEBD occurs very slow; although NEBD begins in prometaphase with release of several Nups, the nuclear membranes and lamina are not completely disassembled until mid-anaphase (Lee et al., 2000). In general, four steps mark the progress of NEBD (for review see (Antonin, Ellenberg, & Dultz, 2008; Gorjánácz et al., 2007; Güttinger, Laurell, & Kutay, 2009).

The first step of NE disassembly is an increase in the permeability of the NE (Mühlhäusser & Kutay, 2007), which is due to dissociation of Nups from the NPC (Figure 1.18). The temporal trigger for NPC disassembly could be the destabilization of protein–protein interaction in the core of NPC subcomplexes by rapid mitotic phosphorylation of Nups. An important candidate to be phosphorylated and initiate NPC disassembly could be the transmembrane Nup gp210, since *C. elegans* embryos depleted of gp210 show compromises NEBD during the first embryonic divisions (Galy et al., 2008). This phosphorylation is driven partially by Cdk1 (Mühlhäusser & Kutay, 2007).

After their dissociation from the NPC, some mitotically stable Nup-subcomplexes diffuse in the cytoplasm until the end of mitosis. However, some Nups specifically relocate to kinetochores in various species. In *C. elegans* these include MEL-28, and the Nup107–160 subcomplex, suggesting they might play functions in kinetochore assembly, spindle microtubules attachment and chromosome segregation (Chatel & Fahrenkrog, 2011; Fernandez & Piano, 2006; Galy, Askjaer, Franz, Lopez-Iglesias, & Mattaj, 2006).

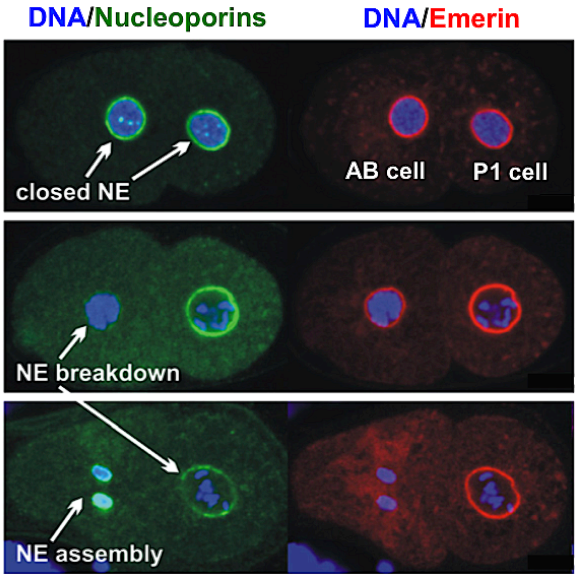

Figure 1.18. Nuclear envelope breakdown and reassembly in *C. elegans* embryos. Confocal immunofluorescence of 2-cell stage embryos immunostained to visualize Nups (green), Emerin (red) and DNA (blue). In the top, a closed NE is observed during interphase. In the middle, during NEBD of AB cell, NPC starts to disassemble, whereas Emerin protein is intact. In the bottom, the new NEs are reassembled around the segregated chromatids during anaphase and the presence of Nups is visible. Adapted from (Gorjánácz et al., 2007).

The second step in NEBD is the formation of holes and the full opening of the nucleus. In mammalian cells, the holes are subsequently expanded by the microtubule-mediated breaking of the nuclear lamina (Beaudouin, Gerlich, Daigle, Eils, & Ellenberg, 2002), which is controlled by Ran and importin β regulator (Mühlhäusser & Kutay, 2007). This collapse of nucleo-cytoplasmic compartmentalization increases the microtubule nucleation (Schuh & Ellenberg, 2007).

The third step is the redistribution of nuclear membranes into the ER. Most evidence suggests that nuclear membranes are directly associated in the ER (L. Yang, Guan, & Gerace, 1997). Interestingly, in *C. elegans* it has been reported that depletion of proteins involved in peripheral ER structure blocks the release of INM components into the peripheral ER, which prevents the complete NE disassembly (Audhya, Desai, & Oegema, 2007).

The last step of nuclear disassembly is the depolymerization of the nuclear lamina, which occurs only after complete opening of the nuclear membranes and depends on PKCβII mediated phosphorylation (Goss et al., 1994). Prevailing lamina carrying NE fragments are removed from chromatin along microtubules and migrate towards the centrosomes, and then the lamins are completely dissolved latest in metaphase. In addition, has been shown that polo-like kinase (PLK-1) is required for proper nuclear lamin disassembly in one-cell embryos as well as for complete NPC dissociation from the NE after the pronuclear meeting (Rahman et al., 2015). The partial inactivation of PLK-1 blocks mixing of the parental genome and causes the formation of paired nuclei in daughter cells. Interestingly, down-regulation of some NPC subunits or LMN-1 suppressed this phenotype. PLK-1 functions are needed not only for the first cell division but also in all subsequent divisions.

Nuclear Envelope Assembly

During late anaphase, after chromosome segregation, the NE starts to reforms on the decondensing chromatin, completing the nuclear reassembly in telophase and reestablishing the nucleocytoplasmic barrier. In each new daughter cell, the NE reassembly must guarantee the enclosure of the entire set of chromosomes into a single nucleus. This demands coordination between processes that affect chromatin status, as well as the recruitment of membranes and NPC insertion.

As the nuclear membranes are continuous with the ER membranes, the NE can be

considered as a subdomain of the ER. Two models of NE reformation at the end of mitosis have been proposed according to the perception of the ER (for review see (Schellhaus et al., 2015)). One model suggests that ER tubules extend from the ER network, then they contact the decondensing chromatin, become immobilized and flatten and extend to give rise to INM and ONM sheets (Anderson & Hetzer, 2007) (Figure 1.19, Ia and Ib). Another model works with ER membrane sheets, which contact and subsequently enclose the chromatin to form the NE (Lu, Ladinsky, & Kirchhausen, 2011) (Figure 1.19, IIa and IIb). Since both interphasic and mitotic ER network morphologies differ between cell types, it is possible that both modes of NE formation exist, according to the cell type. In addition, a novel role of ESCRT-III proteins in stimulating membrane fission has recently been identified in human cells, (Olmos, Hodgson, Mantell, Verkade, & Carlton, 2015).

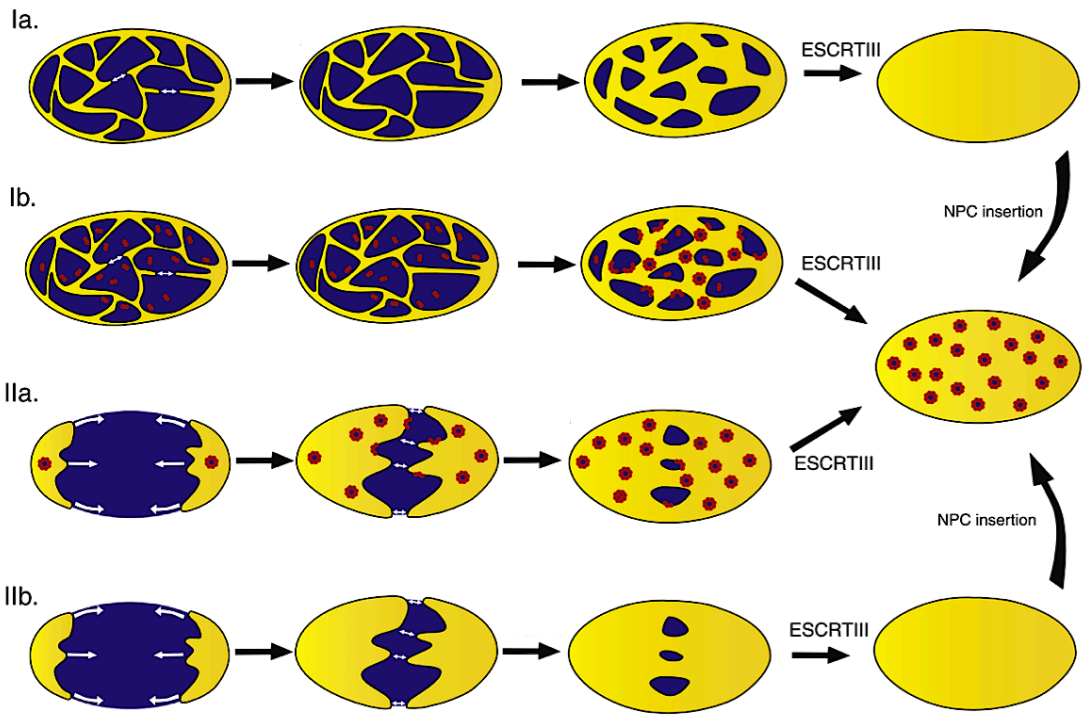

Figure 1.19. Nuclear envelope reformation by ER reorganization. Tubular ER structures are suggested to contact the chromatin, form a network on the surface, flatten and close the remaining holes to form a closed NE (Ia and Ib). Alternative models propose that ER membrane sheets contact the chromatin, spread on its surface and enclose it (IIa and IIb). Both types of models are compatible with any of the existing NPC (in red) reassembly models, enclosure (Ib and IIa) or insertion models (Ia and IIb). Adapted from (Schellhaus et al., 2015)

Nuclear Pore Complex Assembly at the end of Mitosis

In metazoans, NPCs are assembled twice during the cell cycle, during interphase and at the end of mitosis; and each one of them has different preconditions. During interphase, NPC formation requires the insertion of Nups into sealed double nuclear membranes from both sides (D'Angelo, Anderson, Richard, & Hetzer, 2006). Moreover, CDK activity is required for NPCs formation during interphase, but not in post-mitosis assembly (Maeshima et al., 2010).

At the end of mitosis, NPC assembly occurs in a highly temporally and spatially regulated mode (Dultz et al., 2008). There are two different models proposed for NPC reassembly at the end of mitosis, insertion or enclosure (Figure 1.20A-B, for review see (Schellhaus et al., 2015; Schooley et al., 2012)). The insertion model suggests that NPCs are assembled and integrated into pre-existing double membrane sheets of an intact NE (Lu et al., 2011), requiring the fusion of the ONM and INM across the NE lumen. This model is comparable to interphase NPC formation. In contrast, the enclosure model proposes that formation of a pre-pore structure takes place on chromatin prior to membrane attachment and fusion by the outgrowing ER-derived membranes (Antonin et al., 2008). Both modes of NE formation previously mentioned are compatible with one and another NPC reassembly model.

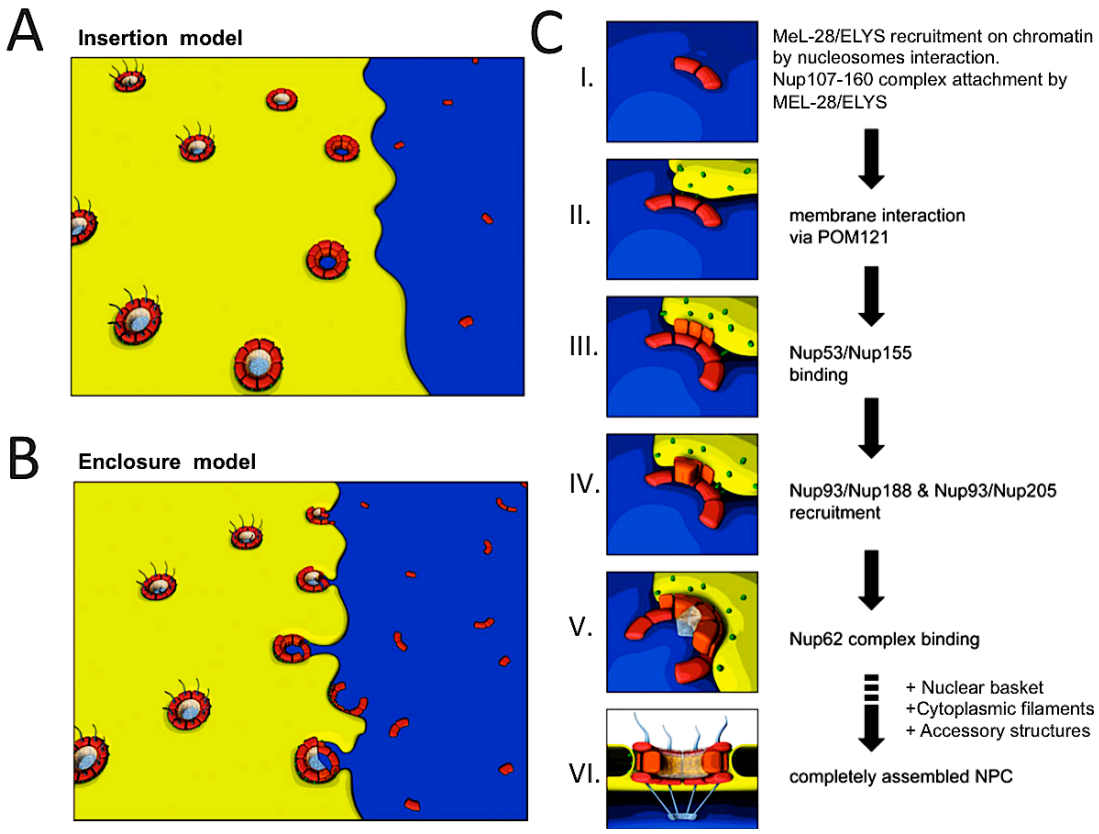

Figure 1.20. Models for the ordered assembly of NPCs at the end of mitosis. (A) Insertion model. As the cisternal sheets of the nuclear membrane wrap around chromatin, NPC assembly is inserted to intact NE. (B) Enclosure model. A second model suggests that pre-pore structures are assembled in the outgrowing membranes. (C) In both models, Mel-28/ELYS initiates NPC assembly on the chromatin by recruiting the Nup107-160 complex. Following the initial contact between nuclear membranes and the Nup107-160 complex, additional Nups are incorporated in the assembling NPCs (see text for details). Adapted from (Schooley et al., 2012).

NE Reformation through MEL28/ELYS and other Nups.

Despite the differences in the postmitotic models of NPC reassembly, a common aspect between both is that the process is initiated on chromatin (Figure 1.20C) by the Nup MEL28/ELYS (Franz et al., 2007; Gillespie, Khoudoli, Stewart, Swedlow, & Blow, 2007a; Beth A Rasala et al., 2006; Rotem et al., 2009). Recently, we demonstrated that MEL-28/ELYS's chromatin binding domain is placed at the C-terminal part of the protein (Gómez-Saldivar, Fernandez, et al., 2016), and it does not require the AT-hook domains, as previously thought (B. A. Rasala, Ramos, Harel, & Forbes, 2008); this is discussed in detail in chapter IV. Moreover, reconstitution experiments show that ELYS binding to histone-containing chromatin is an essential step for NPC assembly (Inoue & Zhang, 2014; Zierhut, Jenness, Kimura, & Funabiki, 2014a). MEL28/ELYS works as a seeding point on chromatin for NPC formation and recruits the Nup107-160 complex to assembly sites (Franz et al., 2007).

The Nup107-160 complex is an indispensable scaffolding component of NPCs and forms the largest part of the cytoplasmic and nucleoplasmic rings (the precise order of Nups assembly has been described in several reviews (Antonin et al., 2008; Schellhaus et al., 2015; Schooley et al., 2012)). Later, the transmembrane Nup POM121 established the first connection between nuclear membranes and the newly forming pores, through its interaction with the Nup107-160 complex. In the next step, Nups of the second major structural complex within NPCs, the Nup93 complex, join to the assembling pore, presumably forming the majority of the inner ring. In contrast to the Nup107-160 complex, which is recruited as a preassembled complex, the Nup93 complex builds from individual components. In the assembly process of the Nup93 complex, first Nup53 associates with the nascent pore, followed by Nup155. Both proteins can interact with the transmembrane Nups NDC1 and POM121, forming the second connection between the NPC and membranes at the pore. Later, Nup93 interacts with Nup53 for its incorporation, together with its binding partners

Nup188 and Nup205, and thus form the structural backbone of the pore. Posteriorly, Nup93 recruits the FG-repeat-containing Nups of the Nup62 complex. The Nup62 complex members Nup62, Nup58, and Nup54/45, together with the FG-containing Nup98, which is recruited at the same time as the Nup93 complex, form a large part of the hydrophobic meshwork localized in the center of the pore.

The assembly of peripheral NPC structures, i.e., the nuclear basket on the nucleoplasmic side and the cytoplasmic filaments, follows the establishment of the structural pore and central channel. On the nuclear side, Nup153 is needed for the recruitment of Nup50 and TPR. The sequence of events in the assembly of the cytoplasmic filaments is less defined but is dependent of Nup358.

When functional NPCs have reassembled in the closed NE, the nucleus further extends, and it starts to assemble and accommodate more NPCs in a process that continues during interphase. Interestingly, whereas NPC reformation at the end of mitosis requires MEL28/ELYS (Franz et al., 2007; Beth A Rasala et al., 2006), it seems dispensable for NPC formation during interphase (Doucet, Talamas, & Hetzer, 2010). Some studies suggest that Nup153 replaces the function of MEL28/ELYS as initiating assembly point in interphase (Vollmer et al., 2015).

NPC role as Translocator, Organizer and Regulator

NPC and Nuclearcytoplasmic Transport

Historically the main function of the NPC has been nucleocytoplasmic transport, which is highly conserved across eukaryotes (Devos et al., 2014), (Cook, Bono, Jinek, & Conti, 2007; Fahrenkrog & Aebi, 2003; Terry, Shows, & Wente, 2007; Wente & Rout, 2010). Electron microscopy reveals that the NPC has a diameter and thickness of 100–150 nm and 50–70 nm, respectively, according to the organism. Each NPC has a central channel of approximately 30 nm diameter and 50 nm long, where macromolecular exchange occurs (Wente & Rout, 2010). NPCs regulate the flow of cellular components, extending from ions to megadalton-sized protein complexes; this process is bidirectional, selective, rapid and energy-dependent, and depends on the precise function and positioning of critical Nups in the NPC structure (Cohen-Fix & Askjaer, 2017; Strawn, Shen, Shulga, Goldfarb, & Wente, 2004; Terry et al., 2007). For example, have been reported that depletion of NPP-19/Nup35

(Ródenas et al., 2009), NPP-13/Nup93, and NPP-3/Nup205 (Galy, Mattaj, & Askjaer, 2003) in *C. elegans* embryos produces a failure in nuclear protein import and NPC permeability, respectively. Similarly, in yeast it was found that Nup188p and Nup170p are implicated in passive NE permeability by establishing the functional resting diameter of the central transport channel (Shulga, Mosammaparast, Wozniak, & Goldfarb, 2000).

There are two modes of nucleocytoplasmic transport: passive diffusion, where molecules smaller than 5 nm can freely diffuse through the pore; and facilitated translocation, where molecules larger than ~40 Kilodalton (kDa) need to be actively transported by nuclear transport receptors (NTRs), which mostly belong to the family of karyopherin β proteins (kap; Cook et al., 2007; Görlich & Kutay, 1999). NTRs mediate translocation of macromolecules (commonly called cargo) from one side of the NE to the other, through the permeability barrier of NPCs, which is mediated by interactions between NTR-cargo complexes and phenylalanine-glycine (FG) repeats in Nups (FG-Nups). Regarding the direction of transport, NTRs can be classified as importins or exportins and can recognize and bind to specific nuclear import (NLS) or export (NES) signals in their cargos (Görlich & Kutay, 1999). There are different types of NLSs and NESs. For instance, the classical NLS (cNLS) is formed by 5 amino acid (aa) residues -KKKRK-, which are required and sufficient for targeting proteins to the nucleus (Goldfarb, Gariépy, Schoolnik, & Kornberg, 1986). However, several proteins present a more complex NLS called bipartite NLS, consisting of two clusters of basic aa, separated by a spacer of ~10 aa (Robbins, Dilworth, Laskey, & Dingwall, 1991). Interestingly, although most of the β-karyopherins bind their cargoes directly, Importin β needs an adaptor to bind to the classical NLS. This adaptor is Importin α, which present an importin β-binding domain in its N-terminal part, and the armadillo domain in the C-terminal part, which connects to the NLS forming a ternary complex (for review see (Cook et al., 2007)). However, other non-classical NLSs have been characterized, for example, the proline-tyrosine-rich and arginine–glycine-rich NLSs (PY-NLS and RG-NLS, respectively). These new classes of NLS are structurally disordered, have a general basic character, and present a weak consensus motif (for review see (Cautain, Hill, de Pedro, & Link, 2015)). Interestingly, an unconventional NLS has been identified in the extensive coiled-coil domain of the STAT5 protein (H. Y. Shin & Reich, 2013).

A GTPase called RAN supply the energy for NTR-mediated transport, and the RAN-GTP gradient between the nucleus and the cytoplasm controls the directionality of nucleocytoplasmic transport (for review see (Cautain et al., 2015; Cook et al., 2007; Wente & Rout, 2010)). Briefly, during nuclear import, cargo release occurs due to the interaction of the NTR with RAN-GTP inside the nucleus, which stimulates its disassembly. In opposite

way, during nuclear export RAN-GTP is needed for the assembly of the NTR–cargo complex and GTP hydrolysis is required for cargo release. Finally, export complexes are dissociated at the cytoplasmic filaments of the NPC by the action of RAN-binding protein 1 (RANBP1) or RANBP2 and RAN GTPase-activating protein (RANGAP) called RAN-2 in *C. elegans* (P. Askjaer, Galy, Hannak, & Mattaj, 2002).

Nup/gene Association at NPCs

Electron microscopy images of interphase nuclei have served to exhibit that heterochromatin is tightly connected to the NE, whereas NPCs are surrounded by decondensed euchromatin. This fact was used to suggest that the NPC tethers active chromatin to form a stimulating environment for gene regulation and coining the gene gating hypothesis (Blobel, 1985). It was proposed that such organization increases accessibility of euchromatin to cytoplasmic factors, promotes messenger RNA (mRNA) production and facilitates its export into the cytoplasm.

Some studies in yeast support this idea (Figure 1.21A), showing that upon activation, certain inducible genes i.e., HSP104, HXK1, INO1, SUC2, and GAL, moves from the center of the nucleus to NPCs (For review see (Burns & Wente, 2014; Ibarra & Hetzer, 2015)). Moreover, specific DNA sequence motif in the promoter region of some genes were identified that interact with NPC/Nups (i.e., Nup2, Mlp1, Mlp2, Nup60, or Nup116), called gene recruitment sequences (GRSs) which also function as DNA zip codes, being able to target an ectopic locus to the NE (Ahmed et al., 2010; Light, Brickner, Brand, & Brickner, 2010). Interestingly, mutation of GRSs produces loss of gene-NPC interaction (Ahmed & Brickner, 2010). A similar mechanism has also been observed in other species, such as *C. elegans*. Embryos expressing a small integrated LacO arrays system carrying the *hsp-16.2* promoter were analyzed to test array positioning by live imaging (Rohner et al., 2013). This study showed that the *hsp-16.2* promoter usually localizes at the periphery in regions devoid of NPCs, and under heat shock (HS) activation, *hsp-16.2* promoter repositions closer to NPCs (Figure 1.21B). This direct promoter-NPC association was confirmed by both super-resolution microscopy and chromatin immunoprecipitation (ChIP). In addition, it was demonstrated that such peripheral positioning requires both HS elements (HSE) and HS-associated site (HSAS) sequence. In another hand, it has been suggested that NPC might regulate the interactions between Nups and chromatin. In *Drosophila* oocytes and nurse cells, a regulatory loop of NPC components has been reported to control the global chromatin attachment state (Breuer & Ohkura, 2015). Depletion of NPC components, Nup62 or Nup93,

produces an excessive chromatin attachment to the NE, which can be reversed by codepletion of a chromatin-binding NPC component, Nup155, implying an interplay between Nups in large-scale genome organization.

More direct evidence about how the dynamic chromatin–Nup association regulates gene expression was provided by studies on Nup155 in cardiomyocytes. These studies identified a mechanism of gene expression regulation by class IIa histone deacetylase (HDAC), HDAC4, in which Nup155 participates (Kehat, Accornero, Aronow, & Molkentin, 2011). It was found that HDAC4 is enriched at the NE, showing a partial colocalization with the mAb414 antibody, which stain FG-repeat Nups (including Nup62 and Nup153). Besides, overexpression of HDAC4 decreased the association of specific target loci with the Nups. Interestingly, overexpression of a truncated Nup155 mutant, lacking the HDAC4-interacting domain altered the expression pattern of genes regulated by HDAC4 and restored the association of many target loci with Nups. This result was reproduced using trichostatin A (TSA) treatments, an inhibitor of HDAC.

In addition, other study performed in *C. elegans* noted that NPC works as a physical meeting point for RNA polymerase (Pol) III transcription and the RNA processing (Ikegami & Lieb, 2013). RNA-sequencing (RNA-seq) analysis reveals a novel role of NPP-13/Nup93, an integral Nups that presumably localizes exclusively in the NPC, in small nucleolar RNAs (snoRNA) and transfer RNA (tRNAs) processing. ChIP of two integral Nups, NPP-13/Nup93 and NPP-3/Nup205, showed that Nups are directly associated with tRNA and snoRNA genes which are transcribed by Pol III, however, its role does not encompass the recruitment of this protein. Nups bind downstream of the Pol III preinitiation complex, and NPP-13/Nup93 is required for cleavage of tRNA and snoRNA precursors into mature RNAs, indicating a possible role in the recruitment of RNA processing enzymes to the site of cleavage. Given the positions of these Nups, the authors suggested that the Nups anchor Pol III-transcribing genes inside the NPC (Figure 1.21B). Interestingly, after NPP-13/Nup93 depletion, an increase of Pol III-snoRNA and tRNA level was observed, but Pol II-transcribed snoRNA levels remained constant, which proposes a potential function of NPP-13/Nup93 controlling the production of Pol III transcripts, possibly coordinating DNA transcription and RNA processing.

Recently, a study using DNA adenine methyltransferase identification technique (DamID; (Van Steensel & Henikoff, 2000)) with two NPC components (the nuclear basket subunit Nup153, and the scaffold subunit Nup93) reported Nup–chromatin interactions at or close to NPCs (Ibarra, Benner, Tyagi, Cool, & Hetzer, 2016). The authors found that in

osteosarcoma cells, Nup153 and Nup93 binding sites localize close to transcription start sites (TSS), mostly in promoter-distal regions, which were enriched for active histone marks. Interestingly, genomic binding sites for both Nups were significantly enriched in super-enhancers (SEs; Figure 1.21C). The Nup-SE associated genes proved to be cell type specific when they evaluate them in unrelated cells types of osteosarcoma (U2OS) and lung fibroblasts (IMR90). Moreover, using fluorescence in situ hybridization (FISH), the autohs determined that NUP-SE association localize preferentially close to the NE. Moreover, depletion of Nup153 and Nup93 produces strong changes in transcriptional profiles of SE-associated genes. This investigation revealed a novel role of Nups in the regulation of cell type-specifying genes.

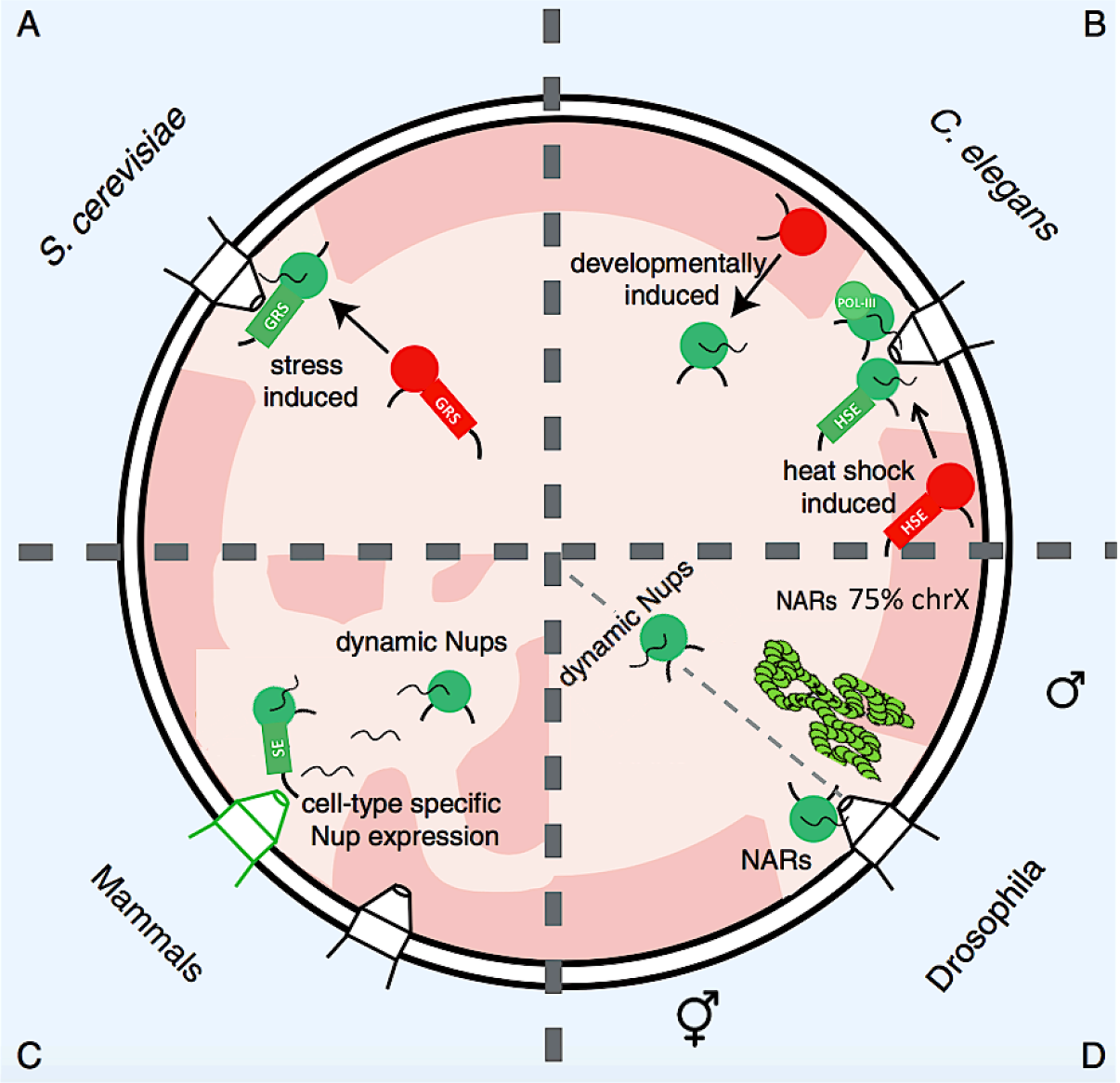

Figure 1.21. Nucleoporins and gene gating hypothesis across different model systems. (A) In *S. cerevisiae*, Nups are required to recruit some induced genes to the NPC for its expression. This mechanism requires DNA gene recruitment sequence (GRS) in the promoters. (B) In *C. elegans*, some developmentally induced promoters are positioned in the nucleoplasmic interior when transcriptionally active, whereas the heat shock-induced promoter hsp-16.2 shuttle to the NPC. Also, NPC works as a physical meeting point for RNA Pol III transcription and RNA processing. (C) Nup153 and Nup93 interact with the chromatin close to NE. Genomic binding sites of both Nups are enriched in super-enhancers (SEs). (D) *Drosophila* Nups (i.e., Nup98, Sec13, Nup50, and Nup62) regulate transcriptional events in the nucleoplasm and at the NPC. Nucleoporin association regions (NARs) are defined genomic regions that interact with the Nup153 and Megator Nups; in males shown an occupancy of 75% of the X-chromosome. Active genes (green circles), inactive genes (red circles), euchromatin and interchromatin compartments (light pink), and heterochromatin (dark pink) are indicated. The figure is not drawn to scale. Adapted from (Burns & Wente, 2014).

Nup/gene Association at Nucleoplasm

In the last two decades, several studies have focused on Nups with a more dynamic behavior. Since these Nups are not spatially confined to the NPC, has been postulated they can interact with the chromatin in the nuclear interior and not exclusively at sites associated with the NPC. In fact, it has been reported that dynamics Nups do not locate randomly in the nucleoplasm, but Nup presents its own pattern of localization, which is different from the others. For example, the nuclear pool of Nup98 discretely accumulates at intranuclear GLFG bodies and is lightly enriched inside nucleoli (E. R. Griffis, Altan, Lippincott-Schwartz, & Powers, 2002; Eric R Griffis, Craige, Dimaano, Ullman, & Powers, 2004); Interestingly, C-terminal domain of Nup98 recruits Nup107-160 complex (Y-complex) and ELYS in GLFG bodies (Morchoisne-Bolhy et al., 2015). Nup50 is diffused in the nucleus with a general exclusion from nucleoli (Buchwalter, Liang, & Hetzer, 2014) and, although Nup153 has a structural role at the NPC, fluorescence recovery after photobleaching (FRAP) experiments support the presence of at least two pools of mobile Nup153 (Eric R Griffis et al., 2004). Likewise, quantitative FRAP analysis of GFP-Nup107 reveals that contrary at NPC, in the nucleoplasm the Y-complex moves into and out of GLFG bodies, founding Nup107 is present in three pools: the very mobile, the dynamic and the immobile (Morchoisne-Bolhy et al., 2015). These different localization patterns suggest that every Nups plays singular transcription-related functions and can interact with multiple gene loci. In addition, dynamics Nups like Nup153, Nup98, or Nup50 are been associated with process regulated by Pol II activity, proposing that off-pore Nup-genome interactions might participate in gene expression regulation (Buchwalter et al., 2014; Eric R Griffis et al., 2004).

Recalling the hypothesis of gene gating, the gene repositioning upon transcriptional activation event appears in two general classes of genes in *C. elegans*: in the stress-induced genes mention above (Figure 1.21B) and in developmentally induced genes which shuttle from the periphery to the nuclear interior (Figure 1.21B, Figure 1.22 and Figure 1.25B). Interestingly, several studies indicate that mutations in specific Nups can produce specific developmental defects rather than a global cell defect (as would happen by a general inhibition of nucleocytoplasmic transport), suggesting a possible involvement of Nups in regulation of developmental genetic programs (Maya Capelson et al., 2010; D 'Angelo, Gomez-Cavazos, Mei, Lackner, & Hetzer, 2012; Gomez-Cavazos & Hetzer, 2015; Kalverda, Pickersgill, Shloma, & Fornerod, 2010; Liang et al., 2013; Raices & D'Angelo, 2012).

In Drosophila the chromatin-binding dynamics of some NUPs have been investigated using different methods such as immuno-staining of polytene chromosomes, ChIP, and DamID. This has revealed an association of mobile Nups with active genes in the nucleoplasm and, moreover, their binding is required for the transcription of their targets genes (Maya Capelson et al., 2010; Kalverda et al., 2010; Vaquerizas et al., 2010). Kalverda and collaborators reported a genome-wide mapping of the *Drosophila* Nup98, Nup50, and Nup62 by DamID (Kalverda et al., 2010).

Intriguingly, they also compared Nup-chromatin interaction of Nup98 permanently tethered to NPCs and a Nup98 fragment that exclusively localizes in the nucleoplasm. Interestingly, association to transcriptionally active genes was observed only in the nucleoplasmic version of Nup98. Moreover, those genes were mostly implicated in developmental regulation and the cell cycle and were downregulated by Nup98 depletion. In the other hand, the NPC-embedded version of Nup98 appears to interact with inactive genes. Additionally, also in *Drosophila*, Capelson and collaborators found that Sec13 and Nup98, as well as a group of FG-Nups, bind to the different regions of the genome mostly in the nuclear interior, specifically in developmentally regulated genes that undergoing transcription induction (Maya Capelson et al., 2010). Contrary they found that NUP88 associates to silent loci (Figure 1.22). Moreover, depletion of intranuclear Sec13 and Nup98 by RNAi produced transcription inhibition under heat shock induction of their target genes. Together, these studies show that Nups can shuttle to the nucleoplasm to regulate gene expression.

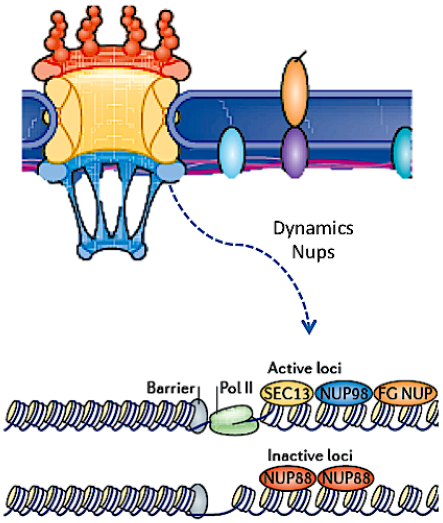

Figure 1.22. Nucleoporins and gene expression regulation. In *D. melanogaster*, Nups regulate gene expression in an NPC-independent mode. They bind to active and silent loci in the genome at nucleoplasm. For example, NUP88 was observed to localize to silent loci, whereas SEC13, NUP98 and a group of FG-Nups were found to bind to actively transcribed genes. Adapted from (Raices & D'Angelo, 2012).

NPC/X-chromosome Association and Dosage Compensation

To date several studies have helped to establish the molecular mechanism of regulation of the X chromosome in different species [Cline & Meyer, 1996; Crane et al., 2015; Sevinç Ercan, 2015; Sevinc Ercan et al., 2007]); interestingly, each time more evidence suggests a link between positioning and gene regulation, proposing that the subnuclear positioning of the X towards the NE might play a role in this. Strikingly, the NPC and some Nups have emerged as factors required for X chromosome activation in males.

Recently, we have reported a novel role of the NPC in dosage compensation (DC; appendix I, (Sharma et al., 2014)) in *C. elegans*, finding that the X chromosome exhibits a sex-specific spatial positioning within the nucleus (Figure 1.23). We detected by FISH and live imaging a preferential peripheral localization of the single X chromosome in males. In contrast, in hermaphrodites, the two X chromosomes displayed a random localization around the nuclei, except for its chromosome arms, which interact with the nuclear periphery, as has been characterized before (González-Aguilera et al., 2014; Ikegami et al., 2010; Towbin et al., 2012). Interestingly, we showed that the X chromosome in male nuclei associates with the nuclear periphery through sequence elements called MEX, and these interactions appear to facilitate increased transcription of X-linked genes. Presumably in hermaphrodites, DCC

binds to MEX elements preventing perinuclear association and increasing X chromosome compaction (Lau, Nabeshima, & Csankovszki, 2014; Sharma & Meister, 2015; Sharma et al., 2014), with a resultant twofold reduction in transcription rates at X-linked genes when compared to the males. Moreover, using DamID we could evaluate with which component of the NE the X chromosome is interacting. After mapping the genomic regions interacting with two NE elements, Lamin and the Nup MEL-28, we found the Lamin DamID profile was similar between hermaphrodites and males for all chromosomes. In contrast, the MEL-28 DamID profile showed very similar signal in autosomal chromosomes between hermaphrodites and males, whereas the signal was remarkably enriched on X chromosome only in males. As discussed in appendix I, this suggests a possible role of NPC association and global chromatin positioning in sex-specific regulation of gene expression.

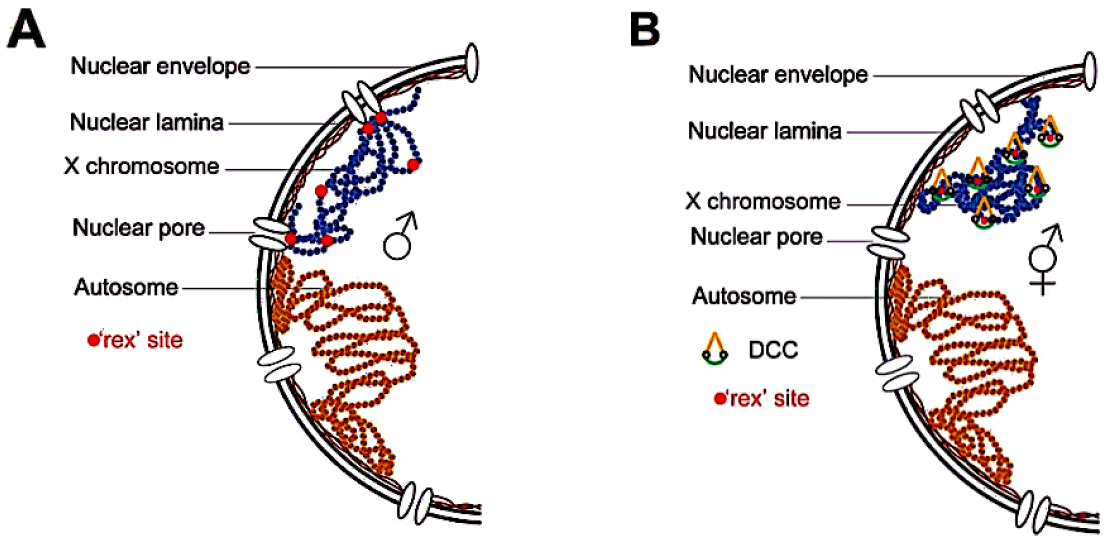

Figure 1.23. Schematic representation of chromosome organization. (A) In males, rex sites direct the interaction of the X chromosome with the NE, which in turn leads to NPC interactions. (B) In hermaphrodites, DCC binding to rex sites and spreading on X chromatin reduces NE localization and interaction with NPC, thereby impairing activation of X-linked transcripts and inducing chromosomal compaction. Adapted from (Sharma & Meister, 2015).

In another hand, in *Drosophila* the DC works to equal the imbalance in gene content by doubling the expression of the single X chromosome in XY males (for review see (Sevinç Ercan, 2015)). A high-resolution genome-wide study revealed that Nup153 and Megator (Mtor, Nup homologous to TPR in vertebrates) bind to 25% of the genome in actively

transcribing chromatin domains extending 10 kb to 500 kb, called Nucleoporin-Associated Regions (NARs, (Vaquerizas et al., 2010)). These NARs are more enriched in male than in female cells, finding an occupancy of 75% of X chromosome's length (Figure 1.21D). Interestingly knockdown by RNAi of Nup153 modified the expression of ~5,700 genes and inhibited the function of DCC in males, what indicates its role in the equalization of gene expression during DC. Moreover, 3D imaging showed that NARs are contributed by both peripheral as well as intranuclear pool of these proteins. Finally, the authors suggest that NAR–binding is used for chromosomal organization that enables gene expression control.

MEL-28/ELYS

One of the mobiles Nups that stands out for having a very dynamic behavior during the cell cycle is MEL-28/ELYS (Fernandez & Piano, 2006; Galy, Askjaer, Franz, López-Iglesias, et al., 2006a; Gillespie et al., 2007a; Beth A Rasala et al., 2006). As we mention above, MEL-28/ELYS binding to chromatin represents the first step in the post-mitotic building of the pore, and all other steps in its manufacture are dependent on this ELYS/chromatin interaction.

ELYS, a large AT-hook domain protein, was originally identified in a cDNA subtraction screen seeking genes expressed at high levels in the mouse embryonic sac (Kimura et al., 2002), from here its name "Embryonic Large molecule derived from Yolk Sac". Mouse *elys* knockouts die in the preimplantation stage because of cell death within the inner cell mass (Okita et al., 2004). ELYS function is essential in all metazoa and is particularly important in rapidly dividing cells (Davuluri et al., 2008; Gao et al., 2011). The orthologous MEL-28 (maternal-effect embryonic-lethal mutation 28) protein, was identified based on its nuclear appearance defect phenotype in a large-scale RNAi screen (Pierre Gönczy et al., 2000; Sönnichsen et al., 2005), In *C. elegans*, MEL-28 dynamically localizes to the nucleoplasm and NPC at interphase and then at the kinetochore and spindle at metaphase (Fernandez & Piano, 2006; Galy, Askjaer, Franz, López-Iglesias, & Mattaj, 2006b; Figure 1.24 and Figure 4.4A in chapter IV). Consistent with its localization pattern, embryos that lack *mel-28* function have severe defects with NE function, mitotic spindle assembly and chromosome segregation and are unviable.

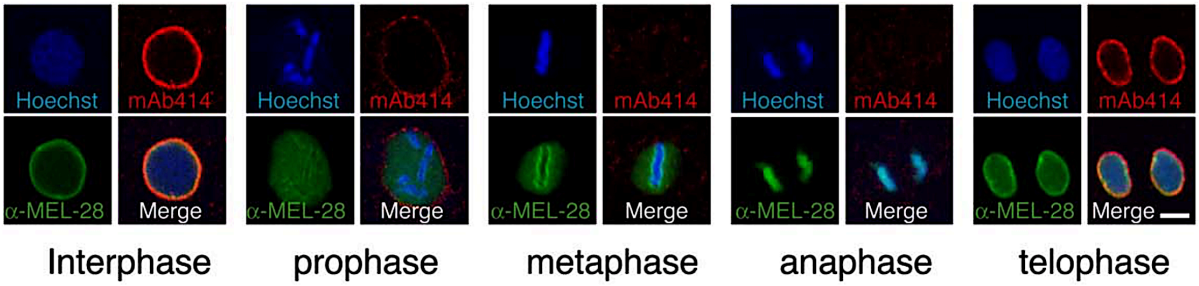

Figure 1.24. Dynamic localization of MEL-28 during the cell cycle. Immunofluorescence of MEL-28 reveals its dynamic behavior, showing NPC accumulation during interphase and chromosomes and kinetochore association during metaphase for MEL-28. MEL-28 appears in green, Nups in red (Ab414), and chromatin in blue (Hoechst). The scale bar represents 5 mm. Adapted from (Galy, Askjaer, Franz, López-Iglesias, et al., 2006b).

The ELYS/chromatin interaction has been studied extensively *in vitro* using *Xenopus* cell extracts. ELYS binds to chromatin during interphase but not at metaphase (Gillespie et al., 2007a), when it instead associates with the spindle and kinetochore (Yokoyama et al., 2014). Chromatin immobilization assays have shown that the most C-terminal fragment of ELYS, corresponding to aa. 2281-2408, is sufficient for chromatin binding. This region includes the AT hook, a motif that binds to AT-rich DNA. However the aa. 2281-2408 fragment with a mutated AT hook and a C-terminal fragment that excludes the AT hook (aa. 2359-2408) also bound to chromatin (B. A. Rasala et al., 2008). A nucleosome binding assay showed that a large C-terminal fragment that includes the AT hook (aa. 2281-2408) was sufficient to bind to nucleosomes, whereas a piece that includes just the AT hook (aa. 2281-2358) or just the region C-terminal to the AT hook (aa. 2359-2408) could not bind to nucleosomes (Zierhut et al., 2014a). Additionally, incubation of *Xenopus* extracts with the C-terminal 208-aa. fragment of ELYS prevented native ELYS from binding to sperm chromatin and also prevented the recruitment of other Nups to the nuclear rim, phenocopying the *elys* loss-of-function phenotype (Gillespie et al., 2007a). However, introducing a C-terminal fragment with a mutated AT hook does not disrupt nuclear pore assembly and is less effective at outcompeting the endogenous ELYS from binding to chromatin (B. A. Rasala et al., 2008). These *in vitro* experiments suggest that both the AT hook and other domains of the C terminus are important for the ELYS/chromatin interaction and the subsequent rebuilding of the pore.

The ELYS/chromatin association has also been studied using mouse *in vitro* fertilization. During fertilization in mice, sperm chromatin is rebuilt *de novo* using histones present in the oocyte. Experiments using *in vitro* fertilized mouse oocytes depleted of histones showed that ELYS does not localize to the NE of the sperm pronucleus in the absence of histones, which in turn prevents the recruitment of other Nups (Inoue & Zhang, 2014). ELYS can be

artificially targeted to the NE in the absence of histones by fusing it with a domain from an inner NE protein. This chimeric ELYS protein not only localizes to the NE but also recruits the other Nups. This suggests that ELYS binding to chromatin is required for its localization to the nuclear rim, which in turn allows the remainder of the nuclear pore to be built.

The overall architecture of MEL-28/ELYS is similar throughout the metazoan (see schematic representations in Figure 4.4C and 4.11B in chapter IV). All metazoan MEL-28/ELYS homologs include an N-terminal β-propeller domain, a central α-helical domain, and a C-terminal domain that includes at least one AT hook. Crystal structure determination of the N-terminal domain of mammalian ELYS showed that it forms a seven bladed β-propeller structure with an extra loop decorating each of the propeller blades (Silvija Bilokapic & Schwartz, 2013a). In human cells, the N-terminal 1018-aa. fragment of ELYS (which includes the β-propeller domain and the central α-helical domain but not the C-terminal AT hook) is sufficient to localize the protein to the NPC (Silvija Bilokapic & Schwartz, 2013a). Mutational disruption of the conserved loop on blade 6 of the β-propeller domain ("loop2") prevents the aa. 1-1018 fragment from localizing to the nuclear rim.

Despite the interest in defining the functional domains of MEL-28/ELYS, until now there have been no studies in which the phenotypic consequences of disrupting specific domains have been studied in developing animals. In this thesis, we have dissected the MEL-28 protein and studied its localization and function in live *C. elegans* embryos.

The Nuclear Envelope as Chromatin Organizer

In *C. elegans*, the global picture of NE associated with silent DNA, is established by several studies which have shown that NE proteins like LMN-1, EMR-1 and LEM-2 are involved in anchoring of silent heterochromatin to the nuclear periphery (González-Aguilera et al., 2014; Ikegami et al., 2010; Snyder et al., 2016; Towbin et al., 2012). Interestingly, a genetic screen done in *C. elegans* showed that histone H3 lysine 9 (H3K9) methylation targets repetitive heterochromatin to the NE (Towbin et al., 2012). This was corroborated by depletion of two histone H3K9 methyltransferases, MET-2 and SET-25, which produced the loss of peripheral localization.

At the nuclear periphery, the NL and NPCs can generate different microenvironments of active or inactive chromatin, such as LADs (Guelen et al., 2008) and NARs (Vaquerizas et

al., 2010). In *C. elegans*, Gonzalez-Aguilera and collaborators found that EMR-1/emerin is associated with two class of chromatin domains: a primary class consisting of LADs and a secondary class lacking LMN-1 and enriched for genes expressed in specific tissues (González-Aguilera et al., 2014). Interestingly, the second class is enriched for genes implicated in muscle and neuronal function, which might be relevant to better understand the human disease Emery-Dreifuss muscular dystrophy, which is caused by mutations in emerin.

LADs are delimited by relatively fine borders, with interesting characteristics (for review see (Collas, Lund, & Oldenburg, 2014)). LAD borders are enriched in binding elements for the chromatin insulator protein CCCTC- binding factor (CTCF), and CTCF protein itself (Guelen et al., 2008). LAD borders also often contain promoters that are oriented away from the LADs, consistent with the insulator function of CTCF, which are enriched in H3K4me2, a histone mark typical of TSS of active genes, and in RNA POL-II. Therefore LADs seem to define regions of silent chromatin, outlined by domains that are transcriptionally active.

In the other hand, high-resolution images show that heterochromatin seems to be interspersed by NPCs, then these could be working as a boundary between condensed and decondensed chromatin and permissive and non-permissive environment (Figure 1.25A; for review see (Pascual-Garcia & Capelson, 2014)). In addition, Nups can have a dual role in this model. Stable Nups which are NE-embedded at NPCs can be associated with silencing, boundary or inactive transcription processes (M Capelson, Doucet, & Hetzer, 2010; Kehat et al., 2011); while peripheral and possibly specialized off-pore Nups can act at nucleoplasm and perform functions in transcription activation and cell differentiation (Figure 1.25B), which has been widely discussed previously.

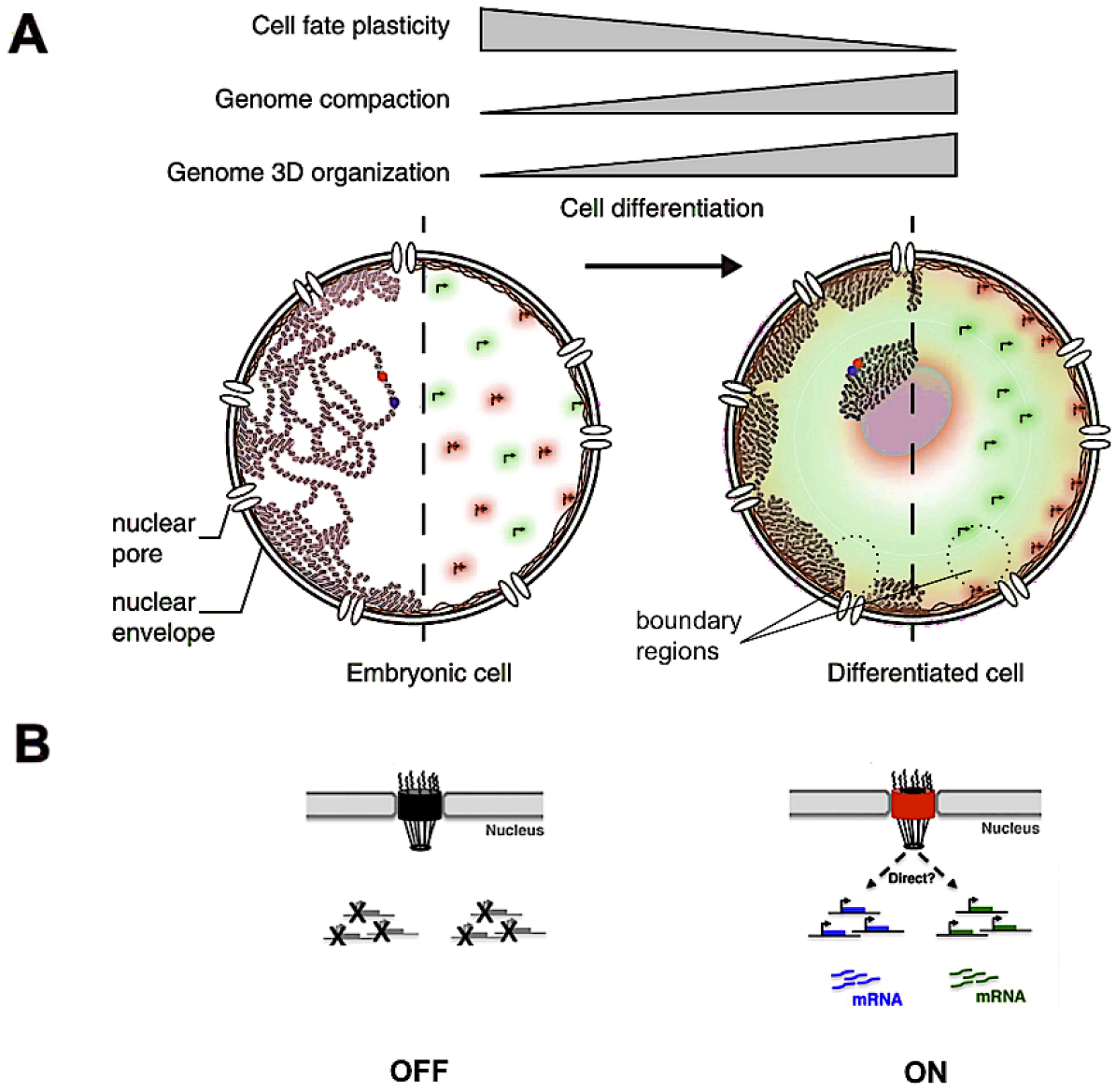

Figure 1.25. Nuclear organization and its changes during development. (A) On the left side, the decrease in cellular plasticity during fate specification is associated with an overall increase in genome compaction level and progressive heterochromatin compartmentalization, generating boundaries of active and inactive regions. On the right side, nuclei become more organized during differentiation, with active developmentally regulated promoters (arrows with green halo) being internalized during differentiation, while inactive ones are segregated at the periphery (arrows with red halo). (B) Some developmentally regulated genes are controlled or induced by direct and indirect Nups interactions. Adapted from (Sharma & Meister, 2013).

Chromatin Architecture

Metazoan genomes are organized in chromatin regions, loops, domains and chromosomal territories, which represents higher-order structures of the chromatin (Figure 1.26). In turn, the combination of all DNA-DNA interactions determines the formation of specific macro-domains of active and inactive chromatin, called topological associated domains (TADs; for

review (Cohen-Fix & Askjaer, 2017; Fraser et al., 2015)). Genomic loci show more interactions within TADs than between adjacent TADs. Moreover, during development, some loci can alternatively interact with two adjacent TADs. For example, in mouse limb development, Hoxd genes are transcribed in two rounds, early and late. The transition between early and later regulations requires a switch of a promoter between two opposite TADs, from telomeric to centromeric domain.(Andrey et al., 2013). Intriguingly, there are similarities between subdomains within TADs and LADs; thus some LADs can be formed by clusters of repressive TADs to the NE, however, not all TADs relate to LADs (for review see (Collas et al., 2014; Gonzalez-sandoval & Gasser, 2016)).

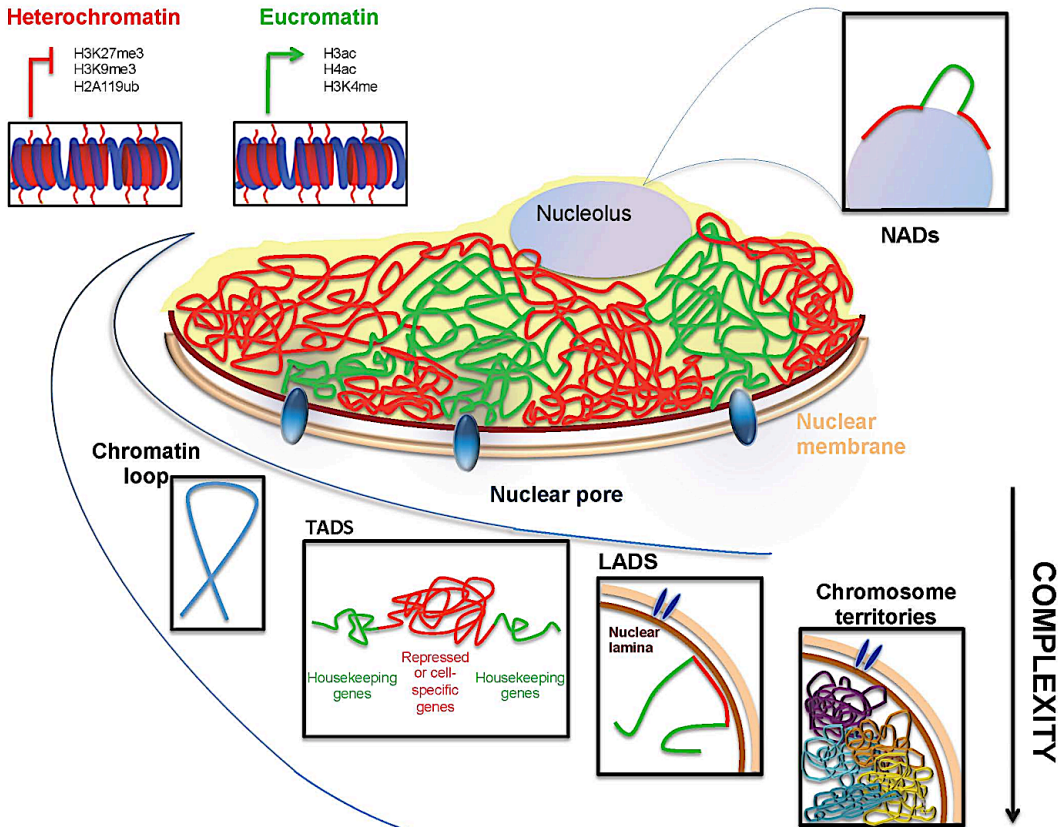

Figure 1.26. Chromatin architecture. Scheme of chromatin organization. Euchromatin (green) appears decondensed, tightly associated to NPC and enriched by histonemodifications H3ac, H4ac and H3K4me. The heterochromatin (red) appears at nuclear periphery, often associatedto NL, condensed and enriched of H3K27me3, H3K9me3, H2A119ub. Inside the nucleus, euchromatin and heterochromatin give rise to several grades ofhigher order structures: chromosome loops, TADs, LADs and chromosomal territories. Also the nucleolus presents specific NADs. Adapted from (Bianchi & Lanzuolo, 2015).

Besides, regions of repressed heterochromatin have also been identified at the periphery of nucleoli, called nucleolus-associated domains (NADs), which are gene poor and enriched for satellite DNA repeats. Surprisingly, NADs overlap with LADs, sharing the same DNA region Moreover, live imaging microscopy has exposed an interchange between NL and nucleolus perimeter after mitosis (for review see (Bianchi & Lanzuolo, 2015)). Certainly, NE invaginations may explain the overlapping between TADs and LADs, the similar size range of LADs, TADs and NADs, and why LADs or NADs can apparently relocate to the NE or to the nucleoplasm after mitosis.

In conclusion, it is evident that the nuclear architecture influences chromatin function and its link with NE components, such as NL or NPCs. The correct functioning of the nucleus can be altered by mutations of NE proteins and produces alterations in the proper development generating pathologies and diseases.

DamID as Tool to Study Chromatin

Since the early classification of chromatin into euchromatin and heterochromatin, the concept of a close interplay between chromatin organization and gene expression has been suggested (Jost, Bertulat, & Cardoso, 2012). Nucleosomes are the main structural component of chromatin and the impact of histone posttranslational modifications on gene regulation is well established (Tessarz & Kouzarides, 2014; Xu, Zhang, & Grunstein, 2005; Zhou, Luo, Wise, & Lou, 2014). Moreover, activation or repression of genes relies on interactions between transcription factors and specific sequences within gene bodies or in surrounding regulatory elements (Giresi, Kim, McDaniell, Iyer, & Lieb, 2007). Finally, the NL is responsible for anchoring of large chromatin domains (LADs) that typically encompass transcriptionally silent genes (Guelen et al., 2008; Pickersgill et al., 2006). In the last two decades our knowledge on global nuclear organization has greatly increased with the development of microarray and next generation sequencing (NGS) technologies. Combined with chromatin immunoprecipitation (ChIP) these advances have provided detailed chromatin profiles across species, developmental stages, and cell types (see for example ENCODE [https://www.encodeproject.org] and modENCODE [http:// modencode.org] for references).

ChIP is a powerful and popular method but depends on the availability of highly specific and efficient antibodies as well as stringent fixation protocols. As an alternative to ChIP, van Steensel and Henikoff developed DamID for in vivo mapping of chromatin binding sites (Van Steensel & Henikoff, 2000); Table 2 lists major differences between ChIP and DamID; a more detailed comparison is reviewed in (Peter Askjaer, Ercan, & Meister, 2014). The versatility of DamID is reflected by its application to evaluate a wide range of chromatin-associating proteins, such as transcription factors (Orian et al., 2003; S. Song, Cooperman, Letting, Blobel, & Choi, 2004; T. D. Southall & Brand, 2007), components of the RNAi machinery (Woolcock, Gaidatzis, Punga, & Bühler, 2011), histones (Braunschweig, Hogan, Pagie, & van Steensel, 2009), and NE proteins in *Drosophila* (Kalverda & Fornerod, 2010; Pickersgill et al., 2006), *C. elegans* (González-Aguilera et al., 2014), fission yeast (Steglich, Filion, van Steensel, & Ekwall, 2012), and mammalian cells (Guelen et al., 2008). DamID can also be used to test association to a single gene of interest using a Southern blot approach (S. Song et al., 2004) or to evaluate the effect of modifications or truncations of chromatin binding proteins (Gómez-Saldivar, Fernandez, et al., 2016). In addition to not involve fixation or antibodies, DamID has the advantage of being able to identify binding sites within compact chromatin with poor solubility, or when the chromatin-associated proteins are very dynamic or present in low abundance (Peter Askjaer, Ercan, et al., 2014).

Table 2. Comparison of advantages and disadvantages of DamID Compared with ChIP technique

	DamID	ChIP
Specific reagents required	Transgenic cells expressing Dam-fusion protein of interest	Antibody with good specificity and high affinity
Resolution	Resolution depends on the distribution of GATC in the genome, but is still comparable to ChIP. *C. elegans* has a median of 210 bp	High resolution
Applicable organism	Any genetically tractable animal or cell type	Any organism for which high-affinity antibody can be obtained
Detection of post-translational modifications	Not possible	Possible but depends on the antibody
Tissue-specific profiling	Dam-fusions can be expressed in a tissue-specific manner	Requires physical separation of cells or nuclei
Detection of long range or transient interactions	Methylation of transiently Dam- associated sequences is possible	Not possible due to specific binding required
Requires 'fixing' of samples	Not. Methylation occurs *in vivo*. DNA can be extracted from unfixed or even live cells	Yes. *In vitro* technique, equires formaldehyde crosslinking of samples
Temporal resolution	Dam must be expressed for several hours	Limited only by time taken for fixing (minutes)
Isoform specificity	A specific sequence must be expressed; therefore, binding of only one isoform is assayed	ChIP antibodies may bind to multiple isoforms of the same protein
Proteins expressed at low levels	Possible, actually Dam-fusions have to be expressed at very low levels	Difficult, depends on the purification efficiency of ChIP antibody

Adapted from (Aughey & Southall, 2016)

The principle of DamID is based on the fusion of the enzyme DNA adenine methyltransferase (Dam) from *E. coli* to a protein of interest (POI). Dam methylates adenine at the N6-position within GATC sequences. When the fusion protein is expressed in vivo, it binds directly or indirectly to the native genomic binding sites of the POI and creates specific GmATC methylation tags in the surrounding chromatin (Figure 1.27). Through a serie of enzymatic reactions, methylated sites are amplified and identified by DNA array or sequencing techniques.

DamID is feasible because adenine methylation is very rare in eukaryotic cells and the high frequency of GATC motifs in the genome (Greer et al., 2015; Greil, Moorman, & van Steensel, 2006), accessing almost every region of the genome. *C. elegans* has 269,049 GATC sequences per haploid genome (Sha et al., 2010a), corresponding to on average one site for every 374 bp (median 210 bp). To compensate for differences in chromatin compactness and unspecific methylation, the signal from the Dam::POI fusion protein is compared to a diffusible "Dam-only" control, which typically is Dam fused to GFP.

We initially identified chromatin-association profiles for *C. elegans* NE proteins by hybridization to tilling-arrays (González-Aguilera et al., 2014; Towbin et al., 2012) and more recently by NGS (Sharma et al., 2014). NGS provides definite counts for methylation of each GATC site, from which the chromatin binding profile of the POI can be established. Applying NGS to DamID has required the development of novel scripts for data processing but provides also advantages compared to microarrays: sequencing discards hybridization biases and provides absolute measures rather than fluorescence ratios. NGS also allows discarding signals arising from nonspecific DNA breakage during sample preparation because such fragments are most often not flanked by GATC sites.

In chapter III (materials and methods) we describe the DamID workflow from sample preparation to bioinformatics analysis. We devote particular attention to data processing (Figure 1.28), but details in sample preparation can been reviewed in (Peter Askjaer, Ercan, et al., 2014; Dobrzynska, Askjaer, & Gruenbaum, 2016).

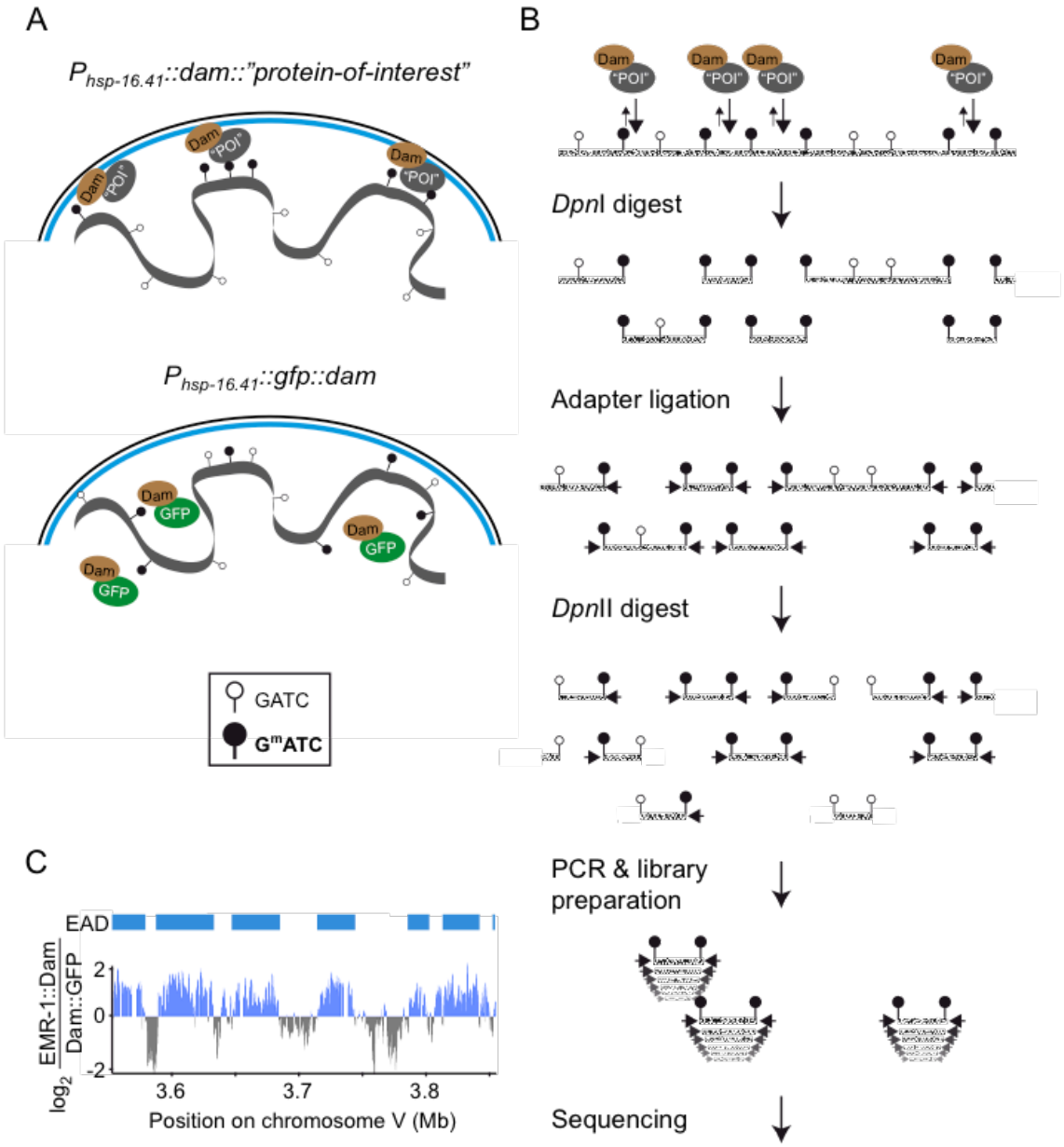

Figure 1.27. Principle and workflow of DamID. (A) DamID is based on in vivo methylation of genomic GATC sites (pins) by Dam fusion proteins expressed at very low concentrations. Top panels shows a nuclear envelope "protein of interest" (POI) fused to Dam whereas the bottom panel represents a diffusible GFP::Dam control. (B) Methylated GATC sites are isolated and amplified trough a series of enzymatic reactions followed by next generation sequencing. (C) Comparison of DamID signals from Dam::POI and GFP::Dam identifies POI associated domains. The graph illustrates results obtained for emerin/EMR-1 with blue bars indicating EMR-1 associated domains; data from (González-Aguilera et al., 2014). Figure from (Gómez-Saldivar, Meister, et al., 2016).

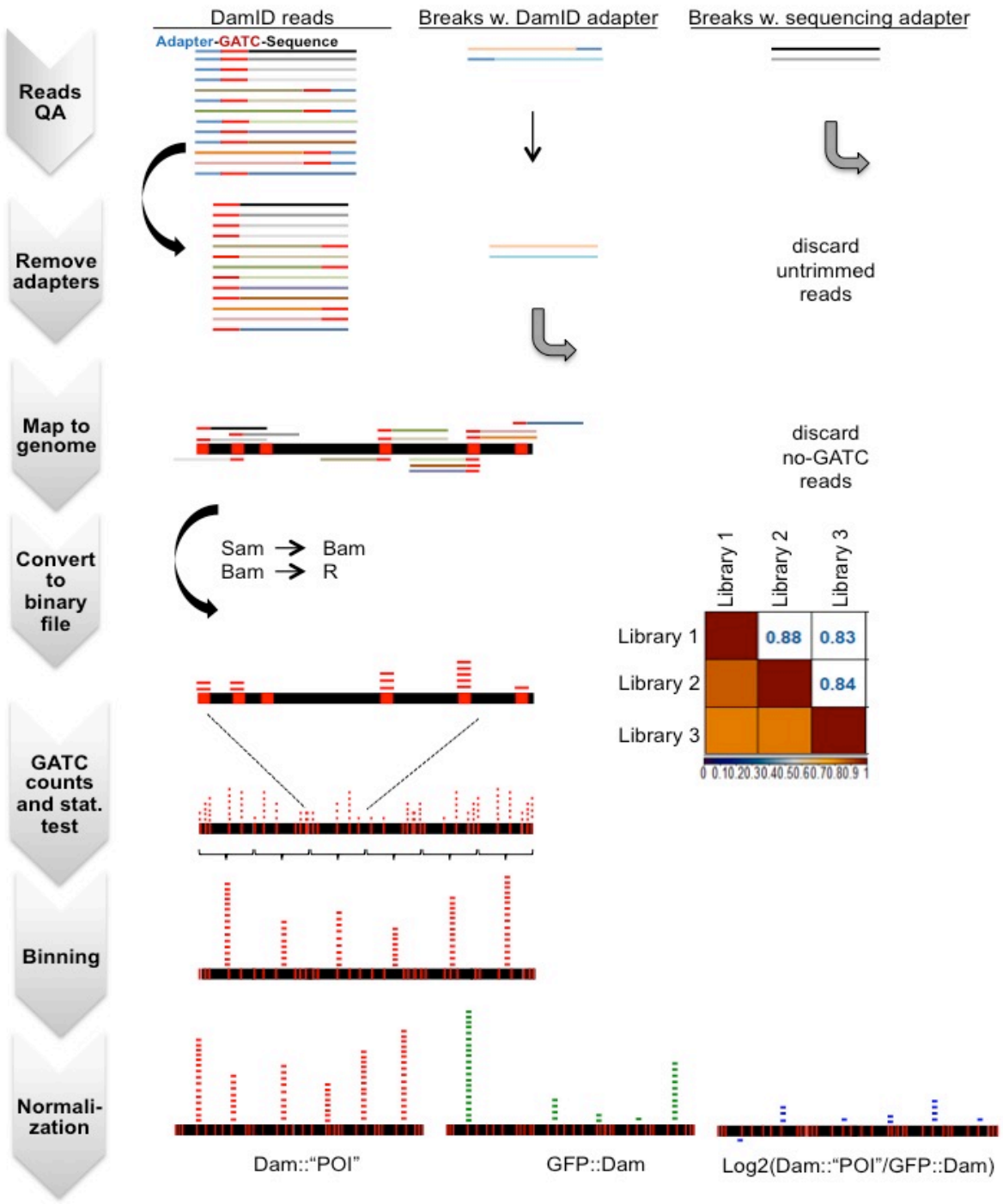

Figure 1.28. Workflow to map and count methylated GATC sites. Once the quality of the reads has been evaluated, the adapters are removed from the reads. Next, the clean reads are mapped to the reference genome. The output is converted to a BAM le, which is processed in R. The next step is identification and counting of GATC sites followed by statistical evaluation and evaluation of the correlation between replicates. To increase the correlation, the signals are binned and finally normalized with the total number of genomic GATC sites and with the GFP::Dam control samples. Figure from (Gómez-Saldivar, Meister, et al., 2016).

Chapter II

Objectives

Objective 1:

Identification and characterization of MEL-28 functional domains, including the domains that regulate MEL-28's location in the nuclear pore complex and to kinetochores.

Objective 2:

Optimize DamID-sequencing technique for the study of nuclear organization in *C. elegans*.

Objective 3:

Characterize the interaction of MEL-28 with chromatin in the nucleoplasm and at the nuclear pore complex.

Chapter III

Materials and Methods

Plasmid constructions

DNA fragments to express MEL-28 full length and truncations were generated by PCR amplification (KAPA HiFi; KAPA Biosystems, Wilmington, USA) or restriction enzyme digestion and inserted into appropriate cloning vectors. In all cases, *mel-28* introns were maintained. Plasmid details are listed in Table 3.1. Some coding region fragments of MEL-28 were PCR-amplified using primers listed in Table 3.2.

To construct GFP-human ELYS (NCBI accession number: NP_056261.4), total RNAs from HeLa, K562 and WI-38 cells were isolated by FastPure RNA kit (TaKaRa Bio Inc., Shiga, Japan), and then cDNAs were generated by using SuperScript III First-Strand synthesis system (Invitrogen, Waltham, MA) according to manufacturer's protocol. The coding region of ELYS was PCR-amplified using primers listed in Table 3.2 and inserted into the pEGFP-C1 vector (Clontech Laboratories, Palo Alto, CA) at the *Xho*I site by In-Fusion reaction (Clontech). Other ELYS fragments were amplified by PCR using the plasmid harboring full-length ELYS as a template and inserted into the pEGFP-C1 vector as describe above. DNA sequencing of all ELYS fusion plasmids was outsourced to the TaKaRa Bio Inc. Compared to the database sequence, 5 out of 5, 6 out of 7 and 2 out of 2 clones from HeLa, K562 and WI-38 cells, respectively, contained a mutation from A to G at position 2648, resulting in an amino acid substitution from N to S at the position 883. Since the mutation was predominant in three different cell lines, we decided to use this ELYS sequence in this report.

Table 3.1. Plasmids used in this study

Plasmid name	Description	Design	Reference
#588	Plasmid containing mel-28 gene	mel-28 gene obtained by subcloning SalI/XmaI fragment from C38D4 cosmid into L4440	Galy et al., 2006
#604	Plasmid encoding MEL-28 with unique XmaI restriction site	Derived from #588; L4440 - contains unique XmaI site immediately before mel-28 stop codon	Galy et al., 2006
#621	pCRII-mel-28		Galy et al., 2006

#630	Plasmid encoding MEL-28::GFP	GFP from inserted into XmaI of #604.	Galy et al., 2006
#1255	Plasmid containing mel-28 fragment with loop2 mutation (l2m; D409S/Y412S/R415A/V416S/P415G).	Two overlapping PCR fragments were produced with primers B466+B585 and B470+B584 using #604 as template. These fragments were next used as template with primers B466+B470and the product was inserted into pSPARK vector.	Gómez-Saldivar et al., 2016
#1263	Plasmid encoding MEL-28_l2m	NdeI/PfoI fragment from #1255 inserted into NdeI/PfoI of #604.	Gómez-Saldivar et al., 2016
#1286	Plasmid to express Cas9		Friedland et al., 2013
#1397	mel-28 repair template	Repair template made by Gibson assembly of gBlock and two PCR fragments; contains silent mutation in PAM sequence (AGG at position 55-57 relative to mel-28 ATG is mutated to AGA).	Gómez-Saldivar et al., 2016
pALI2	pie-1 promoter driving expression of GFP::MEL-28 aa1188-1784	Cut pAF3 with SpeI to excise full-length mel-28 and replaced this with a fragment encoding aa1188-1784 that was amplified from a genomic clone.	Gómez-Saldivar et al., 2016
pALI3	pie-1 promoter driving expression of GFP::MEL-28 aa826-1784	Cut pAF3 with SpeI to excise full-length mel-28 and replaced this with a fragment encoding aa826-1784 that was amplified from a genomic clone.	Gómez-Saldivar et al., 2016
pALI8	pie-1 promoter driving expression of GFP::MEL-28 aa508-1784	Cut pAF3 with SpeI to excise full-length mel-28 and replaced this with a fragment encoding aa508-1784 that was amplified from a genomic clone.	Gómez-Saldivar et al., 2016
pALI9	pie-1 promoter driving expression of GFP::MEL-28 aa1-1744	Cut pAF3 with SpeI to excise full-length mel-28 and replaced this with a fragment encoding aa1-1744 that was amplified from a genomic clone.	Gómez-Saldivar et al., 2016
pBN1	lmn-1 promoter driving ubiquitous expression of mCherry::HIS-58		Rodenas et al., 2012
pBN4	Heat shock inducible hsp-16.41 promoter controlling expression of GFP		Gonzalez-Aguilera et al., 2014

pBN8	Cloning vector for MosSCI into ttTi5605 II		Rodenas et al., 2012
pBN16	Heat shock inducible hsp-16.41 promoter controlling expression of GFP		Gonzalez-Aguilera et al., 2014
pBN23	Heat shock inducible hsp-16.41 promoter controlling expression of GFP::NPP-15		Rodenas et al., 2012
pBN40	lmn-1 promoter driving ubiquitous expression of GFP::HIS-58		Morales-Martínez et al, 2015
pBN41	myo-2 promoter driving expression of GFP in the pharynx		Morales-Martínez et al., 2015
pBN42	myo-3 promoter driving expression of GFP in the body muscle		Morales-Martínez et al., 2015
pBN61	Heat shock inducible hsp-16.41 promoter controlling expression of Dam::MYC		Gonzalez-Aguilera et al., 2014
pBN65	Heat shock inducible hsp-16.41 promoter controlling expression of Dam::MYC::LMN-1		Towbin et al., 2012
pBN67	Heat shock inducible hsp-16.41 promoter controlling expression of GFP::MYC::Dam		Towbin et al., 2012
pBN69	Heat shock inducible hsp-16.41 promoter controlling expression of Dam::MYC::MEL-28	mel-28 NheI gDNA fragment from #621 inserted into pBN61	Gómez-Saldivar et al., 2016
pBN97	Heat shock inducible hsp-16.41 promoter controlling expression of GFP::MEL-28	Phsp-16.41::gfp NgoMIV/NotI fragment from pBN23 into pBN69	Gómez-Saldivar et al., 2016
pBN114	Heat shock inducible hsp-16.41 promoter controlling expression of GFP::MEL-28 aa209-709	mel-28 internal fragment amplified with primers B466+B470, cut NgoMIV+NheI, inserted into NgoMIV+NheI of pBN16	Gómez-Saldivar et al., 2016
pBN115	Heat shock inducible hsp-16.41 promoter controlling expression of GFP::MEL-28 aa846-1350	mel-28 internal fragment amplified with primers B468+B471, cut NgoMIV+NheI, inserted into NgoMIV+NheI of pBN16	Gómez-Saldivar et al., 2016

pBN116	Heat shock inducible hsp-16.41 promoter controlling expression of GFP::MEL-28 aa846-1601	mel-28 C-terminal fragment amplified with primers B468+B469, cut Bgl II+NheI; 1340bp fragment inserted into Bgl II+NheI of pBN115	Gómez-Saldivar et al., 2016
pBN117	Heat shock inducible hsp-16.41 promoter controlling expression of GFP::MEL-28 Daa1239-1728	pBN97 digested with Bgl II and re-ligation of 9970 + 4165bp fragments	Gómez-Saldivar et al., 2016
pBN123	mel-28 promoter (1.1kb) driving expresion of MEL-28::GFP	mel-28::gfp SpeI/NgoMIV fragment from #630 inserted into SpeI/NgoMIV of pBN8	Gómez-Saldivar et al., 2016
pBN128	Heat shock inducible hsp-16.41 promoter controlling expression of GFP::MEL-28 aa846-1167	mel-28 internal fragment amplified with B468+B542, cut NgoMIV+NheI, inserted into NgoMIV+NheI of pBN16	Gómez-Saldivar et al., 2016
pBN129	Heat shock inducible hsp-16.41 promoter controlling expression of GFP::MEL-28 aa1161-1601	mel-28 internal fragment amplified with B469+B541, cut NgoMIV+NheI, inserted into NgoMIV+NheI of pBN16	Gómez-Saldivar et al., 2016
pBN131	Heat shock inducible hsp-16.41 promoter controlling expression of GFP::MEL-28 aa681-1350	mel-28 internal fragment amplified with B548+B471, cut NgoMIV+NheI, inserted into NgoMIV+NheI of pBN16	Gómez-Saldivar et al., 2016
pBN146	Heat shock inducible hsp-16.41 promoter controlling expression of GFP::MEL-28 aa846-1071	pBN115 digested with MscI/NheI and re-ligation of backbone vector .	Gómez-Saldivar et al., 2016
pBN150	Heat shock inducible hsp-16.41 promoter controlling expression of GFP::MEL-28 aa681-929	mel-28 internal fragment amplified with B548+B467, cut NgoMIV+NheI, inserted into NgoMIV+NheI of pBN16	Gómez-Saldivar et al., 2016
pBN157	Heat shock inducible hsp-16.41 promoter controlling expression of GFP::MEL-28 aa1239-1601	pBN98 digested with Bgl II and re-ligation of backbone vector	Gómez-Saldivar et al., 2016
pBN169	mex-5 promoter driving expression of GFP	Pmex-5 amplified with primers B586 + B587 (using gDNA), insert in pSpark vector, cut with SphI + Acc65I and Insert into SphI + Acc65I of pBN4	Gómez-Saldivar et al., 2016
pBN170	Plasmid encoding MEL-28_l2m::GFP	Insert XmaI-GFP-XmaI fragment from #630 into Xma site of #1263	Gómez-Saldivar et al., 2016
pBN171	Plasmid encoding MEL-28_l2m::GFP	NgoMIV/SpeI fragment from pBN170 inserted into NgomIV/SpeI site of pBN8	Gómez-Saldivar et al., 2016

pBN179	mex-5 promoter driving expression of GFP::MEL-28	Pmex-5::gfp amplified with primers B586 + B588 (using pBN169), cut with NotI + NgomIV and Insert into NotI + NgomIV of pBN97	Gómez-Saldivar et al., 2016
pBN180	Empty sgRNA plasmid	sgRNA plasmid derived from pDD162 by whole-plasmid PCR with B633+B634 (to deleted Cas9 cassette)	Gómez-Saldivar et al., 2016
pBN183	Heat shock inducible hsp-16.41 promoter controlling expression of NPP-22::Dam::MYC::MEL-28	Gibson assembly to insert fragments 1 (amplified with primers B662+B663), 2 (B664+B665) and 3 (B667+B668) into pBN97 cut with NotI/NgoMIV.	This study
pBN185	Heat shock inducible hsp-16.41 promoter controlling expression of NPP-22::Dam::MYC	pBN183 cut with NheI, religated. (Note: Includes approximately 60bp fromUNC-54 and 40 bp from MCS before unc-54 stop codon).	This study
pBN194	Heat shock inducible hsp-16.41 promoter controlling expression of DAM::MYC::MEL-28 aa835-end	mel-28 SpeI gDNA fragment from pALI3 inserted into pBN69 previously cuted w NheI and purify the vector.	This study
pBN195	Heat shock inducible hsp-16.41 promoter controlling expression of DAM::MYC::MEL-28 aa508-end	mel-28 SpeI gDNA fragment from pALI8 inserted into pBN69 previously cuted w NheI and purify the vector.	This study
pBN186	mel-28 promoter driving expression of MEL-28_aa1-956_l2m::GFP	Q5 site-directed mutagenesis with primers B673+B7669 on pBN171	Gómez-Saldivar et al., 2016
pBN187	mel-28 promoter driving expression of MEL-28_aa1-956::GFP	Q5 site-directed mutagenesis with primers B673+B7669 on pBN123	Gómez-Saldivar et al., 2016
pBN198	Heat shock inducible hsp-16.41 promoter controlling expression of GFP::MEL-28 aa846-956	mel-28 internal fragment amplified with B726+B468, cut NgoMIV+NheI, inserted into NgoMIV+NheI of pBN16	Gómez-Saldivar et al., 2016
pBN207	U6 promoter driving expression of dpy-10 sgRNA	Q5 site-directed mutagenesis with primers B635+B724 on pBN180	Gómez-Saldivar et al., 2016
pBN220	U6 promoter driving expression of mel-28 sgRNA	Q5 site-directed mutagenesis with primers B635+B790 on pBN180	Gómez-Saldivar et al., 2016
pBN247	mKate2_mel-28 plasmid for SEC protocol	pDD285 cut with SpeI+ClaI; Gibson assembly with 5' homology arm (amplified with B854+B855 on pBN123) and 3'homology arm (amplified with B856+B857 on #1397. Mutated PAM seq but only approx 200 bp homology).	This study

pCFJ90	myo-2 promoter driving expression of mCherry in the pharynx		Frøkjær-Jensen et al., 2008
pCFJ104	myo-3 promoter driving expression of mCherry in the body muscle		Frokjaer-Jensen et al., 2008
pCFJ601	eft-3 promoter driving expression of Mos transposase in the germ line		Frokjaer-Jensen et al., 2012
pDD162	Plasmid to express Cas9 and empty sgRNA		Dickinson et al., 2013
pDD285	mKate2-SEC vector - requires ccdB-resistant bacteria for amplification.		Dickinson et al., 2016
pJL43.1	glh-2 promoter driving expression of Mos transposase in the germ line		Frokjaer-Jensen et al., 2008
pMA122	Heat shock inducible hsp-16.41 promoter controlling expression of PEEL-1		Frokjaer-Jensen et al., 2012
pMSM3	pie-1 promoter driving expression of GFP::MEL-28 aa1740-1784	Cut pAF3 with SpeI to excise full-length mel-28 and replaced this with a fragment encoding aa1740-1784 that was amplified from a genomic clone using SpeI.	Gómez-Saldivar et al., 2016
pMSM4	pie-1 promoter driving expression of GFP::MEL-28 aa1624-1784	Cut pAF3 with SpeI to excise full-length mel-28 and replaced with fragment encoding aa1624-1784 that was amplified from a genomic clone.	Gómez-Saldivar et al., 2016
pMSM5	mex-5 promoter driving expression of GFP::MEL-28 Daa498-956	Amplified 5' fragment from a genomic clone and ligated into pBSKS SpeI/NotI, then amplified 3' fragment from a genomic clone and ligated adjacent to 5' fragment using NotI/SacI. Excised entire cassette using SpeI and ligated into pBN179/NheI.	Gómez-Saldivar et al., 2016
pMSM6	mex-5 promoter driving expression of GFP::MEL-28 aa957-1784	Cut pBN179 with NheI to excise full-length mel-28 and used SpeI to replace this with a mel-28 fragment amplifiied from a genomic clone that represents aa957-1784.	Gómez-Saldivar et al., 2016
pAF3	pie-1 promoter driving expression of GFP::MEL-28		Fernandez et al., 2006

pAF66	pie-1 promoter driving expression of GFP::MEL-28 aa1-765	Cut pAF3 with SpeI to excise full-length mel-28 and replaced this with a fragment encoding aa1-765 that was amplified from a genomic clone.	Gómez-Saldivar et al., 2016
pAF67	pie-1 promoter driving expression of GFP::MEL-28 aa1-1629 (ΔAThooks)	Cut pAF3 with SpeI to excise full-length mel-28 and replaced this with a fragment encoding aa1-1629 that was amplified from a genomic clone.	Gómez-Saldivar et al., 2016
pAF86	pie-1 promoter driving expression of GFP::MEL-28 Δaa566-778	Amplified 5' fragment from a genomic clone and ligated into pBSKS SpeI/NotI, then amplified 3' fragment from a genomic clone and ligated adjacent to 5' fragment using NotI/SacI. Excised entire cassette using SpeI and ligated into pAF3 backbone.	Gómez-Saldivar et al., 2016
pAF114	pie-1 promoter driving expression of GFP::MEL-28 Δaa1140-1186	Amplified 5' fragment from a genomic clone and ligated into pBSKS SpeI/NotI, then amplified 3' fragment from a genomic clone and ligated adjacent to 5' fragment using NotI/SacI. Excised entire cassette using SpeI and ligated into pAF3 backbone.	Gómez-Saldivar et al., 2016

Table 3.2. Primers used in this study

Construct name	Forward primer	Reverse primer
ELYS(1-2275)	5'-gtccggactcagatctcgagctATGGCGGCGGAGCGGCGCTGTGGAAGTATG-3'	5'-gaagcttgagctcgagTTACAGCATTTTTCTGCGTAAAATTTGCTT-3'
ELYS(1-329)	5'-gtccggactcagatctcgagctATGGCGGCGGAGCGGCGCTGTGGAAGTATG-3'	5'-gaagcttgagctcgagTAAGATTTGTCCTGATGCC-3'
ELYS(1-1101)	5'-gtccggactcagatctcgagctATGGCGGCGGAGCGGCGCTGTGGAAGTATG-3'	5'-gaagcttgagctcgagCGAATACACTATAGGAGATGG-3'
ELYS(1-1700)	5'-gtccggactcagatctcgagctATGGCGGCGGAGCGGCGCTGTGGAAGTATG-3'	5'-gaagcttgagctcgagCTGTTCCATTGTATCTGAAGT-3'
ELYS(600-1700)	5'-gtccggactcagatctcgagctGTGGTTCTCACAAAAGAG-3'	5'-gaagcttgagctcgagCTGTTCCATTGTATCTGAAGT-3'
ELYS(1430-1700)	5'-gtccggactcagatctcgagctATCTTCACCCAGAAGTCC-3'	5'-gaagcttgagctcgagCTGTTCCATTGTATCTGAAGT-3'
ELYS(179-22759	5'-gtccggactcagatctcgagctCTATGTTTGGATGACTTGTC-3'	5'-gaagcttgagctcgagTTACAGCATTTTTCTGCGTAAAATTTGCTT-3'
ELYS(476-	5'-	5'-

2275)	gtccggactcagatctcgagctGAGCAGTTTTTTAATCCAAG-3’	gaagcttgagctcgagTTACAGCATTTTTCTGCGTAAAATTTGCTT-3’
ELYS(600-2275)	5’-gtccggactcagatctcgagctGTGGTTCTCACAAAAGAG-3’	5’-gaagcttgagctcgagTTACAGCATTTTTCTGCGTAAAATTTGCTT-3’
ELYS(1430-2275)	5’-gtccggactcagatctcgagctATCTTCACCCAGAAGTCC-3’	5’-gaagcttgagctcgagTTACAGCATTTTTCTGCGTAAAATTTGCTT-3’
ELYS(1700-2275)	5’-gtccggactcagatctcgagctCAGTCCATTCATGAAAC-3’	5’-gaagcttgagctcgagTTACAGCATTTTTCTGCGTAAAATTTGCTT-3’
ELYS(1851-2275)	5’-gtccggactcagatctcgagctAAAAGATTAAAATCATCTCA-3’	5’-gaagcttgagctcgagTTACAGCATTTTTCTGCGTAAAATTTGCTT-3’
ELYS(1851-2034)	5’-gtccggactcagatctcgagctAAAAGATTAAAATCATCTCA-3’	5’-gaagcttgagctcgagTGGTTTTCCAACATCAAC-3’
ELYS(2034-2275)	5’-gtccggactcagatctcgagctCCAGCTTTAGGAAAATCC-3’	5’-gaagcttgagctcgagTTACAGCATTTTTCTGCGTAAAATTTGCTT-3’
pBN180	(B633) 5'-aacgtcgtgactgggaaaac-3'	(B634) 5'-ggtgccaacttttctatacaaag-3'
pBN207	(B724) 5'-CTACCATAGGCACCACGAGgttttagagctagaaatagcaagt-3'	(B635) 5'-caagacatctcgcaataggag-3'
pBN220	(B790) 5'-ATCAAGGATACGAGTGTTGGgttttagagctagaaatagcaagt-3'	(B635) 5'-caagacatctcgcaataggag-3'
pBN114	(B466) 5'-gagccggcGACGATGGAGCATATCGTGA-3'	(B470) 5'-cagctagctcaTTGAACGGGTAGAGATGATCTGA-3'
pBN115	(B468) 5'-gagccggcGCTCCGATGACAGTGACAATCGGA-3'	(B471) 5'-cagctagctcatcaTGGTCTATCTTCCTCAACAGC-3'
pBN116	(B468) 5'-gagccggcGCTCCGATGACAGTGACAATCGGA-3'	(B469) 5'-gcgctagCTAAAGTGCAGATGACGA-3'
pBN128	(B468) 5'-gagccggcGCTCCGATGACAGTGACAATCGGA-3'	(B542) 5'-cagctagctcaatcgtcttggttttcgaaag-3'
pBN129	(B541) 5'-gagccggcACTTTCGAAAACCAAGACGA-3'	(B469) 5'-gcgctagCTAAAGTGCAGATGACGA-3'
pBN131	(B548) 5'-gagccggcGACCCGATCAGACAGCAAAGA-3'	(B471) 5'-cagctagctcatcaTGGTCTATCTTCCTCAACAGC-3'
pBN150	(B548) 5'-gagccggcGACCCGATCAGACAGCAAAGA-3'	(B467) 5'-cagctagctcaCGCAGTCTTCTGACGACCTCTT-3'
pBN169	(B586) 5'-gcGCATGCgcggccgcATATCAGTTTTTAAAAAATTAAACCATAAAACAAATAATATAAC-3'	(B587) 5'-gcggtaccTCTCTGTCTGAAACATTCAATTG-3'
pBN171	(B466) 5'-gagccggcGACGATGGAGCATATCGTGA-3'	(B635) 5'-caagacatctcgcaataggag-3'
pBN179	(B586) 5'-gcGCATGCgcggccgcATATCAGTTTTTAAAAAATTAAACCATAAAACAAATAATATAAC-3'	(B588) 5'-tgagccggcTTTGTATAGTTCATCCATGCC-3'
pBN183 fragment 1	(B662) 5'-CCAGATATCCTGCAGGTAGC-3'	(B663) 5'-TATCACCCATCATCTCGAGGTCGACGGTA-3'
pBN183 fragment 2	(B664) 5'-CCTCGAGATGATGGGTGATAGTCATTCTTCATTCAC-3'	(B665) 5'-tcatCAATTCATCTGTGAGACAAATCATCC-3'
pBN183 fragment 3	(B667) 5'-TGTCTCACAGATGAATTGATGaagaaaaatcgcgctttttg-3'	(B668) 5'-cACGCGTtgcAGATCTtgaG-3'
pBN186	(B669) 5'-	(B673) 5'-

	AACTTCAGGCATATCTTCGTCGTC-3'	cccgggCTGCAGGAATTCGATATCAAGCT-3'
pBN187	(B669) 5'-AACTTCAGGCATATCTTCGTCGTC-3'	(B673) 5'-cccgggCTGCAGGAATTCGATATCAAGCT-3'
pBN198	(B468) 5'-gagccggcGCTCCGATGACAGTGACAATCGGA-3'	(B726) 5'-cagctagctcaAACTTCAGGCATATCTTCGTCGTC-3'
pBN247 fragment 1	(B854) 5'-acgttgtaaaacgacggccagtcgccggcacccctgcatcctgttttg-3'	(B855) 5'-CATGTTTTCTTTAATGAGCTCGGAGACCATTctgaaaaaaaataaacc-3'
pBN247 fragment 2	(B856) 5'-CGTGATTACAAGGATGACGATGACAAGAGAggtaccggatcagctgga-3'	(B857) 5'-tcacacaggaaacagctatgaccatgttatGAGTCCGCATCGATCAAA-3'
PCR1 (l2m)	(B466) 5'-gagccggcGACGATGGAGCATATCGTGA-3'	(B585) 5'-cAgaTgcTTTGTAGgACCATGAAgaTATATCAAAAATAGCTGC-3'
PCR2 (l2m)	(B584) 5'-TTCATGGTcCTACAAAgcAtcTggCGGTCGAGTATCTACAGAT-3'	(B470) 5'-cagctagctcaTTGAACGGGTAGAGATGATCTGA-3'
#1255	(B466) 5'-gagccggcGACGATGGAGCATATCGTGA-3'	(B470) 5'-cagctagctcaTTGAACGGGTAGAGATGATCTGA-3'
dpy-10(cn64) Donor oligo-nucleotide for CRISPR	(B725) 5'-CACTTGAACTTCAATACGGCAAGATGAGAATGACTGGAAACCGTACCGCATGCGGTGCCTATGGTAGCGGAGCTTCACATGGCTTCAGACCAACAGCCTAT-3'	
pAF3	5'-aaactagtATGGATAATGAAAATTCGTCC-3'	5'-aaactagtCTATTGTTTAGCACGGCGAGC-3'
pAF66	5'-aaactagtATGGATAATGAAAATTCGTCC-3'	5'-aaactagttCAATCAATGACATATTGGACAACG-3'
pAF67	5'-aaactagtATGGATAATGAAAATTCGTCC-3'	5'-ttaactagtctaCGTCGGTGCCGATTTGTCGTC-3'
pAF86 fragment 1	5'-aaactagtATGGATAATGAAAATTCGTCC-3'	5'-aaaaaaagcggccgcGTAGTAGACGATAACGTTG-3'
pAF86 fragment 2	5'-aaaaaaagcggccgcAAAACAATTGGCACTTGAAACTATCAAAATCATGAC-3'	5'-aagagctcactagtCTATTGTTTAGCACGGCGAG-3'
pAF114 fragment 1	5'-aaactagtATGGATAATGAAAATTCGTCC-3'	5'-aaaaaaagcggccgcCACTACATTTTTCTCTGAATCC-3'
pAF114 fragment 2	5'-aagcggccgcGGAAACTCCTCCCATGGAAG -3'	5'-aagagctcactagtCTATTGTTTAGCACGGCGAG-3'
pALI2	5'-aaactagtatgACTCCTCCCATGGAAGATACG-3'	5'-aaactagtCTATTGTTTAGCACGGCGAGC-3'
pALI3	5'-aaactagtatgGAGAAAGTATTCTCAATGAAAGATGACG-3'	5'-aaactagtCTATTGTTTAGCACGGCGAGC-3'
pALI8	5'-aaactagtatgGTCAAACTGCCTGCTCTCATCAGG-3'	5'-aaactagtCTATTGTTTAGCACGGCGAGC-3'
pALI9	5'-aaactagtATGGATAATGAAAATTCGTCC-3'	5'-aaactagtctaTGGAGTGGTTGGCTCTTCCACC-3'
pMSM3	5'-aaactagtatgGAAGAGCCAACCACTCCAAAACGC-3'	5'-aaactagtCTATTGTTTAGCACGGCGAGC-3'
pMSM4	5'-aaactagtatgGACAAATCGGCACCGACGAC	5'-aaactagtCTATTGTTTAGCACGGCGAGC-3'

	GCC-3’	
pMSM5 fragment 1	5’-aaactagtATGGATAATGAAAATTCGTCC-3’	5’-aagcggccgcGTTCTGGATCTTCATCCAGTCAATTCTGG-3’
pMSM5 fragment 2	5’-aagcggccgcTTTCGCTTCTGTCAATGACAAAACAGAAAGAAAGCGG -3’	5’-aagagctcactagtCTATTGTTTAGCACGGCGAG-3’
pMSM6	5’-aaactagtatgTTCGCTTCTGTCAATGACAAAACAGAAAGAAAGCGG-3’	5’-aaactagtCTATTGTTTAGCACGGCGAGC-3’

For primers used to clone ELYS fragments, capital and small letters indicate the sequences for hELYS and In-Fusion reaction, respectively. Underlines indicate XhoI sit.

For primers used for pAF, pALI, and pMSM plasmids, capital letters indicate mel-28 sequences and underlined letters indicate restriction enzyme sites.

Nematode strains and transgenesis

The wild type strain used was the *C. elegans* Bristol strain N2. Transgenic strains were generated by any of three different methods: MosSCI (Frøkjær-Jensen, Davis, Ailion, & Jorgensen, 2012), CRISPR-Cas9 (Dobrzynska, Askjaer, et al., 2016) or microparticle bombardment (Praitis, 2006). GE2633 (*mel-28(t1684)*) was obtained from the *Caenorhabditis* Genetic Centers. Other strains are listed in Table 3.3. Strains were cultured at 15-25°C using standard *C. elegans* methods (Stiernagle, 2006).

Table 3.3. Strains used in this study

Strain	Description	Genotype	Method	Ref
N2	Wild-type Bristol strain			CGC
AGF001	Balanced mel-28(t1684) mutant	mel-28(t1684)/qC1 dpy-19(e1259) glp-1(q339) [qIs26] III	PF405 crossed to N2, self-fertilized F1 then crossed to PF405 again	Fernandez et al., 2014
AGF009	Expression of GFP::MEL-28 aa1-1629 (ΔAT-hook)	unc-119(ed3) III; Is[unc-119(+) + Ppie-1::GFP::MEL-28 aa1-1629] ?	Particle bombardment of plasmid pAF67 into DP38.	Gómez-Saldivar et al., 2016
AGF024	Expression of GFP::MEL-28 Δaa1140-1186	unc-119(ed3) III; Is[unc-119(+) + Ppie-1::GFP::MEL-28 Δaa1140-1186] ?	Particle bombardment of plasmid pAF114 into DP38.	Gómez-Saldivar et al., 2016
AGF031	Balanced mel-28(t1684) mutant expressing GFP::MEL-28 Δaa1140-1186	mel-28(t1684) III; Is[unc-119(+) + Ppie-1::GFP::MEL-28 Δaa1140-1186] ? May carry unc-119(ed3) III	AGF024 crossed with AGF001 twice	Gómez-Saldivar et al., 2016

AGF033	Balanced mel-28(t1684) mutant expressing GFP::MEL-28 aa1-1629 (ΔAT-hooks)	mel-28(t1684) III; Is[unc-119(+) + Ppie-1::GFP::MEL-28 aa1-1629] ? May carry unc-119(ed3) III	AGF009 crossed with AGF001 twice	Gómez-Saldivar et al., 2016
AGF039-AGF040	Expression of GFP::MEL-28 aa1188-1784	unc-119(ed3) III; Is[unc-119(+) + Ppie-1::GFP::MEL-28 aa1188-1784] ?	Particle bombardment of plasmid pALI2 into DP38.	Gómez-Saldivar et al., 2016
AGF041-AGF043	Expression of GFP::MEL-28 aa826-1784	unc-119(ed3) III; Is[unc-119(+) + Ppie-1::GFP::MEL-28 aa826-1784] ?	Particle bombardment of plasmid pALI3 into DP38.	Gómez-Saldivar et al., 2016
AGF047-AGF049	Expression of GFP::MEL-28 aa508-1784	unc-119(ed3) III; Is[unc-119(+) + Ppie-1::GFP::MEL-28 aa508-1784] ?	Particle bombardment of plasmid pALI8 into DP38.	Gómez-Saldivar et al., 2016
AGF050	Balanced mel-28(t1684) mutant expressing GFP::MEL-28 aa508-1784	mel-28(t1684) III; Is[unc-119(+) + Ppie-1::GFP::MEL-28 aa508-1784] ? May carry unc-119(ed3) III	AGF047 crossed with AGF001 twice	Gómez-Saldivar et al., 2016
AGF055-AGF058	Expression of GFP::MEL-28 aa1624-1784	unc-119(ed3) III; Is[unc-119(+) + Ppie-1::GFP::MEL-28 aa1624-1784 ?	Particle bombardment of plasmid pMSM4 into DP38.	Gómez-Saldivar et al., 2016
AGF059	Expression of GFP::MEL-28 Δaa1745-1784 (Δlast AT-hook)	unc-119(ed3) III; Is[unc-119(+) + Ppie-1::GFP::MEL-28 aa1-1744] ?	Particle bombardment of plasmid pALI9 into DP38.	Gómez-Saldivar et al., 2016
AGF060-AGF065	Expression of GFP::MEL-28 aa1740-1784	unc-119(ed3) III; Is[unc-119(+) + Ppie-1::GFP::MEL-28 aa1740-1784] ?	Particle bombardment of plasmid pMSM3 into DP38.	Gómez-Saldivar et al., 2016
AGF066	Expression of GFP::MEL-28 Δaa498-956	unc-119(ed3) III; Is[unc-119(+) + Pmex-5::GFP::MEL-28 Δaa498-956] ?	Particle bombardment of plasmid pMSM5 into DP38.	Gómez-Saldivar et al., 2016
AGF072-AGF077	Expression of GFP::MEL-28 aa1-765	unc-119(ed3) III; Is[unc-119(+) + Ppie-1::GFP::MEL-28 aa1-765] ?	Particle bombardment of plasmid pAF66 into DP38.	Gómez-Saldivar et al., 2016
AGF089	Balanced mel-28(t1684) mutant expressing GFP::MEL-28 Δaa498-956	mel-28(t1684)/qC1 III; Is[unc-119(+) + Pmex-5::GFP::MEL-28 Δaa498-956] ? May carry unc-119(ed3) III	AGF066 crossed with AGF001 twice	Gómez-Saldivar et al., 2016
AGF091	Balanced mel-28(t1684) mutant expressing GFP::MEL-28 Δaa1745-1784 (Δlast AT-hook)	mel-28(t1684)/qC1 III; Is[unc-119(+) + Ppie-1::GFP::MEL-28 aa1-1744] ? May carry unc-119(ed3) III	AGF059 crossed with AGF001 twice	Gómez-Saldivar et al., 2016
BN189	Expression of mCherry::HIS-58	bqSi189[pBN13(unc-119(+) Plmn-1::mCherry::his-58)] II; may carry unc-119(ed9) III.	MosSCI co-injection of EG4322 with plasmids pBN13, pBN40, pBN41, pBN42 and pJL43.1; outcrossed twice with N2.	Gómez-Saldivar et al., 2016
BN195	Expression of Dam::LMN-1	bqSi195[pBN65(unc-119(+); hsp16.41p::dam::myc::lmn-1)] II.		Towbin et al., 2012
BN196	Expression of GFP::Dam	bqSi196[pBN67(unc-119(+); hsp16.41p::gfp::myc::dam)] II.		Towbin et al., 2012

BN208	Expression of Dam::MEL-28 full length	bqSi208[pBN69(unc-119(+); Phsp-16.41::dam::myc::mel-28)] II.	MosSCI co-injection of EG4322 with plasmids pBN1, pBN69, pCFJ90, pCFJ104 and pJL43.1; outcrossed twice with N2.	Sharma et al., 2014
BN215	Expression of GFP::MEL-28 full length	bqSi215[pBN97(unc-119(+) Phsp-16.41::gfp::mel-28)] II	MosSCI co-injection of EG4322 with plasmids pBN1, pBN97, pCFJ90, pCFJ104 and pJL43.1; outcrossed twice with N2.	Gómez-Saldivar et al., 2016
BN245	Expression of mCherry::HIS-58, GFP::TBA-2 and GFP::TBB-2	ltIs37[Ppie-1::mCherry::his-58] IV; Ppie-1::GFP::tba-2; ojIs1[Ppie-1::GFP::tbb-2]		Morales-Martínez et al., 2015
BN248	Expression of GFP::MEL-28 Δaa1239-1728	bqSi248[pBN117(unc-119(+) Phsp-16.41::gfp::mel-28 Δaa1239-1728)] II	MosSCI co-injection of EG4322 with plasmids pBN1, pBN117, pCFJ90, pCFJ104 and pJL43.1; outcrossed twice with N2.	Gómez-Saldivar et al., 2016
BN249	Expression of GFP::MEL-28 aa209-709	bqSi249[pBN114(unc-119(+) Phsp-16.41::gfp::mel-28 aa209-709)] II	MosSCI co-injection of EG4322 with plasmids pBN1, pBN114, pCFJ90, pCFJ104 and pJL43.1; outcrossed twice with N2.	Gómez-Saldivar et al., 2016
BN250	Expression of GFP::MEL-28 aa846-1601	bqSi250[pBN116(unc-119(+) Phsp-16.41::gfp::mel-28 aa846-1601)] II	MosSCI co-injection of EG4322 with plasmids pBN1, pBN116, pCFJ90, pCFJ104 and pJL43.1; outcrossed twice with N2.	Gómez-Saldivar et al., 2016
BN251	Expression of GFP::MEL-28 aa846-1350	bqSi251[pBN115(unc-119(+) Phsp-16.41::gfp::mel-28 aa846-1350)] II	MosSCI co-injection of EG4322 with plasmids pBN1, pBN115, pCFJ90, pCFJ104 and pJL43.1; outcrossed twice with N2.	Gómez-Saldivar et al., 2016
BN276	Expression of GFP::MEL-28 aa846-1071	bqSi276[pBN146(unc-119(+) Phsp-16.41::gfp::mel-28 aa846-1071)] II	MosSCI co-injection of EG4322 with plasmids pBN1, pBN146, pCFJ90, pCFJ104 and pJL43.1; outcrossed twice with N2.	Gómez-Saldivar et al., 2016
BN277	Expression of GFP::MEL-28 aa1161-1601	bqSi277[pBN129(unc-119(+) Phsp-16.41::gfp::mel-28 aa1161-1601)] II	MosSCI co-injection of EG4322 with plasmids pBN1, pBN129, pCFJ90, pCFJ104 and pJL43.1; outcrossed twice with N2.	Gómez-Saldivar et al., 2016
BN282	Expression of GFP::MEL-28 aa846-1167	bqSi282[pBN128(unc-119(+) Phsp-16.41::gfp::mel-28 aa846-1167)] II	MosSCI co-injection of EG4322 with plasmids pBN1, pBN128, pCFJ90, pCFJ104 and pJL43.1; outcrossed twice with N2.	Gómez-Saldivar et al., 2016
BN283	Expression of GFP::MEL-28 aa681-1350	bqSi283[pBN131(unc-119(+) Phsp-16.41::gfp::mel-28 aa681-1350)] II	MosSCI co-injection of EG4322 with plasmids pBN1, pBN131, pCFJ90, pCFJ104 and pJL43.1; outcrossed twice with N2.	Gómez-Saldivar et al., 2016
BN295	Expression of GFP::MEL-28 aa681-929	bqSi295[pBN150(unc-119(+) Phsp-16.41::gfp::mel-28 aa681-929)] II	MosSCI co-injection of EG4322 with plasmids pBN1, pBN150, pCFJ90, pCFJ104 and pJL43.1; outcrossed twice with N2.	Gómez-Saldivar et al., 2016
BN297 and BN384	Expression of GFP::MEL-28 aa1239-1601	bqSi297/384[pBN157(unc-119(+) Phsp-16.41::gfp::mel-28 aa1239-1601)] II	MosSCI co-injection of EG4322 with plasmids pBN1, pBN157, pCFJ90, pCFJ104 and pJL43.1; outcrossed twice with N2.	Gómez-Saldivar et al., 2016

BN311	Expression of GFP::MEL-28 full length	bqSi311[pBN179(unc-119(+) Pmex-5::gfp::mel-28)] II	MosSCI co-injection of EG4322 with plasmids pBN1, pBN179, pCFJ90, pCFJ104, pCFJ601 and pMA122; outcrossed twice with N2.	Gómez-Saldivar et al., 2016
BN312, BN344-BN348	Expression of MEL-28_l2m::GFP	bqSi312/344-348[pBN171(unc-119(+) Pmel-28(1.1kb)::mel-28_loop2mut::gfp)] II	MosSCI co-injection of EG4322 with plasmids pBN1, pBN171, pCFJ90, pCFJ104, pCFJ601 and pMA122; outcrossed twice with N2.	Gómez-Saldivar et al., 2016
BN315	Expression of GFP::MEL-28 and mCherry::H2B	bqSi311[pBN179(unc-119(+) Pmex-5::gfp::mel-28)] II; ltIs37[Ppie-1::mCherry::his-58; unc-119 (+)] IV	BN245 crossed with BN311	Gómez-Saldivar et al., 2016
BN337	Balanced mel-28 deletion strain expressing MEL-28_l2m::GFP	bqSi312[pBN171(unc-119(+) Pmel-28(1.1kb)::mel-28loop2mut::gfp)] II; mel-28(t1684) unc-32(e189)/qC1 dpy-19(e1259) glp-1(q339) III; possibly also him-3(e1147) IV.	BN312 crossed with GE2633 twice	Gómez-Saldivar et al., 2016
BN339	Balanced mel-28(t1684) mutant expressing GFP::MEL-28 Δaa1239-1728	bqSi248[pBN117(unc-119(+) Phsp16.41::gfp::mel-28] II; mel-28(t1684) unc-32(e189) III; possibly also him-3(e1147) IV.	BN248 crossed with GE2633 twice	Gómez-Saldivar et al., 2016
BN373	Expression of MEL-28_aa1-956_l2m::GFP	bqSi373[pBN186(unc-119(+) Pmel-28(1.1kb)::mel-28_loop2mut aa1-956::gfp)] II	MosSCI co-injection of EG4322 with plasmids pBN1, pBN186, pCFJ90, pCFJ104, pCFJ601 and pMA122; outcrossed twice with N2.	Gómez-Saldivar et al., 2016
BN374	Expression of NPP-22::Dam::MEL-28	bqSi374[pBN183(unc-119(+); Phsp-16.41::dam::myc::mel-28)] II.	MosSCI co-injection of EG4322 with plasmids pBN1, pBN183, pCFJ90, pCFJ104 and pJL43.1; outcrossed twice with N2.	This study
BN375	Expression of NPP-22::Dam	bqSi375[pBN185(unc-119(+) Phsp16.41::npp-22::Dam::MYC)] II	MosSCI co-injection of EG4322 with plasmids pBN1, pBN185, pCFJ90, pCFJ104 and pJL43.1; outcrossed twice with N2.	This study
BN376	Expression of Dam::MEL-28 aa. 508-end	bqSi376[pBN195(unc-119(+) Phsp16.41::Dam::MYC::mel-28_aa508-end)] II	MosSCI co-injection of EG4322 with plasmids pBN1, pBN195, pCFJ90, pCFJ104 and pJL43.1; outcrossed twice with N2.	This study
BN382	Expression of Dam::MEL-28 aa. 835-end	bqSi382[pBN194(unc-119(+) Phsp16.41::Dam::MYC::mel-28_aa835-end)] II	MosSCI co-injection of EG4322 with plasmids pBN1, pBN194, pCFJ90, pCFJ104 and pJL43.1; outcrossed twice with N2.	This study
BN409 and BN427	Expression of MEL-28_aa1-956::GFP	bqSi409/427[pBN187(unc-119(+) Pmel-28(1.1kb)::mel-28 aa1-956::gfp)] II	MosSCI co-injection of EG4322 with plasmids pBN1, pBN187, pCFJ90, pCFJ104, pCFJ601 and pMA122.	Gómez-Saldivar et al., 2016

BN410	Expression of GFP::MEL-28 Δaa498-956	bqSi410[pMSM5(unc-119(+) Pmex-5::gfp::mel-28 Δaa498-956)] II	MosSCI co-injection of EG4322 with plasmids pBN1, pMSM5, pCFJ90, pCFJ104, pCFJ601 and pMA122.	Gómez-Saldivar et al., 2016
BN411	Expression of GFP::MEL-28 aa957-1784	bqSi411[pMSM6(unc-119(+) Pmex-5::gfp::mel-28 aa957-1784)] II	MosSCI co-injection of EG4322 with plasmids pBN1, pMSM6, pCFJ90, pCFJ104, pCFJ601 and pMA122.	Gómez-Saldivar et al., 2016
BN414-BN416	Expression of GFP::MEL-28 aa846-956	bqSi414-416[pBN198(unc-119(+) Phsp-16.41::gfp::mel-28 aa846-956)] II	MosSCI co-injection of EG4322 with plasmids pBN1, pBN198, pCFJ90, pCFJ104, pCFJ601 and pMA122. outcrossed twice with N2.	Gómez-Saldivar et al., 2016
BN419	Expression of GFP	bqSi419[pBN16(unc-119(+) Phsp-16.41::gfp)] II	MosSCI co-injection of EG4322 with plasmids pBN1, pBN16, pCFJ90, pCFJ104, pCFJ601 and pMA122.	Gómez-Saldivar et al., 2016
BN426	GFP knock-in into the mel-28 locus	mel-28(bq5[gfp::mel-28]) III	CRISPR-Cas9 co-injection of N2 with plasmids #1286 Cas9, pBN207 dpy-10 sgRNA, #1397 mel-28 repair template, pBN220 mel-28 sgRNA and primer B725 dpy-10(cn64). Outcrossed to N2 twice.	Gómez-Saldivar et al., 2016
BN440	Balanced mel-28(t1684) mutant expressing mCherry::HIS-58	bqSi189[pBN13(unc-119(+) Plmn-1::mCherry::his-58)] II; mel-28(t1684) unc-32(e189)/qC1 dpy-19(e1259) glp-1(q339) III. May carry him-3(e1147) IV.	BN189 crossed with GE2633 twice	Gómez-Saldivar et al., 2016
BN452	Expression of GFP::MEL-28 and mCherry::HIS-58	bqSi189[pBN13(unc-119(+) Plmn-1::mCherry::his-58)] II; mel-28(bq5[gfp::mel-28]) III	BN440 crossed with BN426	Gómez-Saldivar et al., 2016
BN464	Balanced mel-28(t1684) mutant expressing mCherry::HIS-58 and GFP::TBB-2	bqSi189[pBN13(unc-119(+) Plmn-1::mCherry::his-58)] II; mel-28(t1684) unc-32(e189)/qC1 dpy-19(e1259) glp-1(q339) III; ojIs1[unc-119(+) pie-1::GFP::tbb-2] V (?). May carry him-3(e1147) IV.	XA3531 crossed with BN440.	Gómez-Saldivar et al., 2016
BN468	mKate2 knock-in into the mel-28 locus	mel-28(bq6[mkate2::mel-28]) III	CRISPR-Cas9 co-injection of N2 using SEC protocol with plasmids #1286, pBN41, pBN42, pBN220 and pBN247	This study
BN513	Expression of mKate2::MEL-28 and GFP::KNL-3 (	mel-28(bq6[mkate2::mel-28]) III; unc-119(ed3) III; ltIs1[pIC22; pie-1/GFP-knl-3; unc-119(+)]	BN468 crossed with OD1	This study
DP38	Strain for bombardment	unc-119(ed3) III		CGC

EG4322	Strain for integration on chr II by MosSCI	ttTi5605 II; unc-119(ed3) III		Frokjaer-Jensen et al., 2008
GE2633	Balanced mel-28(t1684) mutant	mel-28(t1684) unc-32(e189)/qC1 dpy-19(e1259) glp-1(q339) III; him-3(e1147) IV.		Gönczy et al., 1999
OD1	Expression of GFP::KNL-3	unc-119(ed3) III; ltIs1[pIC22; pie-1/GFP-knl-3; unc-119(+)].		Cheeseman et al., 2004
PF402	Expression of GFP::MEL-28 full length	unc-119(ed3) III; Is[unc-119(+) + Ppie-1::GFP::MEL-28] ?	Particle bombardment of plasmid pAF3 into DP38.	Fernandez and Piano, 2006
PF404	mel-28(t1684) mutant expressing GFP::MEL-28 full-length	mel-28(t1684) unc-32(e189) III; Is[unc-119(+) + Ppie-1::GFP::MEL-28] ?	PF402 crossed with GE2633	Gómez-Saldivar et al., 2016
PF405	mel-28(t1684) unc-32(e189) balanced by qC1	mel-28(t1684) unc-32(e189)/qC1 dpy-19(e1259) glp-1(q339) [qIs26] III		Fernandez et al., 2014
PF407-PF408	Expression of GFP::MEL-28 Δaa566-778	unc-119(ed3) III; Is[unc-119(+) + Ppie-1::GFP::MEL-28 Δaa566-778] ?	Particle bombardment of plasmid pAF86 into DP38.	Gómez-Saldivar et al., 2016
XA3531	Balanced mel-28(t1684) mutant expressing GFP::TBB-2	mel-28(t1684) unc-32(e189)/qC1 dpy-19(e1259) glp-1(q339) III; ojIs1[unc-119(+) pie-1::GFP::tbb-2] V (?)		Galy et al., 2006

C. elegans embryonic lethality rescue experiments

Rescue experiments were performed according to the promoter used to express the different MEL-28 fragments. For constitutive promoters homozygous L4 larvae were placed on individual plates to develop and lay eggs for 24 h at 20ºC. Then, the adults were removed and the number of eggs was determined. Twenty-four hours later embryonic lethality was calculated by counting unhatched embryos. For constructs with the *hsp-16.41* heat shock inducible promoter, young gravid adults were incubated for 1 h at 32ºC and allowed to recover and lay eggs for 24 h at 20ºC. The adults were then removed and rescue of embryonic lethality was determined by the presence of viable offspring after 24 h at 20ºC.

C. elegans RNAi

We carried out RNAi as described (Peter Askjaer, Galy, & Meister, 2014) with minor adaptations. In total, 10–15 synchronized L4 hermaphrodites were placed on NGM plates (+ 1 mM IPTG + 100 µg/ml ampicillin) seeded with *E. coli* producing double-stranded RNA (*alt-*

1 RNAi clone sjj_T06E4.3 from (Kamath et al., 2003)) and incubated for 20-24h at 20ºC before analysis of cell cycle timing by live DIC microscopy.

Cell Culture

HeLa cells were a gift from Dr. Hiroshi Kimura (see (Hayashi-Takanaka et al., 2015) for the cell origin). WI-38 cells were purchased from ATCC (Manassas, VA, USA). These cells were maintained in DME medium containing 10% fetal bovine serum (FBS) at 37 °C in a humidified 5% CO_2. K562 cells were obtained from the Riken Cell Bank (Tsukuba, Japan) and maintained in RPMI1640 medium containing 10% FBS. HeLa cells were grown in a glass-bottom culture dish (MatTech, USA). GFP fusion plasmids (1 μg) were transfected into the cells with Lipofectamine 2000 (Invitrogen) according to manufacturer's protocol. After 24 hours transfection, the cells were fixed with 4% formaldehyde for 10 min, permeabilized with 0.1% Triton X-100 in PBS for 5 min. For immunostaining, the cells were blocked by blocking buffer (PBS containing 10% Blocking One (Nacalai tesque, Japan) and 0.1% Triton X-100), and then probed with anti-CENP-A antibody (generous gift from Dr. Tatsuo Fukagawa (Osaka University), (Ando, Yang, Nozaki, Okazaki, & Yoda, 2002)), followed by Alexa Fluor 568-conjugated anti-mouse IgG secondary antibody (1:500, Lifetechnologies, USA). The cells were stained with 4′,6-diamidino-2-phenylindole (DAPI) at 100 ng/ml for 10 min at room temperature. After washing 3-times with 0.1% Triton X-100 in PBS, the cells were mounted on ProLong Diamond antifade mountant (Molecular Probes, Carlsbad, CA). The cells were observed by confocal microscopy (LSM510META and LSM780; Zeiss; operated by built-in software) equipped with a C-Apo 40x NA 1.2 water immersion lens.

C. elegans immunofluorescence

C. elegans embryos and larvae were collected and processed by freeze cracking and methanol fixation as described (Ródenas, González-Aguilera, Ayuso, & Askjaer, 2012). For Figures 5.2 and 5.16 nematodes grown at 20°C were heat-shocked 1 h at 33°C and left to recover for 2 h at 20°C. Next, embryos were collected and processed as the rest. The following primary antibodies were used: mouse monoclonal antibody (mAb) 414 (Covance, Princeton, NJ, USA,1:250), mouse monoclonal antibody MH27 (1:50; (Francis & Waterston, 1991), provided by the Developmental Studies Hybridoma Bank), rabbit polyclonal α-HCP-3 antiserum MH3N (1:200; generous gift from Dr. Mark Roth (Buchwitz et al., 1999)), rabbit polyclonal α-NPP10-C/NUP96 antiserum GBLC (1:300; (Galy et al., 2003)), rabbit polyclonal

α-MEL-28 antiserum BUD3 (1:200-250; (Galy, Askjaer, Franz, López-Iglesias, et al., 2006b)), mouse α-Myc (Cell Signalling 1:500). Secondary antibodies were Alexa Fluor 546-conjugated goat anti-mouse antibodies (Invitrogen, 1:1000), Alexa Fluor 488- and Alexa Fluor 633-conjugated goat anti-rabbit antibodies (Invitrogen, 1:1000). For DNA staining, Hoechst 33258 (Hoechst) was used at 5 µg/ml. Confocal images for Figure 4.1 were obtained with a Nikon A1R microscope through a Plan Apo VC 60x/1.4 objective (Nikon, Tokyo, Japan) using a pinhole of 1 airy unit. All other immunofluorescence images were acquired with a confocal Leica SPE microscope equipped with an ACS APO 63X/1.3 objective (Leica, Wetzlar, Germany) using a pinhole of 1 airy unit.

Live imaging

C. elegans samples were mounted between a coverslip and a 2% agarose pad; embryos were released by dissecting young adult hermaphrodites and mounted in 3 µL M9 buffer, whereas larvae and adults were mounted in 3 µL 10 mM levamisole HCl (Sigma-Aldrich, St. Louis, MI, USA). For *in utero* imaging of oocytes and newly fertilized embryos, young adult hermaphrodites were anesthetized in 20 µL 5 mM ethyl 3-aminobenzoate methanesulfonate (aka Tricaine; Sigma-Aldrich), 0.5 mM levamisole HCl, 0.5x M9 for 15-20 minutes prior to mounting in 3 µL of the same buffer on 2% agarose pads. Vaseline was added between the slide and the coverslip to avoid compression of the animals and melted VALAP (1:1:1 mixture of Vaseline, lanolin, and paraffin) was used to seal the cover slip. Confocal epifluorescence and DIC images were recorded at 22–24 ℃ with a Nikon A1R microscope through a Plan Apo VC 60x/1.4 objective (Nikon, Tokyo, Japan) using a pinhole of 1.2-1.4 airy unit.

Image processing and analysis

For preparation of Figure panels images were processed with FIJI (fiji.sc/Fiji) and Adobe Photoshop CS5 or CS6 (Adobe, San Jose, CA, USA). Identical adjustment of brightness and contrast was applied to all comparable panels within each Figure without changing gamma. Quantification of fluorescence signal at the NE, kinetochore, cytoplasm and nucleoplasm was performed on raw 12 bit images. Fluorescence intensity was normalized by background subtraction; for *C. elegans*, images of wild type embryos acquired with identical microscope settings were used, with exception of Figure 4.3B

Statistical analysis

Statistical analysis was performed with Origin 8.0 (OriginLab, Northampton, MA, USA), Microsoft Excel (Microsoft, Redmond, WA, USA), online Graphpad tools (http://graphpad.com).

DamID-array experiments

DamID-array experiments were performed as in (González-Aguilera et al., 2014), in each experiment were used two biological replicates and all cultures were grown in parallel. Briefly, DamID strains were synchronized by hypochlorite treatment. From each strain, approximately 35,000 L1s were grown in 50 ml S-medium containing GM119, a Dam- *E. coli* strain. Cultures were grown with continuous agitation at 20°C for 53 h. Non-gravid young adults were frozen at −80°C until further processing. Using 30 mg nematodes, methylated genomic DNA (gDNA) was purified with DNAeasy kit (QIAGEN, Venlo, Limburg, Netherlands). 2.5 µg of gDNA was digested overnight with DpnI (New England Biolabs, Ipswich, MA, USA). After DpnI inactivation, gDNA was ligated to double-stranded adaptors with T4 DNA ligase (5 U/µl; Roche, Basel, Switzerland). After ligase inactivation, DNA fragments were digested with DpnII (New England Biolabs). Then, Methylated DNA was amplified with PCR Advantage enzyme mix (50×; Clontech, Otsu, Shiga, Japan) using adaptor-specific primers. Amplified Dam-methylated DNA was labeled and hybridized by the Roche Nimblegen Service Laboratory.

DamID-array normalization and visualization

Nimblegen 2.1 M whole genome tiling arrays, with 50 bp probes, designed against WS180 (ce5) *C. elegans* genome assembly, were used for all experiments. Data were normalized with MA2C (J. S. Song et al., 2007), the resultant values are MA2C scores in log2 ratio (log2 [Dam::POI/GFP::Dam control]). MA2C automatically creates a directory with output files with information of quality control of normalization and peak detection steps (enriched domains). Besides, MA2Cscore files are created for visualization using in Genome Browser, we used UCSC Genome Browser (http://genome.ucsc.edu/), and the Integrative Genomics Viewer (IGV) software (Thorvaldsdottir, Robinson, & Mesirov, 2013). We then converted the chromosome coordinates to WS220 (ce10) *C. elegans* genome assembly using the LiftOver tool from the UCSC genome browser (http://genome.ucsc.edu/). The overall Pearson

correlations for MA2C scores of all probes between two biological replicates were processed in Rstudio. Finally, the mean of normalized MA2C scores from the two independent biological replicates was calculated, then, these values were used for the subsequent enrichment domain calling.

DamID-array data processing

Peak calling. MADs were identified using the peak calling protocol used by (Vastenhouw et al., 2010) with minor changes. Briefly, first, MA2C was applied to detect enriched peaks under two different threshold cutoffs: FDR 5% and FDR 20%. Second, using peak calling with FDR 20%, were kept all the peaks larger than 1.5 kb, in total 6,068 peaks. Third, peaks from FDR 20% that were smaller than 1.5 kb and did not contain peaks overlapping under FDR 5% were discarded, then we kept 756 small peaks. Fourth, we combine resultant peaks from second and third steps and we got a total of 6,824 MADs. Non-associated regions, gaps, were obtained using complement intervals function from Galaxy toolbox from Cistrome Analysis Pipeline Browser (http://cistrome.org/ap/).

Metagenomic profile. The metagenomic profile was generated from the average MA2C scores using. Analyses for enrichment at promoters (up to 3 kb before the transcription start site), exons, introns and 3' and 5' UTR regions, were performed using the CEAS program (H. Shin, Liu, Manrai, & Liu, 2009). Signaling profiling plots were done with the SitePro program from Cistrome toolbox (http://cistrome.org/ap/). We graph the average MA2C score profile around MADs or EADs boundaries, which corresponding to the left edges of all MEL-28 or EMR-1 domains. ChIP-chip and ChIP-seq data of young adult H3K4me3, H3K36me3 and POL-II/AMA-1 (Gerstein et al., 2010), and embryonic NPP-13 (Ikegami & Lieb, 2013) are from modENCODE (http://www.modencode.org/), accession IDs modENCODE_3552, modENCODE_3559, modENCODE_2441 and modENCODE_2738, respectively. DamID-chip data of young adult LMN-1 and EMR-1 (González-Aguilera et al., 2014) are from Gene Expression Omnibus (GEO; https://www.ncbi.nlm.nih.gov/geo/), accession ID GSE44188.

Expression profile in MADs. Ensambl gene database, including genomic position and gene identifier, was downloaded using table browser tool from UCSC Genome Browser (https://genome.ucsc.edu). RNA sequencing (RNA-seq) data (González-Aguilera et al., 2014) is from Gene Expression Omnibus (GEO; https://www.ncbi.nlm.nih.gov/geo/), accession ID GSE44682. First, RNA-seq table with the mean expression values of genes (from N2 worms), was intersected with Ensamble gene table and we keep columns with

gene name, gene expression score and genomic position. Second, the resulting table was intersected with DamID peaks and DamID gaps. All intersections were performed by BEDtools (version 2.25.0) (Quinlan & Hall, 2010). Data were load in Rstudio (https://www.rstudio.com/) to perform a Boxplot from gene score versus peaks and versus gaps, respectively. Statistical significance was obtained running wilcox.test function.

Probe distribution in MADs. Together with the results, Nimblegen provides raw data, and the experimental design of the tiling array. Probe position and %GC content were obtained from the file '100718_Celegans180_ChIP_HX1.pos' present in the folder 'Design_Information'. Then, %AT was calculated for each probe in Galaxi/Cistrome Browser (http://cistrome.org/ap/). Density plot was done in Rstudio (https://www.rstudio.com/). Finally Boxplot of probe distribution in MADs versus genome was plotted in Rstudio. Statistical significance was obtained running wilcox.test function.

DamID-Seq experiments

The optimized protocol (Gómez-Saldivar, Meister, et al., 2016) is described at the end of this section. There we present the DamID-seq workflow from sample preparation to bioinformatics analysis.

DamID-seq normalization and visualization

Samples libraries were analyzed using the workflow shown below (Gómez-Saldivar, Meister, et al., 2016) or RDamIDSeq pipeline (https://github.com/damidseq/RDamIDSeq; (Sharma, Dominic, & Meister, 2016)). Briefly, sequencing reads in fastq format and their corresponding quality strings are imported into R for each sample. First, read quality is tested using package QuasR in R (version 1.8.4/3.2.2). Reads missing the adapter (CGCGGCCGAG) followed by the DpnI motif (GATC) were removed. Remaining reads (DamID reads) were cut after the adapter and the remaining sequence mapped to the ce10 *C. elegans* genome using RBowtie (version 1.8.0, parameters: -m 1 --best --strata - S) (Langmead, Trapnell, Pop, & Salzberg, 2009). Once mapped, the number of reads per GATC motif is counted. For binning, the *C. elegans* genome (ce10) was divided in 1 kb regions and the total GATC read numbers was calculated within this 1 kb regions. The total read number per 1 kb was then normalized using the total number of DamID reads. The ratio between Dam::POI/GFP::Dam is calculated for each replica and the mean ratio is plotted

using a log2 scale, generating also a bedGraph file with the score in log2 at GATC level and bin level and a heatmap with Pearson correlation between samples. Replicates were combined for subsequent analyses. BedGraph files were visualized using UCSC Genome Browser (http://genome.ucsc.edu/).

DamID-seq data processing

Peak Calling. Normalized bedGraph files were used to identify significant regions of enrichment (peaks) using MACS2 (version 2.1.0) and bdgpeakcall subcommand. We evaluate cutoff from 0.3 to 1, running Loop_MACS2.sh script (Table 5.3). Finally we decide to use cutoff=0.6. Gaps were obtained using complement intervals function from Galaxy toolbox from Cistrome Analysis Pipeline Browser (http://cistrome.org/ap/). Chromosome occupancy of each fusion protein was obtained using table browser tool from UCSC Genome Browser (https://genome.ucsc.edu). Peak intersection to designate common peaks between fusion proteins was determined by BEDtools (version 2.25.0) (Quinlan & Hall, 2010), using cutoff parameter –f 0.3.

Gene Ontology. RefSeq or WormID databases, including genomic position and gene identifier (curated RefSeq records), were downloaded using table browser tool from UCSC Genome Browser (https://genome.ucsc.edu/) or BioMart tools from Ensemble gene Browser (http://www.ensembl.org/), respectively. Peaks and genes intersection was performed by BEDtools (version 2.25.0) (Quinlan & Hall, 2010), running Loop_intersect_RefGene.sh or Loop_intersect_wID.sh and Loop_GO.sh scripts (Table 5.3). GO analyses were performed using DAVID (Huang et al., 2007) version 6.8 with updated Knowledgebase. Only the 'Biological Processes' tree was used in our study. We selected GO-term with p-value ≤0.01.

Correlation analysis with CenH3. Signal profiling plot was done with normalized log2-ratios from cenH3 -ChIP-chip or -ChIP-seq. Using Rstudio (https://www.rstudio.com/), log2 scores were intersected with MEL-28 peaks or gaps from both DamID-array and DamID-seq. Next, we graph a Boxplot from log2 score versus peaks or versus gaps. Statistical significance was obtained running wilcox.test function. ChIP-chip and ChIP-seq data of embryonic CENP-A/CenH3 (Gassmann et al., 2012; Steiner & Henikoff, 2014) are from modENCODE (http://www.modencode.org/), accession ID modENCODE_3540 and GEO (https://www.ncbi.nlm.nih.gov/geo/), accession ID GSE44412, respectively.

DamID Statistical analysis

Statistical analysis was performed with R package for statistical computing (www.cran.r-project.org/ and https://www.rstudio.com/). Descriptive statistics of peaks was performed using the summary function from Rstudio, including the mean, standard deviation, range, and percentiles. Statistical significance was obtained running the Wilcoxon rank sum test and Pearson correlation using wilcox.test and cor.test functions, respectively. Scatterplot function was used to plot pairs up values of data set and make a quantitative comparison.

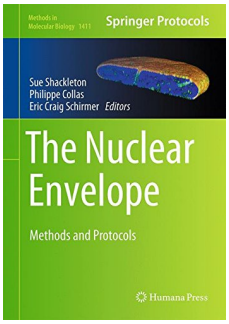

Book Chapter

DamID Analysis of Nuclear Organization in *Caenorhabditis elegans*

Georgina Gómez-Saldivar[1], Peter Meister[2], and Peter Askjaer[1]

[1] Andalusian Center for Developmental Biology (CABD), CSIC/Junta de Andalucia/Universidad Pablo de Olavide, Seville, Spain.
[2] Cell Fate and Nuclear Organization, Institute of Cell Biology, University of Bern, Switzerland.

Sue Shackleton et al. (eds.), *The Nuclear Envelope: Methods and Protocols*, Methods in Molecular Biology, vol. 1411, DOI: 10.1007/978-1-4939-3530-7_22,

DamID-seq workflow

1. Materials

1.1. Expression plasmids for Dam fusions

1.1.1. Plasmid containing the Dam coding sequence and suitable cloning sites, e.g., pBN61 (Phsp-16.41::dam::myc::MCS::unc-54 3' UTR; (González-Aguilera et al., 2014) (see Note 1).

1.1.2. C. elegans genomic DNA (gDNA) or vector bearing the gene of interest.

1.1.3. Plasmid encoding the Dam-only control, e.g., pBN67 (Phsp-16.41::gfp::myc::dam; (González-Aguilera et al., 2014).

1.1.4. Standard molecular biology reagents and materials of high analytic grade for cloning (e.g., primers to amplify the gene of interest, high-fidelity polymerase, agarose, restriction enzymes, ligase, competent E. coli cells).

1.2. Generation and validation of DamID strains

1.2.1. Materials required for Mos1-mediated Single-Copy Integration (MosSCI), including microinjection equipment, nematode host strains, co-injection plasmids, etc. (Dobrzynska, Askjaer, et al., 2016).

1.2.2. Primary antibodies against the Myc epitope (e.g., Sigma-Aldrich C3956 or 9E 10 from Developmental Studies Hybridoma Bank) and nuclear envelope proteins as control (e.g., mAb414 Covance MMS-120R); secondary anti-rabbit and anti-mouse antibodies for immunofluorescence and Western blot analysis (Peter Askjaer, Ercan, et al., 2014).

1.3. Nematode culture

1.3.1. According to personal According to personal preference nematodes can be grown in liquid medium (Peter Askjaer, Ercan, et al., 2014) or on NGM plates (Dobrzynska, Askjaer, et al., 2016); we typically use 3000–4000 animals (~30

mg) per sample, although as little as 20 nematodes can be analyzed (Sharma et al., 2014).

1.3.2. *Dam-E. coli* (e.g., strain GM119 or SCS110; *see* **Note 2**).

1.3.3. M9 buffer: 22 mM KH2PO4, 34 mM Na2HPO4, 86 mM NaCl, 1 mM MgSO4.

1.3.4. Tween 20.

1.3.5. Hypochlorite solution: 1 N NaOH, 30 % household bleach solution.

1.4. Purification and amplification of Dam-methylated DNA

1.4.1. DNeasy Blood and Tissue Kit including RNase A (QIAGEN cat. #69504 and #19101).

1.4.2. Ammonium acetate 3 M.

1.4.3. 96 % and 70 % ethanol.

1.4.4. Thermocycler.

1.4.5. *Dpn*I and *Dpn*II restriction enzymes (NEB cat. #R0176S and #R0543S).

1.4.6. Primers for the preparation of the AdR double-stranded adapter (50 µM): AdRt (5′-CTAATACGACTCACTATAGGGCAGCGTGGTCGCGGCCGAGGA; 100 µM) and AdRb (5′-TCCTCGGCCGCG; 100 µM).

1.4.7. T4 DNA ligase (Roche, cat. # 10799009001, 5 U/µL).

1.4.8. Agencourt AMPure XP® (Beckman Coulter, Inc., cat. #A63880).

1.4.9. Magnetic particle concentrator.

1.4.10. Advantage® cDNA Polymerase Mix (Clontech cat. #639105) and dNTP mix.

1.4.11. PCR Primer AdR (5′-NNNNGTGGTCGCGGCCGAGG ATC; 50 µM).

1.4.12. QIAquick PCR Purification Kit (QIAGEN cat. #28104).

1.4.13. Guanidine hydrochloride 35 %.

1.4.14. Standard materials and equipment for DNA agarose gel electrophoresis.

1.5. Library preparation

1.5.1. End-It™ DNA End-Repair Kit (Epicentre cat. #ER0720).

1.5.2. QIAquick PCR Purification Kit.

1.5.3. Guanidine hydrochloride 35 %.

1.5.4. 10× NEB buffer 2.

1.5.5. Klenow Fragment (3′–5′ exo-) (NEB cat. #M0212M) and dATP.

1.5.6. Primers for the preparation of the Y-shaped Illumina adapters: upper strand (5′-ACACTCTTTCCCTACACGACGCTCTTCCGATCT; 100 μM) and phosphorylated lower strand (P-5′- GATCGGAAGAGCACACGTCT; 100 μM).

1.5.7. T4 DNA ligase.

1.5.8. MyTaqTM Mix (BIOLINE cat. #BIO-25041).

1.5.9. Illumina P7/index primer (index sequence underlined, choose according to NGS facility for easy multiplexing; 5′-CAAGCAGAAGACGGCATACG AGATNNNNNNGTGACTGGAGTTCAGACGTGTGCTCTTCCGATCT; 5 μM).

1.5.10. Forward P5 primer (5′-AATGATACGGCGACCACCGAGATCTACACTCTTT CCCTACACGACGCTCTTCCGATCT; 5 μM).

1.5.11. Agencourt AMPure XP®.

1.5.12. QUBIT® fluorometer or NanoDrop.

1.6. DamID quantification and bioinformatics analysis

1.6.1. Computer with UNIX environment.

1.6.2. Free software tools, e.g. Cutadapt, Bowtie, R/Bioconductor and Galaxy.

2. Methods

2.1. Construction of DamID vector

2.1.1. Using standard molecular cloning techniques, clone the gene of interest into a Dam expression plasmid of choice, e.g. pBN61 (*see* **Note 3**). The transgene must be under the control of an inducible promoter with low basal activity and a characterized 3'UTR (*see* **Notes 4** and **5**).

2.1.2. Verify the sequence of the insertion.

2.2. Nematode culture

2.2.1. Inject the DamID vector into the appropriate *C. elegans* host strain for Mos-mediated single-copy integration and isolate transgenic lines according to standard MosSCI protocols (Frøkjær-Jensen et al., 2012).

2.2.2. Verify correct localization and size of the fusion protein by immunofluorescence and Western blot, respectively, using α-Myc antibodies (*see* **Note 6**).

2.2.3. Collect embryos from asynchronous cultures by standard hypochlorite treatment. Check the nematodes regularly in a dissection stereoscope. Proceed to the next step when half of the nematodes are broken up.

2.2.4. Wash embryos five times in 12 mL M9. Pellet the embryos by centrifugation at 2000 rpm for 3 min. After the last wash, resuspend in 5 mL of M9 with 0.01 % Tween 20.

2.2.5. Count number of embryos in 2–10 µL aliquots.

2.2.6. Leave embryos to hatch overnight at 16–20 °C with gentle agitation.

2.2.7. Assay quantity of hatched L1 larvae in 2–10 µL aliquots.

2.2.8. Place 500–1000 L1s per 85 mm plate containing a thick lawn of Dam-*E. coli* bacteria as food source. Use a total of four plates per strain, multiplied by number of replicas (typically three).

2.2.9. Incubate nematodes at 20 °C and collect when they are enriched for the life stage to be analyzed (e.g., 53 h for non-gravid young adults; 66 h for accumulation of young embryos). Harvest either embryos (Towbin et al., 2012) or, for better signal/noise ratio, adult nematodes (González-Aguilera et al., 2014).

2.2.10. Make aliquots containing ~30 µL embryo or adult material. Remove excess liquid and snap-freeze in liquid nitrogen before −80 °C storage until further processing.

2.3. Purification and amplification of Dam-methylated DNA

2.3.1. Purify genomic DNA (gDNA) with QIAGEN DNeasy Blood and Tissue Kit. All steps should be as gentle as possible to avoid shearing of the gDNA.

2.3.2. Elute the gDNA in 200 µL and determine its concentration. Expected yield is 4–7 µg; concentrate by ethanol precipitation if needed.

2.3.3. Incubate 500 ng of adult gDNA with 10 U *Dpn*I in 10 µL for 6 h at 37 °C in a thermocycler to cut methylated GmATC. Include an additional reaction with *Dpn*I for one of the biological samples to be used as ligation control (control A)

and also a control reaction without *Dpn*I (control B; *see* **Note 7**). Heat-inactivate *Dpn*I for 20 min at 80 °C.

2.3.4. Anneal double-stranded adapters: combine 50 µL of primers AdRt and 50 µL of AdRb. Heat to 95 °C and let cool down slowly to room temperature.

2.3.5. Assemble the adapter ligation reaction on ice and incubate at 16 °C overnight. Prepare also a reaction without T4 DNA ligase (control A).

ddH_2O	6.2 µL
*Dpn*I digested gDNA	10 µL
10× Ligation Buffer	2 µL
Double-stranded adapters	0.8 µL
T4 DNA ligase	1 µL

2.3.6. Heat-inactivate the T4 DNA ligase for 10 min at 65 °C.

2.3.7. Purify the reaction with 36 µL of AMPure XP bead suspension (Agencourt AMPure XP®) using a magnetic particle concentrator and elute in 20 µL.

2.3.8. Incubate the ligation reactions with 10 U of *Dpn*II in a volume of 50 µL for 1 h at 37 °C to cut unmethylated GATC sites. Heat-inactivate *Dpn*II for 20 min at 80 °C.

2.3.9. Purify the reaction with 90 µL of Agencourt AMPure XP® bead suspension and elute in 25 µL.

2.3.10. Amplify methylated DNA using Advantage® cDNA Polymerase Mix. Include a control reaction without DNA template (control C).

ddH_2O	13.75 µL
10× PCR reaction buffer	5 µL
*Dpn*II digested DNA	25 µL
Primer AdR	1.25 µL
dNTP mix (each 2.5 mM)	4 µL
Advantage cDNA Polymerase Mix	1 µL

PCR parameters:

I	68°C: 10 min
II	94°C: 1 min
III	65°C: 5 min
IV	68°C: 15 min
V	94°C: 1 min
VI	65°C: 1 min
VII	68°C: 10 min
VIII	Go to step 5 3x
IX	94°C: 1 min
X	65°C: 1 min
XI	68°C: 2 min
XII	Go to step IX 23x (embryos) or 20x (adults) (*see* **Note 8**).

2.3.11. Analyze 5 µL of PCR reaction on an agarose gel. Amplification of Dam-methylated DNA should produce a smear from 300 to 1000 bp.

2.3.12. Purify the PCR products using QIAquick PCR Purification Kit. Include an extra wash with 700 µL guanidine hydrochloride 35% before PE washing (*see* **Note 9**). Elute in 30 µL. Quantify the concentration of the DNA.

2.4. Library preparation

2.4.1. Blunt the PCR products with End-It™ DNA End-Repair Kit for 45 min at room temperature.

ddH_2O	to a final volume of 50 µL
PCR product	1 µg
10× End-Repair Buffer	5 µL
dNTP mix	5 µL
ATP	5 µL
End-Repair Enzyme Mix	1 µL

2.4.2. Purify the DNA using QIAquick PCR Purification Kit. Include an extra wash with 700 µL guanidine hydrochloride 35% before PE washing. Elute the DNA in 25 µL.

2.4.3. Incubate blunt-ended DNA fragments with Klenow for 30 min at 37°C to add 3'-A overhangs, then put the tubes on ice.

ddH_2O	18.5 µL
Blunt ended DNA	25 µL
10× NEB buffer 2	5 µL
dATP 10 mM	1 µL
Klenow Fragment	0.5 µL

2.4.4. Purify the DNA using QIAquick PCR Purification Kit. Include an extra wash with 400 µL guanidine hydrochloride 35% before PE washing. Elute the DNA in 20 µL.

2.4.5. Anneal Y-shaped Illumina adapters: combine 1:1 of upper and lower strand primers. Heat to 95°C and let cool down slowly to room temperature (annealed adapters can be stored frozen).

2.4.6. Ligate Y-shaped Illumina adapters. Incubate for 2 h at 25°C and heat-inactivate T4 ligase for 10 min at 65°C.

DNA with 3′-A overhang	8 µL (~250 ng)
10× Ligation buffer	1 µL
T4 DNA Ligase	0.5 µL
Illumina Y-Adapter	0.5 µL

2.4.7. Purify the DNA using QIAquick PCR Purification Kit. Elute the DNA in 20 µL.

2.4.8. Amplify by Illumina Index PCR (*see* **Note 10**) using the forward P5 primer and Illumina Trueseq Index primers for multiplexing.

DNA with Y-adapter	8 µL (~100 ng)
Illumina Index primer	1 µL
Forward P5 primer	1 µL
2× MyTaq enzyme mix	10 µL

PCR parameters

I	94°C:	1 min
II	94°C:	30 sec
III	58°C:	30 sec
IV	72°C:	30 sec
V	Go to step II 6-10x	
VI	72°C:	2 min

2.4.9. Purify the Index PCR material with 36 µL Agencourt AMPure XP® beads and elute in 20 µL.

2.4.10. Quantify libraries using preferably QUBIT® fluorometer or NanoDrop and submit for NGS.

3. DamID quantification and bioinformatics analysis

3.1. Evaluate the quality of raw reads and discard those reads that do not meet quality standards (*see* **Note 11**) (Dai et al., 2010). This is sometimes performed by the NGS facility, otherwise use programs such as FastQC (http://www.bioinformatics.babraham.ac.uk/projects/fastqc/). Beware that due to the peculiar nature of the DamID-seq libraries (all reads start with the same sequence of the adapter), FastQC reports a low variability in the first 20 nucleotides. To avoid this, FastQC can also be performed on the sequences once the adapter has been removed (in which case only the first four nucleotides show a high bias towards GATC).

3.2. Remove the DamID adapters using Cutadapt (Martin, 2011); (https://code.google.com/p/cutadapt/). It reads a FASTA or FASTQ file, and writes the changed sequence to standard output. Assuming your sequencing data is available as a FASTQ file, use this command line in your UNIX window:

```
$ cutadapt -g CGCGGCCGAG –e 0.15 --discard-untrimmed input.fastq -o output.fastq
```

Parameters:

-g CGCGGCCGAG; the adapter ligated to the 5′ end. -e 0.15; maximum allowed error rate (default: 0.1). This means that a single error per adapter is allowed. --

discard-untrimmed; discard untrimmed reads, i.e., removes reads resulting from DNA breaks and hence do not carry the DamID adapters.

3.3. Mapping reads to a reference genome. Currently, the main source for reference genome assembly is from the University of California Santa Cruz (UCSC). To align the reads we use Bowtie (Langmead & Salzberg, 2012); (http://bowtie-bio.sourceforge.net/index.shtml) and the *C. elegans* genome sequence (ce10, corresponding to WormBase release WS220; *see* **Note 12**). The mapping parameters are set to only map unique and best alignments (-m 1, --best):

```
$ /path-to-bowtie-programs/bowtie /path to ce10 bowtie index/genome -m 1 --best -q input_cut.fastq -S output_cut.sam
```

3.4. Read mapping programs normally use files in FASTQ format as input, and often store output in files with sequence alignment/map (SAM) format; this implies that you need to convert the file to a machine-readable binary file (BAM) before further analysis using the R/Bioconductor program. We use Samtools (http://samtools.sourceforge.net/) to convert the SAM to BAM format:

```
$ samtools view -bS input_cut_mapped. sam > output_cut_mapped.bam
```

3.5. Mapping GATC sites using RStudio (www.cran.r-project.org and http://www.rstudio.com), the packages "BSgenome. Celegans.UCSC.ce10" and "Biostring", as well as custom-made R scripts (*see* **Notes 13** and **14** and Table 3.4). The library consists of GATC-flanking DNA sequences that are used to map these to the genome. We first identify all GATC sites in the *C. elegans* genome on either strand using the "DNAstring" function. Next, the intervals corresponding to the reads are checked for the presence of a GATC sequence at the beginning (+ strand) or the end (− strand), providing an additional filtering of true DamID reads versus break-produced sequences. Mapped reads are then assigned to individual GATC in the genome and counted for each genomic GATC (*see* **Note 15**).

Table 3.4. Examples of functions used in custom-made R scripts

Function	Purpose
DNAstring	Identify and store GATC sequences.
vmatchPattern	Find all the hits of GATC pattern in *C. elegans* reference sequence.
which	Give the true indices of a logical object, in this case, strand sense.
Rle	Compute the length (frequency) and values (strand sense) of runs.
cor	Estimate correlations between libraries at GATC level.
corrplot	Generate a graphical display of correlation between libraries at GATC level, with confidence interval.
CreateSlidingRegions	Bins the *C. elegans* genome according to the parameters optStep and optWin.

3.6. Comparison of biological replicates and binning. At this step, a correlation coefficient at the GATC level can be calculated, providing a measure of the reproducibility of the observed DamID pattern. This greatly depends on the number of individual reads, but is normally very high ($R > 0.8$). As methylation of a single GATC carries a certain degree of stochasticity, it is recommended to bin the genome in fragments ranging from 1 to 100 kb, depending on the biological question. The correlation coefficient usually improves when analyzing larger genomic segments, but at the same time resolution is reduced. Thus, running the analysis several times may be advantageous for determining the ideal bin size for the protein of interest.

3.7. Normalize DamID reads per bin by the total number of DamID reads, taking into account the sequencing depth. To adjust for the accessibility of the individual GATC sites in the genome, normalize the signal for each POI by the Dam-only scores (GFP::Dam).

3.8. Averaging across replicates. It is good practice to keep replicates separated until the final step (individual Dam::POI and GFP::Dam samples). At this last stage, the average of at least two independent replicates is calculated. The data are then ready to be processed (*see* **Note 16**).

3.9. Peak Calling. Determination of the chromatin domains to which the POI associates is a central part of DamID analysis. For this, we need to assign regions with significant numbers of mapped reads (peaks). Because peak calling tools have typically been developed for ChIP-seq we must choose or adapt a peak-calling algorithm and normalization method considering: (a) the balance between sensitivity and specificity, (b) the type and dynamics of POI chromatin association (point-

source binding [e.g., transcription factors], broadly enriched [e.g., nuclear lamins]). According to the selected parameters we can affect the number and quality of the peaks called. Note that using the same enrichment metric values, such as *p*-value or false discovery rate (FDR) threshold does not ensure that the peaks are comparable across libraries. Instead, it is better to use the irreproducible discovery rate (IDR) threshold (Ivers et al., 2011), which also can guide in selecting the best peak calling algorithm and parameter settings. Existing peak callers (e.g., SPP (Kharchenko, Tolstorukov, & Park, 2008), MACS (Zhang et al., 2008), SICER (Zang et al., 2009), RSEG (Q. Song & Smith, 2011), and ZINBA (Rashid, Giresi, Ibrahim, Sun, & Lieb, 2011)) differ in terms of background modeling and signal smoothing, but most use a windows-based method to define peaks (Bailey et al., 2013). Finally, using R packages "polyaPeak" and "NarrowPeaks" we can improve the resolution through analysis of the shape of the peaks, including optimizing the bandwidth and peak cutoff parameters, and rerank and refine the final peak-calling list. Once the POI association domains are defined we can continue doing more routine analysis as peak annotation and motif analysis, according to the biological question(-s) to answer.

4. Notes

4.1. Additional cloning strategies are discussed on the van Steensel laboratory website (http://research.nki.nl/vansteensellab/DamID.htm), which also provides useful tips, FAQs and protocols for DamID in Drosophila and mammalian cells.

4.2. Using a Dam-*E. coli* as a food source is important to avoid contamination by methylated *E. coli* DNA.

4.3. To minimize variation in expression levels between different DamID strains, we recommend transgenesis by MosSCI single-copy integration techniques. MosSCI plasmids are available for fusion of the Dam protein to either the N- or the C-terminus of the POI. In both orientations a Myc-tag serves as linker between the POI and Dam. Prior knowledge on the behavior and biological activity of GFP-tagged versions of the POI might be useful (Dam and GFP are of equal size), but verification of correct localization should always be performed.

4.4. Dam is a highly active enzyme (Urig et al., 2002), and high methylation levels can be detected at both native binding and non-binding sites when Dam is overexpressed. To avoid false-positive methylation marks as well as potential

effects on gene expression or DNA replication DamID experiments are performed with minimal expression of the Dam::POI transgenes. For *C. elegans*, we use an inducible heat shock promoter (*hsp-16.41*) without induction.

4.5. We use the *unc-54* 3′ UTR in our DamID vectors; other 3′ UTRs could potentially be used to alter the relative signal contribution by different cell types in whole-animal DamID (Mangone et al., 2010).

4.6. Upon heat shock induction, signals corresponding to the Dam fusion protein should be detectable by immunofluorescence and Western blot. A sample without induction is included as control, which corroborates the low basal transcriptional activity of the *hsp-16.41* promoter during the DamID experiment.

4.7. Control B is an important indicator of unspecific breaks produced during gDNA purification the technique. Optionally, include also a control with gDNA purified in parallel from wild type nematodes.

4.8. When using a new batch of Advantage cDNA Polymerase Mix, optimize the total number of PCR cycles required for amplification. Collect 10 µL of the PCR reaction after every two cycles ranging from cycle number 14 to 22 (last cycle).

4.9. Guanidine hydrochloride is used to ensure the complete removal of PCR primers and primer dimers, thereby avoiding the amplification of these primers during the sequencing reaction.

4.10. Make two Illumina Index PCR reactions: one to run on a 1 % agarose gel to inspect the quality of the library and one to purify for NGS.

4.11. Analysis of NGS data is a computational intensive process and requires several software tools, most of which are oriented toward UNIX operating systems. Three main approaches to analyze NGS data, either individually or in combination, exist: (1) Programming to run in a UNIX environment (e.g., Linux, Solaris, Mac OS X, or Windows through Cygwin (https:// www.cygwin.com/)), (2) R/Bioconductor packages for the R computing environment. Table 3.5 lists useful packages available for sequence analysis. (3) Upload data to online servers. Currently, the most popular web server is Galaxy (http://galaxyproject.org/), which hosts several analysis tools.

4.12. The genome database release version is very important when mapping NGS reads. Reads mapped to one version are not directly interchangeable with reads mapped to a different version. The UCSC liftover tool is very useful, but note that repeated remapping of data can yield different results. We recommend using genomes curated at UCSC so that you can easily visualize your data later using the UCSC Genome Browser (http://genome.ucsc.edu).

Table 3.5. Examples of Bioconductor packages for NGS analysis

Purpose	Packages
Data representation	Biostrings, Bsgenome, GenomicRanges, Iranges, VariantAnnotation
Input/Output	ShortRead (FASTQ), Rsamtools (BAM), rtracklayer (GFF, WIG, BED), VariantAnnotation (VCF)
Annotation	AnnotationHub, biomaRT, ChIPpeakANNo, GenomicFeatures, VarianAnnotation
Alignment	Biostrings, gmapR, Rsubread
Visualization	Gviz, ggbio, corrplot
Peak calling	PolyaPeak, NarrowPeaks, Bayespeak, ChIPpeakAnno

4.13. Each replicate should have three to nine million uniquely mapped reads, of which two to eight million reads start with GATC. We are usually able to identify between 65 and 89 % of genomic GATC sites.

4.14. From this point the data analysis becomes more specific to the technique of DamID-seq (compared to for example ChIP-seq) due to the focus exclusively on GATC sites in the genome. The existing algorithms to analyze ChIP-seq data (e.g., SPP and MACS) are based on the assumption that signals are symmetrically distributed. In DamID-seq experiments, one cannot assume that the adenine methylation signals are symmetrical, because the enzymatic process is affected by many factors, such as chromatin 3D structure (Sha et al., 2010b). This challenged us to develop new scripts ((Sharma et al., 2014, 2016); available upon request).

4.15. At this point we generate in R a GenomicRange file (GRanges) containing all the GATC counts as well as a series of genomic features. The GRanges class represents a collection of genomic features that each have a single start and end location on the genome. This includes features or annotations (metadata elements) such as score, transcripts, and exons. These objects can be created by using the GRanges constructor function. Then, we add the data-frame containing the counts of the individual GATC sites as a metadata column in the GRanges file.

4.16. It is good practice, and a requirement by several journals, to deposit data at the public genomic data repository Gene Expression Omnibus (GEO; http://www.ncbi.nlm.nih.gov/geo/).

Chapter IV

Results From Objective 1

Research paper

Identification of Conserved MEL-28/ELYS Domains with Essential Roles in Nuclear Assembly and Chromosome Segregation

Georgina Gómez-Saldivar[1*], Anita Fernandez[2*+], Yasuhiro Hirano[3], Michael Mauro[2], Allison Lai[2], Cristina Ayuso[1], Tokuko Haraguchi[3,4], Yasushi Hiraoka[3,4], Fabio Piano[5,6] and Peter Askjaer[1+]

1 Andalusian Center for Developmental Biology (CABD), CSIC/Junta de Andalucia/Universidad Pablo de Olavide, Seville, Spain, **2** Biology Department, Fairfield University, Fairfield, Connecticut, United States of America, **3** Graduate School of Frontier Biosciences, Osaka University, Suita, Japan, **4** Advanced ICT Research Institute Kobe, National Institute of Information and Communications Technology, Kobe, Japan, **5** Department of Biology and Center for Genomics and Systems Biology, New York University, New York, New York, United States of America, **6** New York University, Abu Dhabi, United Arab Emirates.

*These authors contributed equally to this work.

+ Corresponding authors: afernandez@fairfield.edu (AF); pask@upo.es (PA)

PLoS Genet. 2016 Jun 24;12(6):e1006131. doi: 10.1371/journal.pgen.1006131. eCollection 2016.

Results

MEL-28 is required for meiotic chromosome segregation

We previously reported that *C. elegans* MEL-28 is broadly expressed (Galy, Askjaer, Franz, López-Iglesias, et al., 2006a). However, a promoter study of 127 genes in *C. elegans* embryos suggested that MEL-28 is highly enriched in the intestinal E lineage ~200 min after fertilization (Murray et al., 2012). We therefore revisited MEL-28 expression to analyze it in greater detail. Immunofluorescence analysis detected similar levels of MEL-28 in nuclei of all embryonic cells (Figure 4.1A) and all postembryonic tissues (Figure 4.1B). Next, using CRISPR-Cas9 technology (Dobrzynska, Askjaer, et al., 2016), we generated a GFP knock-in *mel-28* allele to analyze the expression of endogenous MEL-28 by live microscopy. Similar to the observations with antibodies against MEL-28, GFP::MEL-28 localized to the NE in all cell types during embryonic and larval development and in adults (Figure 4.1C). Thus, we conclude that MEL-28 is ubiquitously expressed throughout *C. elegans* development.

MEL-28 strongly accumulated on condensed oocyte chromosomes ((Figure 4.1C; (Ertl et al., 2016; Fernandez & Piano, 2006)). Moreover, we noted during our initial studies of *mel-28* mutant or RNAi-treated embryos that formation and migration of the maternal pronucleus was often more severely affected than the paternal pronucleus (Fernandez & Piano, 2006; Galy, Askjaer, Franz, López-Iglesias, et al., 2006a). Based on these observations we speculated that MEL-28 might have important functions in meiosis. *C. elegans* oocytes are arranged in a linear fashion in the proximal part of the gonad, where each oocyte is numbered relative to the spermatheca (-1, -2, -3, etc.) (Greenstein, 2005). The -1 oocyte completes maturation including germinal vesicle breakdown immediately before ovulation and fertilization triggers rapid progression through meiosis I and II. To examine these processes we performed live *in utero* recordings of animals expressing GFP::MEL-28 and mCherry::HisH2B. In the -4 oocyte, MEL-28 localized to the NE and was absent from condensed chromosomes (Figure 4.2A). In the -3 and -2 oocytes MEL-28 gradually moved away from the NE and accumulated uniformly on meiotic chromosomes. Later, in the -1 oocyte MEL-28 redistributed to cover the surface of meiotic chromosomes (Figure 4.2A), in some cases completely enclosing the chromosomes and in other cases similar to the “cup-shaped” localization of kinetochore proteins, such as KNL-1 and KNL-3 (Dumont et al., 2010).

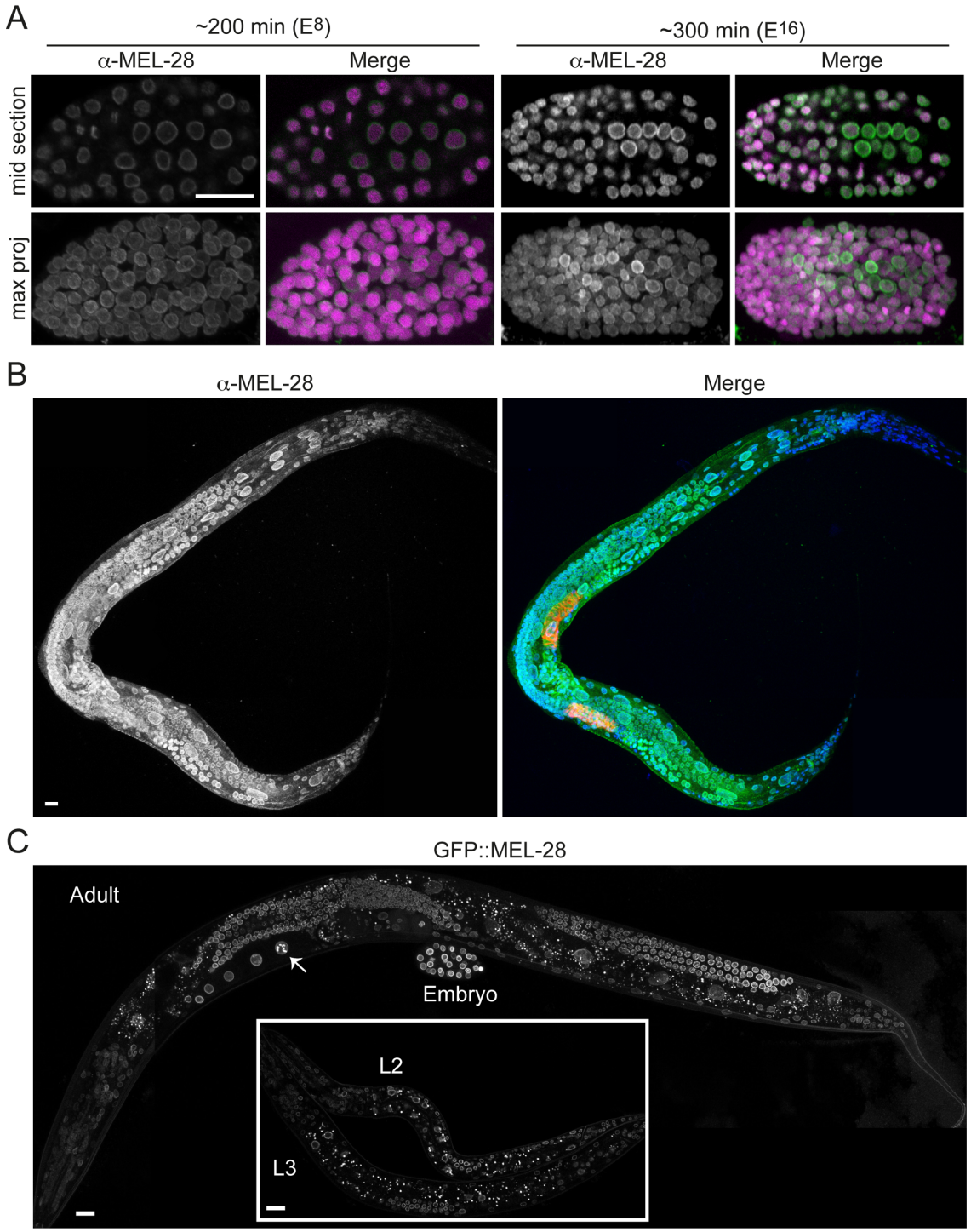

Figure 4.1 MEL-28 is ubiquitously expressed. (A) Embryos were fixed and analyzed with antibodies against MEL-28 and Hoechst to stain DNA (green and magenta in merge, respectively). Single confocal mid sections and maximum projections indicate that MEL-28 is uniformly expressed in all embryonic cells. Approximate developmental time is indicated from fertilization. (B) Maximum projections of confocal sections of L4 larva analyzed with Hoechst (blue in merge) and anti-MEL-28 and MH27 antibodies (green and red, respectively). (C) Maximum projection of confocal sections of adult and embryo showing ubiquitous GFP::MEL-28 expression in GFP knock-in strain. Insert represents a confocal mid section of L2 and L3 larvae. Arrow points to a mature oocyte with MEL-28 localization to condensed chromosomes. Scale bars, 10 µm.

The association of MEL-28 with chromosomes persisted throughout meiosis I and II until pronuclear formation ~30 minutes after germinal vesicle breakdown (Figure 4.2B). The localization pattern of MEL-28 suggested a possible role during segregation of meiotic chromosomes, similar to the situation in mitosis (Fernandez & Piano, 2006; Galy, Askjaer, Franz, López-Iglesias, et al., 2006a). We therefore analyzed *mel-28(t1684)* embryos expressing GFP::β-tubulin and mCherry::HisH2B. *mel-28(t1684)* encodes a premature termination codon at aa. 766 and behaves like a strong loss-of-function of MEL-28, presumably due to nonsense-mediated mRNA decay (Galy, Askjaer, Franz, López-Iglesias, et al., 2006a). Maternal contribution enables homozygous *mel-28(t1684)* hermaphrodites to develop until adulthood but they produce only unviable embryos (hereafter referred to as *mel-28* embryos, whereas embryos produced by heterozygous siblings are referred to as control or *mel-28/+* embryos) with severe NE assembly defects (Galy, Askjaer, Franz, López-Iglesias, et al., 2006a). Strikingly, in *mel-28* embryos chromosomes failed to segregate in anaphase I (n=5/6 embryos) and anaphase II (n=4/6) and, consequently, *mel-28* embryos had either no (n=4/6) or a single (n=2/6) polar body, whereas control embryos had two polar bodies (n=6/6; Figure 4.2C). In addition, chromosomes in *mel-28* embryos were not organized in a pronucleus but appeared scattered in the cytoplasm (Fig 1C; 36:00). To our knowledge, this is the first report describing the involvement of MEL-28/ELYS in meiosis, expanding previously described MEL-28 functions and establishing an important role in chromosome segregation during both meiosis and mitosis.

The MEL-28 N-terminus is required for NPC association

To characterize which regions of MEL-28 are required for its different functions, we examined full-length and truncated versions of MEL-28 fused to GFP and tracked their localization in live *C. elegans* embryos. While most transgenes are expressed (Figure 4.3 and 4.9), some exhibit localization patterns distinct from full-length MEL-28 (see below). During interphase full-length MEL-28 was mainly localized to the NE but was also found in the nucleoplasm (Figure 4.4A). In prophase and prometaphase, MEL-28 left the NE before complete NE breakdown and associated to the condensing chromosomes. By metaphase, MEL-28 appeared as two lines parallel to the metaphase plate, resembling the characteristic pattern of holocentric kinetochore proteins, and less abundantly to the area of the mitotic spindle (Figure 4.4A-D). During anaphase, MEL-28 associated to decondensing chromosomes, and re-localized to reforming NE in telophase (Figure 4.4A).

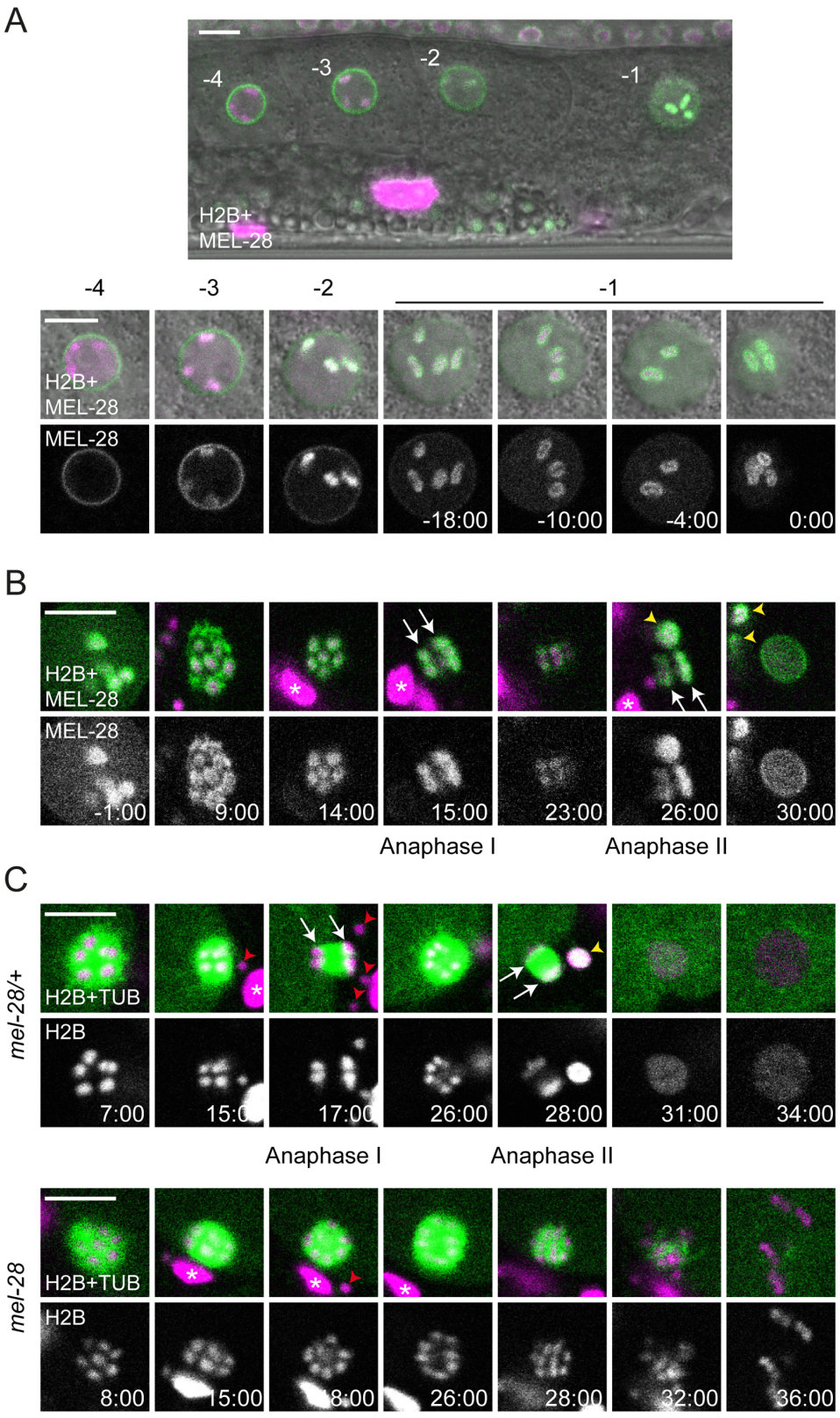

Figure 4.2. MEL-28 is essential for female meiosis. (A) GFP::MEL-28 (green in merged images) was expressed in oocytes and accumulated at kinetochores of meiotic chromosomes (visualized with

mCherry::HisH2B; magenta in merge). Shown are the four most proximal oocytes where position -1 is immediately next to the spermatheca. The -1 oocyte was observed every two minutes until germinal vesicle breakdown. (B) GFP::MEL-28 associated with chromosomes throughout meiosis I and II and accumulated at the NE at pronuclear formation. (C) Chromosomes (magenta) and meiotic spindles (green) were observed *in utero*. Anaphase I and II were characterized by abundant microtubules between segregating chromosomes in control *mel-28/+* animals (top) whereas chromosomes failed to segregate in homozygous *mel-28* mutants (bottom). White arrows point to segregating chromosomes. Red arrowheads and white asterisks mark sperm and somatic nuclei, respectively, outside the fertilized oocyte; yellow arrowheads indicate polar bodies. Time is indicated relative to germinal vesicle breakdown (min:sec). Scale bars, 5 µm.

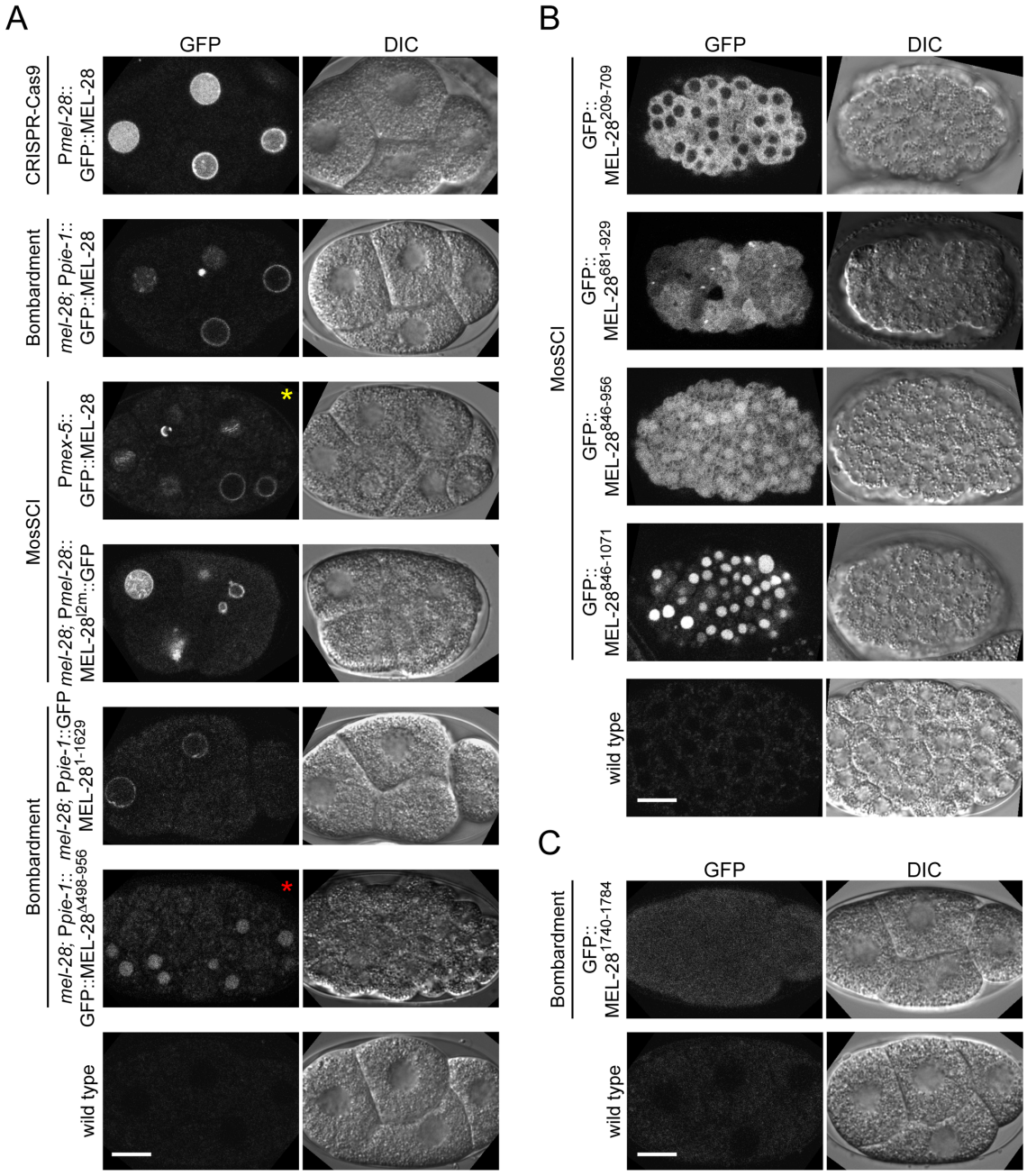

Figure 4.3. Analysis of MEL-28 expression levels. (A) Compared to a strain that expresses GFP::MEL-28 from the endogenous *mel-28* locus after CRISPR/Cas9-mediated GFP knock-in (top panel), expression of GFP::MEL-28 full-length and mutant proteins from transgenes inserted by microparticle bombardment or MosSCI is either similar or lower, thus arguing against the possibility of artifacts induced by overexpression. Confocal images were acquired with identical settings (laser power = 7% and PMT high voltage = 150) except P_{mex-5}::GFP::MEL-28 (yellow asterisk; laser power = 9%) and *mel-28*; P_{pie-1}::GFP::MEL-$28^{\Delta 498-956}$ (red asterisk; laser power = 8%). (B) Comparison of GFP::MEL-28 fragments expressed from heat shock-induced single copy transgenes containing the *hsp-16.41* promoter. Older embryos are shown because induction is inefficient in young embryos. Confocal images were taken with identical settings (laser power = 5% and PMT high voltage = 150). (C) A GFP::MEL-$28^{1740-1784}$ fragment expressed under control of the *pie-1* promoter is visible in early embryos and localizes diffusely throughout the cell (laser power = 8% and PMT high voltage = 160). Wild type embryos not expressing GFP were observed with identical microscope settings and included as controls in A-C. Scale bars, 10 µm.

We next analyzed a putative coiled-coil domain placed in the central part of the protein and which might be engaged in protein–protein interactions. However, GFP::MEL-28 lacking aa. 1140-1186 localized similarly to full-length MEL-28 (Figure 4.4C). During interphase MEL-$28^{\Delta 1140-1186}$ was enriched at the NE and shuttled to kinetochores in mitosis whereas reduced signal was observed at the mitotic spindle (Figure 4.4D). Moreover, expression of GFP::MEL-$28^{\Delta 1140-1186}$ completely rescued the embryonic lethality of *mel-28* mutant embryos (Table 4.1). This demonstrated that the putative coiled-coil domain as well as enrichment at the mitotic spindle is dispensable for MEL-28 function.

Table 4.1. Rescue efficiencies by MEL-28 fragments

MEL-28 fragment[a]	Promoter	*n*[b]	Embryonic lethality[d]	S.D.[g]
-	-	964	100%	0
GFP::MEL-28	Constitutive	372	7.1%[e]	10.8
GFP::MEL-$28^{\Delta 1140–1186}$	Constitutive	632	1%	1.5
GFP::MEL-28^{1-1744}	Constitutive	1424	65.9%	21.4
GFP::MEL-28^{1-1629}	Constitutive	1384	99.4%	1.3
GFP::MEL-$28^{508-1784}$	Constitutive	240	100%	0
GFP::MEL-$28^{\Delta 498–956}$	Constitutive	202	100%	0
MEL-$28^{loop2mut}$::GFP	Constitutive	512	100%	0
GFP::MEL-28	Inducible	328[c]	No[f]	-
GFP::MEL-28^{1-1601}	Inducible	255[c]	Yes[f]	-
GFP::MEL-$28^{\Delta 1239–1728}$	Inducible	117[c]	Yes[f]	-

[a] GFP::MEL-28 fusions were expressed in *mel-28(t1684)* mutants.

[b,c] The number of embryos[b] or worms[c] analyzed is indicated.

[d] Percentage of unhatched embryos.

[e] This strain was also homozygous for *unc-32(e189)*, which may have influenced the incomplete rescue.

[f] Qualitative analysis was done for fragments under control of an inducible promoter due to heterogeneity of the expression.

[g] Standard deviation.

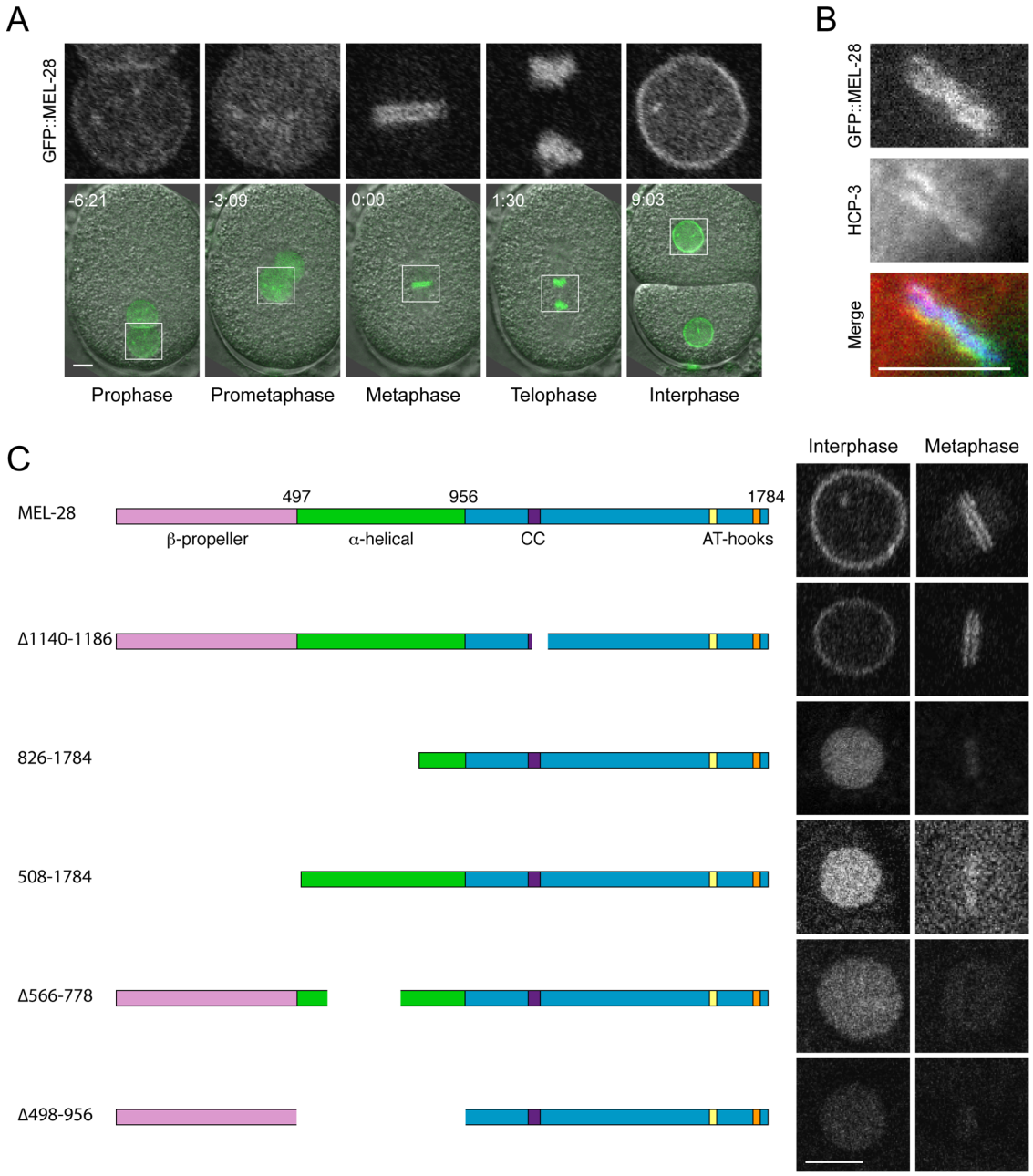

Figure 4.4. MEL-28 N-terminal domains are required for NPC and kinetochore localization. (A) Still images from time-lapse recording of embryo carrying a GFP insertion into the endogenous *mel-28* locus. Time is indicated relative to anaphase onset (min:sec). (B) Metaphase plate of early embryo expressing GFP::MEL-28 (green in merge) analyzed by immunofluorescence with a specific antibody against HCP-3/CENP-A (red in merge) and Hoechst (blue in merge) to visualize chromosomes. MEL-28 localized to kinetochores, which appear as lines on both sides of the chromosomes. (C) Cropped images from embryos expressing different MEL-28 truncations fused to GFP. Except GFP::MEL-28 and GFP::MEL-28$^{\Delta 1140\text{-}1186}$ embryos, all embryos also expressed un-tagged endogenous MEL-28. Purple boxes in MEL-28 cartoons indicate a putative coiled-coil domain (aa. 1127-1160) whereas yellow (aa. 1630-1642) and orange (aa. 1746-1758) boxes indicate AT-hook sequences: their homology to the consensus AT-hook sequence is low and high, respectively. (D) Cropped images from metaphase embryos expressing GFP::MEL-28 or GFP::MEL-28$^{\Delta 1140\text{-}1186}$. Images were processed identically to facilitate visualization of full-length GFP::MEL-28 associated with the mitotic spindle. Signal intensities in boxed areas were quantified in raw images, normalized and plotted (n=5, GFP::MEL-28; n=2, GFP::MEL-28$^{\Delta 1140\text{-}1186}$). * $p<0.05$ by unpaired two-tailed t-test. Scale bars, 5 µm.

Recently, Bilokapic and Schwartz found that the N-terminal half of ELYS containing the β-propeller and α-helical domains localized to the NE in HeLa cells (Silvija Bilokapic & Schwartz, 2013a). However, the relevance of these domains has not been analyzed in the context of full-length MEL-28/ELYS. We first deleted the β-propeller and most of the α-helical domain (GFP::MEL-28$^{826\text{-}1784}$) and found that both NE localization during interphase and kinetochore localization in mitosis were abrogated (Figure 4.4C). Instead, the truncated protein was found in the nucleoplasm and weakly associated with chromosomes during interphase and metaphase, respectively (note that kinetochore localization appears as two parallel lines whereas a single line reflects more uniform chromosome association). Similar mis-localization was observed on deletion of aa. 1-507 (GFP::MEL-28$^{508\text{-}1784}$) or aa. 498-956 (GFP::MEL-28$^{\Delta 498\text{-}956}$), whereas deletion of aa. 566-778 (GFP::MEL-28$^{\Delta 566\text{-}778}$) also abolished the weak association to mitotic chromosomes (Figure 4.4C). Together, these results demonstrate that both the β-propeller and the α-helical domain are required for targeting MEL-28 to NPCs and to kinetochores. All four N-terminally truncated MEL-28 proteins accumulated in the nucleus in interphase, suggesting that the C-terminal unstructured domain of MEL-28 contains one or more nuclear localization signals (NLS's; see below).

Finally, we assessed whether the truncations in the β-propeller and α-helical domains interfered with MEL-28 function. As expected from the severe mis-localization, ectopic expression of any of the four MEL-28 truncations failed to restore viability of *mel-28* embryos (Table 4.1), suggesting that the localization of MEL-28 to NPCs and kinetochores is essential to MEL-28 function. We conclude from these experiments that the N terminus of MEL-28 is required for proper MEL-28 localization and functions. Whereas its importance for

NPC localization is concordant with data on ELYS our experiments revealed a novel role in kinetochore association.

MEL-28 loop2 is required during meiosis and mitosis

Bilokapic and Schwartz identified through protein crystallization and sequence alignments two conserved loops (loop1 and loop2) on the surface of the β-propeller of ELYS (Silvija Bilokapic & Schwartz, 2013a). When they substituted 5 aa. within loop2 the structural fold of the β-propeller was maintained but NPC localization of the N-terminal half of ELYS (aa. 1-1018) fused to GFP was abrogated in HeLa cells. To test the relevance of loop2 in the context of full-length protein we introduced the equivalent aa. substitutions in MEL-28 (D409S/Y412S/R415A/V416S/P417G; MEL-28loop2mut; Figure 4.5A).

In mel-28/+ embryos MEL-28loop2mut::GFP localized normally during interphase and mitosis (Figure 4.5A, left panels; compare with wild type GFP::MEL-28 in Figure 4.4A), suggesting that loop2 residues are not essential for association of full-length MEL-28 with NPCs or kinetochores. However, MEL-28^{loop2mut}::GFP was not able to substitute for endogenous MEL-28: *mel-28* embryos expressing MEL-28^{loop2mut}::GFP were unviable (Table 4.1) and had frequent meiosis defects as evidenced by failure in polar body extrusion and presence of multiple female pronuclei (Figure 4.5A, right panels; Figure 4.5B). Moreover, pronuclei were abnormally small, contained less MEL-28^{loop2mut}::GFP and did not position properly. In 83% of *mel-28*; MEL-28^{loop2mut}::GFP embryos (n=10/12) female and male pronuclei did not meet before the first mitotic division. Instead, only the male pronucleus was positioned between the centrosomes, whereas female pronuclei exhibited shorter migration and remained in the anterior of the embryo.

During mitosis chromosomes failed to congress to the metaphase plate (Figure 4.5A; 0:00) and severe segregation defects were observed (Figure 4.5A; 20:00-31:45). We also noticed alterations in cell cycle timing, in particular for the posterior P1 blastomere at the two-cell stage. In *mel-28*; GFP::MEL-28 and *mel-28/+*; MEL-28^{loop2mut}::GFP embryos the cell cycle of P1 lasted ~1075 sec, whereas it lasted ~1513 sec (41% delay) in *mel-28* embryos expressing MEL-28^{loop2mut}::GFP (Figure 4.5C). Other frequent defects included cleavage furrow regression (37%; n=6/16) and abnormal positioning of cells within the eggshell (53%; n=8/15).

To analyze if the conserved loop2 is required for MEL-28's role in NPC assembly we performed immunofluorescence on *mel-28*; MEL-28^{loop2mut}::GFP embryos and compared

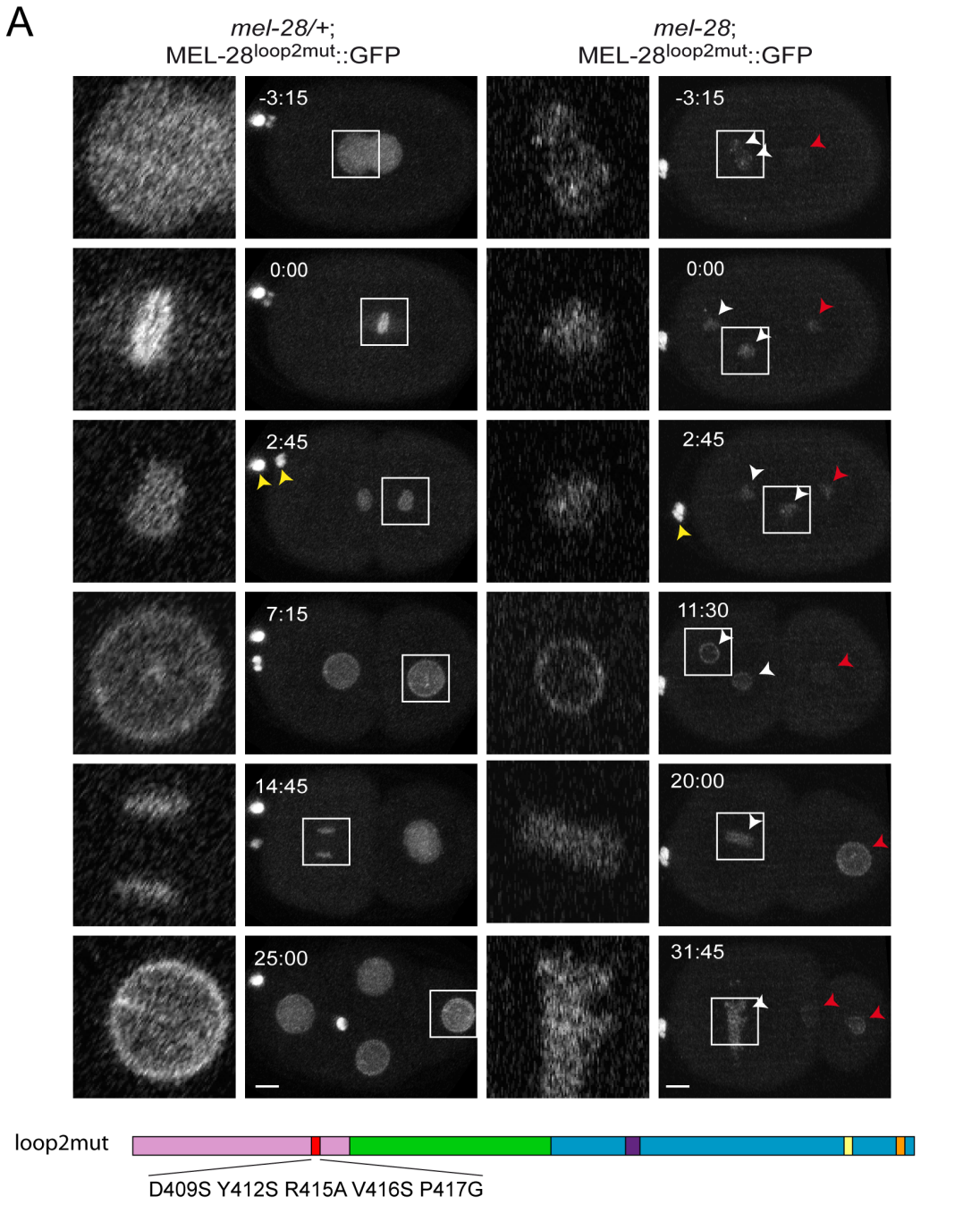
A
mel-28/+;
MEL-28loop2mut::GFP
mel-28;
MEL-28loop2mut::GFP
-3:15
0:00
2:45
7:15
14:45
25:00
11:30
20:00
31:45
loop2mut
D409S Y412S R415A V416S P417G
B
Frequency (%)
Polar bodies
1
2
n=7
n=14
mel-28/+;
mel-28;
MEL-28loop2mut::GFP
C
P1 cell cycle duration (sec)
n=7
n=6
n=6
mel-28;
GFP::MEL-28
mel-28/+;
mel-28;
MEL-28loop2mut::GFP

Fig 4.5. MEL-28 loop2 is required during meiosis and mitosis. (A) Still images from time-lapse recordings of control (left) and *mel-28* (right) embryos expressing MEL-28^{loop2mut}::GFP. Note the presence of two polar bodies in the left embryo but only a single polar body in the right embryo (yellow arrowheads). Concordantly, two oocyte-derived pronuclei were observed in the right embryo (white arrowheads). Red arrowheads indicate sperm-derived chromosomes. Whole-embryo images are max projections; inserts are single confocal sections. Scale bars, 5 µm. (B) Frequency of embryos with a single or two polar bodies. ** p<0.01 by Fisher exact test. (C) Timing from P0 division to P1 division is significantly delayed in *mel-28* embryos expressing MEL-28^{loop2mut}::GFP. *** p<0.001 by unpaired two-tailed t-test.

them with wild type, *mel-28*, and *mel-28*; GFP::MEL-28 embryos. One-cell and four-cell stage embryos were analyzed for meiotic and mitotic defects, respectively, using mAb414 to visualize multiple Nups and specific antibodies against NPP-10C/NUP96, which is a component of the NUP107 complex (Galy et al., 2003). Uniform peripheral signal was observed at pronuclei of wild type and *mel-28*; GFP::MEL-28 one-cell stage embryos, whereas fragmented pronuclei with inconsistent Nup signal was detected in *mel-28*; MEL-28^{loop2mut}::GFP and *mel-28* embryos (Figure 4.6A). Analysis of four-cell stage *mel-28*; MEL-28^{loop2mut}::GFP embryos confirmed the defects in chromosome segregation observed by live imaging and revealed that although nuclei with peripheral Nup localization are formed, these are smaller than in wild type and *mel-28*; GFP::MEL-28 embryos (Figure 4.6B). The NE phenotypes in *mel-28*; MEL-28^{loop2mut}::GFP embryos were less severe when compared to *mel-28* embryos. As previously reported, nuclear reformation and NPC assembly was strongly inhibited in *mel-28* embryos although a few cells had larger nuclei with irregular NE-structure (Figure 4.6B; bottom *mel-28* embryo). From these data we conclude that MEL-28's loop2 is essential for correct chromosome segregation both in meiosis and mitosis but not strictly required for post mitotic NPC assembly, nor for incorporation into the NE.

Identification of MEL-28 nuclear localization and chromatin association domains

The observation that perturbations in MEL-28's N-terminal half do not prevent nuclear accumulation of MEL-28 prompted us to analyze the C-terminus for functional domains. We first expressed GFP::MEL-28$^{1-1744}$, which lacks 40 aa. from the C-terminal end including one of the two AT-hook motifs. This short truncation did not interfere with MEL-28 localization in interphase nor during mitosis (Figure 4.7). However, expression of GFP::MEL-28$^{1-1744}$ res-

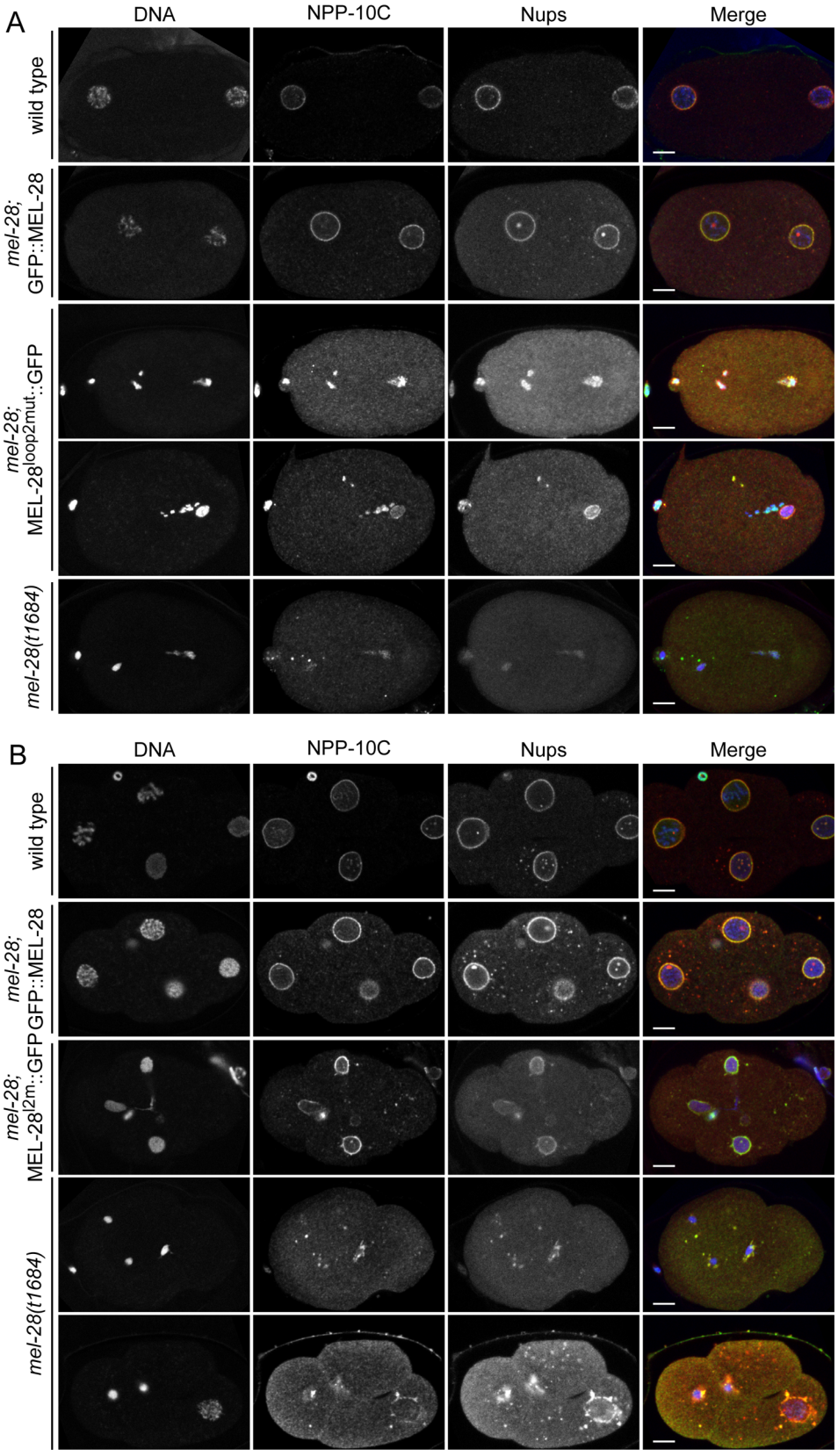

Figure 4.6. Mutation of MEL-28 loop2 impairs chromosome segregation. One-cell stage (A) and 4-cell stage (B) embryos from *mel-28* mutants expressing either GFP::MEL-28 or MEL-28$^{loop2mut.}$::GFP were compared with wild type and *mel-28* embryos by immunofluorescence. Embryos were analyzed with Hoechst (blue in merge), a

specific antibody against NPP-10C/NUP96 (green in merge) and mAb414 recognizing multiple nups (red in merge). Scale bars, 5 μm.

cued lethality in only ~35% of *mel-28* embryos (Table 4.1), indicating that the C-terminal AT hook of MEL-28 contributed significantly to MEL-28 activity. Next, we deleted aa. 1239-1728, including the other AT-hook motif. This reduced slightly the NE accumulation at interphase (Figure 4.7; GFP::MEL-28$^{\Delta 1239\text{-}1728}$). Importantly, expression of GFP::MEL-28$^{\Delta 1239\text{-}1728}$ was not able to rescue the embryonic lethality of *mel-28* embryos (Table 4.1), which suggests that there are domains within this region required for MEL-28 function. Despite several attempts, we were unable to express a MEL-28 aa. 1-956 fragment consisting of wild type β-propeller and α-helical domains (Figure 4.8). In contrast, a similar fragment, but with the five aa. substitutions in loop2 described above was efficiently expressed (MEL-28$^{1\text{-}956_l2m}$::GFP). MEL-28$^{1\text{-}956_l2m}$::GFP localized to the cytoplasm and NE, but its relative NE accumulation compared to kinetochore localization was dramatically reduced (Figure 4.9). As expected, expression of MEL-28$^{1\text{-}956_l2m}$::GFP did not rescue the embryonic lethality of *mel-28* embryos (Table 4.1). Taken together with the results presented in Figure 4.4, we conclude that although the N-terminal β-propeller and α-helical domains are the main determinants for NPC and kinetochore localization, the C-terminal portion of MEL-28 also contributes significantly.

A divergent ~300 aa. MEL -28/ELYS homolog termed ELY5 was recently identified in several fungi (Asakawa et al., 2010; H.-L. Liu, De Souza, Osmani, & Osmani, 2009). Although our experiments presented above would suggest that the part of MEL-28 equivalent to ELY5 (identified as aa. 696-927 by (S. Bilokapic & Schwartz, 2012)) does not contain the domains required for NPC localization we nevertheless expressed a fragment containing aa. 681-929 fused to GFP. As expected, this fragment did not localize to the NE or to kinetochores but showed instead diffuse cytoplasmic signal throughout the cell cycle (Figure 4.7; GFP::MEL-28$^{681\text{-}929}$; Figure 4.3B).

We next expressed a series of overlapping fragments from aa. 681 to the C-terminal end. All fragments that contained aa. 846-1071 accumulated efficiently in the nucleus (Figure 4.7; GFP::MEL-28$^{681\text{-}1350}$, GFP::MEL-28$^{846\text{-}1071}$, GFP::MEL-28$^{846\text{-}1350}$, and GFP::MEL-28$^{846\text{-}1601}$; Figure 4.8A; GFP::MEL-28$^{846\text{-}1167}$). A shorter fragment consisting of aa. 846-956 behaved similarly to free GFP (Figure 4.8A; GFP::MEL-28$^{846\text{-}956}$). Nuclear accumulation was also detected for GFP::MEL-28$^{1188\text{-}1784}$, but not for GFP::MEL-28$^{1161\text{-}1601}$ or GFP::MEL-28$^{1239\text{-}1601}$

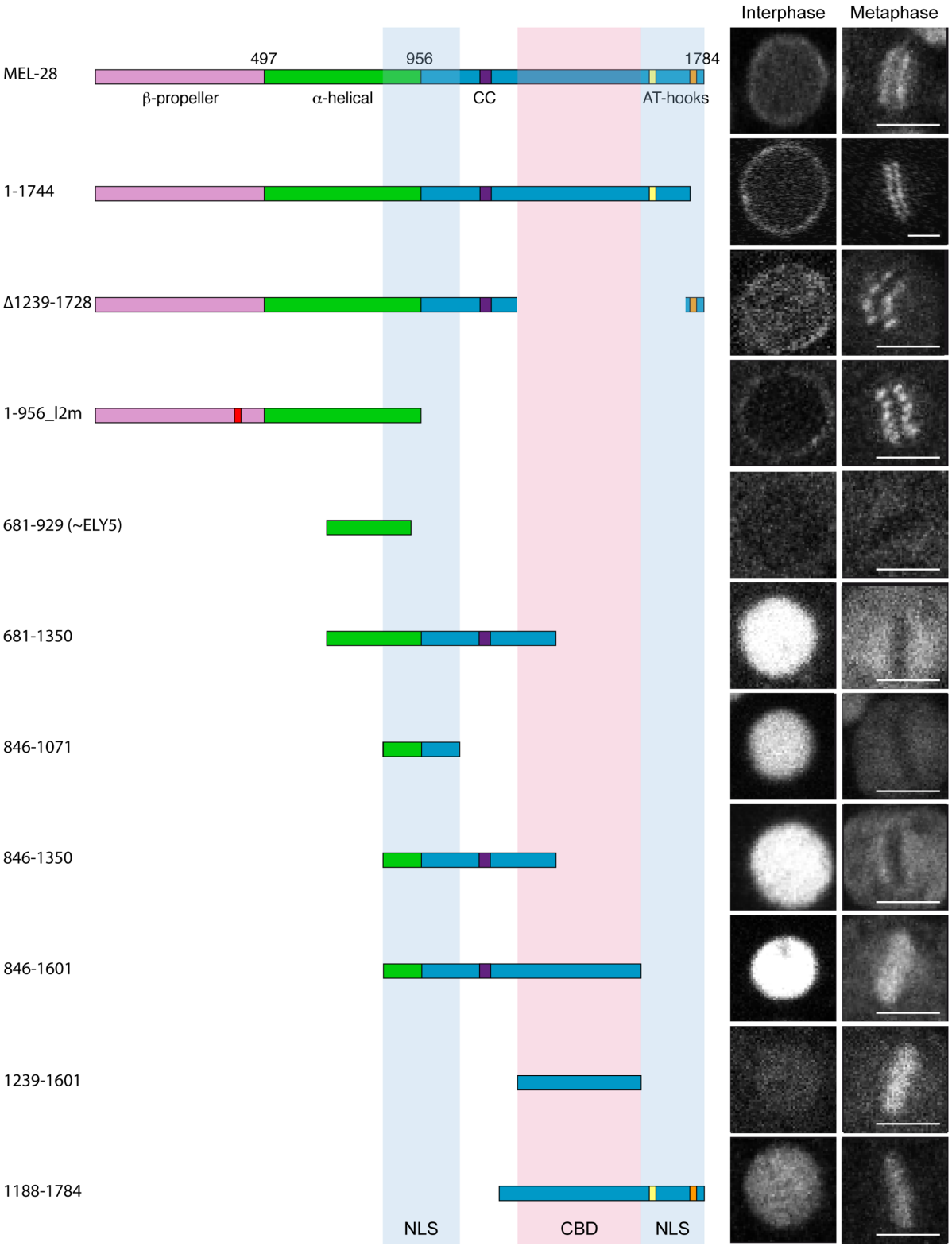

Figure 4.7. Identification of MEL-28 chromatin binding domain and nuclear localization signals. Cropped images from embryos expressing different MEL-28 truncations fused to GFP. Except GFP::MEL-28$^{1-1744}$ and GFP::MEL-28$^{1188-1784}$, fusion proteins were expressed from the *hsp-16.41* promoter in gastrulating embryos. Excluding GFP::MEL-28$^{1-1744}$ embryos, all embryos also expressed un-tagged endogenous MEL-28. Truncations containing MEL-28 residues 846-1071 and/or residues 1602-1784 (blue shading) were efficiently imported

whereas truncations containing residues 1239-1601 (red shading) associated with chromatin in mitosis. Scale bars, 3 µm.

(Figure 4.7 and 4.8A). These observations are consistent with MEL-28 having at least two NLS's mapping to the regions 846-1071 and 1601-1784. Moreover, using the NLS prediction software "cNLS Mapper" (Kosugi, Hasebe, Tomita, & Yanagawa, 2009) we identified several putative mono- and bipartite NLSs in these regions: two in the central region (aa. 942-970 and 1033-1062 with scores 5.9 and 5.2, respectively) and three in the C-terminal region (aa. 1606-1636, 1682-1709 and 1741-1773 with scores 5.7, 7.4 and 5.3, respectively). Analysis of these C-terminal fragments also revealed that aa. 1239-1601 confer strong chromatin binding during mitosis (Figure 4.7).

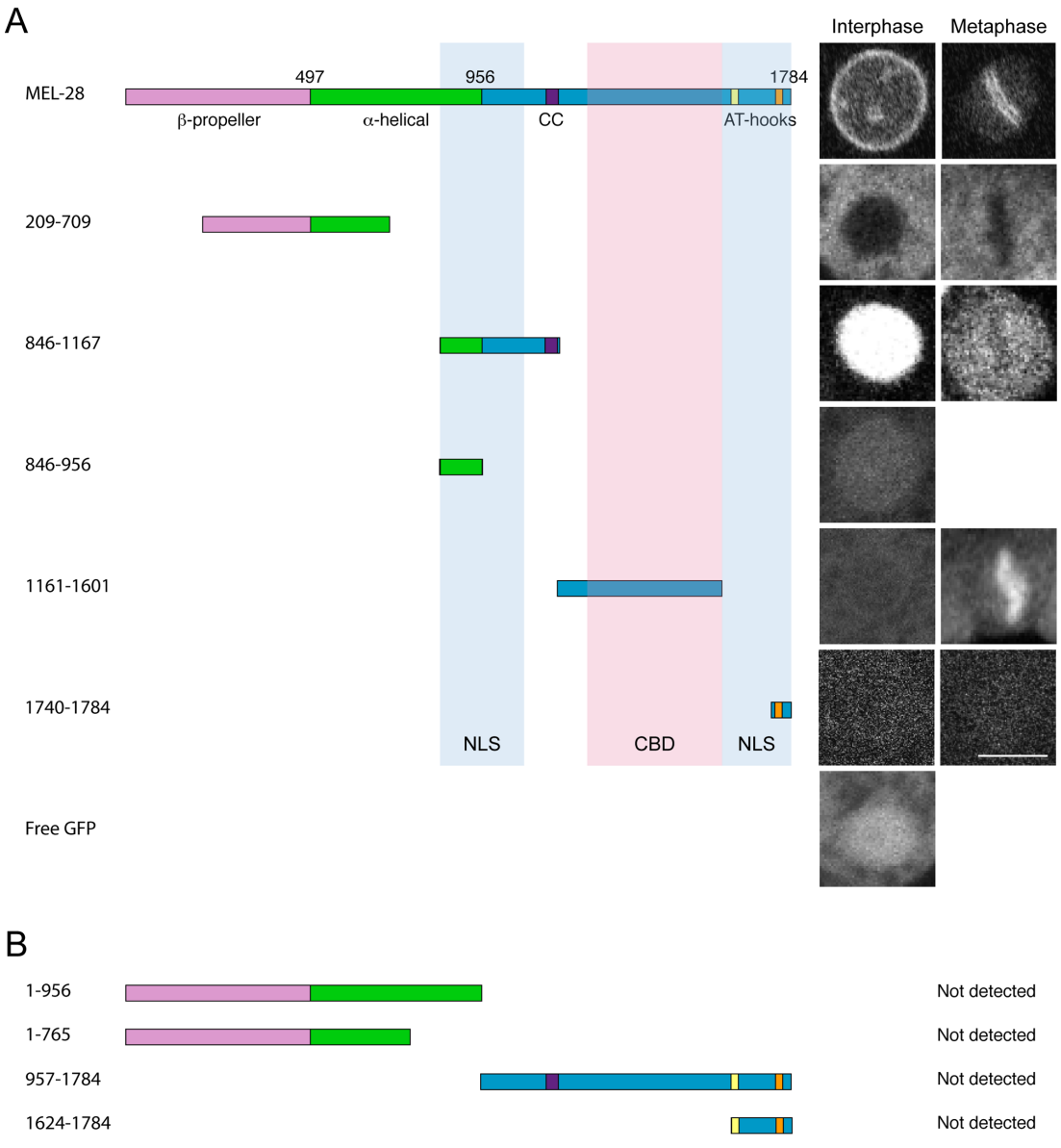

Figure 4.8. Analysis of additional MEL-28 fragments. (A) Cropped images from embryos expressing different MEL-28 truncations fused to GFP. Except GFP::MEL-28 all embryos also expressed untagged endogenous MEL-28. (B) MEL-28 truncations for which several transgenic lines were obtained but without showing GFP expression, potentially reflecting reduced mRNA or protein stability.

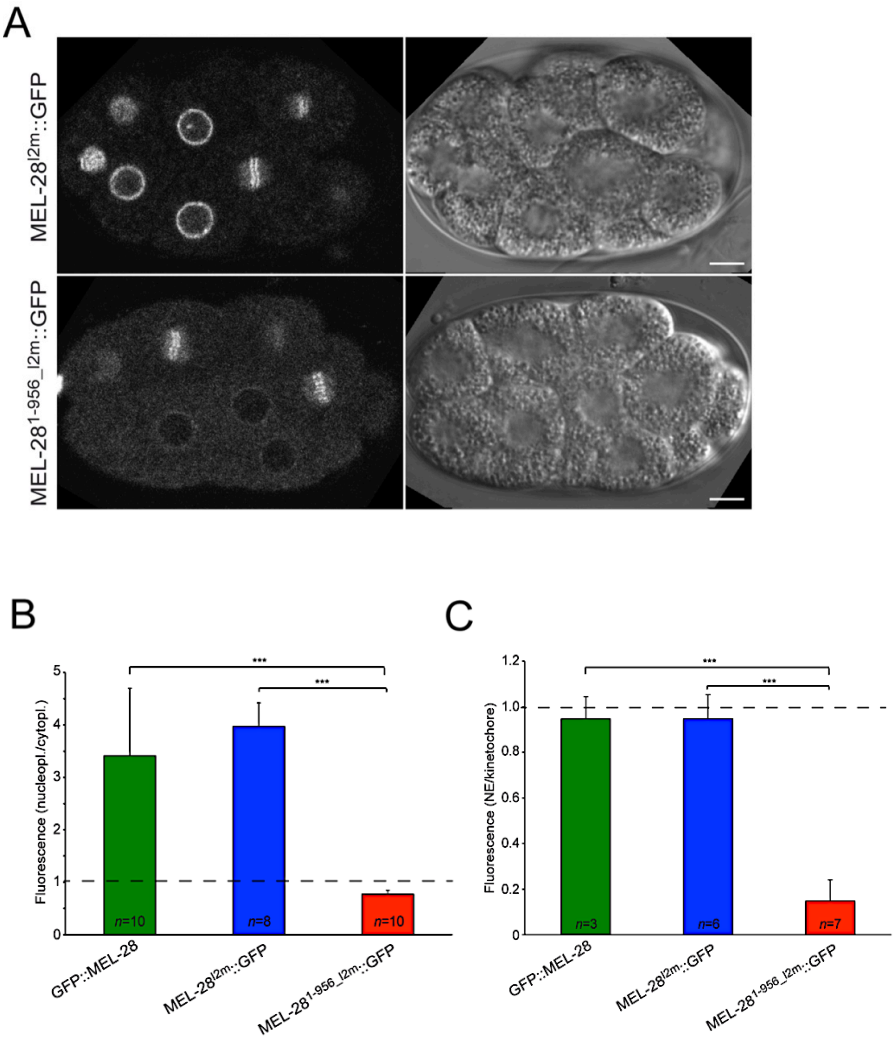

Figure 4.9. Impaired nuclear import and NPC localization of MEL-28$^{1\text{-}956_loop2mut}$. (A) Confocal images of embryos expressing GFP::MEL-28 or MEL-28$^{1\text{-}956_loop2m}$::GFP. Both embryos also expressed endogenous untagged MEL-28. Scale bars, 5 µm. (B) In interphase, the ratio of nucleoplasmic versus cytoplasmic GFP signal was ~4.4-fold higher for full-length MEL-28 compared to MEL-28$^{1\text{-}956_loop2m}$ (3.41 ± 1.28 versus 0.77 ± 0.07). Mutation of MEL-28 loop2 (MEL-28^{loop2m}::GFP) in the context of full-length protein did not reduce nuclear enrichment (3.97 ± 0.44), suggesting that the impaired import of MEL-28$^{1\text{-}956_loop2m}$::GFP was mainly due to deletion of the C-terminal domain. (C) Accumulation of MEL-28$^{1\text{-}956_loop2m}$::GFP at the NE (relative to kinetochore localization) was also specifically reduced (0.94 ± 0.09, 0.94 ± 0.1, and 0.14 ± 0.09, respectively). *** p<0.001 by unpaired two-tailed t-test.

The AT-hook domain is dispensable for MEL-28 localization, but essential for its functions

Comparing the behavior of GFP::MEL-28$^{1239\text{-}1601}$ and GFP::MEL-28$^{1188\text{-}1784}$ indicated that MEL-28's two AT hooks are not required for chromatin association, at least during mitosis (Figure 4.7). Moreover, *in vitro* binding experiments found no difference in chromatin affinity between recombinant peptides that contained either the C-terminal 128 aa of *Xenopus* ELYS including the single ELYS AT hook or a variant with mutated AT hook although the former was more efficient in competition assays (B. A. Rasala et al., 2008). In agreement with the competition assay, it was independently demonstrated that the same 128-aa. peptide efficiently binds nucleosome beads but not when the AT hook is mutated (Zierhut et al., 2014a). However, both studies concluded that the 128-aa. peptide contains residues outside the AT hook important for chromatin and nucleosome interaction. We attempted to address this in further detail, but we were unable to detect expression of a construct encoding the C-terminal 161 aa. of MEL-28 fused to GFP (Figure 4.8B; GFP::MEL-28$^{1624\text{-}1784}$). A shorter 48-aa. fragment containing a single AT hook localized similarly to free GFP (Figure 4.8A; GFP::MEL-28$^{1740\text{-}1784}$).

As a complementary approach, we examined the consequences of deleting the AT hooks from full-length MEL-28. We first compared *mel-28/+* embryos expressing GFP::MEL-28$^{1\text{-}1629}$ (GFP::MEL-28$^{\Delta AT}$) with *mel-28* embryos expressing full-length MEL-28 fused to GFP. Time-lapse confocal microscopy demonstrated that the *mel-28/+*; GFP::MEL-28$^{1\text{-}1629}$ embryos developed normally and the fluorescent protein localized similarly to GFP::MEL-28 (Figure 4.10A; compare left and middle panels). In the absence of endogenous MEL-28, GFP::MEL-28$^{1\text{-}1629}$ still accumulated at the periphery of interphase nuclei and to kinetochores of mitotic chromosomes (Figure 4.10A; right panels). This was in contrast to the severe phenotypes observed in MEL-28^{loop2mut}::GFP embryos (Figure 4.5A) and suggested that MEL-28's function in post-mitotic nuclear assembly is not strictly dependent on the AT hook domain. However, *mel-28;* GFP::MEL-28$^{1\text{-}1629}$ embryos were unviable (Table 4.1) and displayed several defects. Most prominently, daughter nuclei were often (n=5/7) trapped at the cleavage furrow during cytokinesis of the anterior AB blastomere of two-cell stage embryos (Figure 4.10A, right panels; 27:31-34:30). More direct evidence for chromosome segregation failure was obtained by immunofluorescence analysis of four-cell stage embryos, which also demonstrated that NPP-10C/NUP96 and other Nups accumulated at the NE of *mel-28;* GFP::MEL-28$^{1\text{-}1629}$ embryos, albeit in an irregular pattern (Figure 4.10E).

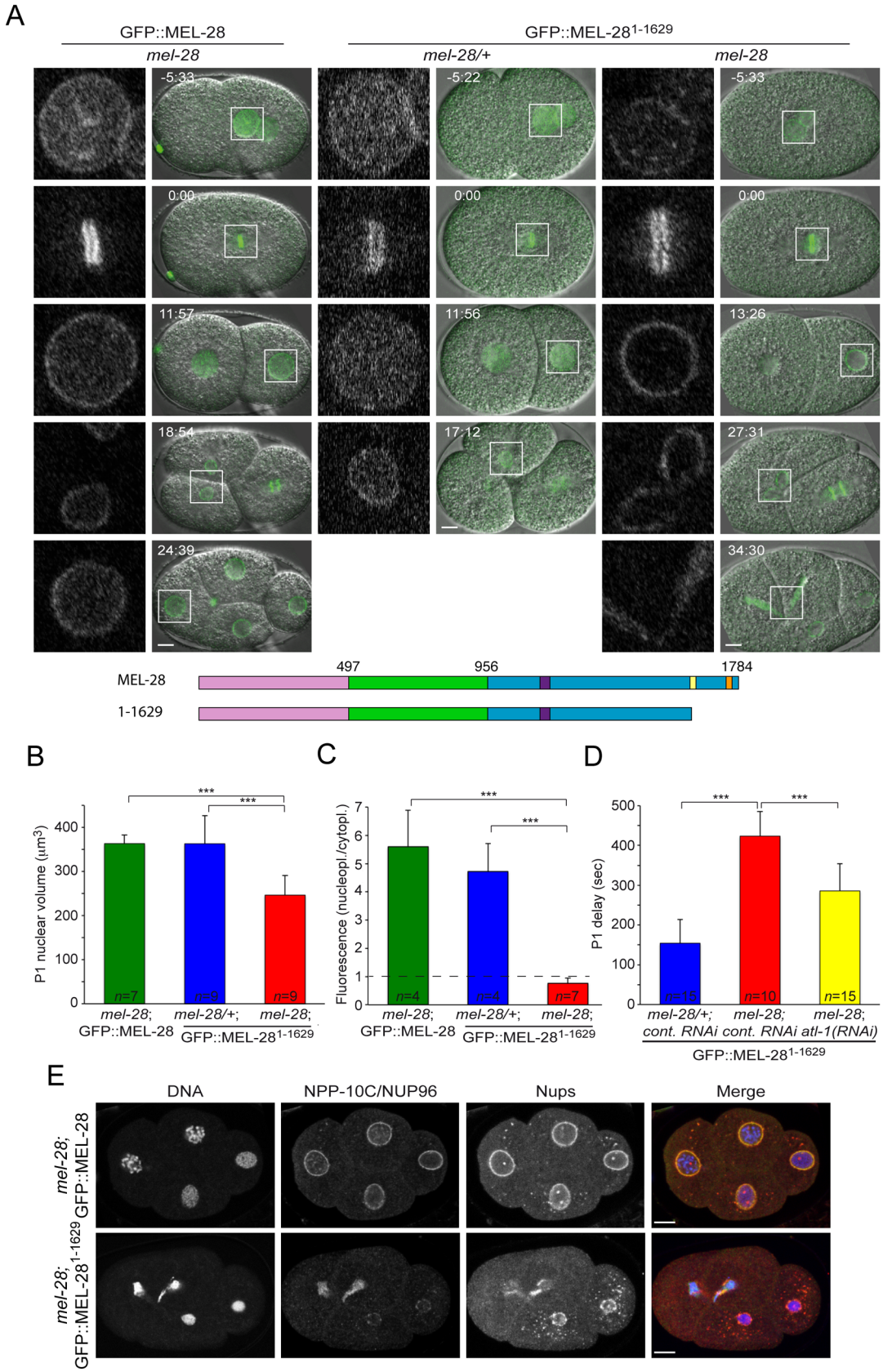

Figure 4.10. The AT-hook domain of MEL-28 is required for nuclear growth, chromosome segregation and cell cycle timing. (A) Still images from time-lapse recordings of control (middle) and *mel-28* (right) embryos

expressing GFP::MEL-28$^{1-1629}$ as well as a *mel-28* embryo expressing GFP::MEL-28 (left). Note defective chromosome segregation in the right embryo. Scale bars, 5 µm. Nuclear growth (B) and distribution of GFP fusion protein between nucleoplasm and cytoplasm (C) was specifically reduced in *mel-28* embryos expressing GFP::MEL-28$^{1-1629}$. Measurements were performed on fully-grown P1 nuclei. (D) Asynchrony between division of AB and P1 blastomeres was significantly delayed in *mel-28* embryos expressing GFP::MEL-28$^{1-1629}$; this delay was partially reduced by depletion of ATL-1. (E) Four-cell stage embryos from *mel-28* mutants expressing either GFP::MEL-28 or GFP::MEL-28$^{1-1629}$ were analyzed with Hoechst (blue in merge), a specific antibody against NPP-10C/NUP96 (green in merge) and mAb414 recognizing multiple nups (red in merge). Scale bars, 5 µm. *** $p<0.001$ by unpaired two-tailed t-test.

In addition, nuclear growth was significantly reduced in GFP::MEL-28$^{1-1629}$ embryos (Figure 4.10A, third row; Figure 4.10B), consistent with defects in NPC-mediated nucleocytoplasmic transport (Levy & Heald, 2010). While nuclei from *mel-28*; GFP::MEL-28 and *mel-28/+*; GFP::MEL-28$^{1-1629}$ grew to the same size (363.8 ± 19 µm^3 and 363.3 ± 63 µm^3; respectively), the maximum volume of P1 nuclei was reduced by 32% in *mel-28*; GFP::MEL-28$^{1-1629}$ embryos (346.6 ± 44 µm^3). We also noticed that the nucleoplasmic pool of GFP::MEL-28$^{1-1629}$ was strongly diminished in *mel-28* embryos compared to GFP::MEL-28 in *mel-28* embryos and GFP::MEL-28$^{1-1629}$ in *mel-28/+* embryos (Figure 4.10A and C). Whereas the ratio between nucleoplasmic and cytoplasmic GFP signal was similar between *mel-28*; GFP::MEL-28 and *mel-28/+*; GFP::MEL-28$^{1-1629}$ embryos (5.60 ± 1.29 and 4.72 ± 0.99; respectively), the ratio was 87% lower in *mel-28*; GFP::MEL-28$^{1-1629}$ embryos (0.76 ± 0.18). These data are compatible with a model in which GFP::MEL-28$^{1-1629}$ has reduced affinity for interphase chromatin and therefore accumulates at NPCs: in *mel-28/+* embryos interaction of GFP::MEL-28$^{1-1629}$ with endogenous MEL-28 accumulates the former in the nucleoplasm, potentially interacting with chromatin.

During time-lapse recordings of 2-cell stage *mel-28* embryos, we realized that division of the P1 blastomere was much delayed relatively to the AB division. In wild-type embryos the P1 cell division is delayed by ~2.5 min compared to AB division. This P1 delay is dependent on checkpoint proteins and is thought to have evolved to protect the germ-line lineage from aneuploidy. Thus, inhibition of DNA replication or induction of DNA damage is typically associated with extended P1 delay. When we compared embryos expressing GFP::MEL-28$^{1-1629}$ an increase in P1 delays by 176% was observed in *mel-28* versus m*el-28/+* embryos (423.5 ± 61.9 sec versus 154.1 ± 59.2 sec; Table 4.2; Figure 4.10D). The presence of chromatin bridges in *mel-28;* GFP::MEL-28$^{1-1629}$ embryos (Figure 4.10E) suggested that chromosomes might be entangled, potentially as consequence of stalled replication and/or double-stranded DNA breaks. To address if the DNA damage checkpoint indeed is involved

in the extended P1 delay in *mel-28;* GFP::MEL-28$^{1-1629}$ embryos, we depleted ATL-1, the *C. elegans* homolog of ATR by RNAi (Budirahardja & Gönczy, 2009). This mitigated the P1 delay (285.7 ± 67.9 sec), which suggested that removal of the AT-hook domain from MEL-28 activates DNA damage and thereby an exaggerated delay of P1 cell division. However, depletion of ATL-1 did not fully rescue P1 cell-cycle timing, which suggests that other checkpoints are also activated in *mel-28;* GFP::MEL-28$^{1-1629}$ embryos. In conclusion, although GFP::MEL-28$^{1-1629}$ localizes properly to the NE and kinetochores, depletion of MEL-28's AT-hook domain causes reduced nuclear growth, mis-segregation of chromosomes and activates the ATR DNA damage checkpoint.

Table 4.2. Loss of MEL-28's AT Hooks causes checkpoint-dependent cell division delays

Strain	n[a]	AB division[b] (average +/- S.D.[c])	P1 division[d] (average +/- S.D.)	P1 delay[e] (average +/- S.D.)	P1/AB ratio[f] (average +/- S.D.)
mel-28/+; GFP::MEL-28$^{1-1629}$; Control RNAi	15	828.6 +/- 33.1	982.7 +/- 81.4	154.1 +/- 59.2	1.2 +/-0.06
mel-28; GFP::MEL-28$^{1-1629}$; Control RNAi	10	775.8 +/- 145.7	1199.3 +/- 151.2**	423.5 +/- 61.9***	1.6 +/-0.17***
mel-28; GFP::MEL-28$^{1-1629}$; *atl-1 RNAi*	15	807.3 +/- 128.9	1093 +/- 133.2	285.7 +/- 67.9$^{\Psi\Psi}$	1.4 +/-0.11$^{\Psi}$

Significant differences by two-tailed t-test: ** different from control *mel-28*/+ embryos, p<0.01; *** different from control *mel-28*/+ embryos, p<0.001;$^{\Psi}$ different from *mel-28* control RNAi embryos p<0.01; $^{\Psi\Psi}$ different from *mel-28* control RNAi embryos p<0.001.

[a] Number of embryos analyzed via real-time DIC microscopy.

[b] Time in seconds between P0 cytokinesis onset and AB cytokinesis onset

[c] Standard deviation.

[d] Time in seconds between P0 cytokinesis onset and P1 cytokinesis onset.

[e] Time in seconds between AB cytokinesis onset and P1 cytokinesis onset.

[f] ratio of time to P1 over time to AB cytokinesis onset.

MEL-28/ELYS localization domains are evolutionary conserved

To explore the degree of conservation of localization domains we expressed human full-length ELYS (ELYS$^{1-2275}$) and 14 ELYS truncations fused to GFP in HeLa cells. As reported, ELYS$^{1-2275}$ was enriched at the NE in interphase and in a pattern coincident with kinetochores in metaphase (Figure 4.11A and 4.12; punctate localization on metaphase chromosomes was observed in single confocal sections as well as in maximum intensity pro-

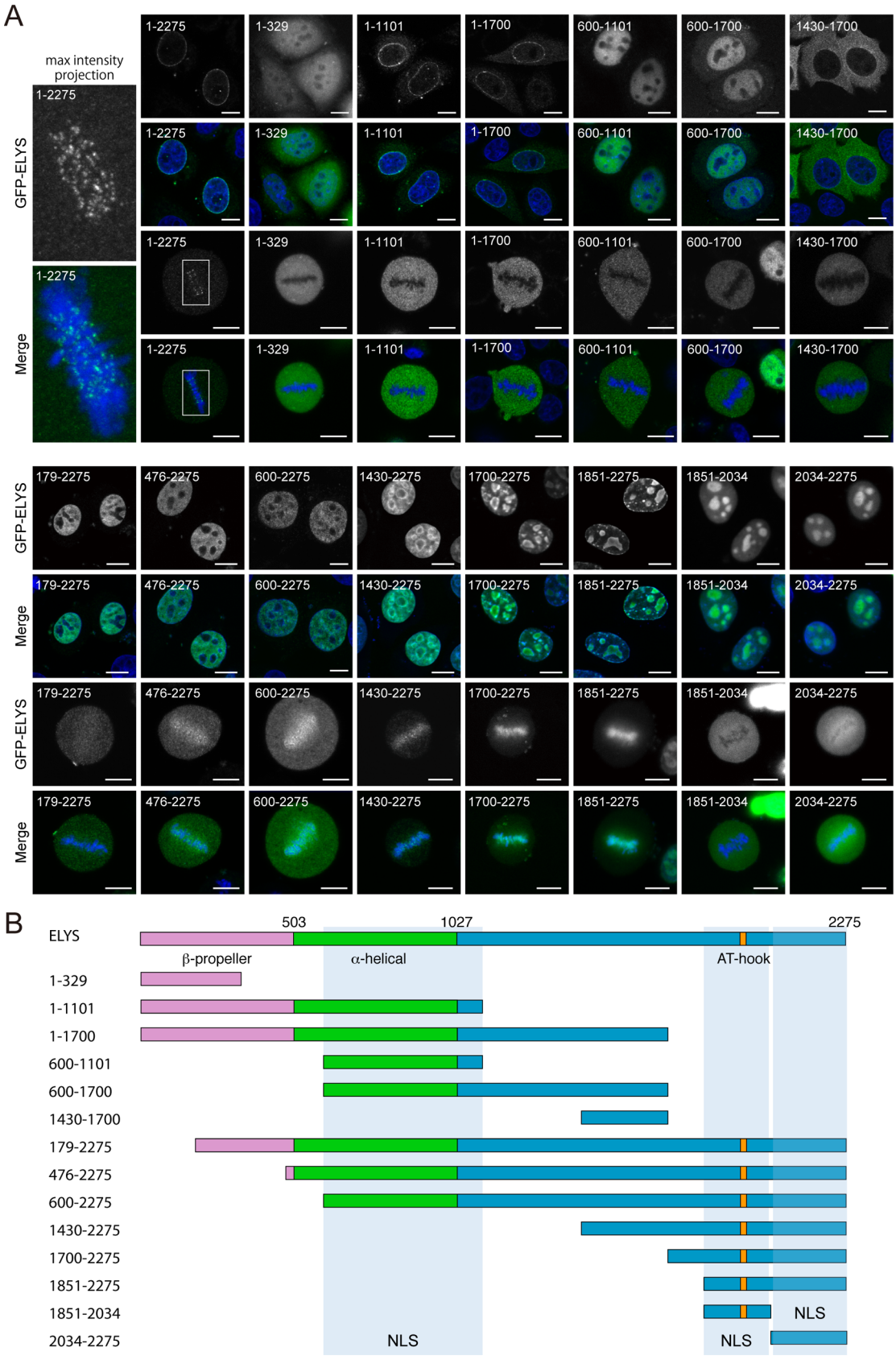

Figure 4.11. Mapping of ELYS localization domains. (A) Transiently transfected HeLa cells expressing full-length human ELYS (1-2275) or ELYS fragments fused to GFP (green in merge) were fixed and counterstained

to visualize DNA (blue in merge). Maximum intensity projection of z-sections spanning the metaphase plate is shown for ELYS; other images represent single confocal sections. Scale bars, 10 µm. (B) Schematic representation of ELYS and analyzed fragments. Orange (aa. 1980-1989) boxes indicate AT-hook sequences. Truncations containing ELYS aa. residues 600-1101, 1851-2024 and/or residues 2034-2275 (blue shading) were efficiently imported.

jections). Two fragments containing the entire β-propeller and α-helical domains (ELYS$^{1-1101}$ and ELYS$^{1-1700}$) still accumulated at the NE but had increased cytoplasmic signal, suggesting that, like for MEL-28, sequences outside the β-propeller and α-helical domains contribute to efficient NPC targeting (Figure 4.11A and 4.13). In contrast, all truncations from the N-terminal end abolished NE signal, including a deletion of ELYS aa. 1-178 (ELYS$^{179-2275}$), indicating that the β-propeller is critically required for incorporation of ELYS into the NE. A short N-terminal fragment, ELYS$^{1-329}$, was also not detected at the NE, which implies that although the first 178 aa. of ELYS are needed for NPC localization, they are not sufficient.

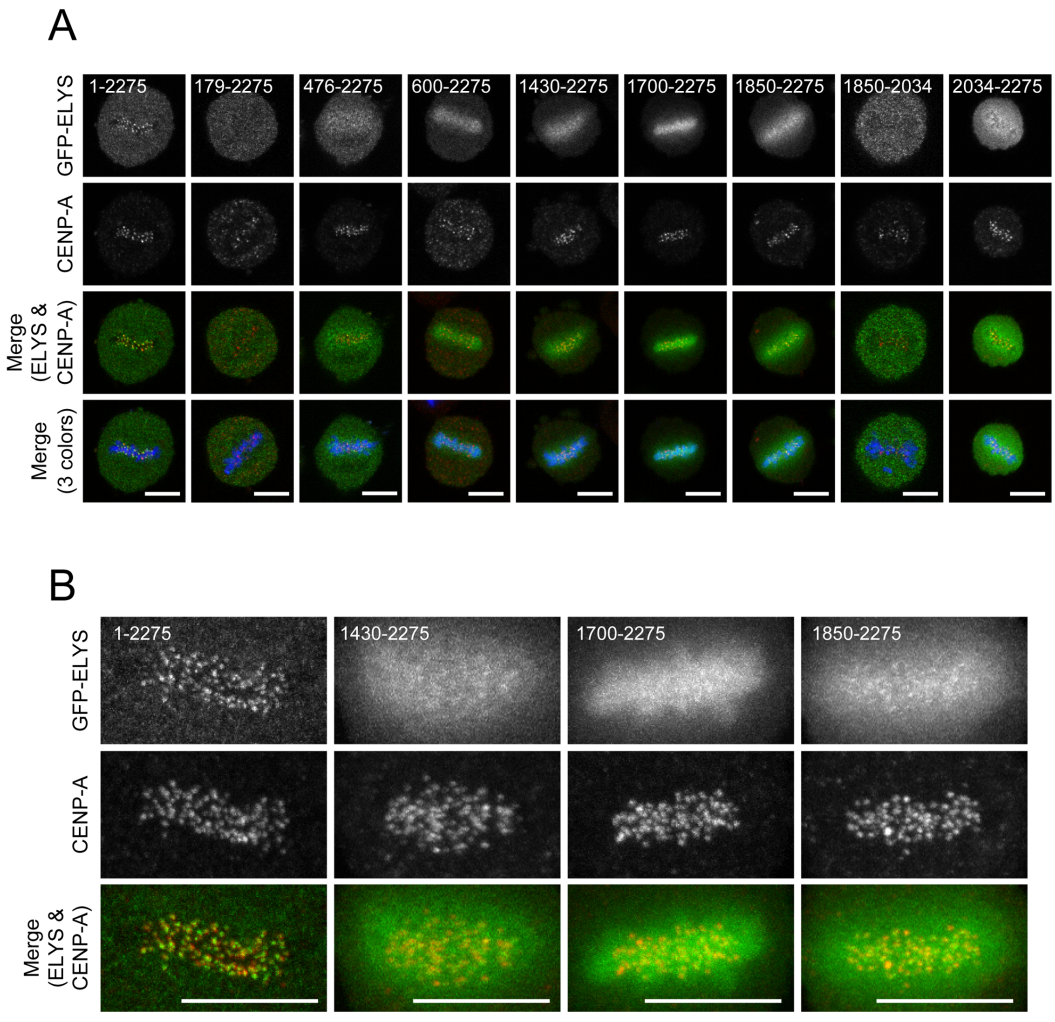

Figure 4.12. Full-length ELYS, but not ELYS fragments, strongly accumulates at kinetochores at mitosis. Cells expressing full-length or truncated GFP-ELYS (green in merge) were analyzed by immunofluorescence with a specific antibody against kinetochore protein CENP-A (red in merge) and DAPI (blue in merge). Single confocal sections (A) and maximum projection images (B) of metaphase cells are shown. Full-length ELYS co-localizes extensively with CENP-A whereas several C-terminal fragments are diffusely associated with metaphase chromosomes. Scale bars, 10 μm.

Two internal fragments, ELYS$^{600\text{-}1101}$ and ELYS$^{600\text{-}1700}$, were nuclear in interphase whereas ELYS$^{1430\text{-}1700}$ was mostly cytoplasmic (Figure 4.11). This suggests that both MEL-28 (Figure 4.7; MEL-28$^{846\text{-}1071}$) and ELYS have at least one NLS at equivalent locations within the central region of the protein. Nuclear accumulation was also observed for two non-overlapping C-terminal fragments, ELYS$^{1851\text{-}2034}$ and ELYS$^{2034\text{-}2275}$. In agreement with earlier predictions (Kimura et al., 2002), this suggests the presence of NLS's in the AT-hook-containing last 425 aa. of ELYS, similar to our mapping of a potential NLS to the AT-hook domain of MEL-28 (Figure 4.7; MEL-28$^{1188\text{-}1784}$) and would represent another functional conservation between ELYS and MEL-28. We also noted that the shortest C-terminal ELYS fragments were enriched in nucleoli, whereas longer fragments (e.g. ELYS$^{179\text{-}2275}$, ELYS$^{476\text{-}2275}$, and ELYS$^{600\text{-}2275}$) were excluded from these compartments (Figure 4.11).

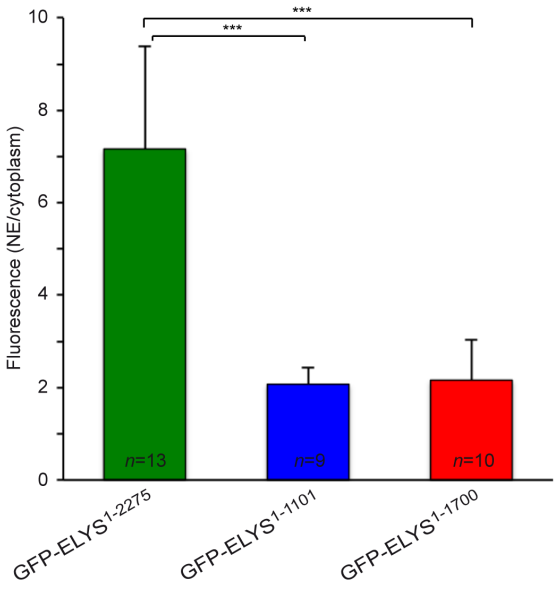

Figure 4.13. The C-terminal domain of ELYS is required for efficient targeting to the nuclear envelope. Fluorescence intensity of the NE and cytoplasm was determined for HeLa cells transiently expressing GFP fused to full-length ELYS (ELYS$^{1\text{-}2275}$), ELYS$^{1\text{-}1101}$, or ELYS$^{1\text{-}1700}$. The ratio of NE versus cytoplasmic fluorescence was reduced by 70-71% for the two truncated ELYS proteins. *** $p<0.001$ by unpaired two-tailed t-test.

Interestingly, all 14 ELYS truncations localized differently from full-length ELYS during metaphase. The three N-terminal fragments (ELYS$^{1-329}$, ELYS$^{1-1101}$, and ELYS$^{1-1700}$) and the three internal fragments (ELYS$^{600-1101}$, ELYS$^{600-1700}$, and ELYS$^{1430-1700}$) were not detected on mitotic chromosomes (Figure 4.11). In contrast, truncations from the N-terminal end increased the abundance of ELYS on chromosomes aligned on the metaphase plate. Importantly, the pattern was more diffuse on the chromosomes compared to the punctate pattern of full-length ELYS (Figure 4.12). This was particularly prominent for ELYS$^{1700-2275}$ and ELYS$^{1851-2275}$, but was also observed for the longer ELYS$^{476-2275}$, ELYS$^{600-2275}$, and ELYS$^{1430-2275}$ fragments. These results suggest that the C-terminus of ELYS has affinity for chromatin but that the ability to interact with chromosomes is reduced in the context of full-length ELYS, which specifically localizes to kinetochores. Thus, we conclude that association with mitotic chromosomes is also conserved from *C. elegans* to humans. Because of the similarity between MEL-28 and ELYS in terms of structural organization despite low primary sequence homology, we propose that the functional assignments for MEL-28 domains presented in this work are likely to be relevant in more complex animals, including humans (Figure 4.14).

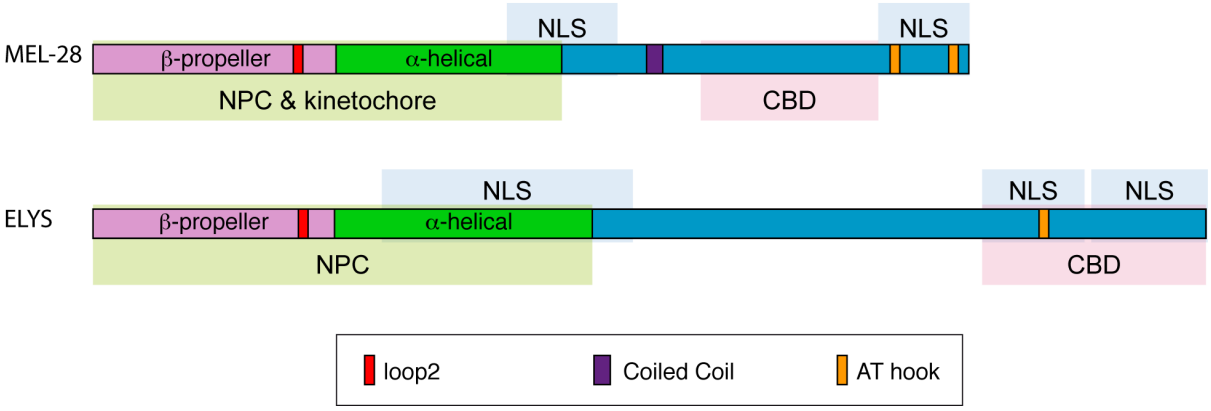

Figure 4.14. Overview of MEL-28 and ELYS localization domains. The N-terminal halves of MEL-28 and ELYS are sufficient to localize to NPCs (green shading) although less efficiently than full-length proteins. In the case of MEL-28, the N-terminus is also sufficient to localize to kinetochores. Both proteins contain central and C-terminal domains that are imported into nuclei (blue shading) and C-terminal domains that confer binding to chromatin (pink shading). A conserved loop2 motif in the N-terminal β-propeller is important for NPC localization in the context of truncated proteins. Both the loop2 motif and the AT-hook domain of MEL-28 are essential for embryonic viability.

Chapter V

Results From Objectives 2 and 3

Article 4: Research paper

(Manuscript in preparation)

Characterization of genome-nucleoporin interactions in *Caenorhabditis elegans*

Georgina Gómez-Saldivar[1], Dominic Ritler[2], Peter Meister[2], and Peter Askjaer[1]

[1] Andalusian Center for Developmental Biology (CABD), CSIC/Junta de Andalucia/Universidad Pablo de Olavide, Seville, Spain.

[2] Cell Fate and Nuclear Organization, Institute of Cell Biology, University of Bern, Switzerland.

Results

MEL-28 binds chromatin in a genome-wide fashion

To investigate Nup-chromatin interactions, we generated genome-wide interaction maps of Nups with different dynamics and localization (Figure 5.1) We initially analyzed MEL-28 full-length protein in young adult worms using the DamID in vivo mapping assay (Van Steensel & Henikoff, 2000). With this technique, a protein of interest is fused to *E. coli* Dam methylase and expressed at very low levels; in our case we used the inducible heat shock protein promoter (*Phsp16.41*) without induction. This led to adenine methylation in GATC sites in the genomic loci bound by the protein of interest. Then, the genomic DNA was isolated and subsequently, fragments flanked by methylated GATC sites were amplified with a series of enzymatic reactions and identified by microarray analysis or high-throughput sequencing; details of the technique were reviewed in chapter III. Using DamID technique we avoid a series of constraints that we could find given the nature of certain NE proteins such as insolubility; since DamID does not rely on *in vivo* crosslinking of DNA with the protein of interest, sonication, and pull-down with a specific antibody. On the other hand, ChIP results could reflect indirect interactions due to high interactivity between all the NPC components. (For review see (Askjaer et al. 2014; Georgina Gómez-Saldivar et al. 2016)).

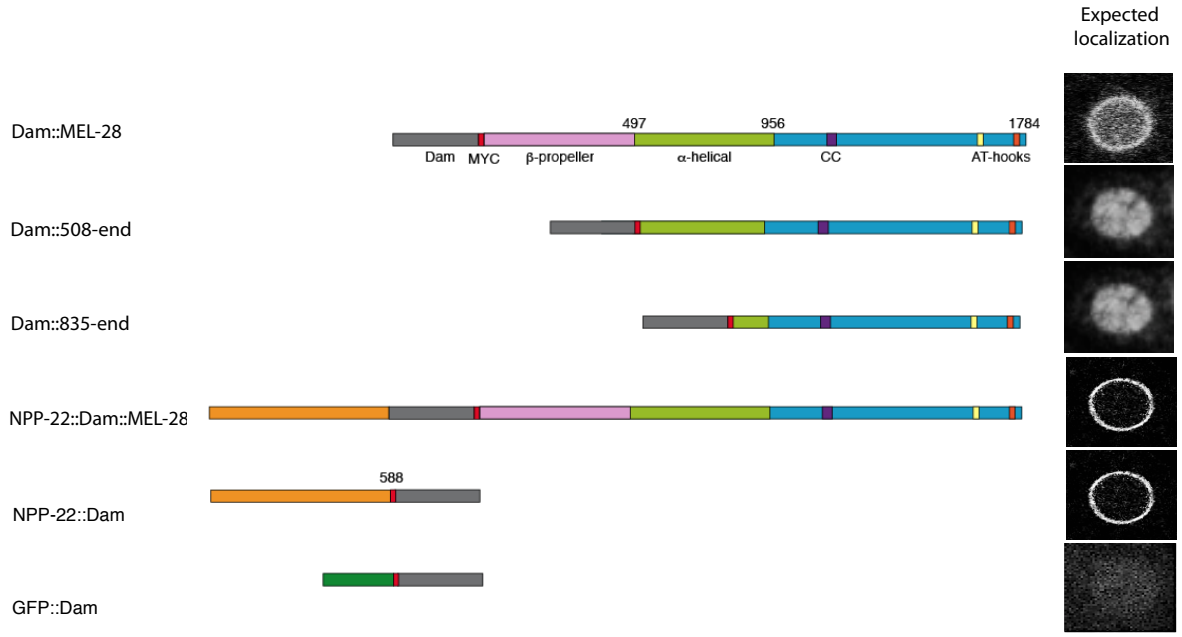

Figure 5.1. Experimental setup. Schematic drawing showing the Dam::Nups fusion constructs used for the generation of Nup-chromatin maps. Three different behavior are expected to find: i) Dam::MEL-28 is expected to localize at NPCs and in the nucleoplasm; ii) Dam::MEL-28 fragments are expected to localize exclusively to the nucleoplasm; and iii) NPP-22::Dam::MEL-28 and NPP-22::Dam are expected to localize exclusively at NPC because of NPP-22's transmembrane domain. GFP::Dam fusion protein was used as a control of chromatin accessibility, showing a diffuse localization. MYC tag (small red domain) can be used to detect fusion proteins by immunofluorescense.

Firstly we evaluated the expression and localization of Dam::MEL-28 fusion protein by immunofluorescence (IF) microscopy. After activation of the heat-shock promoter, the fusion protein was easily observed, although in a heterogeneous pattern as typically observed with the *hsp-16.41* promoter. Dam::MEL-28 localized in two pools, at the nuclear periphery associated to NPC and throughout the nucleoplasm as was expected (Figure 5.2, top). The localization correlates with our previous results, where we fused MEL-28 to GFP instead of Dam, due to both proteins have very similar size, the similar behavior between both chimeric proteins was expeced (Figure 4.4A and C in chapter IV). Although in the IF experiment the construct was overexpressed by heat shock induction, in DamID experiments the expression variation is minimal due to i) we generated *C. elegans* strains containing single copy insertions of the chimeric transgenes by MosSCI (Frøkjær-Jensen et al., 2012); ii) as we mention above, the heat shock promoter is not induced. Therefore, we conclude that Dam::MEL-28 fusion protein reproduces the normal localization of MEL-28 endogenous protein, and their presence does not generate either toxicity or detrimental effects. In fact, the strain can be maintained under normal growth conditions and the worms look healthy and develop identically to N2 worms.

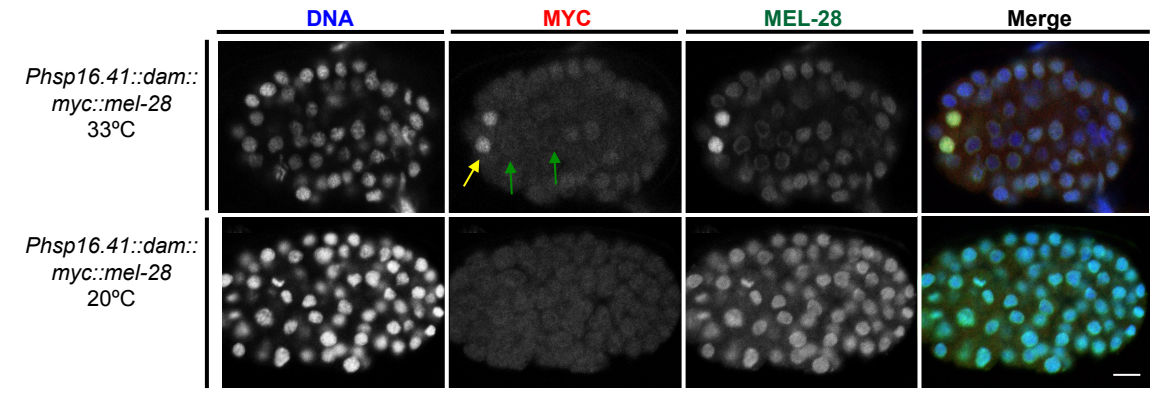

Figure 5.2. Expression and localization of Dam::MEL-28 fusion protein. MEL-28 fusion protein was expressed under the control of the *hsp-16.41* heat-shock promoter. In the top, Dam::MYC::MEL-28 fusion protein localizes properly after the heat-shock treatment, and can be detected in two pools: nuclear envelope (green

arrows) and nucleoplasm (yellow arrows). Note that in mid-stage embryos the degree of induction by the *hsp-16.41* promoter is very heterogeneous (see also Figure 4.3 in chapter IV). Dam::MYC::MEL-28 expressing embryos were fixed and stained with anti-MYC antibody (red in merge), anti-MEL-28 antibody (green in merge) and Hoechst 33258 (blue in merge) to visualize chromatin. Dam::MYC::MEL-28 expressing embryos without heat-shock treatment were used as control. Scale bar 5 µm.

Then, we generate DNA-binding profiles for MEL-28 full-length protein in *C. elegans* young adults using DamID followed by hybridization to *C. elegans* whole-genome high-density tiling microarrays. We normalized raw data to hybridization data from control GFP::Dam cultures to compensate for differences in chromatin accessibility. Then we normalized DamID signals using MA2C program (J. S. Song et al., 2007). We confirmed the reproducibility of results by performing two biological replicates (r= 0.90 at probe level, and r=0.92 after 1kb averaged; Figure 5.3A).

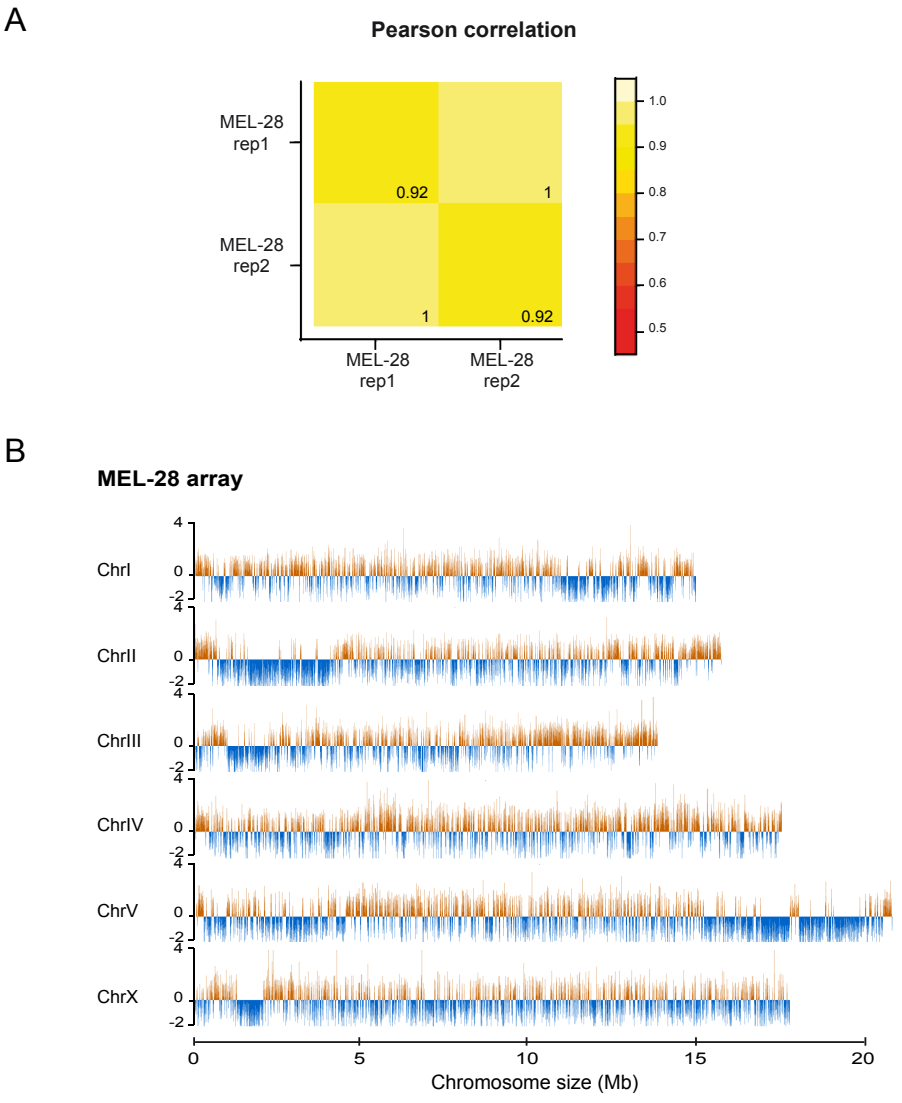

Figure 5.3. MEL-28 protein is distributed along all chromosomes. (A) Heatmap of the quality assessment of MEL-28 DamID replicates by Pearson correlation. Coefficients of two replicates of Dam::MEL-28 DamID experiments are shown. Correlations were calculated based on MA2C scores of all probes on the microarrays (1 kb window averaged). (B) Genome browser views of MEL-28 chromosome binding profile obtained with MA2C after GFP::Dam normalization and binning the genome at 1kb. Each profile represents the average of two independent experiments.

Thus, we average the both replicates to get a final association profile. MEL-28 display binding across the whole genome, and bind to 19.6% of the *C. elegans* genome. This widespread genome association (Figure 5.3B), agrees with the identification of a conserved DNA binding domain in MEL-28 (Franz et al., 2007; Gómez-Saldivar, Fernandez, et al., 2016); in addition, has been demonstrated to associate to nucleosomes with *in vitro* experiments (Zierhut, Jenness, Kimura, & Funabiki, 2014b).

MEL-28 chromatin binding profile is different from other NE proteins

Visual inspection of the DamID profile revealed that MEL-28 associates throughout the length of the chromosome, on all chromosomes (Figure 5.3B), in a different manner to others NE proteins (Figure 5.4). For instance, in autosomes both LMN-1 and EMR-1 associate preferentially to chromosomes arms, leaving the central part with very few LMN-1 and EMR-1 associated domains (LADs and EADs, respectively). On the X chromosome LADs and EADs are found mainly in the left arm (Figure 5.4A; LMN-1 and EMR-1 data from (González-Aguilera et al., 2014)).

Another clear difference was the size of MEL-28 associated domains (MADs). MADs were identified using the peak calling defined by the MA2C algorithm with modifications according to the protocol from (Vastenhouw et al., 2010): First, using FDR=5%, we selected 756 peaks smaller than 1500 bp. Next, using FDR=20%, we selected 6,068 peaks larger than 1500 bp (see materials and methods). A total of 6,824 peaks were identified as MADs (Figure 5.4B) and these were significantly smaller than LADs and EADs previously defined ((González-Aguilera et al., 2014); see also below for comparison of MADs and LADs identified by DamID-seq). LADs and EADs cover 37% of the genome and its size is ranged from 8 to 300 kb with a median size of 22.7 kb and 23.9 kb respectively. While MADs are ranged from 0.65 to 24 kb with a median size of 2.9 kb (Figure 5.4C). Likewise, MEL-28 Gaps were

significantly smaller than LMN-1 and EMR-1 Gaps, which was expected given MEL-28 peaks are more evenly distributed across the genome.

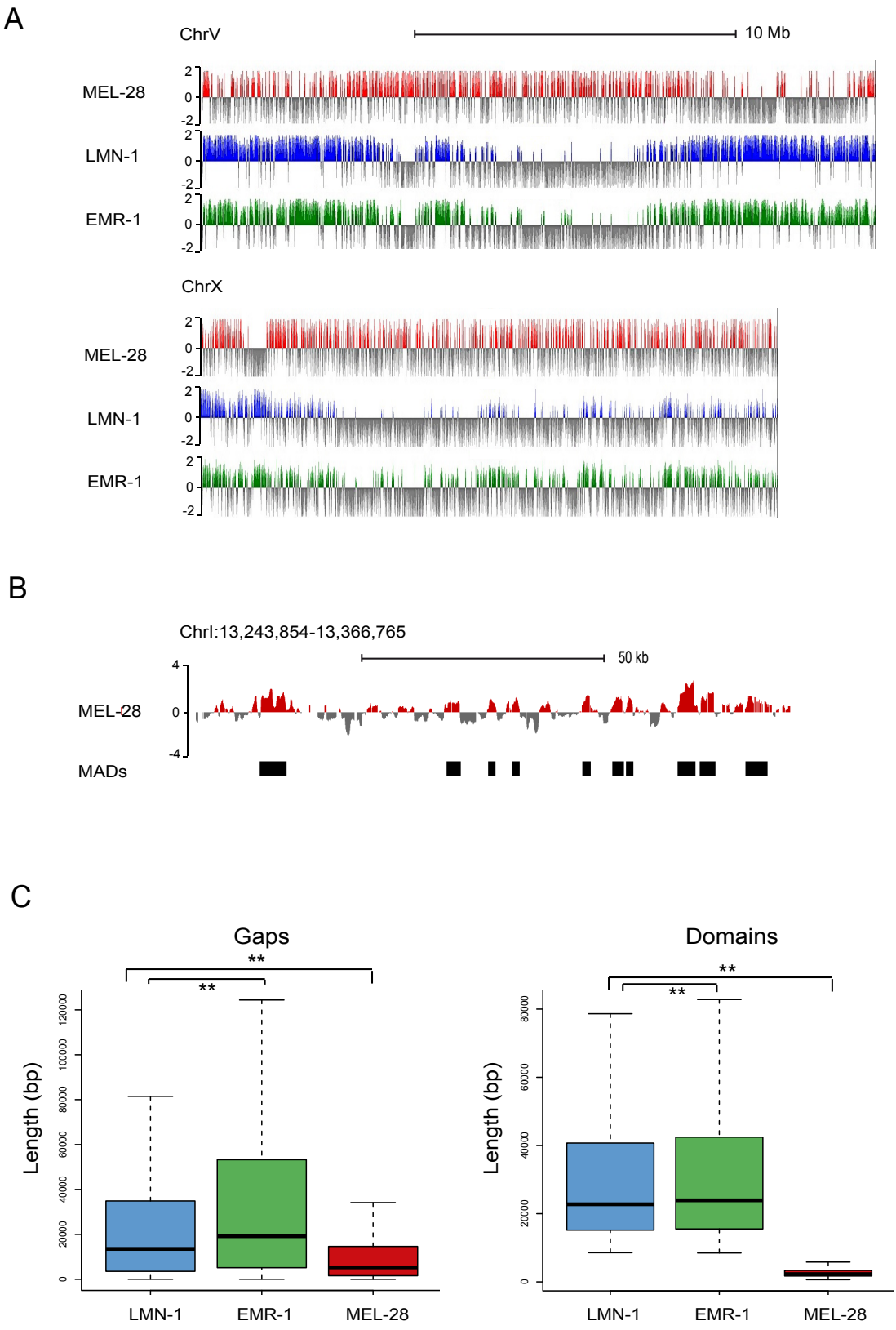

Figure 5.4. MEL-28 interacts with different genomic regions compared with LMN-1 and EMR-1. (A) NE proteins EMR-1 and LMN-1 are enriched in both chromosomes arms in autosomes (chr V is shown as example), and mainly in the left arm of the X chromosome. In contrast, MEL-28 is associated along all chromosomes. Shown are log2 MA2C score of 1 kb window averaged. (B) Zoom-in at chromosome III showing the peak assignment (MEL-28 Associated Domains; MADs) according to the signal intensity obtained with MA2C (score in log2) using a FDR = 0.05 for smaller peaks and FDR = 0.20 for the large domains (see materials and methods). (C) Sizes of LADs, EADs, MADs and regions between domains (Gaps) are shown. Bottom and top of boxes indicate the 25th and 75th percentiles, respectively, and lines in the boxes indicate medians, being visibly smallest domains and gaps of MEL-28. Whiskers indicate the lowest and the highest data points within 1.5x interquartile range from the box. Wilcoxon rank sum test was used to get probability value.** p-value= <2.2e-16. LMN-1 and EMR-1 data from (González-Aguilera et al., 2014).

Interestingly, MEL-28's profile was also different from other reported Nups. For example, in Drosophila Nup153 and Mtor bind extended chromosomal regions alternating between domains of high and low-density binding, covering in total 25% of the genome. These domains correspond to DNA-interactions that occur in both at NPCs and in the nuclear interior and displayed a range size from 10 kb to 100 kb (Vaquerizas et al., 2010).

On the other hand, a component of the nuclear basket, Nup-50 is distributed broadly throughout the nucleoplasm, without apparent nuclear sub-regions, since Nup50 localization responds homogeneously to transcription inhibition treatment, is propose that it can interact actively with euchromatin elements (Buchwalter et al., 2014). In contrast, in *C. elegans* ChIP-chip and ChIP-seq analysis of two integral scaffolds Nups, NPP-13 and NPP-3, suggest that chromatin interaction might take place at the NPCs. For NPP-13 were found 233 significant association sites (Figure 5.5). In conclusion, up to now, there is no characteristic pattern for Nups-binding, and their association with chromatin depends on their nature or position at NPC, suggesting that each Nup has a characteristic pattern of association depending on its specific roles (see discussion).

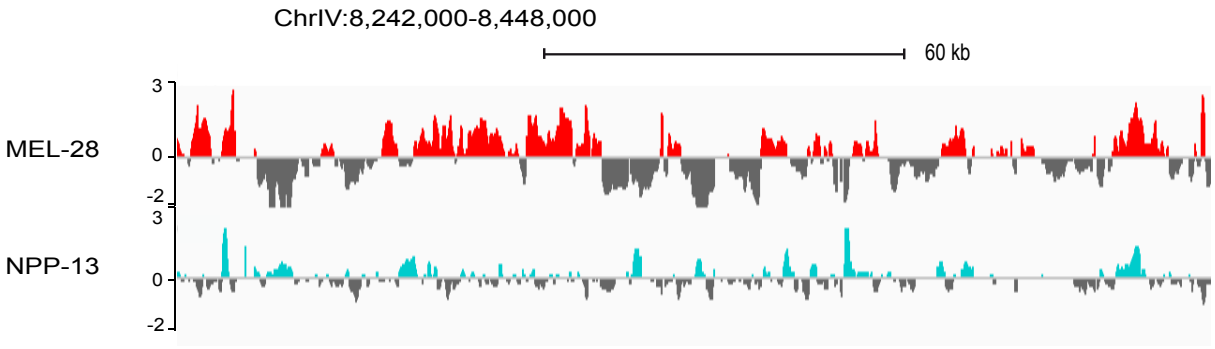

Figure 5.5. MEL-28 shows a different profile to NPP-13. Zoom-in at chromosome IV showing the signal intensity obtained with MA2C (score in log2). NPP-13 displays less association than MEL-28, and this signal is proposed to correspond to NPCs interaction, whereas MEL-28 interactions correspond from both pools NPC and Nucleoplasm. NPP-13 data from (Ikegami & Lieb, 2013).

It has been proposed that MEL-28 might bind to DNA through AT-rich genetic sequences becasue MEL-28's C-terminus harbors 2 AT-hook motifs, putatively able to bind to DNA (Gillespie et al., 2007a; Beth A Rasala et al., 2006). We quantified whether MADs were enriched with array probes with high AT content. Although AT-rich probes were statistically more frequent in MADs compared to the entire genome, the difference between the median values was minimal (Figure 5.6A). A similar conclusion was obtained when plotting the density of all probes from Nimblegen 2.1 M whole genome tiling array versus their AT content (Figure 5.6B). These data are consistent with our previous results where we mapped a chromatin-binding domain of MEL-28 to a C-terminal part lacking AT-hooks, between amino acids 1239-1601 (See Figure 4.8 in chapter IV). Besides, MEL-28 with deletion of its AT-hooks localized identically to the wild-type (See Figure 4.10A in chapter IV).

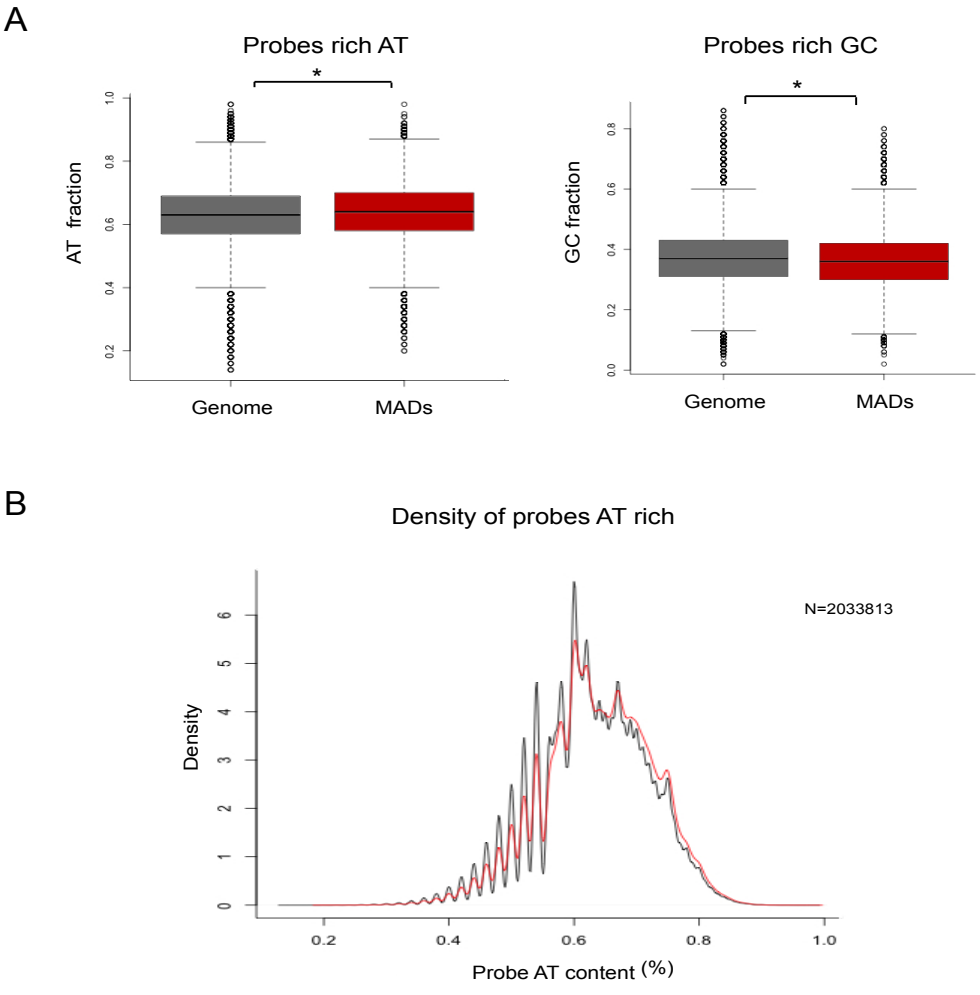

Figure 5.6. Probes distribution in MEL-28 association domains. (A) MADs are slightly enriched in probes with high content of AT, in comparison with probes with high content of GC. Both boxplot took on as reference the whole genome. * p-value= <2.2e-16. (A) Density plot with the distribution of probes according their nucleotide content in both MADs (red line) and genome (black line). N, is the number total of probes plotted from Nimblegen 2.1 M whole genome tiling array.

MEL-28 associates in chromatin actively transcribed

Studies done in several model organism such as *C. elegans* (González-Aguilera et al., 2014; Ikegami et al., 2010), Drosophila (Pickersgill et al., 2006) and human cells (Guelen et al., 2008), support the idea that the chromatin regions associated with the NE are transcriptionally inactive and are marked predominantly by histone markers characteristic of heterochromatin. To investigate if MEL-28 is associated to euchromatin, we analyzed the levels of trimethylated lysine 4 and 36 of histone 3, H3K4me3 and H3K36me3, respectively, two classical histone markers associated with transcription (Gerstein et al., 2010). Besides, we used the Polymerase II (POL-II/AMA-I) binding profile, which is highly enriched at the promoters regions, as an additional indicator for transcriptionally active chromatin (Gerstein et al., 2010),.Together with histone modifications, LADs are robust genome-wide indicators of transcriptional activity, but in this case representing silent chromatin (Kind & van Steensel, 2010; E. Lund et al., 2013). Interestingly, we found a clear correlation of MEL-28 peaks with the three active transcriptions markers and with regions rich in genes (Figure 5.7). In contrast, LMN-1 was mainly enriched outside MADs.

Moreover, analyses across MEL-28 domain boundaries supported that MADs are globally associated with H3K36me3, whereas gaps have lower levels of these histone marks. (Figure 5.8A). Furthermore, we performed analyses across EMR-1 domain boundaries, which display a very similar profile with LADs (González-Aguilera et al., 2014). In active chromatin, represented by EMR-1 gaps, we observed enrichment of MEL-28 together with both H3K4me3 and H3K36me3 markers. In contrast, in silent chromatin enriched in EADs and LADs, lower levels of MEL-28 and histone marks were detected (Figure 5.8B and C).

Finally, the correlation between MEL-28 binding and transcriptional regulation was confirmed by calculating gene expression levels in both MADs and their corresponding gaps. The expression data were obtained by RNA sequencing of N2 wild-type worms (González-Aguilera et al., 2014), and confirmed that MEL-28 is associated with actively transcribed DNA (Figure 5.9A).

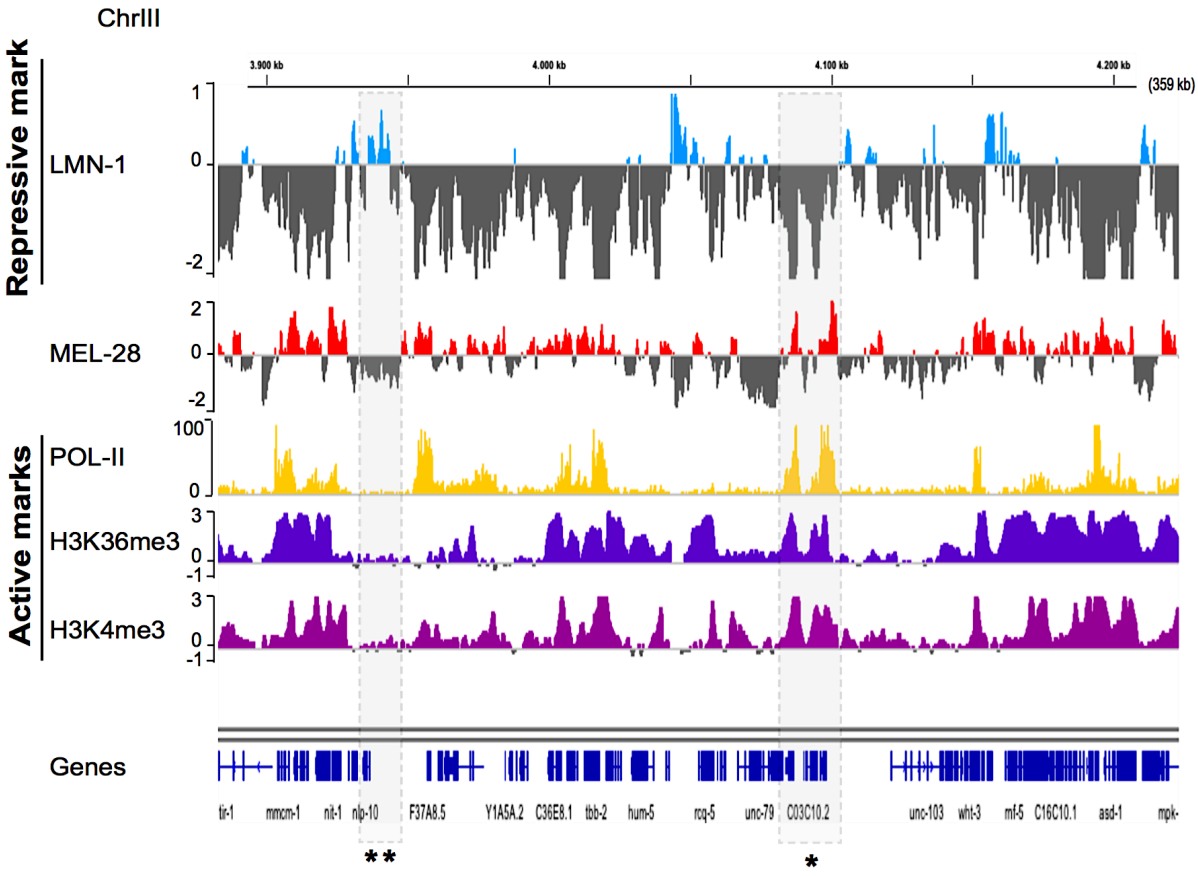

Figure 5.7. MADs are present in transcriptionally active regions of the genome. Genome-track view of 359 kb section on chromosome III show that MEL-28 peaks are rich in genes which accumulate markers of a transcriptionally active chromatin structure: H3K36me3, H3K4me3 and POL-II tracks, but exclude LMN-1 (region shaded with one asterisk) and vice versa (region shaded with two asterisks).

In order to figure out if MEL-28 association domains had any functionally important genomic regions such as gene promoters or exons, we performed *cis*-regulatory element annotation analysis (CEAS software; (H. Shin et al., 2009)). The results of the test indicated that MADs are lightly but significantly enriched in all kind of regulatory regions: promoter= 5.86e-86, intron= 0.036, 3'UTR= 1.25e-5, and 5'UTR= 2.9e-11; with exception of coding exons regions, which were more enriched in the rest of the genome 2.2e-107; (Figure 5. 9B).

These observations indicate that MEL-28 is enriched at transcriptionally active regulators regions of chromatin, which could be interacting close to NPCs. However, we cannot discriminate what part of the signal could reflect chromatin binding corresponding to MEL-28 located in the nucleoplasm.

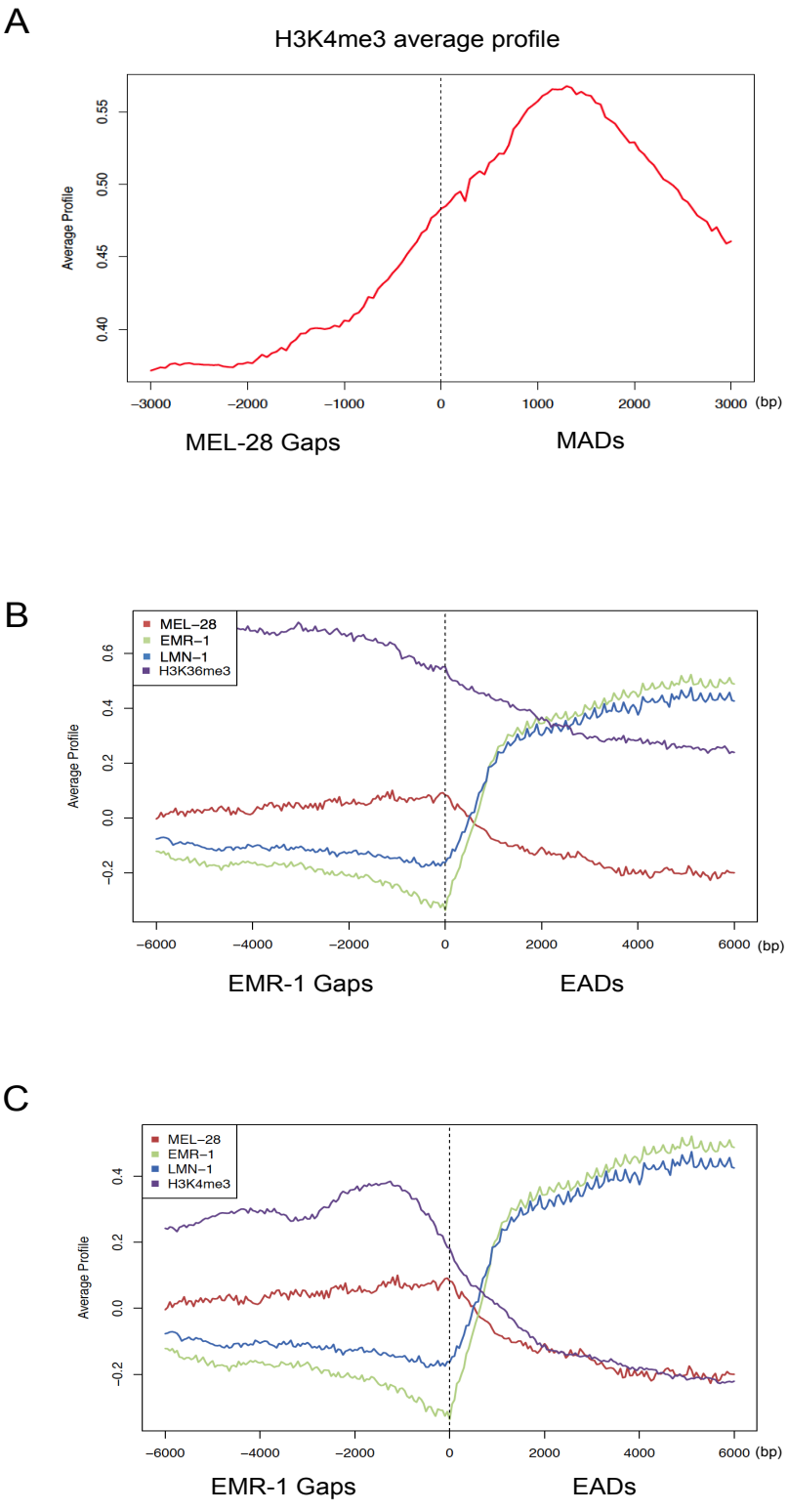

Figure 5.8. Active transcription chromatin marks and MADs are enriched in EMR-1 Gaps. (A) Average H3K4me3 profile at MADs boundaries. (B-C) Average H3K4me3, H3K36me3 and MEL-28 profiles at EADs boundaries. Chromatin immunoprecipitation (ChIP)-chip probe signal scores for indicated histone modifications are plotted. For comparison, averages of LMN-1 and EMR-1 DamID MA2C score are also shown.

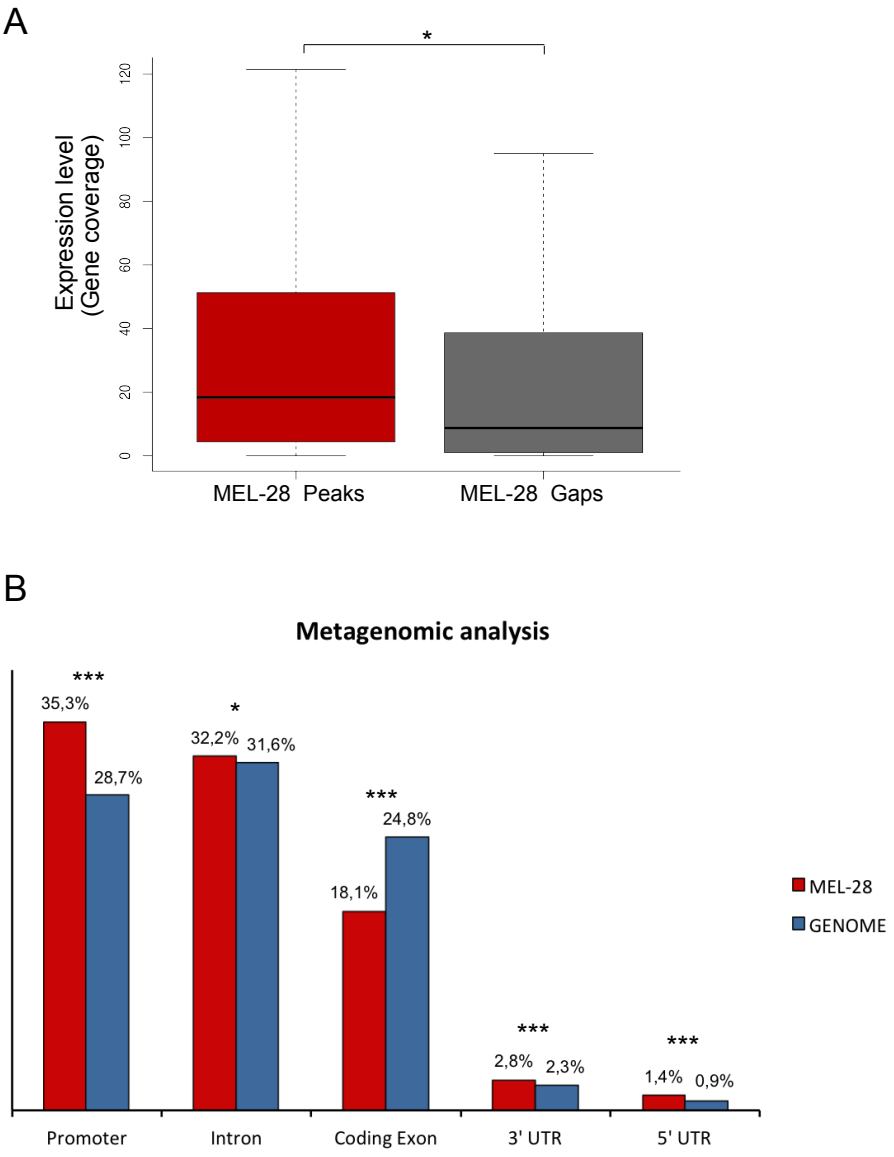

Figure 5.9. MEL-28 is associated to transcriptionally active regions. (A) MEL-28 Peaks are enriched with genes transcriptionally actives. (B) Metagenomic analysis classifies genetic regions into 5 categories. MADs are significantly enriched at all regulatory region with exception of coding exons. *p-value: promoter= 5.86e-86, intron= 0.036, coding exon= 2.2e-107, 3'UTR= 1.25e-5, 5'UTR= 2.9e-11.

Implementation of DamID sequencing

In the second part of the MEL-28 analysis, we found the constraint that NimbleGen® no longer produced tilling arrays; hence we had to adapt the DamID method for its subsequent data analysis with sequencing, hereafter termed DamID-seq. However, this was a positive evolution of the technique, since next-generation sequencing (NGS) technologies allow to

detect the methylated fragments with higher resolution, accuracy and sensitivity. In chapter III, we describe in detail all the steps of the technique; therefore here we just mention some parameters that we modified to improve the analysis of MEL-28.

The first parameter to evaluate was the amount of starting material. It had been suggested that with NGS, DamID could be carried out with less material, taking advantage of this, we and other groups showed results using as little as 10 *C. elegans* worms (Sharma et al., 2014), or even single mammalian cells (Kind et al., 2015). Whereas these protocols were good enough to generate genome-wide maps at a resolution of 100 kb, we aimed to get a better resolution. Our old protocol started with 35,000 worms per sample. We used that number of animals because the hybridization to the microarray required 1 microgram of material. For DamID-seq we reduced this amount to 4000 worms to extract the gDNA and then we evaluated the minimum amount of starting genetic material to generate a good smear of PCR producs amplified from methylated gDNA fragments.

To optimize the protocol we used the strain expressing Dam::LMN-1 since based on our experience, it produces a robust DamID signal. As negative control we used N2 worms, which should not give any signal after the DamID protocol; otherwise, the signal is interpreted as a false positive obtained due to generation of random DNA breaks occurring during gDNA extraction and later ligated to the DamID adapters and PCR-amplified. We found that with a quantity of 500 ng of gDNA and 20 cycles of PCR a good pool of methylated fragments was obtained (Figure 5.10). We can even use 50 ng of gDNA and increase the number of PCR cycles to 22 and still have a nice smear of DamID PCR products versus N2 worms control. The reduction of the starting genetic material represents a clear advantage for the DamID assay in situations where is hard to obtain a big sample, for example, when the genotype of interest cannot be easily selected i.e., different sexes, balanced mutations, specific stages of development, etc., increasing the utility and versatility of the technique.

Interestingly, in 2015 Kind and colleagues published a simplified version of the DamID protocol, which consisted of only a few steps performed in a single PCR tube, avoiding the need for DNA isolation and purification (Kind et al., 2015). Briefly, the optimized protocol consists in: lysis of the sample, digestion with DpnI, ligation with adaptor and PCR amplification. Two key differences with the conventional protocol are i) without prior gDNA purification, worms are placed directly into the single tube used throughout the full experiment; ii) DpnII digestion is eliminated.

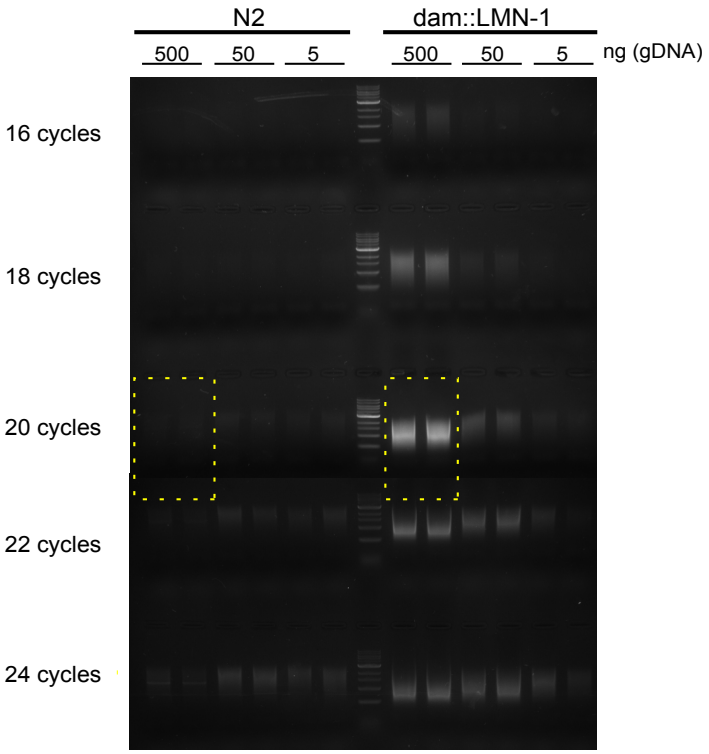

Figure 5.10. Test of starting material and number of PCR cycles for DamID-seq. DamID duplicate samples are visualized on 1% agarose gel. To the right side of the molecular weight shows the optimization done with different concentrations of Dam::LMN-1 gDNA; and on the left side, its corresponding control of N2 gDNA. Yellow dotted rectangles surround a correct smear of PCR-amplified methylated fragments from 300 to 1000 bp obtained with 20 cycles. In the bottom of the gel is shown that with 22-24 PCR cycles false PCR products begin to be amplified.

We tested the simplified version of DamID-seq in duplicate and compared both the methylated fraction smears and the final library smears obtained, either starting with worms or with gDNA (Figure 5.11, in the top). Although this "all in one tube" protocol is quite attractive, using the same tube throughout the experiment, it has the limitation that the volumes at each step are already determined. For example, in the first step, a volume of 10 μL of lysis buffer is used, so it has the restriction that only approximately 10 worms can be employed. To compare both sources of genetic material, we employed in parallel either 10 worms or 50 ng of purified gDNA in 10 μL of lysis buffer and performed DpnI digestion. Subsequently, we continued with the adapter ligation step and PCR amplification. We used 26 cycles of amplification for the 10-worm sample (Figure 5.11, on the left side) as the protocol indicated, whereas for the gDNA sample we used the previously standardized number of 22 cycles (Figure 5.11, on the right side). Since the amount of DNA present in 10 worms is very low, approximately 2.2 ng, the PCR amplicons from the methylated fragments are almost not visible on the agarose gel (Figure 5.11, on the left side).

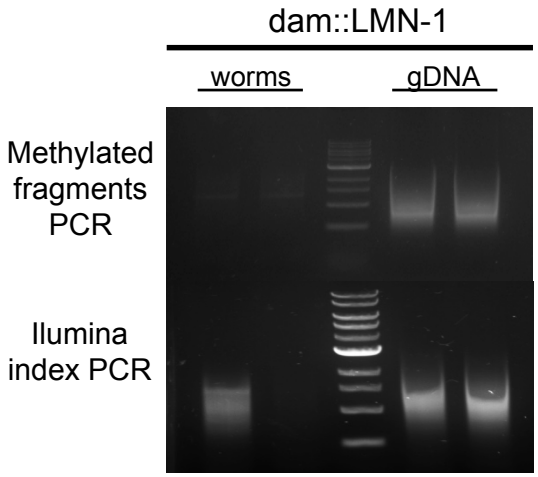

Figure 5.11 Test of different sources of genetic material for dam::LMN-1 DamID-seq. DamID duplicate samples are visualized on 1% agarose gel, 5 μL were loaded of 50 μL reactions. To the left of the molecular weight are shown the results obtained with 10 worms and 26 PCR cycles. In the right side are visualized the results acquired with 50 ng of gDNA and 22 PCR cycles. In the bottom of the gel is shown the size range of the generated libraries.

Finally, we proceed with the preparation of the Illumina libraries and their final verification on agarose gel, where their size range is evaluated. An important note is that the worm library was generated from 2 quantities of PCR products, therefore corresponding to 20 worms. While the libraries generated with gDNA were correct, for the libraries made with worms we found that only one was generated in this round of experiments (Figure 5.11, in the bottom). Despite we were able to set up the new DamID-seq protocol in our lab with two different sources of genetic material, we prefer to work with the protocol using gDNA since we think that the verification of methylated fragment after PCR amplification is an important control step in the assay, since the "all in one tube" protocol can be more prone to failure due to the very low amount of starting material. In addition, we want to generate libraries which mapping can generate genome-wide profiles with higher resolution than 100 kb.

Another point that we wanted to evaluate was the relevance of digestion with DpnII. In the original protocol, it is established that it is an important control point in the technique, which guarantees that only DNA fragments flanked by methylated GATC sites on both sides are amplified (Vogel et al., 2007). However, in the simplified version of the technique, this step was eliminated. We evaluated the incorporation of the digestion directly into the original protocol published with 10 worms (Sharma et al., 2014), minimally modifying the amounts of

distilled water to have a volume sufficient to add 10 units of the DpnII enzyme and its specific buffer. Then, we performed the DamID-seq protocol until the PCR amplification and loaded 30 μL of PCR products to facilitate their visualization in the gel, as control we performed the standard protocol without any modifications. While with the standard protocol smears corresponding to methylated fragments were visible after at 24 and 26 PCR cycles (note the presence of a band originating from PCR bias), in the modified protocol with the addition of DpnII digestion, we did not detect any PCR products (Figure 5.12A). We interpreted the absence of amplification as a possible incompatibility of buffers. Then, we replaced the DpnII enzyme with its isoschizomer MboI that uses a universal buffer to performer its digestion (Figure 5.12B). This time we also included additional DamID-seq controls using N2 worms with both protocols. However, again we did not get any amplification. Finally, we tested the effect of a purification step before the DpnII digestion or one purification step before and one after the DpnII digestion to eliminate the effect of buffer incompatibility. Considering that with the addition of an extra purification step DNA could be lost, we decided to start the protocol with 500 ng of gDNA, eliminating the step of sample lysis (Figure 5.12C).

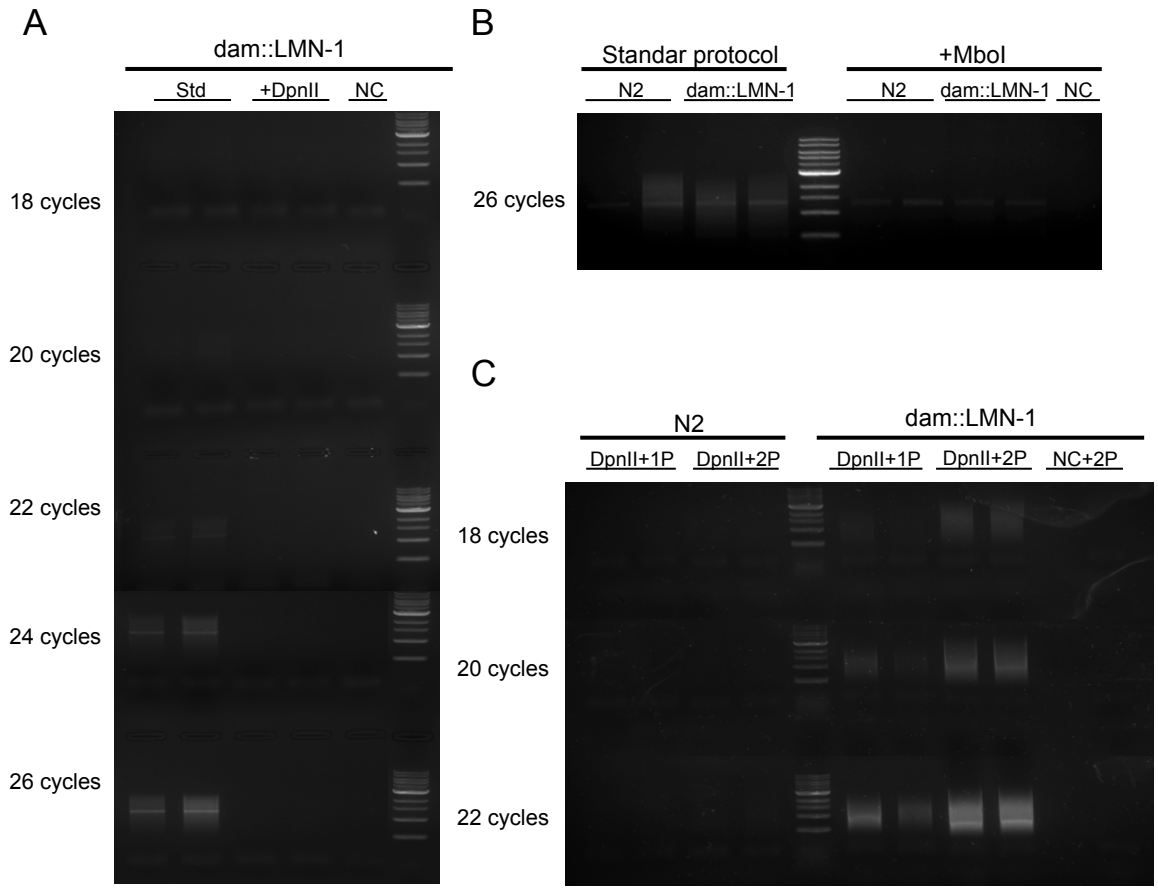

Figure 5.12. Test of addition of DpnII digestion in DamID-seq protocol. DamID samples signal, on 1% agarose gel. (A) Comparison of DamID-seq "all in one tube" standard protocol done with 10 worms and "all in one tube" plus DpnII digestion. 30 µL were loaded for visualization, only standard protocol generated PCR products. (B) Comparison of DamID-seq protocols done with 10 worms. On the left size, "all in one tube" standard protocol is shown. On the right size, "all in one tube" plus MboI digestion protocol is shown. 30 µL were loaded for visualization, only standard protocol generated PCR products, although one of the N2 controls also produced a visible signal, suggesting generation of DNA breaks during the process. (C) Implementation of DpnII digestion plus purification in DamID-seq protocol, using 500 ng of gDNA. Samples from N2 (left side) and Dam::LMN-1 (right side) were processed with DamID-seq protocol plus one (DpnII+1P) or two purifications (DpnII+2P) done just before, or before and after DpnII digestion, respectively. Protocol with two purifications provides better results. NC= negative control.

After this adjustments, we were able to obtain the smear corresponding to methylated fragments in the samples from Dam::LMN-1, whereas the N2 control did not produce any amplification. Moreover, we tested whether just a single purification before DpnII digestion was enough to eliminate any conflict between reactions, or if two purifications were necessary to get amplification. We found two purification steps were more efficient to get a nice smear, getting a very similar result than in our previous optimization (Figure 5.10), determining as optimal 500 ng digested with DpnI and DpnII and been amplificated with 20 PCR cycles when we make two purifications (the entire protocol can be reviewed in chapter III). In the case of performing just one purification before DpnII digestion, 22 PCR cycles are required.

In order to estimate the sensitivity of the new DamID-seq protocol and evaluated whether this technique provides sufficient sensibility to recognize signal from for instance a few cells in a large population, we tested if true signal could be amplified when we mix gDNA from Dam::LMN-1 worms with different concentrations of N2 gDNA (Figure 5.13), assessing the following proportions of gDNA: 1:1 (50ng N2 + 50ng Dam::LMN-1), 1:10 (50ng N2 + 5ng Dam::LMN-1), 1:100 (50ng N2 + 0.5ng Dam::LMN-1), and 1:1000 (50ng N2 + 0.05ng Dam::LMN-1). To minimize any false signal from N2 we did the first test using 20 cycles. We found that signal can be obtained from dilution 1:1, 1:10 and 1:100 (Figure 5.13A). We subsequently did a second assay by increasing the number of PCR cycles and adding a control made with gDNA exclusive of N2 worms, thereby exhibiting any signal that could be originated from DNA breaks. We found specific signal can be achieved from dilution 1:1, 1:10 and 1:100 at 20 and 22 cycles (Figure 5.13B), corresponding to 10% and 1% of Dam::LMN-1, respectively. Using 22 cycles, we recommend using extreme caution during the process since the control made exclusively with N2 gDNA produces a detectable signal.

We conclude that working with dilution 1:1000 produces a signal very similar to N2 indicating that we are seeing mostly unspecific signal. We conclude that specific signal can be achieved with 1% of gDNA derived from Dam::LMN-1 worms. Interestingly this specificity enables to use this technique in cases with low proportion of methylated DNA, for example in tissue specific DamID experiments.

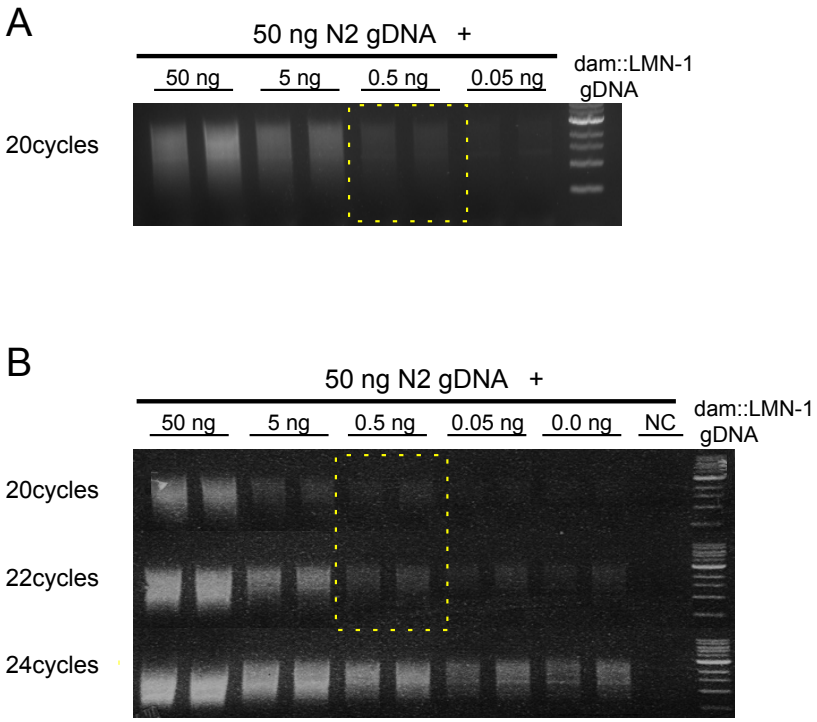

Figure 5.13. Test of DamID sensitivity. DamID samples are visualized on 1% agarose gels. (A-B) DamID-seq performed with a mix of gDNA from both Dam::LMN-1 and N2 worms. Different concentrations were used to evaluated dilutions from 1:1, 1:10, 1:100 and 1:1000 of Dam::LMN-1 in N2 background. Yellow dotted rectangles surround the smear of specific signal from Dam::LMN-1.

We evaluated the correlation between the data from DamID-array and DamID-seq, using again the strain expressing Dam::LMN-1 fusion protein because lamin-associated domain (LADs) are well studied and show similar properties between species such as worms, flies, human cells, etc., (González-Aguilera et al., 2014; Kind & van Steensel, 2014; Kind et al., 2015; E. G. Lund et al., 2015; Pickersgill et al., 2006). We considered this comparison important in order to validate the methods and to facilitate comparisons between different studies. We performed the DamID-seq protocol (using 500ng of gDNA and including DpnII

digestion), and calculated the log2 score of the data previously normalized with GFP::Dam (details are provided below). We binned the genome in 10 kb windows as was done with the data of LMN-1 tiling array (González-Aguilera et al., 2014). We found a high correlation between both methods (r=0.61) at 10 kb bins (Figure 5.14A), but we also estimate the correlation of the data at 1kb and 100 kb windows, to get a broader picture of the similarity of data (Figure 5.14B). As we expected the correlation increase using larger bin size (r=0.73 at 100 kb bin) showing the high similarity of both dataset.

In addition, we compared the LADs that are discovered with both techniques (Figure 5.14C). To make the comparison we worked with the LMN-1 peaks previously published by González-Aguilera and collaborators, which were obtained by DamID-array (González-Aguilera et al., 2014); whereas LMN-1 peaks concerned to DamID-seq were processed with the program MACS2 (details below). We found that 80% of LADs identified with DamID-array were present in the dataset from DamID-seq demonstrating the very good correlation between both methods. On the other hand, we found an overlap of 67% of LADs identified with DamID-seq. This difference corresponds to new LADs discovered with sequencing due to the increase in resolution/sensibility with this technique.

In collaboration with Meister's lab, we assessed the number of reads requires to achieve reproducible results between libraries. We analyzed the behavior of GFP::Dam samples and found that even for sequencing depth higher than 1 million of aligned reads, the number of GATC motifs detected after mapping does not increase over 75-80% of the total mappable motifs (Figure 5.15A). This result was reproducible whether we work with libraries done with 10 worms (Sharma et al., 2016) or purified gDNA (Gómez-Saldivar, Meister, et al., 2016). Another parameter to consider is the size of the windows in which the genome is binned to perform the interaction profile. We evaluate the Pearson correlation between libraries of approximately 2-3 millions of mapped read from two different proteins (LMN-1 and NPP-22; Figure 5.15B). As expected, we found that the correlation is significantly higher using larger windows.

Finally, we compare the DamID Pearson correlation obtained with NPP-22 libraries sequenced with 1 and 10 millions of reads (Figure 5.15C). We found from 1-10 millions of reads the Pearson correlation does not increase too much. This dynamic can be observed better if we plot the correlations vs. the bin size (Figure 5.15D). These data are supported by the parallel analyses done by Sharma and collaborators where it was concluded that sequencing depth is sufficient if the Pearson correlation is at least 0.95 after removing 50% of the reads *in silico* (Sharma et al., 2016).

A

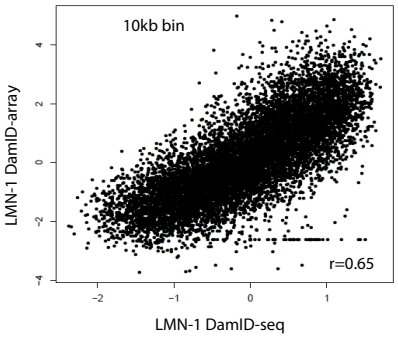

B

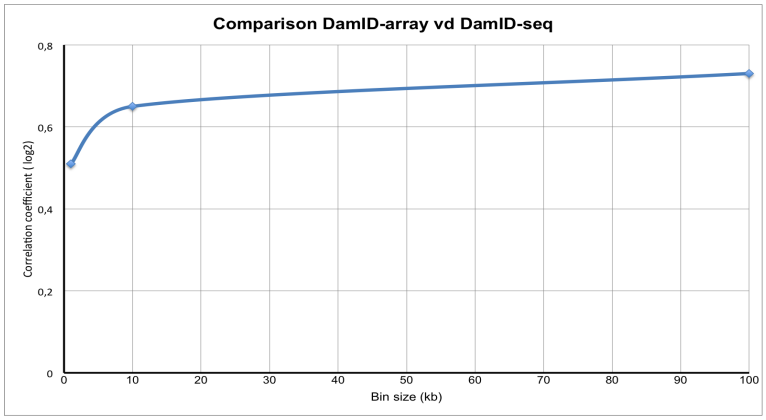

C

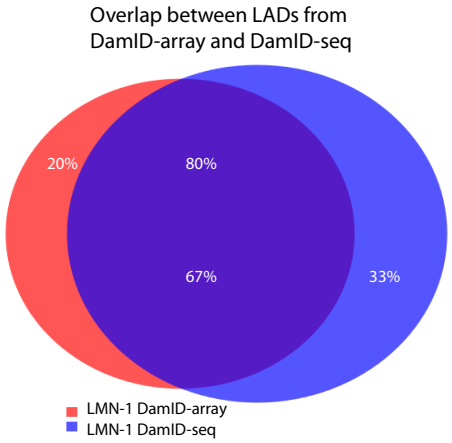

Figure 5.14. Correlation between DamID-array and DamID-seq. (A) Scatter-plot showing the correlation between the normalized data (log 2) binned in 10 kb windows from DamID-seq and DamID-array (r=0.61). (B) Graphic displaying the correlation between DamID done with array versus sequecing at different bin: 1 kb (r=0.51), 10 kb (r=0.61) and 100 kb (r=0.73). (C) Intersecting LADs discovered with DamID-array and DamID-seq (using 10 kb windows), revealed an overlap of 80% and 67% (897 of 1121, and 727 of 1085, respectively), LADs from DamID-array were taken from (González-Aguilera et al. 2014).

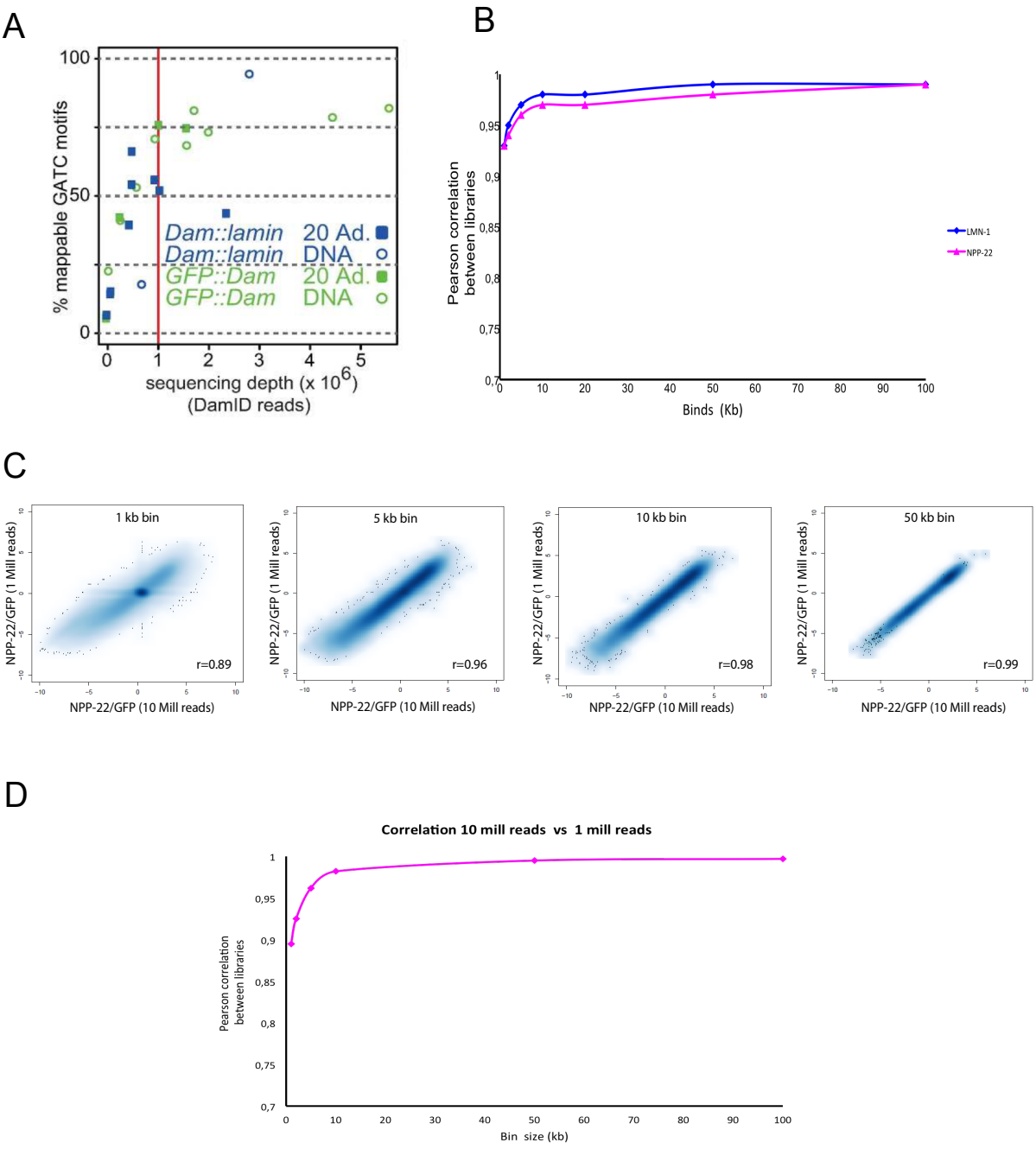

Figure 5.15. Test of sequencing depth required in DamID-seq. (A) Identification of mappable GATC sites (%) found according to the number of DamID reads, GFP::Dam library is shown in green and Dam::LMN-1 in blue, respectively. The red line indicates one million DamID reads. Adapted from (Sharma et al., 2016). (B) Effect of binning size on Pearson correlation between replicates, two Dam::LMN-1 and NPP-22::Dam libraries were sequenced. Libraries showed better correlation at higher bin size (>10 kb). (C) NPP-22::Dam Pearson correlation according to the sequencing depth. We found very well correlation between libraries; in fact, it almost does not change since 10 kb bin.

DamID-seq of MEL-28 specific localization reveals high correlation between MADs from both pools

As we discussed above, one crucial point in the interpretation of Nup-chromatin interactions is if these actually take place at the NPC. Data interpretation can be confusing if the analysis does not separate interactions involving Nups at NPCs from Nups pools in the nucleoplasm. In order to discriminate between MEL-28 chromatin interactions that occur at NPCs level and inside the nucleoplasm, we used our DamID-seq protocol and generated genome-wide interaction maps of MEL-28 versions with different dynamics and localization (Figure 5.1). We worked with (1) the fusion of Dam with MEL-28 full length; moreover we generate two fusions of Dam with different nucleoplasmic version of MEL-28: (2) one lacking the NPC-interacting domain (the entire β-propeller domain and the first aminoacids [aa] of α-helical domain), henceforth called MEL-28$^{508\text{-end}}$; and (3) another version expressing only the C-terminal part plus the last 120 aa of α-helical domain, henceforth called MEL-28$^{835\text{-end}}$. Both fragments were previously characterized in chapter IV. Besides, we generated (4) a fusion of Dam with a constitutive NPC-tethered version of MEL-28, which consists in MEL-28 full-length protein fused to the transmembrane Nup NDC1/NPP-22 (Stavru et al., 2006). In addition, we produced (5) a fusion of Dam with the single Nup NPP-22. Given its localization, more internally inside the NPC, this fusion protein could have lower or no chromatin accessibility, but will exclusively expose NPC-chromatin interaction.

We assessed the localization of fusion proteins after heat shock by IF microscopy using a MYC antibody. Dam::MEL-28 localized in two pools, at the NPC/NE, and throughout the nucleoplasm, as was expected (Figure 5.16, top). Nucleoplasmic Dam::MEL-28 fragments were only detectably localized in the nucleoplasm, as their counterparts fused with GFP (Figure 4.4C in chapter IV,). NPP-22::Dam::MEL-28 localized correctly only in the NPC, as it was designed. However, for NPP-22::Dam the IF did not give satisfactory images. The N2 embryos control (Figure 5.16, bottom) did not show any signal with the MYC antibody. As control of the IF we use an antibody against the N-terminal part of MEL-28, which revealed NPC/NE localization (green arrows) and signal in the nucleoplasm in all the samples; however, logically MEL-28 fragments shown more enrichment in the nucleoplasm in this channel. In addition, without heat-shock treatment fusion protein expression was undetectable (data no shown). We conclude that the Dam-fusion protein localize as we expected (Figure 5.1). For NPP-22::Dam we plan to check its expression by western blot.

Subsequently, we generate the libraries using 500ng of gDNA from *C. elegans* young adults. We found that all the libraries generated a smear of the correct size, with exception of NPP-22::Dam::MEL-28. Despite several attempts to generate this library and increase the concentration of gDNA, we never generated a specific amplification signal. We think that this is due to a problem with the design of the fusion, Dam protein is placed in the middle of two large proteins NPP-22 and MEL-28 with a size of 588 and 1784 aa, respectively. It is possible that Dam has been "trapped" between both proteins, being unable to methylate the DNA. One alternative to try would be to make a new plasmid in where Dam was located after MEL-28.

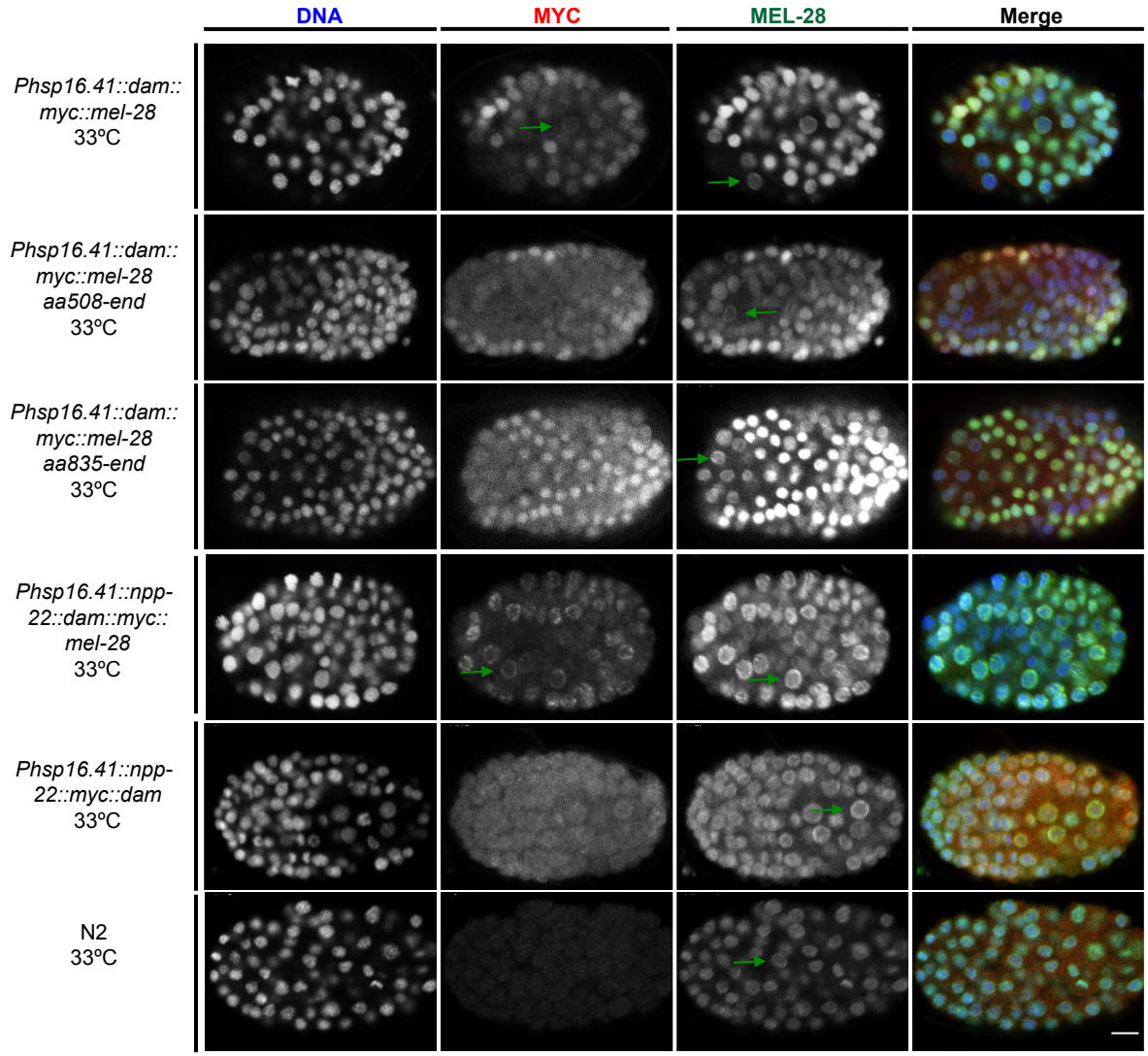

Figure 5.16. DamID fusion proteins expressing MEL-28 full-length and versions localize properly. Fusion proteins were expressed under the control of the hsp-16.41 heat- shock promoter. A MYC epitope inserted between the proteins of interest and Dam was used to detect the expression after the heat-shock treatment.

Embryos expressing the fusion proteins were fixed and stained with anti-MYC antibody (red in merge), anti-MEL-28 antibody (green in merge) and Hoechst 33258 to visualize chromatin (blue in merge). Localization to the NE of endogenous protein is indicated with green arrows in MEL-28 channel, whereas localization to the NE of fusion proteins is in MYC channel. N2 embryos with identical treatment were used as control. Scale bar 5 µm.

From the libraries, we extracted DNA-binding profiles for MEL-28 full-length protein, MEL-28 cytoplasmic versions and NPP-22. Moreover, we added a library generated with Dam::LMN-1 to complete our global view of chromatin interactions that occur at the NPC and NE. We normalized raw data with the GFP::Dam control to avoid bias generated by differences in chromatin accessibility. Then we evaluate the quality of sequencing reads using the pipeline RDamIDSeq (Sharma et al., 2016), which is an R-based pipeline designed for the analysis of DamID-seq data. Interestingly, we found that 70-80% of the total of reads were mappable to GATC motifs (Table 5.1), indicating a high quality of sample preparation.

Table 5.1. Quality control metrics of sequencing libraries from RDamIDSeq data analysis

Sample	Raw Reads	Cut reads	Cut Reads (%)	Mapped reads	Mapped reads (%)	GATC sites	GATC identified (%)
MEL-28 rep1	878660	725497	83%	787507	90%	659263	75%
MEL-28 rep2	1296470	1194654	92%	1058750	82%	990553	76%
GFP rep1	565412	495995	88%	490877	87%	441883	78%
GFP rep2	1344511	1188004	88%	1154746	86%	1052405	78%
NPP-22 rep1	938789	846282	90%	792717	84%	717559	76%
NPP-22 rep2	1213993	1103141	91%	1035431	85%	936933	77%
MEL-28$^{508\text{-end}}$ rep1	779725	680462	87%	705640	90%	617667	79%
MEL-28$^{508\text{-end}}$ rep2	661684	588826	89%	598946	91%	536208	81%
MEL-28$^{835\text{-end}}$ rep1	788437	667661	85%	708084	90%	603291	77%
MEL-28$^{814\text{-end}}$ rep2	1117509	944415	85%	1015734	91%	864438	77%
LMN-1 rep1	4082739	3346615	82%	3303765	81%	2751633	67%
LMN-1 rep2	1834341	1525258	83%	1526910	83%	1285442	70%

Besides, we confirmed the reproducibility of results by comparing two biological replicas, which revealed a very good correlation (MEL-28 r= 0.87, MEL-28$^{508\text{-end}}$ r= 0.89, MEL-28$^{835\text{-end}}$ r= 0.92, NPP-22 r= 0.93, LMN-1 r= 0.96, for 1kb windows; Figure 5.17A). As above, we tested how the genome bin size influenced the correlation of the samples (Figure 5.17B) and decided to work with 1 kb bin. Thus, we averaged the two replicas to get a final association profile (Figure 5.17C). Interestingly, we found high Pearson correlation between MEL-full length and MEL-28 fragments (r=0.84 to MEL-28$^{508\text{-end}}$ and r=0.89 to MEL-28$^{835\text{-end}}$) and between the two MEL-28 fragments (r= 0.88). On the other hand, we found very low

correlation between MEL-28 and LMN-1 (r=0.27), and, surprisingly, even lower correlation between MEL-28 and NPP-22 (r=0.19). NPP-22 shows good correlation with LMN-1 (r=0.70), presumably reflecting that both proteins are strongly enriched at the nuclear periphery.

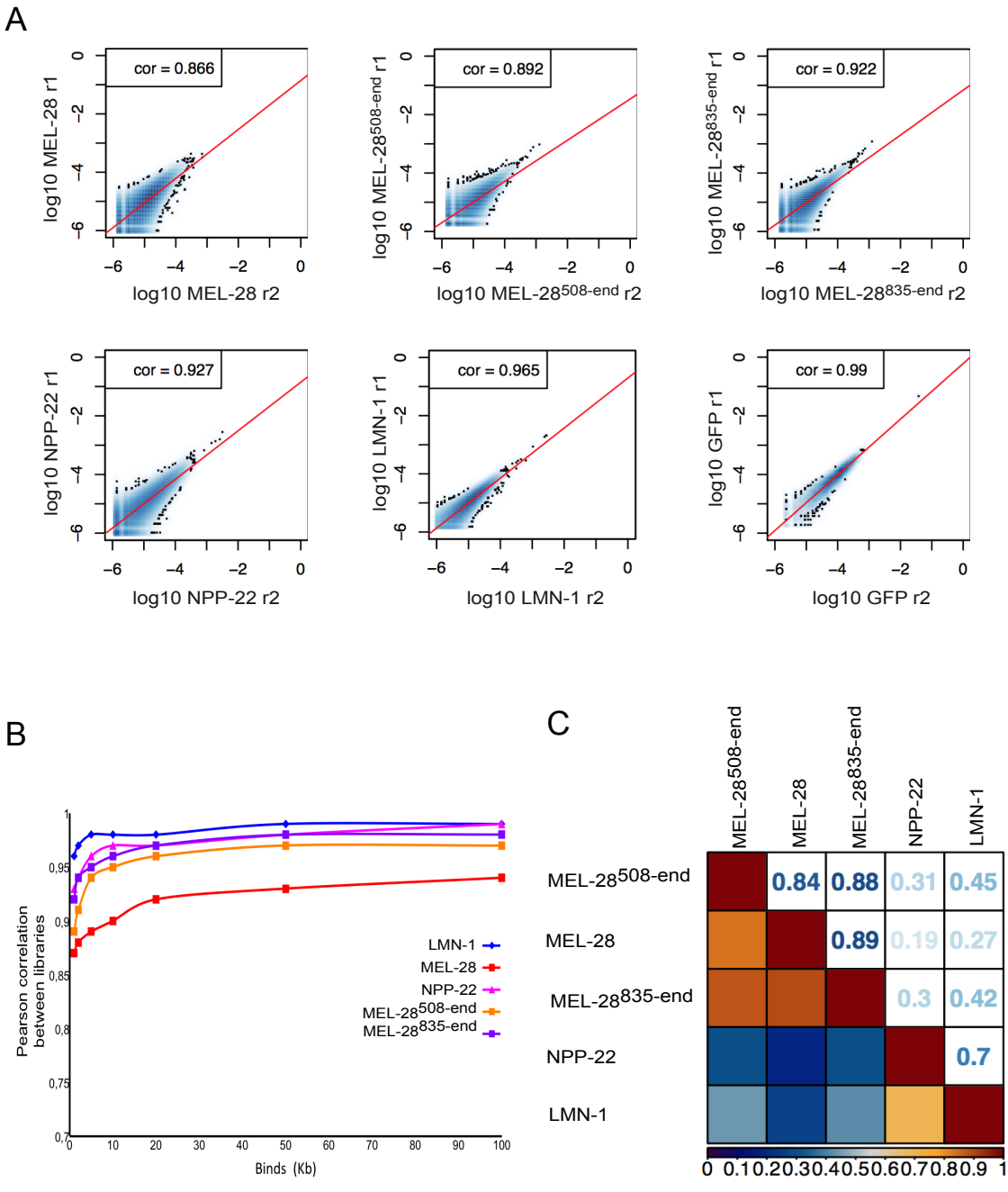

Figure 5.17. Correlation between DamID-seq replicates and libraries. (A) Scatterplots of correlation between replicas of NGS libraries: MEL-28, MEL-28$^{508\text{-end}}$, MEL-28$^{835\text{-end}}$ (top left-right), NPP-22, LMN-1, GFP (bottom left-right). All Samples were smoothed with a bin size of 1 kb. (B) Effect of binning size on Pearson correlation between replicates. We found very well correlation between libraries; in fact, it almost does not change since 5 kb

bin. (C) Genome-wide Pearson correlation matrix for all smoothed samples after normalization with GFP and replica merge.

MEL-28 and MEL-28 fragments interact with functionally different chromatin regions that NPP-22 and LMN-1

The genome-wide interaction map showed that MEL-28 full length and both MEL-28 fragments associates to almost identical regions (Figure 5.18). Moreover, they closely reassemble the profile previously observed with the MEL-28 DamID array: (Figure 5.3B). NPP-22 displayed a profile very similar with LMN-1, associating preferentially to chromosomes arms, leaving the central part with almost no NPP-22 or LMN-1 associated domains. Their similarity was also shared on the X chromosome, finding both proteins mainly at the left arm (Figure 5.18).

Next, we performed peak modeling and identification of regions with significant enrichment of DamID signals. We used the bedGraph file generated with the pipeline RDamIDSeq, in which the reads mapped to *C. elegans* genome were normalized and processed to obtain the log2 score. As we discussed in the Introduction, several programs can be used to analyze the DamID data, however, most of them are designed to ChIP-seq data. We used the peak caller program named Model-based Analysis of ChIP-Seq (Zhang et al., 2008) (MACS version2, MACS2), one of the most popular algorithms used for identifying binding sites. The standard command of MACS2, callpeak, can be easily used for ChIP-seq data alone, or with the control sample with the increase of specificity; this option works with bam files. We used the command bdgpeakcall, which defines peaks from a bedGraph output. Importantly, MACS2 allows analyze your data in a highly customized way using a cutoff parameter.

We tested different peak calling using a cutoff range from 0.3 to 1.0; given that our DamID score is in log2 this mean that using cutoff = 0.3, we select 1.2 times more methylations than control and, using cutoff = 1.0, we select 2 times more methylation than control. As expected, we observed that using lower values of cutoff we discover a higher number of peaks with a larger average size, covering larger genome regions but with less specificity (Table 5.2; for practicality, only the data analysis with the cutoff equal to 0.6, 0.8 and 1.0 are shown, corresponding to 1.52, 1.74 and 2 fold enrichment).

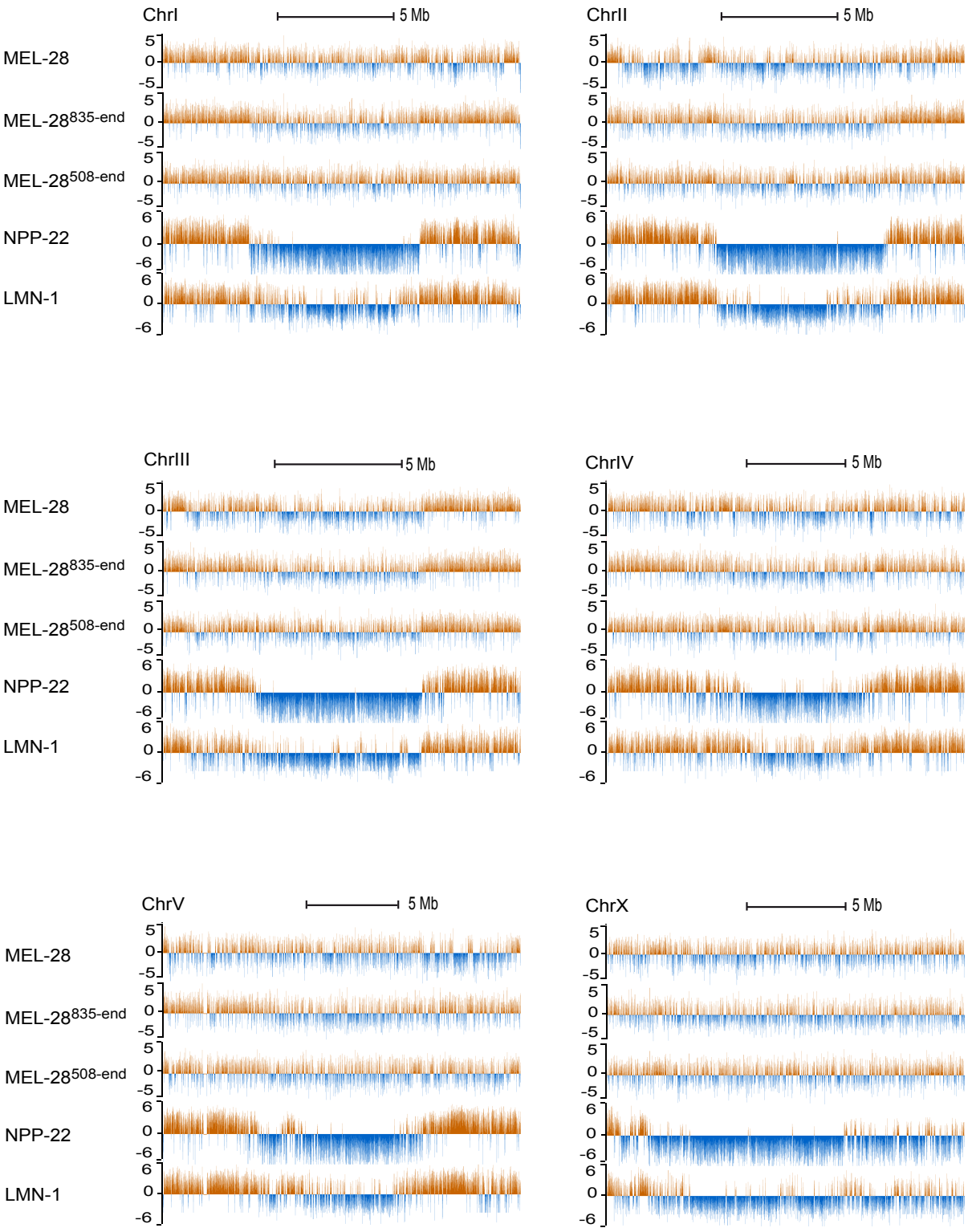

Figure 5.18. MEL-28 is associated along all chromosomes whereas NPP-22 and LMN-1 are associated in chromosomes arms. Genome browser views of interaction profiles in each chromosome of MEL-28, MEL-28$^{508\text{-end}}$, MEL-28$^{835\text{-end}}$, NPP-22 and LMN-1, after GFP::Dam normalization and binning the genome at 1kb. MEL-28 full-length and MEL-28$^{508\text{-end}}$, MEL-28$^{835\text{-end}}$ fragments show almost identical profiles (top). NPP-22 profile is more similar to LMN-1 than MEL-28 (bottom). Each profile represents the average of two independent experiments.

We also compared how the number discovered genes changed depended on the database that we used to identify the genes contained within the peaks; we did the test using *C. elegans* gene identifiers (WormID; http://www.wormbase.org) database, and the Reference Sequence (RefSeq; http://www.ensembl.org) databases (Pruitt, Tatusova, & Maglott, 2005).

Table 5.2. Test of peak calling cutoff

Sample	Cutoff	No. of Peaks	Peak Size Mean (bp)	Genome Coverage	No. Genes	
					Worm ID	RefGene
MEL-28	0.6	14966	1702	25.40%	10368	10882
	0.8	12752	1564	19.88%	8046	8334
	1	10985	1467	16.06%	6483	6643
MEL-28$^{508\text{-end}}$	0.6	15786	1509	23.76%	8871	9593
	0.8	13878	1414	19.57%	7197	7654
	1	10926	1310	14.28%	5003	5327
MEL-28$^{835\text{-end}}$	0.6	16096	1643	26.38%	11110	11599
	0.8	14142	1514	21.35%	8950	9625
	1	11831	1406	16.59%	6829	7074
NPP-22	0.6	8579	3167	27.09%	14223	14176
	0.8	8218	3075	25.29%	13241	13173
	1	7881	2970	23.34%	12301	12167
LMN-1	0.6	13229	2553	33.68%	16190	16730
	0.8	12583	2431	30.51%	14702	15162
	1	11821	2301	27.12%	12987	13349

To be able to process the 5 samples with all combinations of parameters i.e., cutoff from 0.3 to 1.0, two gene databases, and others criteria of the peak calling we designed a simple pipeline in Perl language, consisting of 6 loops scripts (Table 5.3). We start with the bedGraph file with the normalized DamID-seq score and we end up with the list of genes ready to enter into any web-based functional annotation tool, such as David (https://david.ncifcrf.gov) or Panther (http://pantherdb.org). Additionally, the scripts produce other output files that can be useful for further processing with different programs according to the needs of the analysis.

Finally, we decided to focus on the datasets generated by the cutoff = 0.6, which would be interpreted as regions with a methylation enrichment of 1.5 times more than the control. Through visual inspection, we observed that using cutoff from 0.6 to 1.0 the profiles do not present major changes (Figure 5.19). However, the peak calling done with cutoff 0.6 or 0.7 fits better to the signal found in the association profile. For example, the cutoff of 1.0, which in theory would generate peaks with more specificity, generates small peaks and in cases where we have a larger domain, it generates several small peaks instead of a broader peak

(rectangle with the red dotted line in Figure 5.19). Obviously, using a lower cutoff, peaks with less enrichment are also assigned (rectangle with the green dotted line in Figure 5.19). Even so, we decided that the cutoff of 0.6 was the best fit according to our criteria.

Table 5.3. Description of the program used to analyze data from peaks to genes

Script	Input	Output	Usage
Loop_MACS2.sh	bed file with normalized data	*_PEAKS.bed *_num_peaks.txt	To perform peak calling using different parameters in all the bed files containing in the folder. Generates a .txt report with the number of peaks found
Loop_cut_peaks.sh	*_PEAKS.bed	*_SCORE.bed	To produce 4 columns bed file (chr, start, end, score)
Loop_stadistic.sh	*_STAD.bed	*_STAD2.bed	To produce 3 columns bed file (chr, start, end) ready to load in UCSC browser and to get stadistic
Loop_peak_size.sh	*_STAD2.bed	*_peakSIZE.bed *_SIZE.txt	To get the size of the peaks. Generates a .txt file ready to load in Graph Prism, excel, R etc. and plot the results
Loop_intersect_wID.sh Loop_intersect_refGene.sh	*_PEAKS.bed	*_GOfull.bed *_num_genes.txt	Intersects the bed file with the table containing the position of the genes. Generates a .txt report with the number of genes found
Loop_GO.sh	*_GO.txt	*_GOfull_end.txt	Generates a .txt file with the list of genes ready to load into DAVID or another Gene Ontology program

Once the association domains were mapped, we analyzed in more detail the interaction domains of the different samples. For example, we noticed although MEL-28 full-length and fragments have very similar profile the coverage of the genome is slightly different. MEL-28 binds in total to a quarter of the genome (25.4%, 10368 genes, WormID), whereas the fragment lacking the β-propeller domain MEL-28$^{508\text{-end}}$ lightly reduces its association to 23.76% (1515 fewer genes than full-length). This could potentially be explained by the loss of genes associated with the NPC. However, the smaller fragment MEL-28$^{835\text{-end}}$ showed a slightly greater association with the genome, 26.38% (742 more genes than full-length), which was reflected by finding 2239 more genes than with the larger fragment. Although the association of NPP-22 and LMN-1 is confined to the chromosomes arms, they interact with a larger fraction of the genome, showing genome coverage of 27.09% (14223 genes) and 33.68% (16190 genes), respectively (Table 5.2).

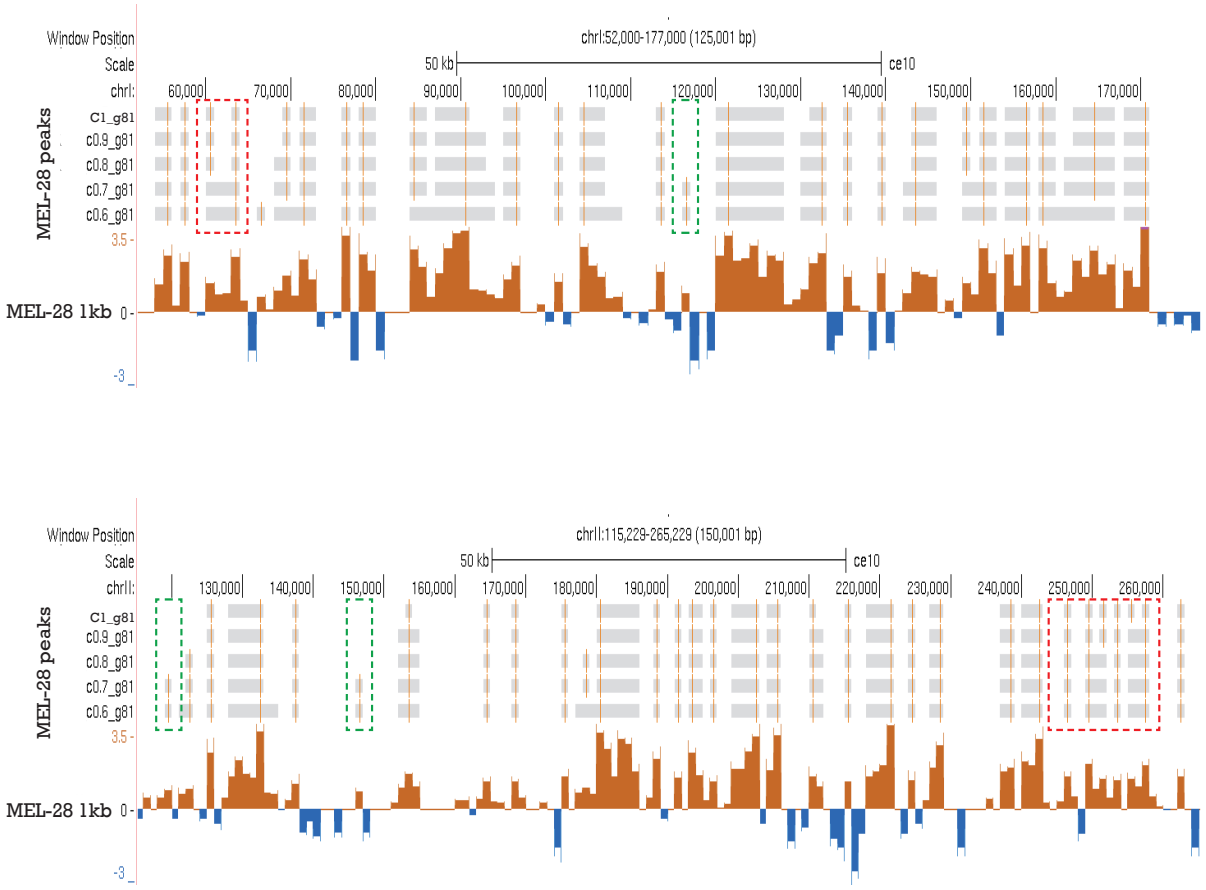

Figure 5.19. Inspection of different cutoff values during MEL-28 peak calling. Genome browser views of MEL-28 interaction profiles in chrI (top) and chrII (bottom); regions with a zoom at 125 kb and 150 kb respectively are displayed. In the top of each chromosome profile appears the different association domains generate with cutoff from 0.6 to 1.0. Inside rectangle with the red dotted line a zone with a broader peak is shown. Inside rectangle with the green dotted line a zone with peaks with less enrichment are shown. These peaks only appear with lower cutoff.

Through observation of the binding pattern at chromosomes arms, we could examine that large proportion of NPP-22 and LMN-1 interaction domains are broader than those of MEL-28 (Figure 5.20A). Besides, as reviewed above, its coverage in the genome is more distributed but smaller than NPP-22 and LMN-1. In contrast, regions, where there is more presence of MEL-28 peaks, are accompanied by gaps of NPP-22 and LMN-1. The domain sizes observed for MEL-28 full length and fragments varied slightly (Figure 5.20B; average peaks for MEL-28 = 1702 bp, MEL-28$^{835\text{-end}}$ = 1643 bp, MEL-28$^{508\text{-end}}$ = 1509 bp). Similarly, although NPP-22 and LMN-1 show very similar profiles NPP-22 peaks were statistically significantly larger (NPP-22 = 3167 bp and LMN-1 = 2553 bp).

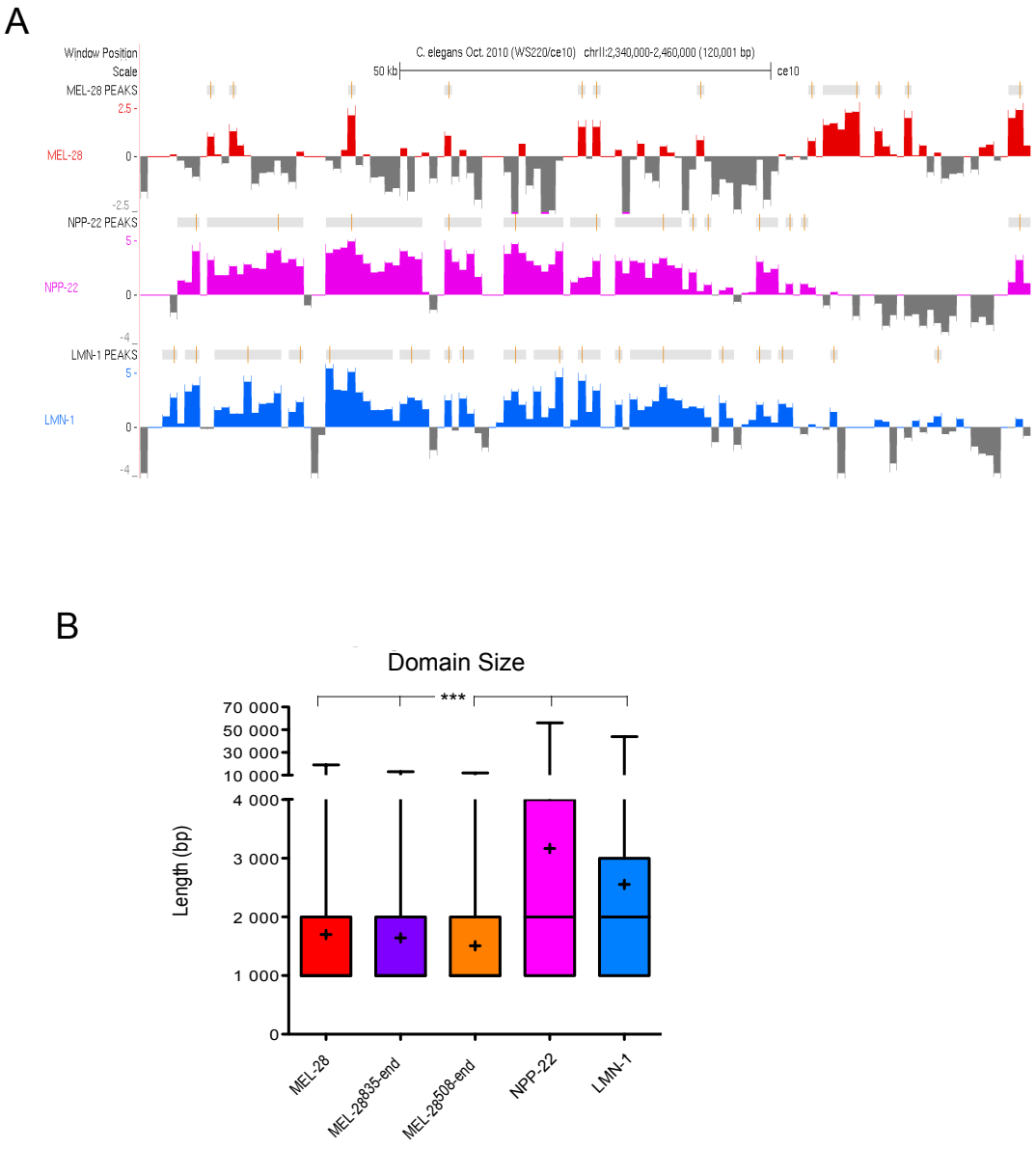

Figure 5.20. Genome-wide view of the left chromosome II arm reveals different chromatin association between MEL-28 and NPP-22 and LMN-1. (A) Zoom-in of the left chrII showing the signal intensity obtained with MA2C (score in log2). MEL-28 (in red) displays less and smaller association than NPP-22 (in pink) and LMN-1 (in blue). (B) Sizes of association domains are shown. Bottom and top of boxes indicate the 25th and 75th percentiles, respectively, lines in the boxes indicate medians, and crosses represents the average size of the peaks (MEL-28 = 1702 bp, MEL-28$^{835\text{-end}}$ = 1643 bp, MEL-28$^{508\text{-end}}$ = 1509 bp, NPP-22 = 3167 bp, and LMN-1 = 2553 bp); being sadistic significative smallest the domains of MEL-28 (in red) and the fragments (orange and purple) in comparison to domains of NPP-22 (in pink) and LMN-1 (in blue). Although MEL-28 and the fragments seem to have very similar peaks, their size is sadistic different. Whiskers indicate the lowest and the highest data points within 1.5x interquartile range from the box. Wilcoxon rank sum test was used to get probability value. *** p-value= <0.001.

It has been reported that NE proteins LEM-2, LMN-1 and EMR-1 shown an autosome chromosome occupancy that positively correlated with the chromosome size (González-Aguilera et al., 2014; Ikegami et al., 2010). In order to examine if MEL-28 and NPPP-22 shared this feature, we measured the percentage of occupancy of fusion proteins at each autosome chromosome and sexual chromosome. Interestingly, whereas NPP-22 and LMN-1 displayed a concordance of association relative to the size, and a low occupancy in the sexual chromosome, MEL-28 showed a very similar association between all chromosomes (Figure 5.21A). This association profile is independent of the MEL-28 localization since the MEL-28 fragments followed the same behavior; due to the binding range of MEL-28 and both fragments with the chromosomes is so uniform that it gives the impression that on the larger chromosomes there is less binding (Figure 5.21B). Intriguingly, it was clear that NPP-22 and MEL-28$^{508\text{-end}}$ bind considerably less to the X chromosome.

In order to appreciate the differences between the interaction of the X chromosome and different NE components, we decided to quantify the association of all fusion proteins exclusively on the X chromosome (Figure 5.21C). MEL-28 was the protein with highest occupancy on the X chromosome. Intriguingly, this association seems to be independent of MEL-28 N-terminal part because MEL-28$^{835\text{-end}}$ showed the same level of association than MEL-28 full length (24%). In contrast, the MEL-28$^{508\text{-end}}$ fragment showed a reduced association (19%), suggesting that the α-helical domain might have a negative effect on X chromosome association. Nevertheless, NPP-22 had the lower association with the X chromosome (11%).

MEL-28 colocalizes with kinetochore components, but does not share the same centromeric association sites

Once the MADs were defined, we decided to explore whether they overlapped with the centromeric sites, which are characterized by the presence of the histone variant CenH3/CENP-A that replaces the canonical histone H3 in centromeric nucleosomes, and inner kinetochore proteins, such as CenH4/CENP-C and the KNL-1/3 complex (Desai et al., 2003; Monen et al., 2005; Oegema & Hyman, 2006). Early studies have shown that MEL-28 colocalizes with kinetochore components (Galy, Askjaer, Franz, López-Iglesias, et al., 2006a); see also Figure 4.4 and 4.9 in chapter IV), and participates in the kinetochore assembly pathway at different levels; for example, CenH3 is required to MEL-28 localization

at kinetochores, and in turn, KNL-3 requires MEL-28 to accumulate at the kinetochore (Fernandez & Piano, 2006).

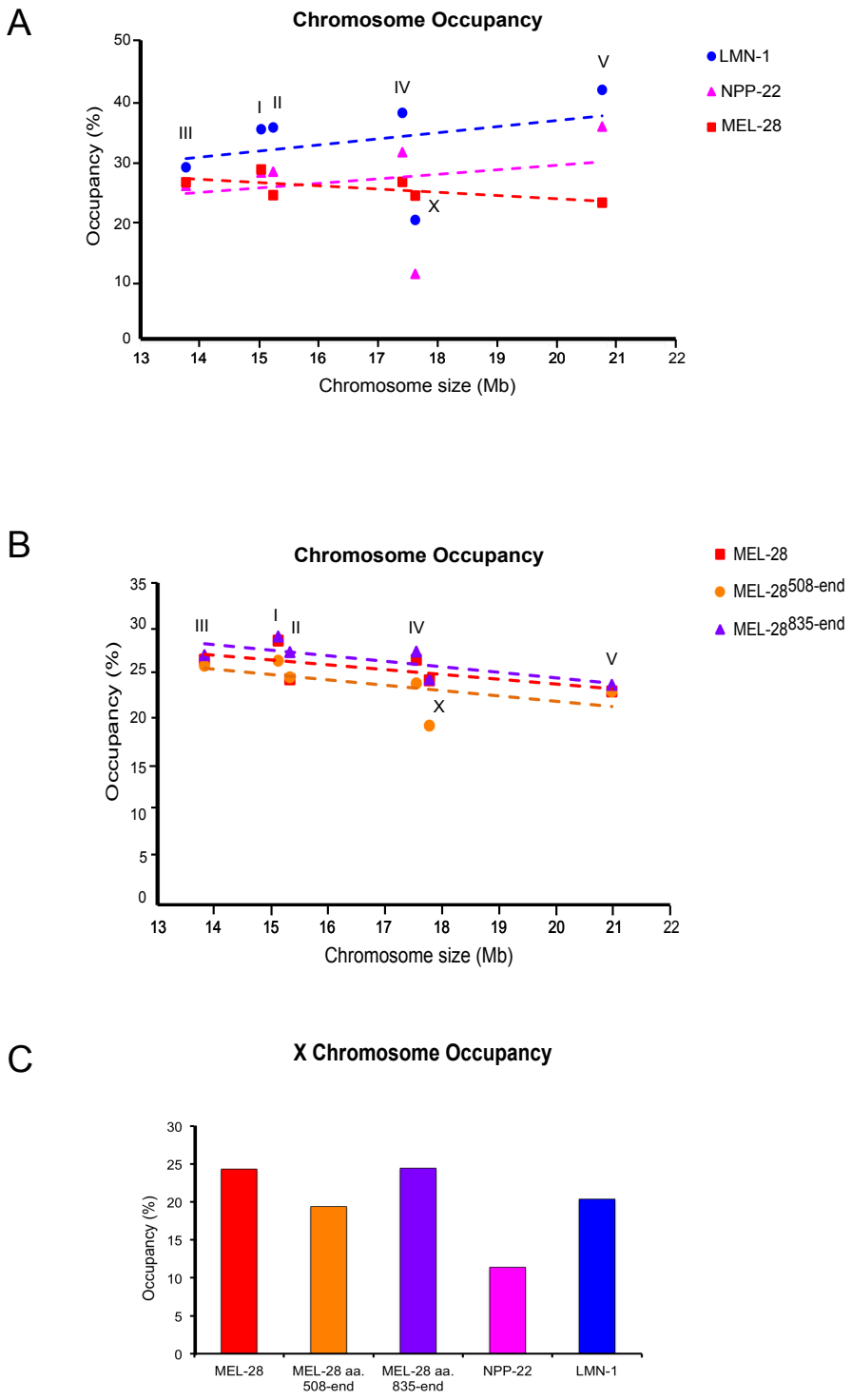

Figure 5.21. Relationship between chromosome size and MEL-28, NPP-22 and LMN-1 relative occupancy. (A) Linear regression lines for MEL-28 (red; r = -0.64), LMN-1 (blue; r = 0.92) and NPP-22 (pink; r = 0.99) occupancy are indicated, illustrating NPP-22 and LMN-1 shown a positive correlation, whereas MEL-28 does not.

(B) Linear regression lines for MEL-28 (red; r = -0.65), MEL-28$^{508\text{-end}}$ (orange; r = -0.88) and MEL-28$^{835\text{-end}}$ (purple; r = -0.80) occupancy are indicated, illustrating the independence of bind correlation with MEL-28 localization. Correlation values in A and B were calculated discarding the X-chromosome. (C) Analysis of fusion proteins interaction with X chromosome. MEL-28 and MEL-28$^{835\text{-end}}$ were the protein that most bind to the X chromosome (24%). While MEL-28$^{508\text{-end}}$ fragment and NPP-22 showed a reduced association (19% and 11%, respectively).

Besides, we found that during oocyte maturation MEL-28 gradually shifted from the NE to meiotic chromosomes, enclosing them in the classical "cup-shaped" patter of kinetochore proteins (Figure 4.2A in chapter IV). In order to achieve a better characterization of the dynamics of MEL-28 and kinetochore proteins *in vivo*, we generated embryos expressing GFP::KNL-3 and knock-in mKate::MEL-28. Confocal microscopy images support the perfect colocalization of these proteins in both meiotic and mitotic chromosomes (Figure 5.22A). After collecting all this evidence, the next step was to investigate a possible relationship between the distribution of MEL-28 and cenH3 in the genome. To date, two studies have mapped the genome-wide association profile of CenH3 in *C. elegans*, showing slightly different results (Figure 5.22B).

On the one hand, Gassmann and collaborators using a microarray-based approach (ChIP-chip) reported that CenH3 occupies ~2900 broad domains and suggested that cenH3 nucleosomes assemble at random positions within the domain (Gassmann et al., 2012). On the other hand, Steiner and Henikoff using a sequencing-based approach (ChIP-seq) with single base-pair resolution, perceived a similar profile with low CenH3 occupancy, but also found approximately 700 small sites with much higher CenH3 occupancy. Also, they showed that these sites are favored for the establishment of centromeric nucleosomes and serve as potential attachment sites for the kinetochore (Steiner & Henikoff, 2014).

Initially, when we only had access to the data of MEL-28 and CenH3 obtained with either DamID or ChIP on microarray-based approach, respectively, we found a negative correlation. Opposite to our expectation, we observed a slight enrichment of the CenH3 signal, in places where MEL-28 was absent (Gaps; Figure 5.22C left). Later, when CenH3 ChIP-seq data were available, we made the comparison again finding the same results (Figure 5.22C right). However, when we made the comparison using the MEL-28 DamID-seq data we obtained slightly different results; whereas with the CenH3 ChIP-chip data signal we found a negative correlation, with CenH3 ChIP-seq data we observed a slight enrichment of the CenH3 signal in MADs (Figure 5.22D).

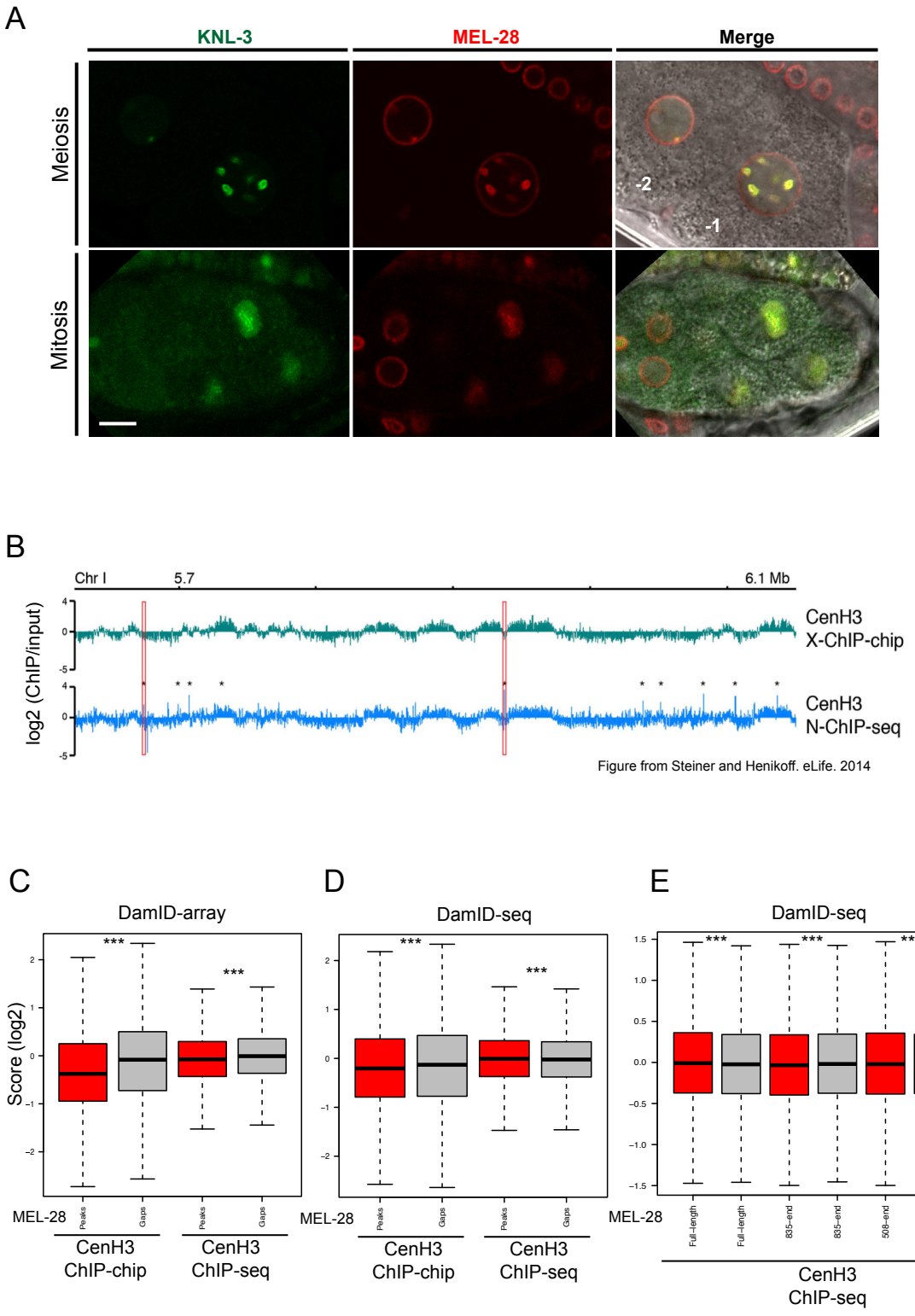

Figure 5.22. Correlation between CenH3 and MEL-28 domains. (A) mKate::MEL-28 (red in merged) was expressed in oocytes and embryos and accumulated together with KNL-3 kinetochore component (green in merge) in both meiotic and mitotic chromosomes (top and bottom of the image, respectively). Shown are the two most proximal oocytes where position -1 is immediately next to the spermatheca. Scale bar 10 µm. (B) Comparison between CenH3 profiles from two studies using ChIP-chip (Gassmann et al., 2012) or ChIP-seq (Steiner & Henikoff, 2014). (C) MEL-28 peaks from DamID-array data have slightly less association with CenH3

compared to MEL-28 gaps (D-E) CenH3 association is similar within MEL-28 peaks and gaps from DamID-seq data although not statistically identical. *** p-value= <0.001.

Consequently, we evaluated the association of the CenH3 in the peaks of the fragments and found that while the CenH3 is enriched in MEL-28$^{508\text{-end}}$ association domains (Gaps; Figure 5.22E right), with the smaller fragment we find the opposite, CenH3 is enriched in MEL-28$^{835\text{-end}}$ absent sites (Gaps; Figure 5.22E middle).

Nucleoplasmic MEL-28-chromatin interactions preferentially occur at developmental genes and genes related to mitotic processes

Through the visual inspection of the association profiles of the different fusion proteins, we found that even though the global profiles of MEL-28 full-length and fragments were highly similar (Figure 5.18), there were also variations between them. For example, local observation of a region of approximately 100 kb of the chrII arm, revealed the presence of three kinds of peaks: (i) peaks that are almost identical between MEL-28 full-length and fragments, (ii) peaks that just appear in MEL-28 fragments, (iii) peaks that just appear in MEL-28 full-length (Figure 5.23).

To perform a more detailed analysis of the differences in the chromatin association of MEL-28 full length and fragments, and at the same time with the Dam-fusion proteins of the nuclear periphery, we extracted the common and different peaks between all datasets We defined as common peaks those that overlap at least 30% with MEL-28 or NPP-22 association domains (Table 5.4, in the top). We found that 72% of the association domains of MEL-28 full length are shared with the smaller fragment MEL-28$^{835\text{-end}}$, while 59% are shared with the MEL-28$^{508\text{-end}}$ fragment. The number of peaks in common was less than we anticipated, especially for MEL-28$^{508\text{-end}}$ fragment, given the high correlation between samples and their similarity in the profile displayed in the Genome browser. However, certain factors have to be considered, for example, (i) If we observe the region shaded with one asterisk in the Figure 5.23, despite the fact that in the three proteins two peaks are identified, they have different extension, therefore there may be regions where the overlap is below to the cutoff and we lose common peaks. (ii) MEL-28$^{508\text{-end}}$ fragment MEL-28

presented slightly smaller peaks and less genome coverage, which could explain that it presented less similarity than the other fragment. (iii) In the region shaded with three asterisks, we can notice visible signal for full-length protein but not for the fragments, but this peak does not show high enrichment, then using parameters more strict in the peak calling we could eliminate these small peaks which could potentially be false positives.

Interestingly, we found a high level of overlap of MEL-28 peaks with LMN-1 and NPP-22 peaks, 60% and 45% respectively. This unexpected percentage may be due to the size of binding domains. If we examine the Figure 5.20A, we can perceive that although the association profile is not similar, the broad peaks of NPP-22 and LMN-1 can contain several smaller MEL-28 peaks; and therefore, the flexible settings in peak calling and peak intersect analysis influence considerably the number peaks scored as common.

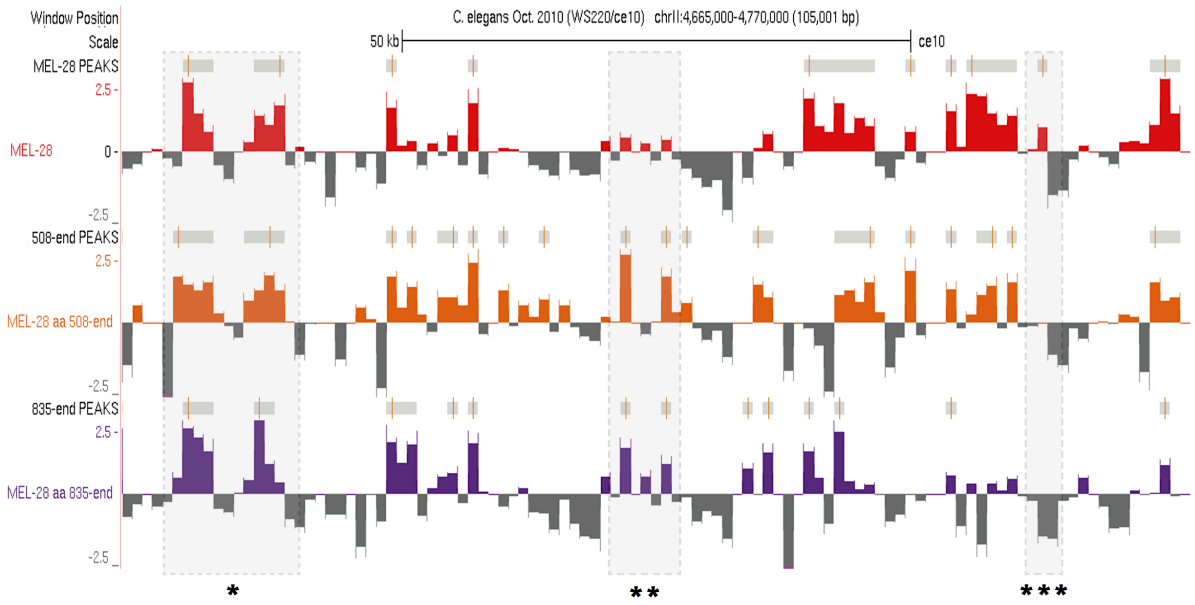

Figure 5.23. Zoom in on chromosome regions reveals different chromatin association between MEL-28 full-length and fragments. **An example of a chrII region that shows three principal classes of MEL-28 peaks: peaks in common between MEL-28 full-length and fragments (region shaded with one asterisk), and peaks that just appear in MEL-28 fragments (region shaded with two asterisks), or in MEL-28 full-length (region shaded with three asterisks).**

Table 5.4. Subset of MEL-28 and NPP-22 peaks according to its presence of absence in other peaks calling

Sample	Sample	Common peaks (50% overlap)	% Peaks	Common peaks (30% overlap)	% Peaks	Different peaks	% Peaks
MEL-28	MEL-28$^{835\text{-end}}$	10095	67%	10773	72%	4146	28%
	MEL-28$^{508\text{-end}}$	7958	53%	8760	59%	5991	40%
	NPP-22	6556	44%	6806	45%	8044	54%
	LMN-1	8449	56%	9008	60%	5788	39%
NPP-22	MEL-28	3764	44%	4574	53%	2944	34%
	MEL-28$^{835\text{-end}}$	3889	45%	4770	55%	2763	32%
	MEL-28$^{508\text{-end}}$	3375	39%	4301	50%	3120	36%
	LMN-1	6132	71%	6885	80%	1721	20%

To further understand the dynamic chromatin-binding behavior of MEL-28, we reviewed the functional categories of genes associated to MEL-28 full length and fragments by gene ontology analysis. Using the genes found in all the peaks of each fusion protein, we found very few significantly enriched categories (Table 5.5); indeed for MEL-28 full-length protein we found a single one GO-term related with neuropeptide signaling pathway. Interestingly, this same category was found for MEL-28$^{835\text{-end}}$ fragment, along with other categories related to vulva development and RNA polyadenylation. MEL-28$^{508\text{-end}}$ fragment matched with GO-terms linked to tRNA methylation, protein folding, and oxidation-reduction process. We think the low number of categories found was due to the fact that the list of genes used was quite extensive (>10,000 genes), which diffused to find statistically significant terms.

Table 5.5. Main gene ontology categories found in DNA-binding regions of MEL-28 full-length and fragments

GO-Term	MEL-28	MEL-28$^{508\text{-end}}$	MEL-28$^{835\text{-end}}$
Neuropeptide signaling pathway	3,80E-04		9,40E-03
Protein folding		4,20E-03	
tRNA methylation		5,30E-03	
Oxidation-reduction process		6,70E-03	
Negative regulation of vulva development			2,60E-03
RNA polyadenylation			8,70E-03

In order to broaden our understanding about which types of genes interacted with the Nups according to their location at the NE or in the nucleoplasm, we compare the gene list corresponding to the subset of peaks that are different between MEL-28 fragments and NPP-22 (Table 5,6).

Table 5.6. Gene ontology categories found in DNA-binding regions from nucleoplasmic MEL-28 fragments that are not common with NPC-tethered NPP-22

MEL-28 Fragments GO-Term	Different with NPP-22	
Embryo development ending in birth or egg hatching	8,80E-06	3,20E-10
Reproduction	1,40E-05	2,70E-08
Oxidation-reduction process	1,60E-04	
Translation	2,10E-04	2,70E-03
Growth	3,30E-04	2,50E-04
tRNA methylation	1,10E-03	
Nematode larval development	1,40E-03	3,90E-08
Ribosomal small subunit assembly	1,70E-03	
Apoptotic process	3,00E-03	5,80E-04
Protein peptidyl-prolyl isomerization	3,60E-03	
Receptor-mediated endocytosis	8,30E-03	
Cytokinesis	8,40E-03	4,10E-04
Protein folding	9,00E-03	
Negative regulation of vulva development		9,00E-06
Hermaphrodite genitalia development		4,50E-05
Oviposition		1,40E-04
Locomotion		3,80E-04
Mitotic cytokinesis		2,90E-03
Maturation of SSU-rNA from tricistronic rRNA transcript		3,80E-03
Neuron migration		5,10E-03
Gonad development		9,10E-03

Interestingly, the genes interacting with nucleoplasmic MEL-28$^{508\text{-end}}$ and MEL-28$^{358\text{-end}}$ fragments were enriched in several GO-term related with development (Table 5.6, in orange color, are shown the p-value from MEL-28$^{508\text{-end}}$ and in purple from MEL-28$^{835\text{-end}}$, respectively). For example, in difference to the static NPP-22, we found embryo development, larval development, vulva development, gonad development, hermaphrodite genitalia development, growth, oviposition, and reproduction. In addition, were enriched GO-term related with the mitotic process such as cytokinesis. The entire list of GO-terms with p-values <0.01 is shown in Table 5.6.

We subsequently performed a global analysis of the genes found in MEL-28 chromatin association domains that are either present or absent in the other DamID data sets (Table 5.7). The entire list of GO-term with p-values <0.01 is shown in Table 5.7. By observing the table is notorious that the terms corresponding to functions that would be performed in the periphery or in the nucleoplasm are very well delimited. For example, with the blue background are highlighted the GO-terms related to processes that would take place to the proximity of NE, that is, in common with NPP-22 and LMN-1 proteins and different from the cytoplasmic fragments.

Table 5.7. Gene ontology categories found in MADs and its comparison with other NE-proteins

MEL-28 GO-Term	Common with fragments	Different from fragments	Common with NPP-22	Common with LMN-1	Different from NPP-22	Different from LMN-1
Protein folding	4,40E-03					
Oxidation-reduction process	4,70E-03					
Neuropeptide signaling pathway		3,10E-04	1,80E-04	5,30E-03		
Striated muscle myosin thick filament assembly		2,40E-03			5,20E-03	
Detection of chemical stimulus involved in sensory perception			1,90E-05	6,30E-03		
Detection of chemical stimulus involved in sensory perception of smell			2,60E-05	1,20E-03		
G-protein coupled receptor signaling pathway			9,30E-05	7,50E-03		
Olfactory behavior			9,50E-05	3,80E-03		
Steroid hormone mediating signaling pathway			1,20E-03	7,90E-03		
Embryo development ending in birth or egg hatching					7,30E-03	2,90E-03
Cytokinesis					7,60E-03	
Translation					7,80E-03	1,20E-04
Negative regulation of vulva development					7,90E-03	
Negative regulation of translational initiation					8,20E-03	1,20E-03
Apoptotic process						4,00E-04
Nematode larval development						2,50E-03

Nuclear envelope proteins-chromatin interactions preferentially occur with genes related to signaling pathways, sensorial perception, and metabolism

We found a high correlation between NPP-22 and LMN-1 samples (r=0.7; Figure 5.17C), and overlapping of 80% of peaks between them (Table 5.4, bottom). However, by visual inspection of the DamID profiles in the Genome browser we noticed an obvious difference between LMN-1-enriched regions, which are also slightly present at central part of the autosomes and on the X chromosome, and NPP-22-enriched regions, which are confined to the chromosomal arms (Figure 5.18).

Table 5.8. Main gene ontology categories found in DNA-binding regions of NPP-22 and LMN-1

GO-Term	NPP-22	LMN-1
Detection of chemical stimulus involved in sensory perception	1,70E-58	2,10E-24
G-protein coupled receptor signaling pathway	3,30E-43	3,40E-21
Detection of chemical stimulus involved in sensory perception of smell	2,80E-37	9,50E-17
Olfactory behavior	1,20E-34	1,30E-14
Steroid hormone mediating signaling pathway	2,00E-10	1,30E-03
Cellullar polysaccharide biosynthetic process	2,80E-10	4,80E-04
Innate immune response	4,60E-06	
Sensory perception of chemical stimulus	1,30E-05	8,20E-04
Fucosylation	1,50E-04	3,00E-03
Misfolder or incompletely synthesized protein catabolic process	2,10E-04	1,40E-03
Glycoprotein catabolic process	2,10E-04	
Protein homooligomerization	9,70E-04	
Macromolecule glycosylation	9,80E-04	5,20E-03
Protein deglycosylation	3,70E-03	
Proteolysis	4,50E-03	3,20E-03
3'-UTR-mediated mRNA destabilization	9,00E-03	1,70E-03
Neuropeptide signaling pathway		1,70E-03
Protein dephosphorylation		3,70E-03
Peptidyl-tyrosine dephosporylation		9,90E-03

Nevertheless, we expected to get differences in the profiles because of the unequal distribution of heterochromatin and euchromatin between NPCs and the NL. Besides, low amounts of lamin protein are also found in the nucleoplasm. Then, we reviewed the functional categories of genes associated to these regions by gene ontology analysis. We found that within the 16 categories identified as significantly enriched for these proteins, 12 were common, indicating their great correlation with the type of chromatin that interacts in the nuclear periphery (Table 5.8). Among the main Go-terms findings are those related to signaling pathways, sensorial perception, behavior, and metabolism.

Finally, to evaluate the interactions with chromatin that are given with different components of the NE we evaluated which types of genes are present in LMN-1 peaks but absent from MEL-28 or NPP-22 peaks (Table 5.9). As we expected, between LMN-1 and NPP-22 there were few different GO-terms enriched, but those were very interesting for example growth and embryo development, which is consistent with recent reports showing that LMNA can interact with euchromatin (E. G. Lund et al., 2015). On the other hand, with respect to MEL-28 were found more different categories, and those reflect the basic functions of the nuclear lamina such as regulation of cell shape and innate immune response.

Table 5.9. Gene ontology categories found in LADs that are not common with NPC components

LMN-1 GO-Term	Different from MEL-28	Different from NPP-22
Regulation cell shape	5,70E-05	
Peptidyl-serine-phosporylation	8,90E-05	
Detection of chemical stimulus involved in sensory perception of smell	3,10E-04	
Detection of chemical stimulus involved in sensory perception	8,10E-04	
Metabolic process	1,10E-03	
Olfactory behavior	1,20E-03	
Innate immune response	1,30E-03	
G-protein coupled receptor signaling pathway	4,20E-03	
Growth		3,80E-03
Embryo development ending in birth or egg hatching		4,60E-03
Heme transport		6,60E-03

Chapter VI

Discussion

Discussion

In this thesis we expand the understanding of MEL-28 behavior and functions. Through a systematic, functional and structural analysis of MEL-28 in *C. elegans* early development and human ELYS in cultured cells, we were thus able to identify several functional domains as well as a novel function of MEL-28 in meiosis.

We found human ELYS and *C. elegans* MEL-28 have similar functional domains. Both orthologs depend on an intact β-propeller and central α-helical domains for NPC and kinetochore localization, and the C-terminus presents a chromatin-binding domain. Thanks to the good conservation among the functional domains, we conclude that results from functional analyses of MEL-28 in *C. elegans* are broadly applicable to vertebrate ELYS.

Besides, we extended the global landscape of NE-chromatin interactions through the comparison between genome-wide profiles of MEL-28, NPP-22 and LMN-1. Using an optimized DamID-seq technique, we found MEL-28 and NPP-22 associated chromatin domains were enriched for different gene classes, highlighting that beyond its role in NE assembly and nuclear transport, Nups can be involved in different functions. Similar to other dynamic Nups, MEL-28 was related to developmental processes.

DamID as tool to study chromatin organization

To evaluate the interactions of genes and chromatin domains with NE components, several techniques such as fluorescence *in situ* hybridization (FISH), chromatin immunoprecipitation ChIP, and DamID, have been developed. We propose DamID as an attractive, powerful and sensitive method to globally characterize chromatin organization in *C. elegans*. The versatility of DamID is reflected by its application to evaluate a wide range of chromatin-associating proteins in several organisms such as yeast (Steglich et al., 2012), flies (Kalverda et al., 2010), worms (González-Aguilera et al., 2014), and mammalian cells (Guelen et al., 2008).

Recently, DamID-seq was used to generate genome-wide maps in single human cells (Kind et al., 2015). This study generated 395 single-cell LAD maps at a resolution of 100 kb, which is below of the median size of human LADs (0.5 Mb; (Guelen et al., 2008)). In addition, due to its high sensitivity, DamID is able to reveal genome interactions of chromatin proteins at

tissue-specific level, *in vivo* without cell isolation from model organisms such as *C. elegans* (Muñoz-Jimenez, unpublished data) and *Drosophila* (Tony D Southall et al., 2013). For this purpose it is necessary to change slightly the approximation of the Dam-fusion protein expression. For example: Targeted DamID, TaDa, (Marshall, Southall, Cheetham, & Brand, 2016; Tony D Southall et al., 2013) combines the GAL4 system to drive tissue-specific, bicistronic transcription (translation of a secondary open reading frame [ORF]) to regulate the expression of Dam::POI, which should be kept very low to avoid both toxicity and high non-specific background methylation of the genome.

In another recent approach in *Drosophila*, a system based on Flipase (FLP) inducible expression of Dam protein in a tissue-specific manner was constructed (Pindyurin, Pagie, Kozhevnikova, van Arensbergen, & van Steensel, 2016). Using a cassette containing a transcription terminator flanked by two DNA recombinase recognition sites (FLP/FRT). Interestingly, the promoter used was a minimal *Phsp* fragment which does not respond to heat shock, ensuring only the basal expression of Dam::POI. Thus, cell type-specific expression of the FLP guarantees the generation of the corresponding DamID profile.

It is clear that more and better applications of this elegant technique are to come. However, one of the main bottlenecks of the technique is the analysis and interpretation of the data generated, as in any genome-scale experiment. DamID analysis has required an implementation of bioinformatics techniques, because until 1 year ago, we simply adapted, to a lesser or greater extent, the existing tools which had been developed for ChIP, since it is a longer established technique. Nevertheless, the bioinformatics tools used to analyze ChIP-array worked well enough for DamID-array.

Interestingly, together with DamID-seq implementation, computational scripts specific for DamID-seq analysis have been developed (Marshall & Brand, 2015). For example, in 2016, three different DamID-seq pipelines have been published (Gutierrez-Triana, Mateo, Ibberson, Ryu, & Wittbrodt, 2016; Maksimov, Laktionov, & Belyakin, 2016; Sharma et al., 2016). Nonetheless, the decision of which analysis method to choose still depends on the dynamics, nature, and behavior of the protein of interest, as well as on the biological question to answer. And surely, new and perhaps easier bioinformatics tools are about to emerge.

MEL-28 is required for meiotic chromosome segregation

Previous work demonstrated that MEL-28/ELYS is essential for mitotic chromosome segregation in *C. elegans* and vertebrates (Fernandez & Piano, 2006; Galy, Askjaer, Franz, López-Iglesias, & Mattaj, 2006; Beth A Rasala, Orjalo, Shen, Briggs, & Forbes, 2006). Here we show that MEL-28 is also essential for proper meiotic chromosome segregation in *C. elegans* oogenesis. We describe for the first time the dynamic of MEL-28 during meiosis. MEL-28 localizes to the NE in the earliest oocyte. In the -3 and -2 oocytes MEL-28 gradually shifted from the NE to meiotic chromosomes, remaining associated throughout meiosis I and II and is required to the precise progression of anaphase I and II. Posteriorly, MEL-28 accumulates at the NE at pronuclear formation. In the absence of MEL-28, defects in anaphase produce an abnormal number of polar bodies; pronuclei remain small and do not expand, driving to perturbed mitosis.

In *C. elegans*, chromosome segregation during female meiosis is kinetochore-independent, and instead depends on microtubule growth in the region between separating chromosomes and lateral microtubule attachments to the separating chromosomes (Dumont et al., 2010; Muscat, Torre-Santiago, Tran, Powers, & Wignall, 2015). It may be that these lateral attachments to chromosomes are less stable in the absence of MEL-28, leading to failure of chromosome segregation. Alternatively there could be defects to the architecture of the meiotic spindle when MEL-28 is disrupted, as has been shown for the mitotic spindle in *mel-28* RNAi-treated embryos (Fernandez & Piano, 2006; Galy et al., 2003).

It is important to note that the cell cycle proceeds in *mel-28* embryos despite the penetrant failure in meiotic chromosome segregation, which suggests that mel-28 does not affect the APC (Furuta et al., 2000; Golden et al., 2000). Protein kinases are one of the key components that control cell-cycle progression activating multiple processes by phosphorylation of several proteins. However, exit from M phase needs the inactivation of phosphorylated proteins. This inactivation occurs principally through proteasome-mediated degradation regulated by APC, but also by dephosphorylation of mitotic phosphoproteins by the protein phosphatases 1 (PP1) and 2A (Bollen, Gerlich, & Lesage, 2009; Lesage et al., 2011).

Interestingly, a recent study in *C. elegans* showed that a mutation preventing MEL-28 from to bind PP1, produced a failure to segregate chromosomes in oocyte meiosis I. Together

with additional experiments this suggests that the recruitment of PP1 by MEL-28 leads to chromosome segregation during anaphase I, which seem to be dependent of kinetochore disassembly, and the nuclear assembly through the transition from M phase to interphase (Hattersley et al., 2016). In contrast, MEL-28 recruitment to chromosomes, formation of bipolar spindle and progression into anaphase were no affected. Remarkably, depletion of Y-complex components NPP-2/Nup85, NPP-6/Nup160 and NPP- 15/Nup133 did not affect meiosis I chromosome segregation, indicating that the MEL-28 meiotic phenotype is not an indirect consequence of defective nuclear compartmentalization.

This mechanism implies that kinetochore disassembly is required in anaphase I segregation, which contrasts with the previously proposed kinetochore-independent model (Dumont et al., 2010). ELYS-mediated phosphorylation network, has been also found in human cell lines, it has been reported that ELYS and PP1 regulate the phosphorylation of Lamin B Receptor, which is required for its recruitment to the NE (Mimura, Takagi, Clever, & Imamoto, 2016).

MEL-28 N-terminal part mediate NPC and kinetochore localization

In both *C. elegans* and HeLa cells, full-length MEL-28/ELYS localizes to the nucleoplasm and NPCs at interphase and to the kinetochore at mitosis (Fernandez & Piano, 2006; Galy, Askjaer, Franz, López-Iglesias, et al., 2006b; Beth A Rasala et al., 2006; Yokoyama et al., 2014). Here we observed that in *C. elegans*, localization to NPCs and the kinetochore is dependent on both the N-terminal β-propeller domain and the central α-helical domain, corresponding to the N-terminal 956 aa. residues. Mammalian ELYS NPC localization also requires the β-propeller and α-helical domains (Silvija Bilokapic & Schwartz, 2013b) and here we have shown that these domains are also necessary for the localization of ELYS to kinetochores at metaphase, similar to previous studies of human ELYS (Silvija Bilokapic & Schwartz, 2013b).

Another essential element for ELYS/MEL-28 function in NPC assembly is the presence of histones (Inoue & Zhang, 2014). During mouse *in vitro* fertilization, sperm chromatin is restored de novo using histones present in the oocyte. When histones are depleted, ELYS does not localize to the NE of the sperm pronucleus and the recruitment of other Nups is blocked. Intriguing, artificial tethering of ELYS to the NE (through fusion to Emerin), rescued the recruitment of other Nups and NPC assembly, suggesting that nucleosome assembly is

upstream of ELYS nuclear periphery localization and ELYS-nucleosome interaction is a requirement for its NE localization and function in NPC assembly.

One major difference between MEL-28 and ELYS is that chromatin and kinetochore binding is strictly dependent on the C-terminal chromatin-binding domain in ELYS. In contrast, MEL-28 fragments lacking the C terminus are still delivered to the kinetochore as long as the N terminus is intact although in a more irregular manner. It is possible that MEL-28 kinetochore localization is more robust to perturbation because of the unique holocentric structure of the kinetochore in *C. elegans*.

Therefore, in spite of the divergent amino acid sequences between MEL-28 and human ELYS (with at best 23% sequence identity) we found that the functional domains of invertebrate and vertebrate orthologs are remarkably well conserved. Other examples of good conserved domains are the 50-aa. docking motif for the catalytic subunit of PP1 (Hattersley et al., 2016) and the loop2 motif (Bilokapic & Schwartz, 2013a).

Loop2 mediated chromosomal functions of MEL-28

Studies on mouse ELYS have shown that disruption of the protein by substitution of five exposed amino acid residues (called loop2) prevented a 1018-aa. N-terminal ELYS fragment from localizing properly to the NE (Silvija Bilokapic & Schwartz, 2013b). We found disruption of loop2 within an equivalent N-terminal fragment of MEL-28 (aa.1-956) caused a reduction of localization at the NPC and nucleoplasm, with a corresponding increase in cytoplasmic fluorescence. Interestingly, the full-length MEL-28 fusion with the loop2 defect had the wild-type localization pattern, suggesting that domains in the C terminus contribute to nuclear rim localization. Even so, mutations of loop2 severely disrupted MEL-28 function and caused cell cycle delay, nuclear expansion defects, problems with chromosome segregation during mitosis and meiosis, abnormal pronuclei formation, and ultimately embryonic death. However, NPC components were recruited to the reforming nuclei relatively efficiently. This suggests that the chromosomal functions of MEL-28 are more sensitive to defects to loop2 than the nuclear pore functions of MEL-28.

MEL-28/ELYS chromatin binding domain is placed in the disorder C-terminal part and is independent from the AT-hook domain

In vitro analyses studying the C-terminal domain of ELYS using *Xenopus* extracts have suggested that there are at least two domains, including the AT hook, required for chromatin binding (Gillespie, Khoudoli, Stewart, Swedlow, & Blow, 2007b; B. A. Rasala et al., 2008; Zierhut et al., 2014a). Our results studying the C terminus of human ELYS are consistent with this. We identified at least two domains needed for metaphase chromatin localization. The C-terminal end of ELYS corresponding to aa. 1851–2275 bound to metaphase chromatin. However the smaller aa. 1851–2034 (which includes the AT hook) and aa. 2034–2275 fragments were both excluded from metaphase chromatin, suggesting that both the AT hook and the domain C-terminal to the AT hook are required for metaphase chromatin binding. In concordance with this, in *Xenopus laevis* egg extracts the interaction of ELYS with nucleosomes depends on C-terminal part containing AT-hook (aa. 2281–2408). Individual fragments including just the AT-hook (aa. 2281–2358) or just the region C-terminal next to the AT-hook (aa. 2359–2408) could not bind to nucleosomes (Zierhut et al., 2014a). Interestingly, nucleosomes present in egg extracts were essential to assemble functional NE and mitotic spindles.

Our *C. elegans* MEL-28 data also suggest that both the AT hooks and other C-terminal domains are involved in chromatin binding. *C. elegans mel-28(t1684)* embryos expressing GFP::MEL-28$^{1\text{-}1629}$ had reduced fluorescence in the nucleoplasm at interphase, consistent with inefficient chromatin binding. These embryos also showed defects in recruitment of NPC components that would be expected if MEL-28 could not effectively bind to chromatin (Franz et al., 2007; B. A. Rasala et al., 2008). We studied multiple C-terminal fragments of MEL-28 (that also lacked the N-terminal β-propeller and the central α-helical domains). Such fragments that include aa. 1239–1601 localized to the metaphase chromatin, but fragments lacking this domain were excluded from metaphase chromatin. This suggests that aa. 1239–1601, just N-terminal to the AT hooks in MEL-28, comprise a chromatin-binding domain.

Notably, MEL-28 fragments with an intact N terminus (including the β-propeller domain and the central α-helical domain) localized to the kinetochore regardless of the presence of aa. 1239–1601, showing that metaphase kinetochore localization does not require this domain. With human ELYS, in contrast, fragments were completely excluded from the chromatin and kinetochores unless they contained the C terminal domain including aa. 1851–2275.

In contrast to the behavior of C-terminal MEL-28 and ELYS fragments, full-length *C. elegans* and human proteins were enriched at kinetochores with no apparent affinity for other parts of the metaphase chromosomes. Moreover, disruption of kinetochores blocks recruitment of MEL-28 to mitotic chromosomes (Fernandez & Piano, 2006). However, several observations indicate that full-length MEL-28 and ELYS also interact with chromatin. Firstly, ELYS bound to chromatin in interphase Xenopus egg extracts (Gillespie et al., 2007b; B. A. Rasala et al., 2008; Zierhut et al., 2014a). Secondly, DamID experiments in *C. elegans* adults showed specific interaction of MEL-28 throughout all chromosomes (this study and Sharma et al., 2014). As a possible explanation for the different behavior at interphase and mitosis we speculate that MEL-28 and ELYS might undergo conformational changes in mitosis that lower their affinity for chromatin. Upon deletion of N-terminal regions, the chromatin association domain(s) in the C-terminus of MEL-28 and ELYS might become more accessible and confer binding to metaphase chromosomes. Such a "shielding" mechanism is concordant with the gradual increase in association to metaphase chromosomes as more residues are deleted from the N-terminus of ELYS. Alternatively, or in combination with conformational changes of MEL-28 and ELYS, condensed mitotic chromosomes might provide a less favorable binding site for MEL-28/ELYS.

The AT hook domain is essential for MEL-28's functions but not for MEL-28 localization

MEL-28 is efficiently targeted to NPCs and kinetochores even without AT hooks. However, the ΔAT-hooks version of MEL-28 clearly lacks MEL-28 function; *mel-28(t1684)* embryos expressing MEL-28$^{1\text{-}1629}$ were defective in NPC assembly and nearly all died before hatching. This shows that having MEL-28 placed at the NE is not sufficient for efficient recruitment of the remaining components of the NPC but that this depends on the AT-hook domain. In addition, these embryos show chromatin bridges and activate a checkpoint associated with DNA breakage. Previous work has suggested a role for MEL-28 in chromosome congression and segregation (Fernandez & Piano, 2006; Galy, Askjaer, Franz, López-Iglesias, et al., 2006b), and our observations suggest that these functions require the AT hooks.

The second, or most C-terminal, of the two predicted AT hooks clustered at the C terminus is a canonical AT hook whereas the penultimate is less well conserved (Galy, Askjaer, Franz, López-Iglesias, et al., 2006b). Interestingly, the MEL-28 fusion missing only its last AT hook retained some MEL-28 function, as *mel-28(t1684)* animals expressing this fusion

showed partial penetrance embryonic lethality, with over one third of the embryos surviving. Since removal of both AT hooks causes 99% embryonic lethality, either the penultimate AT hook or the short domain between the AT hooks must contribute to MEL-28 function. In either case, most *mel-28(t1684)* embryos expressing the version lacking the last AT hook are unviable, so the last AT hook is clearly needed for full MEL-28 function.

We think it will be very interesting to perform DamID on *mel-28* mutants lacking the AT-hook domain, and evaluate how this might affect chromatin association as well as gene expression.

MEL-28 associates with actively transcribed chromatin

Our DamID-array analysis showed that MEL-28 association domains (MADs) are enriched with transcriptionally active genes and congruently, MADs correlate positively with H3K4me3 and H3K36me3 histone mark and Pol-II profiles (Gerstein et al., 2010). In contrast, MADs correlate negatively with LADs, which are been proposed as heterochromatin markers (Kind & van Steensel, 2010; E. Lund et al., 2013). Besides, MEL-28 was enriched in several Cis-regulatory elements such as promoter, introns, 3'-UTR and 5'-UTR regions, and less abundant in coding exons. Therefore, our data suggest that MEL-28 may be involved in regulation of gene expression.

Supporting our data, recently was found a high level of genome-wide correlation between ELYS DNA-binding sites and H3K27acetyl signal (Pascual-Garcia et al., 2017), which correspond to both active enhancers and promoters (Kharchenko et al., 2011). The same study analyzed the mobile Nup98 and the highly stable Nup93 (Rabut et al., 2004). Interestingly, the characterization of common ELYS/Nup98/Nup93 binding sites (which were assumed as interactions placed at NPC), showed an equal correlation with H3K27acetyl and H3K27Me3 mark, suggesting that in the periphery DNA interaction occurs with both active and silent genes.

We expected to be able to perform the DamID experiment with the entire set of MEL-28 proteins (Figure 5.1) in order to discern between MEL-28-chromatin interactions at NPCs and in the nucleoplasm. However, we did not detect any DamID signal from the NPP-22::Dam::MEL-28 fusion protein, but the high correlation between MEL-28 full-length and cytoplasmic fragments suggests the interaction with active chromatin occurs mainly in the

nuclear interior. This is in agree on previous *Drosophila* DamID studies, which found strong enrichment of active chromatin in intranuclear Nups, but not in NPC-attached Nup (Kalverda et al., 2010). Other evidence of nucleoplasmic Nup-chromatin interaction and its link with transcription was described in HeLa cells (Capitanio, Montpetit, & Wozniak, 2017). In this study, was identified the DExH/D-box helicase DHX9 as an intranuclear Nup98 binding partner. Besides, it was shown that binding of Nup98 stimulates the ATPase activity of DHX9 and consequently, DHX9-induced transcription.

An additional and interesting option to evaluate the place where MEL-28-chromatin interactions take place is through FISH on 3D-preserved nuclei (3D-FISH). We can design probes containing chromosomal regions interacting with full-length and nucleoplasmic MEL-28, as well as for some of the genes actively transcribed within the MADs with the highest score. In this way we can assess in which nuclear sub-regions MEL-28-DNA association occurs in interphase nucleus.

Elucidating MEL-28 functions during interphase

The analysis of the interactions of MEL-28 cytoplasmic fragments is of great relevance because until now it is not very clear if MEL-28 has functions during interphase; for example, in interphase, MEL-28 is not relevant for NPC assembly (Doucet et al., 2010), which is one of its key functions during mitosis. We found similar levels of MEL-28 in nuclei of all embryonic cells and all postembryonic tissues in both larva and adults, suggesting that after embryonic development, MEL-28 could be required for other functions.

Direct evidence for the presence of ELYS inside the nucleus has been shown. Using specific HeLa cell lines with a high frequency of GLFG bodies revealed the colocalization of ELYS and several Y-complex members with Nup98 and CRM1 within these structures (Morchoisne-Bolhy et al., 2015). Interestingly, ELYS together with GLFG bodies was disassembled and reformed through cell cycle progression, which discards the possibility that its location is merely a random aggregation.

MEL-28 has unknown postembryonic functions

Several Nups have been involved in transcriptional regulation, showing that their chromatin-association roles are relevant to the control of gene expression programs in developing organisms (Maya Capelson et al., 2010; D 'Angelo et al., 2012; Kalverda et al., 2010; Liang et al., 2013). However, neither the regulatory mechanisms performed by Nups nor their gene targets are completely clear.

Although in chapter IV we have demonstrated that MEL-28 is indispensable for correct meiotic and mitotic progression (Gómez-Saldivar, Fernandez, et al., 2016), we could not exclude that the embryonic lethality phenotype seen in *mel-28* mutants was due largely to nuclear structural defects rather than to genetic transcription implications. Congruently, one study in zebra fish presents an example of the consequences of the reduction of NPCs number during development (Davuluri et al., 2008). A zebra fish mutant called *Flo* showed defects in NPC re-assembly, then in every cell division, the number of NPC was decreasing, producing strong defects in more proliferating tissues, such as retina and intestine and finally producing cell cycle arrest and apoptosis.

Interestingly, we found that genes interacting with nucleoplasmic MEL-28 fragments were enriched in several GO-term related with development such as embryo and larva development, growth, oviposition, and reproduction. This indicates that similarly to other Nups "off-pore" MEL-28-chromatin interactions might be required for proper development. Fernandez and collaborators recently reported a genome-scale screen for *mel-28* in *C. elegans.* They found 65 *mel-28* genetic interactors and identified novel potential postembryonic roles for MEL-28 (Fernandez et al., 2014). This suggests that MEL-28 could participate in larval development and mediate the expression of developmental genes, a possibility that had not been appreciated earlier given its strict condition as a maternal-effect lethal gene.

NPP-22-chromatin interaction reflects its stable NPC localization

Due to transmembrane domain of NPP-22, we speculated that NPP-22 would have lower chromatin accessibility and therefore low DNA interaction. Furthermore, there was an antecedent in a previous Drosophila DamID study, using a similar approach found NDC1::Dam interaction signal was highly reduced in comparison to NPC-tethered Nup98 (NDC1::Nup98Fragment::Dam); although both fusion proteins binds, in general, to the same genomic regions (Kalverda et al., 2010). Beside, ChIP-seq experiments found stable Nup93

present considerably fewer binding peaks than Elys, 385 versus 14336 binding sites, respectively, (genome coverage percentage was not shown), although they overlap 79% (Pascual-Garcia et al., 2017). However, we found 27% of NPP-22 DNA association, very similar to other mobile Nups, such as MEL-28, Nup153 and Mtor, ~25% (this study, (Vaquerizas et al., 2010)). But remarkably, the pattern of DNA-association between NPP-22 and MEL-28 was mainly different.

In contrast, NPP-22 profile was very similar to other NE proteins such as LMN-1, EMR-1, LEM-2 (this study, (González-Aguilera et al., 2014; Ikegami et al., 2010)). Therefore, despite its nature more embedded inside the NPC, is able to connect with the chromatin domains that are placed in nuclear periphery, in a very similar pattern: enriched in chromosome arms, but not in central regions. Supporting that, Gene Ontology analysis showed that it is linked to classical NE processes, for instance, signaling pathways.

Notably, one of the major differences between NPP-22 and LMN-1 association was the interaction with the sexual chromosome. NPP-22 had very low occupancy on the X chromosome (11%), even lower that LMN-1 (19%), which previously was been shown to interact in low proportion with the X chromosome in comparison to EMR-1 (30%; (González-Aguilera et al., 2014)). Although we do not expect to have a prominent interaction between theX chromosome anchored in the periphery and the NPC, MEL-28 presented 24% of occupancy on the X chromosome and this interaction increased in males (Appendix 1, Sharma et al., 2014). It would be interesting to assess whether the interaction between NPP-22 and the X chromosome also increases in males, which would provide additional evidence to support the structural model of dosage compensation (DC) in *C. elegans* wherein the DCC prevents X-chromosome-NPC association in hermaphrodites, whereas in males, X-specific sequences place the X-chromosome in transcriptionally active domains located around NPC (Appendix 1, Sharma et al., 2014).

NPP-22 could be associated with silent chromatin

Based on the high correlation that our results show between the association profiles of NPP-22 and LMN-1, it is very likely that NPP-22 interacts with heterochromatin. It would be relevant to make an analysis of which class of histone marks are in the NPP-22 binding sites. We speculate that similar to LMN-1, EMR-1, and LEM-2 (González-Aguilera et al., 2014; Ikegami et al., 2010), we might find low levels of active transcription markers such as POL-II, H3K36me3, and H3K4me3 across NPP-22 interaction domains.

Furthermore, we found almost no NPP-22 association in the central parts of chromosomes, whereas LMN-1 presented a few binding sites in these regions. This could be related to the low proportion of genes (5-10%) that are active transcribed in LADs (Guelen et al., 2008; D. Peric-Hupkes & van Steensel, 2010); or with recently described lamin-interacting domains, LiDs (E. G. Lund et al., 2015), which can be found in euchromatic regions as promoters, and not necessarily associated with the nuclear lamina, but may also localize to the nuclear interior. Then, it might be that NPP-22 is even more related to heterochromatin than LMN-1. However, classical EM experiments have established that NPCs are generally surrounded by euchromatin so further analyses are required to clarify this.

Several reports argue that NPC-chromatin interactions are frequently related with silent chromatin. For example, in mouse embryonic stem cells was found a new role of Nup153 mediating the recruitment of the polycomb-repressive complex 1 (PRC1). Moreover, Nup153 association with developmentally regulated genes is required to maintain them in a repressed state and the pluripotency of cells (Jacinto, Benner, & Hetzer, 2015a). New evidence shows Nup93 sub-complex regulates the anchorage and repression of HOXA gene cluster expression (Labade, Karmodiya, & Sengupta, 2016). Nup93 was found enriched in HOXA promoters. The depletion of Nup93 sub-complex releases the HOXA gene locus from the nuclear periphery and upregulates its gene expression levels. Congruently, Nup93 knockdown increased transcription elongation and active histone marks, and decreased repressive histone marks.

Curiously, the transmembranes Nups Pom121 and Nup210 have been related with gene expression processes, expanding its functions beyond to initiate nuclear membrane fusion during NPC assembly (Doucet et al., 2010; B. A. Rasala et al., 2008) Nup210 was involved in myogenesis, inducing changes in the expression patterns of genes involved in differentiation (D ’Angelo et al., 2012). On the other hand, in human cells, a soluble variant of POM121, lacking the transmembranal domain, was found to interact with Nup98 in the nucleoplasm and bind to specific gene promoters to regulate transcription (Franks et al., 2016).

Potential mechanisms of Nup–chromatin associations

The mechanisms employed by Nups to interact with DNA are not completely elucidated. Besides, it seems that the interactions involve different components according to the place

where they take place (NPC or nucleoplasm) and their purpose (activate, silence or stabilize genes). However, several findings propose that Nups are implicated in chromatin remodeling due to their association with chromatin modifiers such as histones deacetylases (HDACs) (Kehat et al., 2011), the Spt-Ada-Gcn5-acetyltransferase (SAGA) complex (Rohner et al., 2013), the male specific lethal (MSL) complex (Mendjan et al., 2006; Pascual-Garcia, Jeong, & Capelson, 2014), small ubiquitin-like modifier (SUMO) proteases (Chow, Elgort, Dasso, & Ullman, 2012) and PRC1 (Jacinto, Benner, & Hetzer, 2015b). Interestingly in *C. elegans*, MEL-28 was identified as protein interactor of SWSN-2.2, an accessory subunit of SWI/SNF chromatin-remodeling complexes (Ertl et al., 2016). SWI/SNF complexes are involved in diverse processes, such as chromosomal stability and gene expression regulation. Remarkably, MEL-28 and SWSN-2.2 were found to colocalize in chromatin and mitotic and meiotic chromosomes in early embryos and oocytes.

Another interesting proposal is that NPC can function as scaffolds for topological genome organization. NPC can recruit genes, which are regulated by dynamic Nups. This model is supported by recent evidence showing a novel role of Nup98 in promoting enhancer-promoter looping, and therefore genome architecture regulation (Pascual-Garcia et al., 2017). In this model, silenced genes are recruited at the NPC; upon activation, Nup98 gains new physical interactions, which mediate formation of proper enhancer-promoter contacts, and priming the transcription of inducible genes. In addition, interactions between Nup98 and architectural proteins CTCF, GAF, and Su(Hw), are increased. Interestingly, these interactions were also implied in the epigenetic memory of developing organisms.

Outlooks

With the final purpose of assessing whether MEL-28 is important for gene expression, beyond its role in NE assembly; we have planned to do two critical experiments in the near future, where we will evaluate the consequences of MEL-28 depletion on nuclear organization and gene expression. To address this question we are going to perform LMN-1 DamID-seq and RNA-seq comparative analysis in the presence or absence of MEL-28. Moreover, we could perform FISH-3D experiments to evaluate the modifications of chromatin organization and chromatin architecture in the absence and presence of MEL-28.

Addressing the question whether spatial genome organization correlates with transcription is however not trivial: MEL-28 can be depleted efficiently from *C .elegans* embryos, but it is very difficult to separate the multiple nuclear functions from each other and conclude which it

is cause and effect. To avoid effects caused by defective nuclear reformation, we propose to perform experiments in post-mitotic cells. To this end, we will employ a thermosensitive *glp-4* mutant that fails to develop a germ line at the restrictive temperature. We have already generated *glp-4* (I) mutants, which carrying single copy insertion of *dam::lmn-1*; as well as a balanced strain which generates *mel-28* heterozygous and homozygous mutants.

Additionally, identification of MEL-28 interacting partners would help us to understand MEL-28 non-NPC functions and its roles in different locations. Experiments using yeast-two-hybrid and Bimolecular Fluorescence Complementation assays have already been started by laboratory members.

Finally, it would be interesting to achieve the DamID experiment of MEL-28 associated exclusively in the NPC and to compare with our previous results. As well as a detailed analysis of MEL-28-X-chromosome interaction in males and hermaphrodites in the different MEL-28 contexts: cytoplasmatic (fragments) or peripheral (attached at NPC), with the objective of clarifying, a little more, the model of DC in *C. elegans*. A recent study proposes another mechanism to DC in *C. elegans* (Wheeler et al., 2016), arguing to find some inconsistencies with our NPC-X-chromosome mechanism of upregulation (Sharma & Meister, 2015; Sharma et al., 2014). For instance, in their hands, integration of the same transgenes onto DCC binding to a nearby rex site is not sufficient to drive DC of a gene. These authors are more in favor of a model where the X chromosome is broadly permissive for DC, and the DCC acts via a chromosome-wide mechanism producing changes in X structure that influence expression and therefore balance transcription between sexes.

Chapter VII

Conclusions

Conclusions:

1. MEL-28 localization in nuclear pores is essential to perform its endogenous function.

2. MEL-28 has a novel role during meiosis, intervening in the segregation of chromosomes in anaphase I and II.

3. The AT-Hook motifs are not necessary for MEL-28 localization at the nuclear periphery or for its binding to DNA, but are required for MEL-28 function.

4. Depletion of MEL-28's AT-Hook domain causes reduced nuclear growth, mis-segregation of chromosomes and activates the ATR-dependent DNA damage checkpoint, producing cell division delays.

5. The Coiled Coil domain of MEL-28 is not necessary for nuclear envelope and kinetochore localization, and it is dispensable for viability, but stimulates association to the spindle matrix.

6. MEL-28's N-terminal β-propeller and α-helical domains are both required for localization to the kinetochore and to the nuclear pore.

7. Mutations in the conserved β-propeller loop2 do not affect proper nuclear pore localization of MEL-28 full length but produces defects during meiosis and mitosis.

8. MEL-28 contains two nuclear localization signals (NLSs); one in the central part of the protein (aa. 846-1071) and one in the AT hook domain.

9. The binding of MEL-28 to chromatin is mediated by aa. 1239-1601 in the disordered C-terminal half and is flanked by the two NLSs.

10. MEL-28 functional domains are conserved in human ELYS protein.

11. DamID-seq and DamID array technologies identify similar MEL-28 binding sites in the genome.

12. In contrast to previously described lamina association domains, MEL-28 association domains (MADs) are distributed uniformly throughout all the chromosomes.

13. MEL-28-chromatin interactions occur mostly in the nucleoplasm, although increased association of MEL-28 with the X chromosome in males correlates with chromatin recruitment to the nuclear periphery.

14. MADs are enriched in transcribed genes and active chromatin marks, which suggests that MEL-28 might be involved in transcriptional regulation.

15. MEL-28-associated genes accumulating at the nuclear envelope are related to biological processes involved in sensory perception.

16. MEL-28-chromatin interactions in the nucleoplasm preferentially involve developmental genes and genes related to mitotic process

17. MEL-28 colocalizes with kinetochore components HCP-3, KNL-3, but does not share the same centromeric association sites.

18. The integral membrane nucleoporin NPP-22 interacts mainly with chromosome arms of autosomes and the left arm of the X chromosome left arm, similarly to LMN-1 and EMR-1.

19. LMN-1 and NPP-22 chromatin interactions preferentially involves genes related to signaling pathways, sensorial perception, and metabolism.

20. The increased resolution of DamID-seq suggests that lamina association domains have a median size of 2 kb, significantly smaller than previously established.

Chapter VIII

References

References

Ahmed, S., Brickner, D. G., Light, W. H., Cajigas, I., McDonough, M., Froyshteter, A. B., … Brickner, J. H. (2010). DNA zip codes control an ancient mechanism for gene targeting to the nuclear periphery. *Nature Cell Biology*, *12*(2), 111–118. http://doi.org/10.1038/ncb2011

Ahmed, S., & Brickner, J. H. (2010). A role for DNA sequence in controlling the spatial organization of the genome. *Nucleus*, *1*(5), 402–406. http://doi.org/10.4161/nucl.1.5.12637

Albertson, D. G. (1984). Formation of the first cleavage spindle in nematode embryos. *Developmental Biology*, *101*(1), 61–72. Retrieved from http://www.ncbi.nlm.nih.gov/pubmed/6692980

Albertson, D. G., Rose, A. M., & Villeneuve, A. M. (1997). Chromosome Organization, Mitosis, and Meiosis. In *C. elegans II*. Cold Spring Harbor Laboratory Press. Retrieved from http://www.ncbi.nlm.nih.gov/pubmed/21413226

Albertson, D. G., & Thomson, J. N. (1982). The kinetochores of Caenorhabditis elegans. *Chromosoma*, *86*(3), 409–428. Retrieved from http://www.ncbi.nlm.nih.gov/pubmed/7172865

Altun, Z. F., & Hall, D. H. (2016). Handbook of C. elegans Anatomy. Retrieved from http://www.wormatlas.org/hermaphrodite/hermaphroditehomepage.htm

Anderson, D. J., & Hetzer, M. W. (2007). Nuclear envelope formation by chromatin-mediated reorganization of the endoplasmic reticulum. *Nature Cell Biology*, *9*(10), 1160–1166. http://doi.org/10.1038/ncb1636

Ando, S., Yang, H., Nozaki, N., Okazaki, T., & Yoda, K. (2002). CENP-A, -B, and -C Chromatin Complex That Contains the I-Type Satellite Array Constitutes the Prekinetochore in HeLa Cells. *MOLECULAR AND CELLULAR BIOLOGY*, *22*(7), 2229–2241. http://doi.org/10.1128/MCB.22.7.000–2229–2241.2002

Andrey, G., Montavon, T., Mascrez, B., Gonzalez, F., Noordermeer, D., Leleu, M., … Duboule, D. (2013). A Switch Between Topological Domains Underlies HoxD Genes Collinearity in Mouse Limbs. *Science*, *340*(6137), 1234167–1234167. http://doi.org/10.1126/science.1234167

Ankeny, R. A. (2001). The natural history of Caenorhabditis elegans research. *Nature Reviews. Genetics*, *2*(6), 474–9. http://doi.org/10.1038/35076538

Antonin, W., Ellenberg, J., & Dultz, E. (2008). Nuclear pore complex assembly through the cell cycle: Regulation and membrane organization. *FEBS Letters*, *582*(14), 2004–2016. http://doi.org/10.1016/j.febslet.2008.02.067

Asakawa, H., Kojidani, T., Mori, C., Osakada, H., Sato, M., Ding, D.-Q., … Haraguchi, T. (2010). Report Virtual Breakdown of the Nuclear Envelope in Fission Yeast Meiosis. *Current Biology*, *20*, 1919–1925. http://doi.org/10.1016/j.cub.2010.09.070

Askjaer, P., Ercan, S., & Meister, P. (2014). Modern techniques for the analysis of chromatin and nuclear organization in C. elegans. http://doi.org/10.1895/wormbook.1.169.1

Askjaer, P., Galy, V., Hannak, E., & Mattaj, I. W. (2002). Ran GTPase Cycle and Importins alpha and beta Are Essential for Spindle Formation and Nuclear Envelope Assembly in Living Caenorhabditis elegans Embryos. *Molecular Biology of the Cell*, *13*(12), 4355–4370. http://doi.org/10.1091/mbc.E02-06-0346

Askjaer, P., Galy, V., & Meister, P. (2014). Modern Tools to Study Nuclear Pore Complexes and

Nucleocytoplasmic Transport in Caenorhabditis elegans. In *Methods in cell biology* (Vol. 122, pp. 277–310). Elsevier Inc. http://doi.org/10.1016/B978-0-12-417160-2.00013-8

Audhya, A., Desai, A., & Oegema, K. (2007). A role for Rab5 in structuring the endoplasmic reticulum. *The Journal of Cell Biology*, *178*(1), 43–56. http://doi.org/10.1083/jcb.200701139

Aughey, G. N., & Southall, T. D. (2016). Dam it's good! DamID profiling of protein-DNA interactions. *Wiley Interdisciplinary Reviews: Developmental Biology*, *5*(1), 25–37. http://doi.org/10.1002/wdev.205

Bailey, T., Krajewski, P., Ladunga, I., Lefebvre, C., Li, Q., Liu, T., … Zhang, J. (2013). Practical Guidelines for the Comprehensive Analysis of ChIP-seq Data. *PLoS Computational Biology*, *9*(11), e1003326. http://doi.org/10.1371/journal.pcbi.1003326

Beaudouin, J., Gerlich, D., Daigle, N., Eils, R., & Ellenberg, J. (2002). Nuclear envelope breakdown proceeds by microtubule-induced tearing of the lamina. *Cell*, *108*(1), 83–96. Retrieved from http://www.ncbi.nlm.nih.gov/pubmed/11792323

Bianchi, A., & Lanzuolo, C. (2015). Into the chromatin world: Role of nuclear architecture in epigenome regulation. *AIMS Biophysics*, *2*(4), 585–612. http://doi.org/10.3934/biophy.2015.4.585

Bilokapic, S., & Schwartz, T. U. (2012). Molecular basis for Nup37 and ELY5/ELYS recruitment to the nuclear pore complex. *Proceedings of the National Academy of Sciences*, *109*(38), 15241–15246. http://doi.org/10.1073/pnas.1205151109

Bilokapic, S., & Schwartz, T. U. (2013a). Structural and functional studies of the 252 kDa nucleoporin ELYS reveal distinct roles for its three tethered domains. *Structure*, *21*(4), 572–580. http://doi.org/10.1016/j.str.2013.02.006

Blobel, G. (1985). Gene gating: A hypothesis. *Cell Biology*, *82*, 8527–8529.

Blobel, G. (2010). Three-dimensional organization of chromatids by nuclear envelope-associated structures. *Cold Spring Harbor Symposia on Quantitative Biology*, *75*, 545–554. http://doi.org/10.1101/sqb.2010.75.004

Bollen, M., Gerlich, D. W., & Lesage, B. (2009). Mitotic phosphatases: from entry guards to exit guides. *Trends in Cell Biology*, *19*(10), 531–541. http://doi.org/10.1016/j.tcb.2009.06.005

Bowerman, B., & Kurz, T. (2006). Degrade to create: developmental requirements for ubiquitin-mediated proteolysis during early C. elegans embryogenesis. *Development*, *133*, 773–784. http://doi.org/doi:10.1242/dev.02276

Braunschweig, U., Hogan, G. J., Pagie, L., & van Steensel, B. (2009). Histone H1 binding is inhibited by histone variant H3.3. *The EMBO Journal*, *28*(23), 3635–3645. http://doi.org/10.1038/emboj.2009.301

Brenner, S. (1974). The genetics of Caenorhabditis elegans. *Genetics*, *77*(1), 71–94. Retrieved from http://www.ncbi.nlm.nih.gov/pubmed/4366476

Brenner, S. (2009). In the beginning was the worm.. *Genetics*, *182*(2), 413–415. http://doi.org/10.1534/genetics.109.104976

Breuer, M., & Ohkura, H. (2015). A negative loop within the nuclear pore complex controls global chromatin organization. *Genes & Development*, *29*(17), 1789–1794.

http://doi.org/10.1101/gad.264341.115

Bucher, E. A., & Seydoux, G. (1994). Gastrulation in the nematode Caenorhabditis elegans. *Seminars in Developmental Biology*, *5*(2), 121–130. http://doi.org/10.1006/sedb.1994.1016

Buchwalter, A. L., Liang, Y., & Hetzer, M. W. (2014). Nup50 is required for cell differentiation and exhibits transcription-dependent dynamics. *Molecular Biology of the Cell*, *25*(16), 2472–2484. http://doi.org/10.1091/mbc.E14-04-0865

Buchwitz, B. J., Ahmad, K., Moore, L. L., Roth, M. B., & Henikoff, S. (1999). A histone-H3-like protein in C. elegans. *Nature*, *401*(6753), 547–8. http://doi.org/10.1038/44062

Budirahardja, Y., & Gönczy, P. (2009). Coupling the cell cycle to development. *Development (Cambridge, England)*, *136*(17), 2861–2872. http://doi.org/10.1242/dev.021931

Burns, L. T., & Wente, S. R. (2014). From Hypothesis to Mechanism: Uncovering Nuclear Pore Complex Links to Gene Expression. *Molecular and Cellular Biology*, *34*(12), 2114–2120. http://doi.org/10.1128/MCB.01730-13

Capelson, M., Doucet, C., & Hetzer, M. W. (2010). Nuclear pore complexes: guardians of the nuclear genome. *Cold Spring Harbor Symposia on Quantitative Biology*, *75*, 585–597. http://doi.org/10.1101/sqb.2010.75.059

Capelson, M., & Hetzer, M. W. (2009). The role of nuclear pores in gene regulation, development and disease. *EMBO Reports*, *10*(7), 697–705. http://doi.org/10.1038/embor.2009.147

Capelson, M., Liang, Y., Schulte, R., Mair, W., Wagner, U., & Hetzer, M. W. (2010). Chromatin-Bound Nuclear Pore Components Regulate Gene Expression in Higher Eukaryotes. *Cell*, *140*, 372–383. http://doi.org/10.1016/j.cell.2009.12.054

Capitanio, J. S., Montpetit, B., & Wozniak, R. W. (2017). Human Nup98 regulates the localization and activity of DExH/D-box helicase DHX9. *eLife*, *6*, e18825. http://doi.org/10.7554/eLife.18825

Cautain, B., Hill, R., de Pedro, N., & Link, W. (2015). Components and regulation of nuclear transport processes. *FEBS Journal*, *282*(3), 445–462. http://doi.org/10.1111/febs.13163

Chadrin, A., Hess, B., San Roman, M., Gatti, X., Lombard, B., Loew, D., … Doye, V. (2010). Pom33, a novel transmembrane nucleoporin required for proper nuclear pore complex distribution. *The Journal of Cell Biology*, *189*(5), 795–811. http://doi.org/10.1083/jcb.200910043

Chatel, G., & Fahrenkrog, B. (2011). Nucleoporins: Leaving the nuclear pore complex for a successful mitosis. *Cellular Signalling*, *23*(10), 1555–1562. http://doi.org/10.1016/j.cellsig.2011.05.023

Cheeseman, I. M., Chappie, J. S., Wilson-Kubalek, E. M., & Desai, A. (2006). The Conserved KMN Network Constitutes the Core Microtubule-Binding Site of the Kinetochore. *Cell*, *127*(5), 983–997. http://doi.org/10.1016/j.cell.2006.09.039

Cheeseman, I. M., Niessen, S., Anderson, S., Hyndman, F., Yates, J. R., Oegema, K., & Desai, A. (2004). A conserved protein network controls assembly of the outer kinetochore and its ability to sustain tension. *Genes & Development*, *18*(18), 2255–2268. http://doi.org/10.1101/gad.1234104

Chen, I.-H. B., Huber, M., Guan, T., Bubeck, A., & Gerace, L. (2006). Nuclear envelope transmembrane proteins (NETs) that are up-regulated during myogenesis. *BMC Cell Biology*, *7*, 38. http://doi.org/10.1186/1471-2121-7-38

Chow, K.-H., Elgort, S., Dasso, M., & Ullman, K. S. (2012). Two distinct sites in Nup153 mediate

interaction with the SUMO proteases SENP1 and SENP2. *Nucleus*, *3*(4), 349–358. http://doi.org/10.4161/nucl.20822

Cline, T. W., & Meyer, B. J. (1996). VIVE LA DIFERENCE: Males vs Females in Flies vs Worms. *Annual Review of Genetics*, *30*, 637–702. http://doi.org/10.1146/annurev.genet.30.1.637

Cohen-Fix, O., & Askjaer, P. (2017). Cell Biology of the Caenorhabditis elegans Nucleus. *Genetics*, *205*(1), 25–59. http://doi.org/DOI: 10.1534/genetics.116.197160

Collas, P., Lund, E. G., & Oldenburg, A. R. (2014). Closing the (nuclear) envelope on the genome: How nuclear lamins interact with promoters and modulate gene expression. *BioEssays*, *36*(1), 75–83. http://doi.org/10.1002/bies.201300138

Collette, K. S., Petty, E. L., Golenberg, N., Bembenek, J. N., & Csankovszki, G. (2011). Different roles for Aurora B in condensin targeting during mitosis and meiosis. *Journal of Cell Science*, *124*(Pt 21), 3684–3694. http://doi.org/10.1242/jcs.088336

Colombo, K., Grill, S. W., Kimple, R. J., Willard, F. S., Siderovski, D. P., & Gönczy, P. (2003). Translation of Polarity Cues into Asymmetric Spindle Positioning in Caenorhabditis elegans Embryos. *Science*, *300*(5627), 1957–1961.

Cook, A., Bono, F., Jinek, M., & Conti, E. (2007). Structural Biology of Nucleocytoplasmic Transport. *Annual Review of Biochemistry*, *76*(1), 647–671. http://doi.org/10.1146/annurev.biochem.76.052705.161529

Corsi, A. K., Wightman, B., & Chalfie, M. (2015). A transparent window into biology: A primer on Caenorhabditis elegans. *Genetics*, *200*(2), 387–407. http://doi.org/10.1534/genetics.115.176099

Cortes, D. B., McNally, K. L., Mains, P. E., & McNally, F. J. (2015). The asymmetry of female meiosis reduces the frequency of inheritance of unpaired chromosomes. *eLife*, *4*, e06056. http://doi.org/10.7554/eLife.06056

Cowan, C. R., & Hyman, A. A. (2004). Centrosomes direct cell polarity independently of microtubule assembly in C. elegans embryos. *Nature*, *431*(7004), 92–96. http://doi.org/10.1038/nature02825

Crane, E., Bian, Q., McCord, R. P., Lajoie, B. R., Wheeler, B. S., Ralston, E. J., … Meyer, B. J. (2015). Condensin-driven remodelling of X chromosome topology during dosage compensation. *Nature*, *523*(7559), 240–244. http://doi.org/10.1038/nature14450

Crowder, M. E., Flynn, J. R., McNally, K. P., Cortes, D. B., Price, K. L., Kuehnert, P. a., … McNally, F. J. (2015). Dynactin-dependent cortical dynein and spherical spindle shape correlate temporally with meiotic spindle rotation in Caenorhabditis elegans. *Molecular Biology of the Cell*, *26*(17), 3030–3046. http://doi.org/10.1091/mbc.E15-05-0290

Csankovszki, G., Collette, K., Spahl, K., Carey, J., Snyder, M., Petty, E., … Hagstrom, K. (2009). Three Distinct Condensin Complexes Control C. elegans Chromosome Dynamics. *Current Biology*, *19*(1), 9–19. http://doi.org/10.1016/j.cub.2008.12.006

Csankovszki, G., McDonel, P., & Meyer, B. J. (2004). Recruitment and spreading of the C. elegans dosage compensation complex along X chromosomes. *Science* , *303*(5661), 1182–1185. http://doi.org/10.1126/science.1092938

D ’Angelo, M. A., Gomez-Cavazos, J. S., Mei, A., Lackner, D. H., & Hetzer, M. W. (2012). A Change in Nuclear Pore Complex Composition Regulates Cell Differentiation. *Developmental Cell*, *22*(2),

446–458. http://doi.org/10.1016/j.devcel.2011.11.021

D'Angelo, M. A., Anderson, D. J., Richard, E., & Hetzer, M. W. (2006). Nuclear Pores Form de Novo from Both Sides of the Nuclear Envelope. *Science*, *312*(5772), 440–443.

Dai, M., Thompson, R. C., Maher, C., Contreras-Galindo, R., Kaplan, M. H., Markovitz, D. M., … Meng, F. (2010). NGSQC: cross-platform quality analysis pipeline for deep sequencing data. *BMC Genomics*, *11*(Suppl 4), S7. http://doi.org/10.1186/1471-2164-11-S4-S7

Dauer, W. T., & Worman, H. J. (2009). The Nuclear Envelope as a Signaling Node in Development and Disease. *Developmental Cell*, *17*, 626–638. http://doi.org/10.1016/j.devcel.2009.10.016

Davis, T. L., & Meyer, B. J. (1996). SDC-3 coordinates the assembly of a dosage compensation complex on the nematode X chromosome. *Development*, *124*, 1019–1031.

Davuluri, G., Gong, W., Yusuff, S., Lorent, K., Muthumani, M., Dolan, A. C., & Pack, M. (2008). Mutation of the zebrafish nucleoporin elys sensitizes tissue progenitors to replication stress. *PLoS Genetics*, *4*(10). http://doi.org/10.1371/journal.pgen.1000240

Dawes, H. E., Berlin, D. S., Lapidus, D. M., Nusbaum, C., Davis, T. L., & Meyer, B. J. (1999). Dosage compensation proteins targeted to X chromosomes by a determinant of hermaphrodite fate. *Science*, *284*(5421), 1800–1804. Retrieved from http://www.ncbi.nlm.nih.gov/pubmed/10364546

Desai, A., Rybina, S., M??ller-Reichert, T., Shevchenko, A., Shevchenko, A., Hyman, A., & Oegema, K. (2003). KNL-1 directs assembly of the microtubule-binding interface of the kinetochore in C. elegans. *Genes and Development*, *17*(19), 2421–2435. http://doi.org/10.1101/gad.1126303

Devos, D. P., Gräf, R., & Field, M. (2014). Evolution of the nucleus. *Current Opinion in Cell Biology*, *28*, 8–15. http://doi.org/10.1016/j.ceb.2014.01.004.

Dickinson, D. J., & Goldstein, B. (2016). CRISPR-Based Methods for Caenorhabditis elegans Genome Engineering. *Genetics*, *202*(3), 885–901. http://doi.org/10.1534/genetics.115.182162

Dickinson, D. J., Ward, J. D., Reiner, D. J., & Goldstein, B. (2013). Engineering the Caenorhabditis elegans genome using Cas9-triggered homologous recombination. *Nature Methods*, *10*(10), 1028–1034. http://doi.org/10.1038/nmeth.2641

Dittmer, T., & Misteli, T. (2011). Gene organization and evolutionary history. *Genome Biology*, *12*(5), 222–236.

Dobrzynska, A., Askjaer, P., & Gruenbaum, Y. (2016). Lamin-Binding Proteins in Caenorhabditis elegans. In *Methods in enzymology* (Vol. 569, pp. 455–483). http://doi.org/10.1016/bs.mie.2015.08.036

Dobrzynska, A., Gonzalo, S., Shanahan, C., & Askjaer, P. (2016). The Nuclear Lamina in Health and Disease. *Nucleus (Austin, Tex.)*, *1034*(July), 0. http://doi.org/10.1080/19491034.2016.1183848

Doucet, C. M., Talamas, J. A., & Hetzer, M. W. (2010). Cell cycle-dependent differences in nuclear pore complex assembly in metazoa. *Cell*, *141*(6), 1030–1041. http://doi.org/10.1016/j.cell.2010.04.036

Dougherty, E. C., & Calhoun, H. G. (1948). Possible significance of free-living nematodes in genetic research. *Nature*, *161*(4079), 29. Retrieved from http://www.ncbi.nlm.nih.gov/pubmed/18900748

Dultz, E., Zanin, E., Wurzenberger, C., Braun, M., Rabut, G., Sironi, L., & Ellenberg, J. (2008). Systematic kinetic analysis of mitotic dis- and reassembly of the nuclear pore in living cells. *The*

Journal of Cell Biology, *180*(5), 857–865. http://doi.org/10.1083/jcb.200707026

Dumont, J. (2015). Aurora B/C in Meiosis: Correct Me If I'm Right. *Developmental Cell*, *33*, 499–501. http://doi.org/10.1016/j.devcel.2015.05.018

Dumont, J., Oegema, K., & Desai, A. (2010). A kinetochore-independent mechanism drives anaphase chromosome separation during acentrosomal meiosis. *Nature Cell Biology*, *12*(9), 894–901. http://doi.org/10.1038/ncb2093

Ercan, S. (2015). Mechanisms of X Chromosome Dosage Compensation. *Journal of Genomics*, *3*, 1–19. http://doi.org/10.7150/jgen.10404

Ercan, S., Dick, L. L., & Lieb, J. D. (2009). The C. elegans dosage compensation complex propagates along chromatin dynamically and independently of X-chromosome sequence. *Current Biology*, *19*(21), 1777–1787. http://doi.org/10.1016/j.cub.2009.09.047

Ercan, S., Giresi, P. G., Whittle, C. M., Zhang, X., Green, R. D., & Lieb, J. D. (2007). X chromosome repression by localization of the C. elegans dosage compensation machinery to sites of transcription initiation. *Nature Genetics*, *39*(3), 403–408. http://doi.org/10.1038/ng1983

Ertl, I., Porta-De-La-Riva, M., Gómez-Orte, E., Rubio-Peña, K., Aristizábal-Corrales, D., Cornes, E., … Cerón, J. (2016). Functional Interplay of Two Paralogs Encoding SWI/SNF Chromatin-Remodeling Accessory Subunits During Caenorhabditis elegans Development. *Genetics*, *202*(3), 961–975. http://doi.org/10.1534/genetics.115.183533

Fabritius, A. S., Ellefson, M. L., & McNally, F. J. (2011). Nuclear and spindle positioning during oocyte meiosis. *Current Opinion in Cell Biology*, *23*(1), 78–84. http://doi.org/10.1016/j.ceb.2010.07.008

Fahrenkrog, B., & Aebi, U. (2003). The nuclear pore complex: nucleocytoplasmic transport and beyond. *Nature Reviews Molecular Cell Biology*, *4*(10), 757–766. http://doi.org/10.1038/nrm1230

Fernandez, A. G., Mis, E. K., Lai, A., Mauro, M., Quental, A., Bock, C., & Piano, F. (2014). Uncovering buffered pleiotropy: a genome-scale screen for mel-28 genetic interactors in Caenorhabditis elegans. *G3 (Bethesda, Md.)*, *4*(1), 185–96. http://doi.org/10.1534/g3.113.008532

Fernandez, A. G., & Piano, F. (2006). MEL-28 Is Downstream of the Ran Cycle and Is Required for Nuclear-Envelope Function and Chromatin Maintenance. *Current Biology*, *16*(17), 1757–1763. http://doi.org/10.1016/j.cub.2006.07.071

Ferrai, C., de Castro, I. J., Lavitas, L., Chotalia, M., & Pombo, A. (2010). Gene positioning. *Cold Spring Harbor Perspectives in Biology*, *2*(6), 1–18. http://doi.org/10.1101/cshperspect.a000588

Ferris, H., & Hieb, W. F. (2015). Ellsworth C. Dougherty: A Pioneer in the Selection of Caenorhabditis elegans as a Model Organism. *GENETICS*, *200*(4), 991–1002. http://doi.org/10.1534/genetics.115.178913

Francis, R., & Waterston, R. H. (1991). Muscle Cell Attachment in Caenorhabditis elegans. *Journal of Cell Biology*, *114*(3), 465–479. Retrieved from https://www.ncbi.nlm.nih.gov/pmc/articles/PMC2289102/pdf/jc1143465.pdf

Franks, T. M., Benner, C., Narvaiza, I., Marchetto, M. C. N., Young, J. M., Malik, H. S., … Hetzer, M. W. (2016). Evolution of a transcriptional regulator from a transmembrane nucleoporin. *Genes & Development*, (May), 1–17. http://doi.org/10.1101/gad.280941.116.

Franz, C., Walczak, R., Yavuz, S., Santarella, R., Gentzel, M., Askjaer, P., … Antonin, W. (2007).

MEL-28/ELYS is required for the recruitment of nucleoporins to chromatin and postmitotic nuclear pore complex assembly. *EMBO Reports*, *8*(2), 165–172. http://doi.org/10.1038/sj.embor.7400889

Fraser, J., Williamson, I., Bickmore, W. A., & Dostie, J. (2015). An Overview of Genome Organization and How We Got There: from FISH to Hi-C. *Microbiology and Molecular Biology Reviews*, *79*(3), 347–372. http://doi.org/10.1128/MMBR.00006-15.

Friedland, A. E., Tzur, Y. B., Esvelt, K. M., Colaiácovo, M. P., Church, G. M., & Calarco, J. A. (2013). Heritable genome editing in C. elegans via a CRISPR-Cas9 system. *Nature Methods*, *10*(8), 741–743. http://doi.org/10.1038/nmeth.2532

Frøkjær-Jensen, C., Davis, M. W., Ailion, M., & Jorgensen, E. M. (2012). Improved Mos1-mediated transgenesis in C. elegans. *Nature Methods*, *9*(2), 117–118. http://doi.org/10.1038/nmeth.1865

Frøkjær-Jensen, C., Wayne Davis, M., Hopkins, C. E., Newman, B. J., Thummel, J. M., Olesen, S.-P., … Jorgensen, E. M. (2008). Single-copy insertion of transgenes in Caenorhabditis elegans. *Nature Genetics*, *40*(11), 1375–1383. http://doi.org/10.1038/ng.248

Furuta, T., Tuck, S., Kirchner, J., Koch, B., Auty, R., Kitagawa, R., … Greenstein, D. (2000). EMB-30: an APC4 homologue required for metaphase-to-anaphase transitions during meiosis and mitosis in Caenorhabditis elegans. *Molecular Biology of the Cell*, *11*(4), 1401–1419. Retrieved from http://www.molbiolcell.org/cgi/content/full/11/4/1401\npapers2://publication/uuid/05D314E5-9768-4ABD-8CB9-F931A2609698

Gadde, S., & Heald, R. (2004). Review Mechanisms and Molecules of the Mitotic Spindle. *Current Biology*, *14*, 797–805. http://doi.org/10.1016/j.cub.2004.09.021

Galy, V., Antonin, W., Jaedicke, A., Sachse, M., Santarella, R., Haselmann, U., & Mattaj, I. (2008). A role for gp210 in mitotic nuclear-envelope breakdown. *Journal of Cell Science*, *121*, 317–328. http://doi.org/10.1242/jcs.022525

Galy, V., Askjaer, P., Franz, C., López-Iglesias, C., & Mattaj, I. W. (2006a). MEL-28, a Novel Nuclear-Envelope and Kinetochore Protein Essential for Zygotic Nuclear-Envelope Assembly in C. elegans. *Current Biology*, *16*(17), 1748–1756. http://doi.org/10.1016/j.cub.2006.06.067

Galy, V., Mattaj, I. W., & Askjaer, P. (2003). Caenorhabditis elegans Nucleoporins Nup93 and Nup205 Determine the Limit of Nuclear Pore Complex Size Exclusion In Vivo. *Molecular Biology of the Cell*, *14*, 5104–5115. http://doi.org/10.1091/mbc.E03

Gao, N., Davuluri, G., Gong, W., Seiler, C., Lorent, K., Furth, E. E., … Pack, M. (2011). The nuclear pore complex protein Elys is required for genome stability in mouse intestinal epithelial progenitor cells. *Gastroenterology*, *140*(5), 1547–55 e10. http://doi.org/10.1053/j.gastro.2011.01.048.The

Gassmann, R., Rechtsteiner, A., Yuen, K. W., Muroyama, A., Egelhofer, T., Gaydos, L., … Desai, A. (2012). An inverse relationship to germline transcription defines centromeric chromatin in C. elegans. *Nature*, *484*(7395), 534–7. http://doi.org/10.1038/nature10973

Gerstein, M. B., Lu, Z. J., Van Nostrand, E. L., Cheng, C., Arshinoff, B. I., Liu, T., … Waterston, R. H. (2010). Integrative analysis of the Caenorhabditis elegans genome by the modENCODE project. *Science*, *330*(6012), 1775–1787. http://doi.org/science.1196914 [pii]\r10.1126/science.1196914

Gillespie, P. J., Khoudoli, G. A., Stewart, G., Swedlow, J. R., & Blow, J. ??Julian. (2007a). ELYS/MEL-28 Chromatin Association Coordinates Nuclear Pore Complex Assembly and Replication Licensing. *Current Biology*, *17*(19), 1657–1662. http://doi.org/10.1016/j.cub.2007.08.041

Giresi, P. G., Kim, J., McDaniell, R. M., Iyer, V. R., & Lieb, J. D. (2007). FAIRE (Formaldehyde-Assisted Isolation of Regulatory Elements) isolates active regulatory elements from human chromatin. *Genome Research*, *17*(6), 877–885. http://doi.org/10.1101/gr.5533506

Golden, A., Sadler, P. L., Wallenfang, M. R., Schumacher, J. M., Hamill, D. R., Bates, G., … Shakes, D. C. (2000). Metaphase to Anaphase (mat) Transition–Defective Mutants inCaenorhabditis elegans. *The Journal of Cell Biology*, *151*(7), 1469–1482. Retrieved from http://jcb.rupress.org/content/151/7/1469

Goldfarb, D. S., Gariépy, J., Schoolnik, G., & Kornberg, R. D. (1986). Synthetic peptides as nuclear localization signals. *Nature*, *322*(6080), 641–644. http://doi.org/10.1038/322641a0

Gomez-Cavazos, J. S., & Hetzer, M. W. (2012). Outfits for different occasions: Tissue-specific roles of Nuclear Envelope proteins. *Current Opinion in Cell Biology*, *24*(6), 775–783. http://doi.org/10.1016/j.ceb.2012.08.008

Gomez-Cavazos, J. S., & Hetzer, M. W. (2015). The nucleoporin gp210/Nup210 controls muscle differentiation by regulating nuclear envelope/ER homeostasis. *The Journal of Cell Biology*, *208*(6), 671–681.

Gómez-Saldivar, G., Fernandez, A., Hirano, Y., Mauro, M., Lai, A., Ayuso, C., … Askjaer, P. (2016). Identification of Conserved MEL-28/ELYS Domains with Essential Roles in Nuclear Assembly and Chromosome Segregation. *PLOS Genetics*, *12*(6), e1006131. http://doi.org/10.1371/journal.pgen.1006131

Gómez-Saldivar, G., Meister, P., & Askjaer, P. (2016). DamID Analysis of Nuclear Organization in Caenorhabditis elegans. In S. Shackleton, P. Collas, & E. C. Schirmer (Eds.), *The Nuclear Envelope. Methods in Molecular Biology* (1411th ed., pp. 341–358). New York: Springer Nature. http://doi.org/10.1007/978-1-4939-3530-7_22

Gönczy, P. (2008). Mechanisms of asymmetric cell division: flies and worms pave the way. *Nature Reviews Molecular Cell Biology*, *9*(5), 355–366. http://doi.org/10.1038/nrm2388

Gönczy, P., Grill, S., Stelzer, E. H., Kirkham, M., & Hyman, A. A. (2001). Spindle positioning during the asymmetric first cell division of Caenorhabditis elegans embryos. *Novartis Foundation Symposium*, *237*, 164–175; discussion 176–181. Retrieved from http://www.ncbi.nlm.nih.gov/pubmed/11444042

Gönczy, P., Hyman, A. A., Echeverri, C., Oegema, K., Coulson, A., Jones, S. J. M., … Bork, P. (2000). Functional genomic analysis of cell division in C. elegans using RNAi of genes on chromosome III. *Nature*, *408*(6810), 331–336. http://doi.org/10.1038/35042526

González-Aguilera, C., Ikegami, K., Ayuso, C., de Luis, A., Íñiguez, M., Cabello, J., … Askjaer, P. (2014). Genome-wide analysis links emerin to neuromuscular junction activity in Caenorhabditis elegans. *Genome Biology*, *15*(2), R21. http://doi.org/10.1186/gb-2014-15-2-r21

Gonzalez-sandoval, A., & Gasser, S. M. (2016). On TADs and LADs : Spatial Control Over Gene

Expression. *Trends in Genetics*, *xx*(July), 1–11. http://doi.org/10.1016/j.tig.2016.05.004

Gorjánácz, M., Jaedicke, A., & Mattaj, I. W. (2007). What can *Caenorhabditis elegans* tell us about the nuclear envelope? *FEBS Letters*, *581*(15), 2794–2801. http://doi.org/10.1016/j.febslet.2007.03.052

Görlich, D., & Kutay, U. (1999). Transport Between the Cell Nucleus and the Cytoplasm. *Annual Review of Cell and Developmental Biology*, *15*(1), 607–660. http://doi.org/10.1146/annurev.cellbio.15.1.607

Goss, V. L., Hocevar, B. A., Thompson, L. J., Stratton, C. A., Burns, D. J., & Fields, A. P. (1994). Identification of nuclear beta II protein kinase C as a mitotic lamin kinase. *The Journal of Biological Chemistry*, *269*(29), 19074–19080. Retrieved from http://www.ncbi.nlm.nih.gov/pubmed/8034666

Greenstein, D. (2005). Control of oocyte meiotic maturation and fertilization. http://doi.org/10.1895/wormbook.1.53.1

Greer, E. L., Blanco, M. A., Gu, L., Sendinc, E., Liu, J., Aristizábal-Corrales, D., … Shi, Y. (2015). DNA methylation on N6-adenine in C. elegans. *Cell*, *161*(4), 868–878. http://doi.org/10.1016/j.cell.2015.04.005

Greil, F., Moorman, C., & van Steensel, B. (2006). [16] DamID: Mapping of In Vivo Protein-Genome Interactions Using Tethered DNA Adenine Methyltransferase. *Methods in Enzymology*, *410*(06), 342–359. http://doi.org/10.1016/S0076-6879(06)10016-6

Griffis, E. R., Altan, N., Lippincott-Schwartz, J., & Powers, M. A. (2002). Nup98 Is a Mobile Nucleoporin with Transcription-dependent Dynamics. *Molecular Biology of the Cell*, *13*(4), 1282–1297. http://doi.org/10.1091/mbc.01-11-0538

Griffis, E. R., Craige, B., Dimaano, C., Ullman, K. S., & Powers, M. A. (2004). Distinct Functional Domains within Nucleoporins Nup153 and Nup98 Mediate Transcription-dependent Mobility. *Molecular Biology of the Cell*, *15*, 1991–2002. http://doi.org/10.1091/mbc.E03–10

Guelen, L., Pagie, L., Brasset, E., Meuleman, W., Faza, M. B., Talhout, W., … van Steensel, B. (2008). Domain organization of human chromosomes revealed by mapping of nuclear lamina interactions. *Nature*, *453*(7197), 948–951. http://doi.org/10.1038/nature06947

Gutierrez-Triana, J. A., Mateo, J. L., Ibberson, D., Ryu, S., & Wittbrodt, J. (2016). iDamIDseq and iDEAR: an improved method and computational pipeline to profile chromatin-binding proteins. *Development*, *143*(22), 4272–4278. http://doi.org/10.1242/dev.139261

Güttinger, S., Laurell, E., & Kutay, U. (2009). Orchestrating nuclear envelope disassembly and reassembly during mitosis. *Nature Reviews. Molecular Cell Biology*, *10*(3), 178–191. http://doi.org/10.1038/nrm2641

Hagstrom, K. A., Holmes, V. F., Cozzarelli, N. R., & Meyer, B. J. (2002). C. elegans condensin promotes mitotic chromosome architecture, centromere organization, and sister chromatid segregation during mitosis and meiosis. *Genes & Development*, *16*(6), 729–742. http://doi.org/10.1101/gad.968302

Hagstrom, K. A., & Meyer, B. J. (2003). Condensin and cohesin: more than chromosome compactor and glue. *Nature Reviews Genetics*, *4*(7), 520–534. http://doi.org/10.1038/nrg1110

Hattersley, N., Cheerambathur, D., Moyle, M., Dumont, J., Oegema, K., & Desai, A. (2016). A Nucleoporin Docks Protein Phosphatase 1 to Direct Meiotic Chromosome Segregation and Article A Nucleoporin Docks Protein Phosphatase 1 to Direct Meiotic Chromosome Segregation and Nuclear Assembly. *Developmental Cell*, *38*(5), 463–477. http://doi.org/10.1016/j.devcel.2016.08.006

Hayashi-Takanaka, Y., Maehara, K., Harada, A., Umehara, T., Yokoyama, S., Obuse, C., … Kimura, H. (2015). Distribution of histone H4 modifications as revealed by a panel of specific monoclonal antibodies. *Chromosome Research*, *23*(4), 753–766. http://doi.org/10.1007/s10577-015-9486-4

Hetzer, M. W. (2010). The Nuclear Envelope. *Cold Spring Harbor Perspectives in Biology*, *2*(3), a000539–a000539. http://doi.org/10.1101/cshperspect.a000539

Hillers, K. J., Jantsch, V., Martinez-Perez, E., & Yanowitz, J. L. (2015, December 22). Meiosis. http://doi.org/10.1895/wormbook.1.178.1

Hird, S. N., & White, J. G. (1993). Cortical and cytoplasmic flow polarity in early embryonic cells of Caenorhabditis elegans. *The Journal of Cell Biology*, *121*(6), 1343–1355. Retrieved from http://www.ncbi.nlm.nih.gov/pubmed/8509454

Hirota, T., Gerlich, D., Koch, B., Ellenberg, J., & Peters, J. M. (2004). Distinct functions of condensin I and II in mitotic chromosome assembly. *Journal of Cell Science*, *117*(26), 6435–6445. http://doi.org/10.1242/jcs.01604

Ho, C. Y., & Lammerding, J. (2012). Lamins at a glance. *Journal of Cell Science*, *125*(9), 2087–2093. http://doi.org/10.1242/jcs.087288

Hodgkin, J., Horvitz, H. R., & Brenner, S. (1979). Nondisjunction Mutants of the Nematode CAENORHABDITIS ELEGANS. *Genetics*, *91*(1), 67–94. Retrieved from http://www.ncbi.nlm.nih.gov/pubmed/17248881

Hoelz, A., Debler, E. W., & Blobel, G. (2011). The structure of the nuclear pore complex. *Annual Review of Biochemistry*, *80*, 613–43. http://doi.org/10.1146/annurev-biochem-060109-151030

Howe, M., McDonald, K. L., Albertson, D. G., & Meyer, B. J. (2001). HIM-10 is required for kinetochore structure and function on Caenorhabditis elegans holocentric chromosomes. *Journal of Cell Biology*, *153*(6), 1227–1238. http://doi.org/10.1083/jcb.153.6.1227

Huang, D. W., Sherman, B. T., Tan, Q., Kir, J., Liu, D., Bryant, D., … Lempicki, R. A. (2007). DAVID Bioinformatics Resources: Expanded annotation database and novel algorithms to better extract biology from large gene lists. *Nucleic Acids Research*, *35*(SUPPL.2), 169–175. http://doi.org/10.1093/nar/gkm415

Hudson, D. F., Marshall, K. M., & Earnshaw, W. C. (2009). Condensin: Architect of mitotic chromosomes. *Chromosome Research*, *17*(2), 131–144. http://doi.org/10.1007/s10577-008-9009-7

Ibarra, A., Benner, C., Tyagi, S., Cool, J., & Hetzer, M. W. (2016). Nucleoporin-mediated regulation of cell identity genes. *Genes & Development*, 2253–2258. http://doi.org/10.1101/gad.287417.116

Ibarra, A., & Hetzer, M. W. (2015). Nuclear pore proteins and the control of genome functions. *Genes and Development*, *29*(4), 337–349. http://doi.org/10.1101/gad.256495.114

Ikegami, K., Egelhofer, T. A., Strome, S., & Lieb, J. D. (2010). Caenorhabditis elegans chromosome

arms are anchored to the nuclear membrane via discontinuous association with LEM-2. *Genome Biology*, *11*(12), R120. http://doi.org/10.1186/gb-2010-11-12-r120

Ikegami, K., & Lieb, J. (2013). Integral Nuclear Pore Proteins Bind to Pol III-Transcribed Genes and Are Required for Pol III Transcript Processing in C. elegans. *Molecular Cell*, *51*(6), 840–849. http://doi.org/10.1016/j.molcel.2013.08.001

Inoue, A., & Zhang, Y. (2014). Nucleosome assembly is required for nuclear pore complex assembly in mouse zygotes. *Nature Structural & Molecular Biology*, *21*(7), 609–16. http://doi.org/10.1038/nsmb.2839

Ivers, K. M., Li, C., Patel, N., Sredar, N., Luo, X., Queener, H., … Porter, J. (2011). Reproducibility of measuring lamina cribrosa pore geometry in human and nonhuman primates with in vivo adaptive optics imaging. *Investigative Ophthalmology & Visual Science*, *52*(8), 5473–5480. http://doi.org/10.1167/iovs.11-7347

Jacinto, F. V, Benner, C., & Hetzer, M. W. (2015a). The nucleoporin Nup153 regulates embryonic stem cell pluripotency through gene silencing. *GENES & DEVELOPMENT* , *29*, 1–15. http://doi.org/10.1101/gad.260919.115

Jans, J., Gladden, J. M., Ralston, E. J., Pickle, C. S., Michel, A. H., Pferdehirt, R. R., … Meyer, B. J. (2009). A condensin-like dosage compensation complex acts at a distance to control expression throughout the genome. *Genes & Development*, *23*(5), 602–618. http://doi.org/10.1101/gad.1751109

Jost, K. L., Bertulat, B., & Cardoso, M. C. (2012). Heterochromatin and gene positioning: inside, outside, any side? *Chromosoma*, *121*(6), 555–563. http://doi.org/10.1007/s00412-012-0389-2

Kalverda, B., & Fornerod, M. (2010). Characterization of genome-nucleoporin interactions in Drosophila links chromatin insulators to the nuclear pore complex. *Cell Cycle*, *9*(24), 4812–4817. http://doi.org/10.4161/cc.9.24.14328

Kalverda, B., Pickersgill, H., Shloma, V. V., & Fornerod, M. (2010). Nucleoporins Directly Stimulate Expression of Developmental and Cell-Cycle Genes Inside the Nucleoplasm. *Cell*, *140*(3), 360–371. http://doi.org/10.1016/j.cell.2010.01.011

Kamath, R. S., Fraser, A. G., Dong, Y., Poulin, G., Durbin, R., Gotta, M., … Ahringer, J. (2003). Systematic functional analysis of the Caenorhabditis elegans genome using RNAi. *Nature*, *421*(6920), 231–237. http://doi.org/10.1038/nature01278

Kehat, I., Accornero, F., Aronow, B. J., & Molkentin, J. D. (2011). Modulation of chromatin position and gene expression by HDAC4 interaction with nucleoporins. *Journal of Cell Biology*, *193*(1), 21–29. http://doi.org/10.1083/jcb.201101046

Kharchenko, P. V, Alekseyenko, A. A., Schwartz, Y. B., Minoda, A., Riddle, N. C., Ernst, J., … Park, P. J. (2011). Comprehensive analysis of the chromatin landscape in Drosophila melanogaster. *Nature*, *471*, 480–485. Retrieved from https://pdfs.semanticscholar.org/5337/4f1ee219841cb55d4f11bc15a214a37a78e2.pdf

Kharchenko, P. V, Tolstorukov, M. Y., & Park, P. J. (2008). Design and analysis of ChIP-seq experiments for DNA-binding proteins. *Nature Biotechnology*, *26*(12), 1351–1359. http://doi.org/10.1038/nbt.1508

Kim, D. Y., & Roy, R. (2006). Cell cycle regulators control centrosome elimination during oogenesis in *Caenorhabditis elegans*. *The Journal of Cell Biology*, *174*(6), 751–757. http://doi.org/10.1083/jcb.200512160

Kimura, N., Takizawa, M., Okita, K., Natori, O., Igarashi, K., Ueno, M., … Taga, T. (2002). Identification of a novel transcription factor, ELYS, expressed predominantly in mouse foetal haematopoietic tissues. *Genes to Cells*, *7*(4), 435–446. http://doi.org/10.1046/j.1365-2443.2002.00529.x

Kind, J., Pagie, L., De Vries, S. S., Nahidiazar, L., Dey, S. S., Bienko, M., … Van Steensel, B. (2015). Genome-wide Maps of Nuclear Lamina Interactions in Single Human Cells. *Cell*, *163*(1), 134–147. http://doi.org/10.1016/j.cell.2015.08.040

Kind, J., & van Steensel, B. (2010). Genome-nuclear lamina interactions and gene regulation. *Current Opinion in Cell Biology*, *22*(3), 320–325. http://doi.org/10.1016/j.ceb.2010.04.002

Kind, J., & van Steensel, B. (2014). Stochastic genome-nuclear lamina interactions: Modulating roles of Lamin A and BAF. *Nucleus*, *5*(2), 1–7. http://doi.org/10.4161/nucl.28825

Kitagawa, R. (2009). Key players in chromosome segregation in Caenorhabditis elegans. *Frontiers in Bioscience : A Journal and Virtual Library*, *14*(Figure 1), 1529–1557. http://doi.org/3323 [pii]

Kosugi, S., Hasebe, M., Tomita, M., & Yanagawa, H. (2009). Systematic identification of cell cycle-dependent yeast nucleocytoplasmic shuttling proteins by prediction of composite motifs. *Proceedings of the National Academy of Sciences*, *106*(25), 10171–10176. http://doi.org/10.1073/pnas.0900604106

Labade, A. S., Karmodiya, K., & Sengupta, K. (2016). HOXA repression is mediated by nucleoporin Nup93 assisted by its interactors Nup188 and Nup205. *Epigenetics & Chromatin*, *9*(54). Retrieved from https://www.ncbi.nlm.nih.gov/pmc/articles/PMC5135769/pdf/13072_2016_Article_106.pdf

Labbé, J.-C., McCarthy, E. K., & Goldstein, B. (2004). The forces that position a mitotic spindle asymmetrically are tethered until after the time of spindle assembly. *The Journal of Cell Biology*, *167*(2), 245–256. http://doi.org/10.1083/jcb.200406008

Langmead, B., & Salzberg, S. L. (2012). Fast gapped-read alignment with Bowtie 2. *Nature Methods*, *9*(4), 357–359. http://doi.org/10.1038/nmeth.1923

Langmead, B., Trapnell, C., Pop, M., & Salzberg, S. L. (2009). Ultrafast and memory-efficient alignment of short DNA sequences to the human genome. *Genome Biology*, *10*(3), R25. http://doi.org/10.1186/gb-2009-10-3-r25

Lau, A. C., Nabeshima, K., & Csankovszki, G. (2014). The C. elegans dosage compensation complex mediates interphase X chromosome compaction. *Epigenetics & Chromatin*, *7*(1), 31. http://doi.org/10.1186/1756-8935-7-31

Lee, K. K., Gruenbaum, Y., Spann, P., Liu, J., & Wilson, K. L. (2000). C. elegans Nuclear Envelope Proteins Emerin, MAN1, Lamin, and Nucleoporins Reveal Unique Timing of Nuclear Envelope Breakdown during Mitosis. *Molecular Biology of the Cell*, *11*, 3089–3099.

Lesage, B., Qian, J., Bollen, M., Musacchio, A., Salmon, E. D., Zich, J., … Chen, R. H. (2011). Spindle checkpoint silencing: PP1 tips the balance. *Current Biology*, *21*(21), 898–903.

http://doi.org/10.1016/j.cub.2011.08.063

Levy, D. L., & Heald, R. (2010). Nuclear Size Is Regulated by Importin α and Ntf2 in Xenopus. *Cell*, *143*(2), 288–298. http://doi.org/10.1016/j.cell.2010.09.012

Liang, Y., Franks, T. M., Marchetto, M. C., Gage, F. H., Hetzer, M. W., Harold, G., … Helmsley, H. B. (2013). Dynamic Association of NUP98 with the Human Genome. *PLoS Genet*, *9*(2), e1003308. http://doi.org/10.1371/journal.pgen.1003308

Light, W. H., Brickner, D. G., Brand, V. R., & Brickner, J. H. (2010). Interaction of a DNA zip code with the nuclear pore complex promotes H2A.Z incorporation and INO1 transcriptional memory. *Molecular Cell*, *40*(1), 112–125. http://doi.org/10.1016/j.molcel.2010.09.007

Lints, R., & Hall, D. H. (2016). Reproductive system. http://doi.org/doi:10.3908/wormatlas.2.14

Liu, H.-L., De Souza, C. P. C., Osmani, A. H., & Osmani, S. A. (2009). The Three Fungal Transmembrane Nuclear Pore Complex Proteins of Aspergillus nidulans Are Dispensable in the Presence of an Intact An-Nup84-120 Complex. *Molecular Biology of the Cell*, *20*, 616–630. http://doi.org/10.1091/mbc.E08

Liu, J., Rolef Ben-Shahar, T., Riemer, D., Treinin, M., Spann, P., Weber, K., … Gruenbaum, Y. (2000). Essential roles for Caenorhabditis elegans lamin gene in nuclear organization, cell cycle progression, and spatial organization of nuclear pore complexes. *Molecular Biology of the Cell*, *11*(11), 3937–3947. Retrieved from http://www.ncbi.nlm.nih.gov/pubmed/11071918

Lu, L., Ladinsky, M. S., & Kirchhausen, T. (2011). Formation of the postmitotic nuclear envelope from extended ER cisternae precedes nuclear pore assembly. *Journal of Cell Biology*, *194*(3), 425–440. http://doi.org/10.1083/jcb.201012063

Lucchesi, J. C., Kelly, W. G., & Panning, B. (2005). Chromatin Remodeling in Dosage Compensation. *Annual Review of Genetics*, *39*(1), 615–651. http://doi.org/10.1146/

Lui, D. Y., & Colaiácovo, M. P. (2013). Meiotic development in Caenorhabditis elegans. In T. Schedl (Ed.), *Advances in experimental medicine and biology* (Vol. 757, pp. 133–170). New york: Springer Science Business Media. http://doi.org/10.1007/978-1-4614-4015-4_6

Lund, E., & Collas, P. (2013). Nuclear lamins. *Nucleus*, *4*(6), 424–430. http://doi.org/10.4161/nucl.26865

Lund, E. G., Duband-Goulet, I., Oldenburg, A., Buendia, B., & Collas, P. (2015). Distinct features of lamin A-interacting chromatin domains mapped by ChIP-sequencing from sonicated or micrococcal nuclease-digested chromatin. *Nucleus*, *1034*(February 2016), 0. http://doi.org/10.4161/19491034.2014.990855

Lund, E., Oldenburg, A. R., Delbarre, E., Freberg, C. T., Duband-goulet, I., Eskeland, R., … Collas, P. (2013). Lamin A / C-promoter interactions specify chromatin state – dependent transcription outcomes. *Genome Research*, 1580–1589. http://doi.org/10.1101/gr.159400.113

Luz, J. G., Hassig, C. A., Pickle, C., Godzik, A., Meyer, B. J., & Wilson, I. A. (2003). XOL-1, primary determinant of sexual fate in C. elegans, is a GHMP kinase family member and a structural prototype for a class of developmental regulators. *GENES & DEVELOPMENT*, *17*, 977–990. http://doi.org/10.1101/gad.1082303

Maddox, P. S., Portier, N., Desai, A., & Oegema, K. (2006). Molecular analysis of mitotic chromosome

condensation using a quantitative time-resolved fluorescence microscopy assay. *Proceedings of the National Academy of Sciences of the United States of America*, *103*(41), 15097–15102. http://doi.org/10.1073/pnas.0606993103

Maeshima, K., Iino, H., Hihara, S., Funakoshi, T., Watanabe, A., Nishimura, M., … Imamoto, N. (2010). Nuclear pore formation but not nuclear growth is governed by cyclin-dependent kinases (Cdks) during interphase. *Nature Structural & Molecular Biology*, *17*(9), 1065–1071. http://doi.org/10.1038/nsmb.1878

Maksimov, D. A., Laktionov, P. P., & Belyakin, S. N. (2016). Data analysis algorithm for DamID-seq profiling of chromatin proteins in Drosophila melanogaster. *Chromosome Research*, *24*(4), 481–494. http://doi.org/10.1007/s10577-016-9538-4

Mangone, M., Manoharan, A. P., Thierry-Mieg, D., Thierry-Mieg, J., Han, T., Mackowiak, S. D., … Kim, J. K. (2010). The Landscape of C. elegans 3'UTRs. *Science*, *329*(5990), 432–435. http://doi.org/10.1126/science.1191244

Margalit, A., Segura-Totten, M., Gruenbaum, Y., & Wilson, K. L. (2005). Barrier-to-autointegration factor is required to segregate and enclose chromosomes within the nuclear envelope and assemble the nuclear lamina. *Proceedings of the National Academy of Sciences*, *102*(9), 3290–3295.

Marques, A., & Pedrosa-Harand, A. (2016). Holocentromere identity: from the typical mitotic linear structure to the great plasticity of meiotic holocentromeres. *Chromosoma*, *125*(4), 669–681. http://doi.org/10.1007/s00412-016-0612-7

Marshall, O. J., & Brand, A. H. (2015). damidseq_pipeline: an automated pipeline for processing DamID sequencing datasets. *Bioinformatics*, 1–3. http://doi.org/10.1093/bioinformatics/btv386

Marshall, O. J., Southall, T. D., Cheetham, S. W., & Brand, A. H. (2016). Cell-type-specific profiling of protein-DNA interactions without cell isolation using targeted DamID with next-generation sequencing. *Nature Protocols*, *11*(9), 1586–1598. http://doi.org/10.1038/nprot.2016.084

Martin, M. (2011). Cutadapt removes adapter sequences from high-throughput sequencing reads. *EMBnet.journal*, *17*(1), 10. http://doi.org/10.14806/ej.17.1.200

Mattout, A., Pike, B. L., Towbin, B. D., Bank, E. M., Gonzalez-Sandoval, A., Stadler, M. B., … Gasser, S. M. (2011). Article An EDMD Mutation in C. elegans Lamin Blocks Muscle-Specific Gene Relocation and Compromises Muscle Integrity. *Current Biology*, *21*, 1603–1614. http://doi.org/10.1016/j.cub.2011.08.030

McCarter, J., Bartlett, B., Dang, T., & Schedl, T. (1997). Soma-germ cell interactions in Caenorhabditis elegans: multiple events of hermaphrodite germline development require the somatic sheath and spermathecal lineages. *Developmental Biology*, *181*(2), 121–143. http://doi.org/10.1006/dbio.1996.8429

McCarter, J., Bartlett, B., Dang, T., & Schedl, T. (1999). On the Control of Oocyte Meiotic Maturation and Ovulation in Caenorhabditis elegans. *Developmental Biology*, *205*, 111–128 . http://doi.org/10.1006/dbio.1998.9109

McNally, K., Berg, E., Cortes, D. B., Hernandez, V., Mains, P. E., & McNally, F. J. (2014). Katanin maintains meiotic metaphase chromosome alignment and spindle structure in vivo and has

multiple effects on microtubules in vitro. *Molecular Biology of the Cell*, *25*(7), 1037–1049. http://doi.org/10.1091/mbc.E13-12-0764

McNally, K. L., & McNally, F. J. (2005). Fertilization initiates the transition from anaphase I to metaphase II during female meiosis in C. elegans. *Developmental Biology*, *282*(1), 218–230. http://doi.org/10.1016/j.ydbio.2005.03.009

Meister, P., Towbin, B. D., Pike, B. L., Ponti, A., & Gasser, S. M. (2010). The spatial dynamics of tissue-specific promoters during C. elegans development. *Genes & Development*, *24*(8), 766–782. http://doi.org/10.1101/gad.559610

Melters, D. P., Paliulis, L. V., Korf, I. F., & Chan, S. W. L. (2012). Holocentric chromosomes: convergent evolution, meiotic adaptations, and genomic analysis. *Chromosome Research*, *20*(5), 579–593. http://doi.org/10.1007/s10577-012-9292-1

Mendjan, S., Taipale, M., Kind, J., Holz, H., Gebhardt, P., Schelder, M., … Akhtar, A. (2006). Nuclear Pore Components Are Involved in the Transcriptional Regulation of Dosage Compensation in Drosophila. *Molecular Cell*, *21*(6), 811–823. http://doi.org/10.1016/j.molcel.2006.02.007

Meyer, B. J. (2005). X-Chromosome dosage compensation. http://doi.org/10.1895/wormbook.1.8.1

Michaelis, C., Ciosk, R., & Nasmyth, K. (1997). Cohesins: chromosomal proteins that prevent premature separation of sister chromatids. *Cell*, *91*(1), 35–45. Retrieved from http://www.ncbi.nlm.nih.gov/pubmed/9335333

Miller, L. M., Plenefisch, J. D., Casson, L. R., & Meyer, B. J. (1988). xol-1: A Gene That Controls the Male Modes of Both Sex Determination and X Chromosome Dosage Compensation in C. elegans. *Cell*, *55*(0), 167–183.

Miller, M. A., Ruest, P. J., Kosinski, M., Hanks, S. K., & Greenstein, D. (2003). An Eph receptor sperm-sensing control mechanism for oocyte meiotic maturation in Caenorhabditis elegans. *Genes & Development*, *17*(2), 187–200. http://doi.org/10.1101/gad.1028303

Mimura, Y., Takagi, M., Clever, M., & Imamoto, N. (2016). ELYS regulates the localization of LBR by modulating its phosphorylation state. *Journal of Cell Science*, *129*(22), 4200–4212. http://doi.org/10.1242/jcs.190678

Monen, J., Maddox, P. S., Hyndman, F., Oegema, K., & Desai, A. (2005). Differential role of CENP-A in the segregation of holocentric C. elegans chromosomes during meiosis and mitosis. *Nature Cell Biology*, *7*(12), 1248–1255. http://doi.org/10.1038/ncb1331

Moore, L. L., & Roth, M. B. (2001). HCP-4, a CENP-C-like protein in Caenorhabditis elegans, is required for resolution of sister centromeres. *The Journal of Cell Biology*, *153*(6), 1199–1208. Retrieved from http://www.ncbi.nlm.nih.gov/pubmed/11402064

Morales-Martínez, A., Dobrzynska, A., & Askjaer, P. (2015). Inner nuclear membrane protein LEM-2 is required for correct nuclear separation and morphology in C. elegans. *Journal of Cell Science*, *128*(Journal of Cell Science), 1090–1096. http://doi.org/10.1242/jcs.164202

Morchoisne-Bolhy, S., Geoffroy, M.-C., Bouhlel, I. B., Alves, A., Audugé, N., Baudin, X., … Doye, V. (2015). Intranuclear dynamics of the Nup107-160 complex. *Molecular Biology of the Cell*, *26*(12), 2343–56. http://doi.org/10.1091/mbc.E15-02-0060

Mühlhäusser, P., & Kutay, U. (2007). An in vitro nuclear disassembly system reveals a role for the

RanGTPase system and microtubuledependent steps in nuclear envelope breakdown. *The Journal of Cell Biologuy* , *178*(4), 595–610.

Müller-Reichert, T., Greenan, G., O 'toole, E., & Srayko, M. (2010). The elegans of spindle assembly. *Cellullar and Molecular Life Sciences*, *67*(13), 2195–2213. http://doi.org/10.1007/s00018-010-0324-8

Murray, J. I., Boyle, T. J., Preston, E., Vafeados, D., Mericle, B., Weisdepp, P., … Waterston, R. H. (2012). Multidimensional regulation of gene expression in the C. elegans embryo. *Genome Research*, *22*(7), 1282–1294. http://doi.org/10.1101/gr.131920.111

Muscat, C. C., Torre-Santiago, K. M., Tran, M. V., Powers, J. A., & Wignall, S. M. (2015). Kinetochore-independent chromosome segregation driven by lateral microtubule bundles. *eLife*, *4*(MAY), 1–53. http://doi.org/10.7554/eLife.06462

Nusbaum, C., & Meyer, B. J. (1989). The Caenorhabditis elegans gene sdc-2 controls sex determination and dosage compensation in XX animals. *Genetics*, *122*(3), 579–593. Retrieved from http://www.ncbi.nlm.nih.gov/pubmed/2759421

Oegema, K., Desai, A., Rybina, S., Kirkham, M., & Hyman, A. A. (2001). Functional Analysis of Kinetochore Assembly in Caenorhabditis elegans. *The Journal of Cell Biology*, *153*(6), 1209–1226. Retrieved from http://www.jcb.org/cgi/content/full/153/6/1209

Oegema, K., & Hyman, A. A. (2006). Cell division. http://doi.org/10.1895/wormbook.1.72.1

Ohkura, H. (2016). Meiosis : An Overview of Key Differences from Mitosis, (Paris 6). http://doi.org/10.1101/cshperspect.a015859

Okita, K., Kiyonari, H., Nobuhisa, I., Kimura, N., Aizawa, S., & Taga, T. (2004). Targeted disruption of the mouse ELYS gene results in embryonic death at peri-implantation development. *Genes to Cells*, *9*(11), 1083–1091. http://doi.org/10.1111/j.1365-2443.2004.00791.x

Olmos, Y., Hodgson, L., Mantell, J., Verkade, P., & Carlton, J. G. (2015). ESCRT-III controls nuclear envelope reformation. *Nature*, *522*(7555), 236–239. http://doi.org/10.1038/nature14503

Orian, A., Steensel, B. Van, Delrow, J., Bussemaker, H. J., Li, L., Sawado, T., … Eisenman, R. N. (2003). Genomic binding by the. *Genes & Development*, 1101–1114. http://doi.org/10.1101/gad.1066903.ing

Ozlü, N., Srayko, M., Kinoshita, K., Habermann, B., O'toole, E. T., Müller-Reichert, T., … Desai, A. (2005). An essential function of the C. elegans ortholog of TPX2 is to localize activated aurora A kinase to mitotic spindles. *Developmental Cell*, *9*(2), 237–48. http://doi.org/10.1016/j.devcel.2005.07.002

Pascual-Garcia, P., & Capelson, M. (2014). Nuclear pores as versatile platforms for gene regulation. *Current Opinion in Genetics and Development*, *25*(1), 110–117. http://doi.org/10.1016/j.gde.2013.12.009

Pascual-Garcia, P., Debo, B., Aleman, J. R., Talamas, J. A., Lan, Y., Nguyen, N. H., … Capelson, M. (2017). Metazoan Nuclear Pores Provide a Scaffold for Poised Genes and Mediate Induced EnhancerPromoter Contacts. *Molecular Cell*, *66*(1), 63–76. http://doi.org/10.1016/j.molcel.2017.02.020

Pascual-Garcia, P., Jeong, J., & Capelson, M. (2014). Nucleoporin Nup98 Associates with Trx/MLL

and NSL Histone-Modifying Complexes and Regulates Hox Gene Expression. *Cell Reports*, *9*(2), 433–442. http://doi.org/10.1016/j.celrep.2014.09.002

Pasierbek, P., Födermayr, M., Jantsch, V., Jantsch, M., Schweizer, D., & Loidl, J. (2003). The Caenorhabditis elegans SCC-3 homologue is required for meiotic synapsis and for proper chromosome disjunction in mitosis and meiosis. *Experimental Cell Research*, *289*(2), 245–255. Retrieved from http://www.ncbi.nlm.nih.gov/pubmed/14499625

Peric-Hupkes, D., Meuleman, W., Pagie, L., Bruggeman, S. W. M., Solovei, I., Brugman, W., … van Steensel, B. (2010). Molecular Maps of the Reorganization of Genome-Nuclear Lamina Interactions during Differentiation. *Molecular Cell*, *38*(4), 603–613. http://doi.org/10.1016/j.molcel.2010.03.016

Peric-Hupkes, D., & van Steensel, B. (2010). Role of the Nuclear Lamina in Genome Organization and Gene Expression. *Cold Spring Harbor Symposia on Quantitative Biology*, *75*(0), 517–524. http://doi.org/10.1101/sqb.2010.75.014

Petronczki, M., Siomos, M. F., Nasmyth, K., Adams, R. ., Carmena, M., Earnshaw, W. ., … Kirschner, M. . (2003). Un ménage à quatre: the molecular biology of chromosome segregation in meiosis. *Cell*, *112*(4), 423–440. http://doi.org/10.1016/S0092-8674(03)00083-7

Pickersgill, H., Kalverda, B., de Wit, E., Talhout, W., Fornerod, M., & van Steensel, B. (2006). Characterization of the Drosophila melanogaster genome at the nuclear lamina. *Nature Genetics*, *38*(9), 1005–1014. http://doi.org/10.1038/ng1852

Pindyurin, A. V., Pagie, L., Kozhevnikova, E. N., van Arensbergen, J., & van Steensel, B. (2016). Inducible DamID systems for genomic mapping of chromatin proteins in *Drosophila*. *Nucleic Acids Research*, gkw176. http://doi.org/10.1093/nar/gkw176

Portier, N., Audhya, A., Maddox, P. S., Green, R. A., Dammermann, A., Desai, A., & Oegema, K. (2007). A Microtubule-Independent Role for Centrosomes and Aurora A in Nuclear Envelope Breakdown. *Developmental Cell*, *12*, 515–529. http://doi.org/10.1016/j.devcel.2007.01.019

Powers, J., Rose, D. J., Saunders, A., Dunkelbarger, S., Strome, S., & Saxton, W. M. (2004). Loss of KLP-19 polar ejection force causes misorientation and missegregation of holocentric chromosomes. *The Journal of Cell Biology*, *166*(7), 991–1001. http://doi.org/10.1083/jcb.200403036

Praitis, V. (2006). Creation of Transgenic Lines Using Microparticle Bombardment Methods. *Methods Mol Biol.*, *351*, 93–108. http://doi.org/10.1385/1-59745-151-7:93

Pruitt, K. D., Tatusova, T., & Maglott, D. R. (2005). NCBI Reference Sequence (RefSeq): a curated non-redundant sequence database of genomes, transcripts and proteins. *Nucleic Acids Research*, *33*(Database issue), D501–4. http://doi.org/10.1093/nar/gki025

Quinlan, A. R., & Hall, I. M. (2010). BEDTools: a flexible suite of utilities for comparing genomic features. *Bioinformatics*, *26*(6), 841–842. http://doi.org/10.1093/bioinformatics/btq033

Rabut, G., Doye, V., & Ellenberg, J. (2004). Mapping the dynamic organization of the nuclear pore complex inside single living cells. *NATURE CELL BIOLOGY*, *6*(11). http://doi.org/10.1038/ncb1184

Rahman, M. M., Munzig, M., Kaneshiro, K., Lee, B., Strome, S., Müller-Reichert, T., & Cohen-Fix, O.

(2015). Caenorhabditis elegans polo-like kinase PLK-1 is required for merging parental genomes into a single nucleus. *Molecular Biology of the Cell*, *26*(25), 4718–4735. http://doi.org/10.1091/mbc.E15-04-0244

Raices, M., & D'Angelo, M. a. (2012). Nuclear pore complex composition: a new regulator of tissue-specific and developmental functions. *Nature Reviews Molecular Cell Biology*, *13*(11), 687–699. http://doi.org/10.1038/nrm3461

Rasala, B. A., Orjalo, A. V, Shen, Z., Briggs, S., & Forbes, D. J. (2006). ELYS is a dual nucleoporin¯kinetochore protein required for nuclear pore assembly and proper cell division. *Sciences-New York*, *103*(47), 17801–17806.

Rasala, B. A., Ramos, C., Harel, A., & Forbes, D. J. (2008). Capture of AT-rich Chromatin by ELYS Recruits POM121 and NDC1 to Initiate Nuclear Pore Assembly. *Molecular Biology of the Cell*, *19*(9), 3982–3996. http://doi.org/10.1091/mbc.E08-01-0012

Rashid, N. U., Giresi, P. G., Ibrahim, J. G., Sun, W., & Lieb, J. D. (2011). ZINBA integrates local covariates with DNA-seq data to identify broad and narrow regions of enrichment, even within amplified genomic regions. *Genome Biology*, *12*(7), R67. http://doi.org/10.1186/gb-2011-12-7-r67

Rhind, N. R., Miller, L. M., Kopczynski, J. B., & Meyer, B. J. (1995). xol-1 acts as an early switch in the C. elegans male/hermaphrodite decision. *Cell*, *80*(1), 71–82. Retrieved from http://www.ncbi.nlm.nih.gov/pubmed/7813020

Riddle, D. L., Blumenthal, T., Meyer, B. J., & Priess, J. R. (1997). *Fertilization - C. elegans II.* (D. L. Riddle, T. Blumenthal, B. J. Meyer, & J. R. Priess, Eds.) (2nd ed.). Cold Spring Harbor (NY): Cold Spring Harbor Laboratory Press.

Robbins, J., Dilworth, S. M., Laskey, R. A., & Dingwall, C. (1991). Two interdependent basic domains in nucleoplasmin nuclear targeting sequence: identification of a class of bipartite nuclear targeting sequence. *Cell*, *64*(3), 615–623. Retrieved from http://www.ncbi.nlm.nih.gov/pubmed/1991323

Robertson, S., Lin, R., Robertson, S., Lin, R., & Lin, R. (2013). The Oocyte-to-Embryo Transition. In T. Schedl (Ed.), *Germ Cell Development in C. elegans,, Advances in Experimental Medicine and Biology* (757th ed., pp. 351–372). New York: Springer. http://doi.org/10.1007/978-1-4614-4015-4_12

Ródenas, E., González-Aguilera, C., Ayuso, C., & Askjaer, P. (2012). Dissection of the NUP107 nuclear pore subcomplex reveals a novel interaction with spindle assembly checkpoint protein MAD1 in Caenorhabditis elegans. *Molecular Biology of the Cell*, *23*(5), 930–44. http://doi.org/10.1091/mbc.E11-11-0927

Ródenas, E., Klerkx, E. P., Ayuso, C., Audhya, A., & Askjaer, P. (2009). Early embryonic requirement for nucleoporin Nup35/NPP-19 in nuclear assembly. *Developmental Biology*, *327*(2), 399–409. http://doi.org/10.1016/j.ydbio.2008.12.024

Rogers, E., Bishop, J. D., Waddle, J. A., Schumacher, J. M., & Lin, R. (2002). The aurora kinase AIR-2 functions in the release of chromosome cohesion in *Caenorhabditis elegans* meiosis. *The Journal of Cell Biology*, *157*(2), 219–229. http://doi.org/10.1083/jcb.200110045

Rohner, S., Kalck, V., Wang, X., Ikegami, K., Lieb, J. D., Gasser, S. M., & Meister, P. (2013). Promoter- and RNA polymerase II–dependent *hsp-16* gene association with nuclear pores in *Caenorhabditis elegans*. *The Journal of Cell Biology*, *200*(5), 589–604. http://doi.org/10.1083/jcb.201207024

Rose, L., & Gönczy, P. (2014). Polarity establishment, asymmetric division and segregation of fate determinants in early C. elegans embryos. http://doi.org/10.1895/wormbook.1.30.2

Rotem, A., Gruber, R., Shorer, H., Shaulov, L., Klein, E., & Harel, A. (2009). Importin beta regulates the seeding of chromatin with initiation sites for nuclear pore assembly. *Molecular Biology of the Cell*, *20*(18), 4031–4042. http://doi.org/10.1091/mbc.E09-02-0150

Schellhaus, A. K., De Magistris, P., & Antonin, W. (2015). Nuclear Reformation at the End of Mitosis. *Journal of Molecular Biology*. http://doi.org/10.1016/j.jmb.2015.09.016

Schirmer, E. C., Florens, L., Guan, T., Yates, J. R., & Gerace, L. (2003). Nuclear membrane proteins with potential disease links found by subtractive proteomics. *Science (New York, N.Y.)*, *301*(5638), 1380–1382. http://doi.org/10.1126/science.1088176

Schneider, S. Q., & Bowerman, B. (2003). Cell polarity and the cytoskeleton in the Caenorhabditis elegans zygote. *Annu. Rev. Genet*, *37*, 221–249. http://doi.org/10.1146/annurev.genet.37.110801.142443

Schooley, A., Vollmer, B., & Antonin, W. (2012). Building a nuclear envelope at the end of mitosis: Coordinating membrane reorganization, nuclear pore complex assembly, and chromatin de-condensation. *Chromosoma*, *121*(6), 539–554. http://doi.org/10.1007/s00412-012-0388-3

Schuh, M., & Ellenberg, J. (2007). Self-Organization of MTOCs Replaces Centrosome Function during Acentrosomal Spindle Assembly in Live Mouse Oocytes. *Cell*, *130*(3), 484–498. http://doi.org/10.1016/j.cell.2007.06.025

Schumacher, J. M., Ashcroft, N., Donovan, P. J., & Golden, A. (1998). A highly conserved centrosomal kinase, AIR-1, is required for accurate cell cycle progression and segregation of developmental factors in Caenorhabditis elegans embryos. *Development* , *125*, 4391–4402 .

Schumacher, J. M., Golden, A., & Donovan, P. J. (1998). AIR-2: An Aurora/Ipl1-related Protein Kinase Associated with Chromosomes and Midbody Microtubules Is Required for Polar Body Extrusion and Cytokinesis in Caenorhabditis elegans Embryos. *The Journal of Cell Biology*, *143*(6), 1635–1646. Retrieved from http://www.jcb.org

Severson, A. F., von Dassow, G., & Bowerman, B. (2016). *Oocyte Meiotic Spindle Assembly and Function*. *Current Topics in Developmental Biology* (1st ed., Vol. 116). Elsevier Inc. http://doi.org/10.1016/bs.ctdb.2015.11.031

Sha, K., Gu, S. G., Pantalena-Filho, L. C., Goh, A., Fleenor, J., Blanchard, D., … Fire, A. (2010a). Distributed probing of chromatin structure in vivo reveals pervasive chromatin accessibility for expressed and non-expressed genes during tissue differentiation in C. elegans. *BMC Genomics*, *11*(465). http://doi.org/10.1186/1471-2164-11-465

Sha, K., Gu, S. G., Pantalena-Filho, L. C., Goh, A., Fleenor, J., Blanchard, D., … Fire, A. (2010b). Distributed probing of chromatin structure in vivo reveals pervasive chromatin accessibility for expressed and non-expressed genes during tissue differentiation in C. elegans. *BMC Genomics*,

11, 465. http://doi.org/10.1186/1471-2164-11-465

Sharma, R., Dominic, R., & Meister, P. (2016). Tools for DNA adenine methyltransferase identification analysis of nuclear organization during C. elegans development. *Genesis*, (092403), 1–55. http://doi.org/10.1002/dvg.22925

Sharma, R., Jost, D., Kind, J., Gómez-Saldivar, G., Van Steensel, B., Askjaer, P., … Meister, P. (2014). Differential spatial and structural organization of the X chromosome underlies dosage compensation in C. elegans. *Genes & Development*, *28*, 25–91–2596. http://doi.org/10.1101/gad.248864.114

Sharma, R., & Meister, P. (2013). Nuclear organization in the nematode C. elegans. *Current Opinion in Cell Biology*, *25*(3), 395–402. http://doi.org/10.1016/j.ceb.2013.02.002

Sharma, R., & Meister, P. (2015). Linking dosage compensation and X chromosome nuclear organization in C. elegans. *Nucleus*, *6*(4), 266–272. http://doi.org/10.1080/19491034.2015.1059546

Shin, H., Liu, T., Manrai, A. K., & Liu, X. S. (2009). CEAS: cis-regulatory element annotation system. *Bioinformatics*, *25*(19), 2605–2606. http://doi.org/10.1093/bioinformatics/btp479

Shin, H. Y., & Reich, N. C. (2013). Dynamic trafficking of STAT5 depends on an unconventional nuclear localization signal. *Journal of Cell Science*, *126*(15), 3333–3343. http://doi.org/10.1242/jcs.123042

Shulga, N., Mosammaparast, N., Wozniak, R., & Goldfarb, D. S. (2000). Yeast nucleoporins involved in passive nuclear envelope permeability. *The Journal of Cell Biology*, *149*(5), 1027–1038. Retrieved from http://www.ncbi.nlm.nih.gov/pubmed/10831607

Snyder, M. J., Lau, A. C., Brouhard, E. A., Davis, M. B., Jiang, J., Sifuentes, M. H., & Csankovszki, G. (2016). Anchoring of Heterochromatin to the Nuclear Lamina Reinforces Dosage Compensation-Mediated Gene Repression. *PLOS Genetics*, *12*(9), e1006341. http://doi.org/10.1371/journal.pgen.1006341

Song, J. S., Evan Johnson, W., Zhu, X., Zhang, X., Li, W., Manrai, A. K., … Shirley Liu, X. (2007). Model-based analysis of two-color arrays (MA2C), *8*(8), R178. http://doi.org/10.1186/gb-2007-8-8-r178

Song, Q., & Smith, A. D. (2011). Identifying dispersed epigenomic domains from ChIP-Seq data. *Bioinformatics*, *27*(6), 870–871. http://doi.org/10.1093/bioinformatics/btr030

Song, S., Cooperman, J., Letting, D. L., Blobel, G. A., & Choi, J. K. (2004). Identification of cyclin D3 as a direct target of E2A using DamID. *Mol Cell Biol*, *24*(19), 8790–8802. http://doi.org/10.1128/MCB.24.19.8790-8802.2004

Sönnichsen, B., Koski, L. B., Walsh, A., Marschall, P., Neumann, B., Brehm, M., … Echeverri, C. J. (2005). Full-genome RNAi profiling of early embryogenesis in Caenorhabditis elegans. *Nature*, *434*(7032), 462–469. http://doi.org/10.1038/nature03353

Southall, T. D., & Brand, A. H. (2007). Chromatin profiling in model organisms. *Briefings in Functional Genomics and Proteomics*, *6*(2), 133–140. http://doi.org/10.1093/bfgp/elm013

Southall, T. D., Gold, K. S., Egger, B., Davidson, C. M., Caygill, E. E., Marshall, O. J., & Brand, A. H. (2013). Developmental Cell Resource Cell-Type-Specific Profiling of Gene Expression and

Chromatin Binding without Cell Isolation: Assaying RNA Pol II Occupancy in Neural Stem Cells. *Developmental Cell*, *26*(1), 101–112. http://doi.org/10.1016/j.devcel.2013.05.020

Srayko, M., Buster, D. W., Bazirgan, O. A., McNally, F. J., & Mains, P. E. (2000). MEI-1/MEI-2 katanin-like microtubule severing activity is required for Caenorhabditis elegans meiosis. *Genes & Development*, *14*(9), 1072–1084. Retrieved from http://www.ncbi.nlm.nih.gov/pubmed/10809666

Srayko, M., O'toole, E. T., Hyman, A. A., Müller-Reichert, T., McNally, F. J., Vale, R. D., … McIntosh, J. R. (2006). Katanin disrupts the microtubule lattice and increases polymer number in C. elegans meiosis. *Current Biology : CB*, *16*(19), 1944–1949. http://doi.org/10.1016/j.cub.2006.08.029

Stavru, F., Hülsmann, B. B., Spang, A., Hartmann, E., Cordes, V. C., & Görlich, D. (2006). NDC1: a crucial membrane-integral nucleoporin of metazoan nuclear pore complexes. *The Journal of Cell Biology*, *173*(4), 509–519. http://doi.org/10.1083/jcb.200601001

Steglich, B., Filion, G., van Steensel, B., & Ekwall, K. (2012). The inner nuclear membrane proteins Man1 and Ima1 link to two different types of chromatin at the nuclear periphery in S. pombe. *Nucleus*, *3*(1), 77–87. http://doi.org/10.4161/nucl.18825

Steiner, F. A., & Henikoff, S. (2014). Holocentromeres are dispersed point centromeres localized at transcription factor hotspots. *eLife*, *2014*(3), 1–22. http://doi.org/10.7554/eLife.02025

Stiernagle, T. (2006). Maintenance of C. elegans. http://doi.org/10.1895/wormbook.1.101.1

Strambio-De-Castillia, C., Niepel, M., & Rout, M. P. (2010). The nuclear pore complex: bridging nuclear transport and gene regulation. *Nat Rev Mol Cell Biol*, *11*(7), 490–501. http://doi.org/nrm2928 [pii]\n10.1038/nrm2928

Strawn, L. A., Shen, T., Shulga, N., Goldfarb, D. S., & Wente, S. R. (2004). Minimal nuclear pore complexes define FG repeat domains essential for transport. *Nature Cell Biology*, *6*(3), 197–206. http://doi.org/10.1038/ncb1097

Sulston, J., & Horvitz, H. (1977). Post-embryonic cell lineages of the nematode, Caenorhabditis elegans. *Developmental Biology*, *56*(1), 110–156. Retrieved from http://www.ncbi.nlm.nih.gov/pubmed/838129

Sulston, J., Schierenberg, E., White, J., & Thomson, J. (1983). The embryonic cell lineage of the nematode Caenorhabditis elegans. *Developmental Biology*, *100*(1), 64–119. Retrieved from http://www.ncbi.nlm.nih.gov/pubmed/6684600

Tavernier, N., Labbé, J. C., & Pintard, L. (2015). Cell cycle timing regulation during asynchronous divisions of the early C. elegans embryo. *Experimental Cell Research*, *337*(2), 243–248. http://doi.org/10.1016/j.yexcr.2015.07.022

Terry, L. J., Shows, E. B., & Wente, S. R. (2007). Crossing the Nuclear Envelope: Hierarchical Regulation of Nucleocytoplasmic Transport. *Science*, *318*(5855), 1412–1416. http://doi.org/10.1126/science.1142204

Tessarz, P., & Kouzarides, T. (2014). Histone core modifications regulating nucleosome structure and dynamics. *Nature Reviews Molecular Cell Biology*, *15*(11), 703–708. http://doi.org/10.1038/nrm3890

Thorvaldsdottir, H., Robinson, J. T., & Mesirov, J. P. (2013). Integrative Genomics Viewer (IGV): high-performance genomics data visualization and exploration. *Briefings in Bioinformatics*, *14*(2), 178–192. http://doi.org/10.1093/bib/bbs017

Towbin, B. D., González-Aguilera, C., Sack, R., Gaidatzis, D., Kalck, V., Meister, P., … Gasser, S. M. (2012). Step-wise methylation of histone H3K9 positions heterochromatin at the nuclear periphery. *Cell*, *150*(5), 934–947. http://doi.org/10.1016/j.cell.2012.06.051

Uhlmann, F., Lottspeich, F., & Nasmyth, K. (1999). Sister-chromatid separation at anaphase onset is promoted by cleavage of the cohesin subunit Scc1. *Nature*, *400*(6739), 37–42. http://doi.org/10.1038/21831

Urig, S., Gowher, H., Hermann, A., Beck, C., Fatemi, M., Humeny, A., & Jeltsch, A. (2002). The Escherichia coli Dam DNA Methyltransferase Modifies DNA in a Highly Processive Reaction. *Journal of Molecular Biology*, *319*(5), 1085–1096. http://doi.org/10.1016/S0022-2836(02)00371-6

Van Steensel, B., & Henikoff, S. (2000). Identification of in vivo DNA targets of chromatin proteins using tethered dam methyltransferase. *Nature Biotechnology*, *18*(4), 424–428. http://doi.org/10.1038/74487

Vaquerizas, J. M., Suyama, R., Kind, J., Miura, K., Luscombe, N. M., Akhtar, A., … Kunzelmann, K. (2010). Nuclear Pore Proteins Nup153 and Megator Define Transcriptionally Active Regions in the Drosophila Genome. *PLoS Genetics*, *6*(2), e1000846. http://doi.org/10.1371/journal.pgen.1000846

Vastenhouw, N. L., Zhang, Y., Woods, I. G., Imam, F., Regev, A., Liu, X. S., … Schier, A. F. (2010). Chromatin signature of embryonic pluripotency is established during genome activation. *Nature*, *464*(7290), 922–926. http://doi.org/10.1038/nature08866

Vogel, M. J., Peric-Hupkes, D., & van Steensel, B. (2007). Detection of in vivo protein-DNA interactions using DamID in mammalian cells. *Nature Protocols*, *2*(6), 1467–78. http://doi.org/10.1038/nprot.2007.148

Vollmer, B., Lorenz, M., Moreno-André, D., Flö, M., Leptihn, S., Correspondence, W. A., … Antonin, W. (2015). Nup153 Recruits the Nup107-160 Complex to the Inner Nuclear Membrane for Interphasic Nuclear Pore Complex Assembly. *Developmental Cell*, *33*, 717–728. http://doi.org/10.1016/j.devcel.2015.04.027

Wente, S. R., & Rout, M. P. (2010). The nuclear pore complex and nuclear transport. *Cold Spring Harbor Perspectives in Biology*, *2*(10), a000562. http://doi.org/10.1101/cshperspect.a000562

Wheeler, B. S., Anderson, E., Frøkjær-Jensen, C., Bian, Q., Jorgensen, E., & Meyer, B. J. (2016). Chromosome-wide mechanisms to decouple gene expression from gene dose during sex-chromosome evolution. *eLife*, *5*, e17365. http://doi.org/10.7554/eLife.17365

Woolcock, K. J., Gaidatzis, D., Punga, T., & Bühler, M. (2011). Dicer associates with chromatin to repress genome activity in Schizosaccharomyces pombe. *Nature Structural & Molecular Biology*, *18*(1), 94–99. http://doi.org/10.1038/nsmb.1935

Xu, F., Zhang, K., & Grunstein, M. (2005). Acetylation in Histone H3 Globular Domain Regulates Gene Expression in Yeast. *Cell*, *121*(3), 375–385. http://doi.org/10.1016/j.cell.2005.03.011

Yamamoto, I., Kosinski, M. E., & Greenstein, D. (2006). Start me up: cell signaling and the journey from oocyte to embryo in C. elegans. *Developmental Dynamics*, *235*(3), 571–585. http://doi.org/10.1002/dvdy.20662

Yang, H., Mains, P. E., & McNally, F. J. (2005). Kinesin-1 mediates translocation of the meiotic spindle to the oocyte cortex through KCA-1, a novel cargo adapter. *The Journal of Cell Biology*, *169*(3), 447–457. http://doi.org/10.1083/jcb.200411132

Yang, H., McNally, K., & McNally, F. J. (2003). MEI-1/katanin is required for translocation of the meiosis I spindle to the oocyte cortex in C. elegans☆. *Developmental Biology*, *260*(1), 245–259. http://doi.org/10.1016/S0012-1606(03)00216-1

Yang, L., Guan, T., & Gerace, L. (1997). Integral membrane proteins of the nuclear envelope are dispersed throughout the endoplasmic reticulum during mitosis. *The Journal of Cell Biology*, *137*(6), 1199–1210. Retrieved from http://www.ncbi.nlm.nih.gov/pubmed/9182656

Yokoyama, H., Koch, B., Walczak, R., Ciray-Duygu, F., González-Sánchez, J. C., Devos, D. P., … Gruss, O. J. (2014). The nucleoporin MEL-28 promotes RanGTP-dependent γ-tubulin recruitment and microtubule nucleation in mitotic spindle formation. *Nature Communications*, *5*, 3270. http://doi.org/10.1038/ncomms4270

Yonker, S. A., & Meyer, B. J. (2003). Recruitment of C. elegans dosage compensation proteins for gene-specific versus chromosome-wide repression. *Development (Cambridge, England)*, *130*(26), 6519–6532. http://doi.org/10.1242/dev.00886

Zang, C., Schones, D. E., Zeng, C., Cui, K., Zhao, K., & Peng, W. (2009). A clustering approach for identification of enriched domains from histone modification ChIP-Seq data. *Bioinformatics*, *25*(15), 1952–1958. http://doi.org/10.1093/bioinformatics/btp340

Zarkower, D. (2006). Somatic sex determination. http://doi.org/10.1895/wormbook.1.84.1

Zhang, Y., Liu, T., Meyer, C. A., Eeckhoute, J., Johnson, D. S., Bernstein, B. E., … Liu, X. S. (2008). Model-based analysis of ChIP-Seq (MACS). *Genome Biology*, *9*(9), R137. http://doi.org/10.1186/gb-2008-9-9-r137

Zhou, H.-L., Luo, G., Wise, J. A., & Lou, H. (2014). Regulation of alternative splicing by local histone modifications: potential roles for RNA-guided mechanisms. *Nucleic Acids Research*, *42*(2), 701–713. http://doi.org/10.1093/nar/gkt875

Zierhut, C., Jenness, C., Kimura, H., & Funabiki, H. (2014a). Nucleosomal regulation of chromatin composition and nuclear assembly revealed by histone depletion. *Nature Structural & Molecular Biology*, *21*(7), 617–25. http://doi.org/10.1038/nsmb.2845

Zuleger, N., Robson, M. I., & Schirmer, E. C. (2011). The nuclear envelope as a chromatin organizer. *Nucleus*, *2*(5), 339–349. http://doi.org/10.4161/nucl.2.5.17846

Appendix I

Genes & Development

Research paper

Differential spatial and structural organization of the X chromosome underlies dosage compensation in *Caenorhabditis elegans*

Rahul Sharma, Daniel Jost, Jop Kind, Georgina Gómez-Saldivar, Bas van Stenseel, Peter Askjaer, Cédric Vaillant and Peter Meister

Genes Dev. 2014 Dec 1;28(23):2591-6. DOI: 10.1101/gad.248864.114.

PMID: 25452271.

Differential spatial and structural organization of the X chromosome underlies dosage compensation in *C. elegans*

Rahul Sharma,[1,2] Daniel Jost,[3] Jop Kind,[4] Georgina Gómez-Saldivar,[5] Bas van Steensel,[4] Peter Askjaer,[5,6,7] Cédric Vaillant,[3] and Peter Meister[1]

[1]Cell Fate and Nuclear Organization, Institute of Cell Biology, University of Bern, 3012 Bern, Switzerland; [2]Graduate School for Cellular and Biomedical Sciences, University of Bern, 3012 Bern, Switzerland; [3]Laboratoire de Physique, Ecole Normale Supérieure de Lyon, UMR 5672, Centre National de la Recherche Scientifique (CNRS), 69007 Lyon, France; [4]Division of Gene Regulation, The Netherlands Cancer Institute, 1006 Amsterdam, The Netherlands; [5]Spanish National Research Council (CSIC), [6]The Junta of Andalusia (JA), [7]Universidad Pablo de Olavide, Andalusian Center for Developmental Biology (CABD), 41013 Sevilla, Spain

The adjustment of X-linked gene expression to the X chromosome copy number (dosage compensation [DC]) has been widely studied as a model of chromosome-wide gene regulation. In *Caenorhabditis elegans*, DC is achieved by twofold down-regulation of gene expression from both Xs in hermaphrodites. We show that in males, the single X chromosome interacts with nuclear pore proteins, while in hermaphrodites, the DC complex (DCC) impairs this interaction and alters X localization. Our results put forward a structural model of DC in which X-specific sequences locate the X chromosome in transcriptionally active domains in males, while the DCC prevents this in hermaphrodites.

Supplemental material is available for this article.

Received July 18, 2014; revised version accepted October 20, 2014.

Throughout the animal kingdom, varied strategies have evolved to equalize expression of the X chromosome genes between sexes with different X to autosomes ratios, a process called dosage compensation (DC) (for review, see Ferrari et al. 2014). In *Caenorhabditis elegans*, genetic screens and RNA quantifications showed that DC occurs in hermaphrodites by twofold down-regulation of X-linked transcripts from both Xs (for review, see Strome et al. 2014). A number of mutants were isolated in which overexpression of X-linked genes led to hermaphrodite-specific defects (*dpy* genes) or sex determination and DC deficiency (*sdc* genes). Remarkably, all proteins of the sex-specific Dpy and Sdc classes interact and form a single complex, the DC complex (DCC). Structurally, the DCC is similar to condensin I and loaded on the X chromosome at *rex* (recruitment element on X) sites characterized by a 12-base-pair (bp) *MEX* (motif enriched on X) consensus sequence (Ercan et al. 2009; Jans et al. 2009). Thirty-eight *rex* sites have been experimentally demonstrated, and sequence analysis suggests the presence of 100–300 sites on the X chromosome (Jans et al. 2009). This estimation is due to the fact that the DCC moves and spreads along the X chromosome from its nucleation sites (Csankovszki et al. 2004). The DCC accumulates at promoters upstream of transcription start sites; however, the relationship between DCC accumulation and transcriptional regulation remains disputed (Ercan et al. 2009; Jans et al. 2009). Genome-wide run-on experiments have shown that the DCC reduces transcription from the X chromosome, although RNA polymerase chromatin immunoprecipitation (ChIP) does not show a significant reduction compared with autosomes (Kruesi et al. 2013). How DCC loading regulates RNA polymerase II (Pol II) function still remains unknown. Compared with autosomes, compensated X chromatin is depleted for the histone variant HTZ-1 and H4K16 acetylation, likely a consequence of lower transcription, and carries high H4K20 monomethylation (H4K20me1), spreading with the DCC (Whittle et al. 2008; Petty et al. 2011; Vielle et al. 2012; Wells et al. 2012). Inside the nuclear space, the compensated X displays a peculiar tridimensional conformation: While all autosomes have high interactions of both arms with the nuclear lamina, the X chromosome is only loosely interacting with the periphery at telomeres (Fig. 1D; Ikegami et al. 2010; Towbin et al. 2012). In males, no specific chromosome organization or X-specific chromatin marks have been described. Given the similarity between the DCC and condensins, the presence of a specific higher-order structure of the X chromosomes facilitated by the DCC has been suggested as a model for years but never tested directly (Ferrari et al. 2014).

Results and Discussion

We asked whether DC has an effect on X chromosome tridimensional organization by carrying out fluorescence in situ hybridization (FISH) for a *rex* site located in the center of the *chr X* (*rex-33*) (Fig. 1B). Radial distribution of this locus was scored in 40- to 150-cell stage male and hermaphrodite embryos (after DC establishment) (Chuang et al. 1994; Dawes et al. 1999) using the three-zone scoring assay (Fig. 1A; representative image of FISH data in Supplemental Fig. S1,; Askjaer et al. 2014). For each FISH signal, in the *Z*-plane in which the spot is the brightest, the nuclear section is divided into three zones of equal surface. The spot is then binned into one of these three zones. In hermaphrodite embryos, *rex-33* is randomly localized, although the probe overlaps with a site previously shown as highly enriched for nuclear pore proteins (nucleoporins) (Fig. 1B; Ikegami and Lieb 2013). As the subnuclear localization of this site was not tested previously, our data suggest that pore–chromatin interaction occurs in the nuclear lumen or that this interaction is present in a minor

[*Keywords*: dosage compensation; nuclear organization; *C. elegans*; nuclear pores]
Corresponding author: peter.meister@izb.unibe.ch
Article is online at http://www.genesdev.org/cgi/doi/10.1101/gad.248864.114.

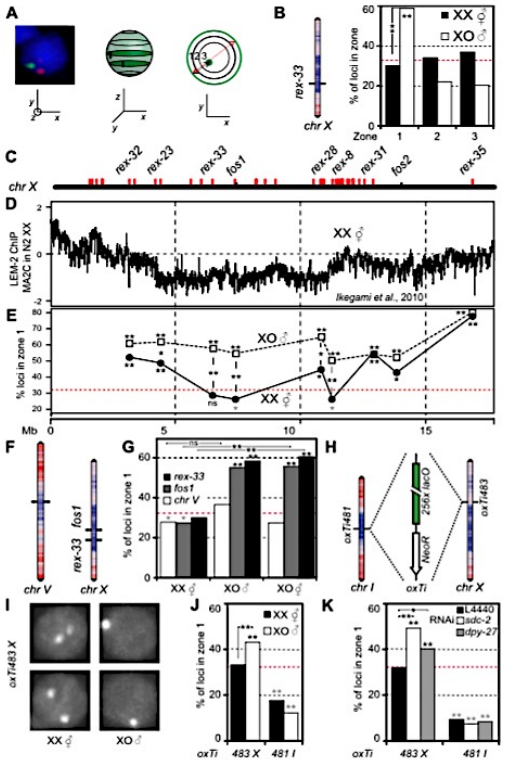

Figure 1. The X chromosome is peripherally located in males, and DC impairs this localization. (*A*) Three-zone assay to quantify the radial position of a locus inside the nucleus. (*B*) Location of *rex-33* on *chr X* with LEM-2 ChIP–chip profile overlay ([red] high LEM-2 interaction; [blue] low LEM-2 interaction) and three-zone scoring for the same locus in hermaphrodites and males. Statistical data for all scorings in Supplemental Table 1: (*) $P < 0.05$; (**) $P < 0.01$; (asterisks on the bars) *P*-value against random in χ^2 test; (gray) significantly internal; (black) significantly peripheral; (asterisks between bars) *P*-value between samples in Fisher exact test. (*C*) Localization of analyzed *rex* and non-*rex* (*fos*) sites along *chr X*. (*D*) LEM-2 ChIP–chip profile along the hermaphrodite X chromosome (data from Ikegami et al. 2010). (*E*) Zone 1 scorings for sites in *C* in hermaphrodite and male. (Red dashed line) Random distribution (33%). (*F*) Location of scored loci on *chr V* and *chr X*, with overlay of the LEM-2 ChIP–chip profile. (*G*) Zone 1 scorings for the sites in *F* in XO males and XX and XO hermaphrodites. (*H*) Location of *lacO* repeats insertions on *chr I* and *chr X*, with overlay of the LEM-2 ChIP–chip profile. (*I*) Representative images of nuclei in male and hermaphrodite embryos for the *chr X* insertion. (*J*) Zone 1 scorings for the insertions in *H* in XX hermaphrodites and XO males. (*K*) Zone 1 scorings for the insertions in *H* in XX hermaphrodites grown on control (L4440), *sdc-2*, and *dpy-27* RNAi.

fraction of cells. In males, *rex-33* was preferentially located in zone 1 (58% of spots) (Fig. 1B). Scoring of eight additional loci distributed along the X chromosome (Fig. 1C,E) showed that in hermaphrodites, our measurements largely agree with LEM-2 ChIP data performed in hermaphrodites: Loci with high LEM-2 enrichment are preferentially located in zone 1 (Fig. 1E), while regions with low LEM-2 enrichment show random distribution inside the nucleus. In male embryos, all sites show highly significant enrichment in the peripheral-most zone (at least 50%) (Fig. 1E). The difference between males and hermaphrodites is particularly visible in the center of the chromosome, as telomeres appear to be anchored at the nuclear envelope similarly in both sexes (Ferreira et al. 2013). Moreover, peripheral positioning does not appear to be *rex* site-specific, as both *rex* and non-*rex* loci are peripherally located (Fig. 1E). It is, however, specific to the X chromosome, as an autosomal site located in the middle of *chr V* is similarly positioned in males and hermaphrodites (Fig. 1F,G). Our data therefore indicate a sex-specific X chromosome localization.

To ensure that the observed differences in X chromosome organization are due to DC and not an outcome of differential gene expression between sexes, we scored the X chromosome position in noncompensated XO hermaphrodite embryos (TY2205) (Csankovszki et al. 2009). These animals have one X chromosome, express a hermaphrodite transcriptional program, and do not initiate DC. Two sites located in the middle of *chr X* were located similarly in males, while the position of the center region of *chr V* was internal or random for all genotypes (Fig. 1F,G). Differences in X chromosome organization are therefore not a consequence of global gene expression differences between sexes but rather reflect DC acting on X. This implies that the "default" localization of the noncompensated X chromosome is at the nuclear periphery as in males and that this localization is impaired by the loading of the DCC on X chromosomes in hermaphrodites, leading to an internal location.

A consequence of the DC-positioning hypothesis above is that down-regulation of the DCC in hermaphrodites should lead to perinuclear localization of the X chromosome. As the localization in XO hermaphrodites suggests, mutation of components of the DCC (*sdc-3*) leads to relocation of the X chromosome to the periphery (Fig. 1G). To test this hypothesis more directly, we used *lacO* repeats inserted in the central region of *chr X* and a control insertion in the center of *chr I*. Expression in *trans* of GFP-lacI leads to the formation of a visible spot of which radial position inside the nucleus can be scored (Fig. 1H,I; Askjaer et al. 2014). Upon DCC knockdown, transcription in the vicinity of these *lacO* insertions is up-regulated for the X chromosome locus and stable around the *chr I* insertion site (Supplemental Fig. S2; Kruesi et al. 2013). As in our FISH analysis, the X-linked locus is randomly positioned in hermaphrodites and significantly enriched at the nuclear periphery in males. In contrast, the locus on *chr I* is internally positioned in both sexes (Fig. 1J). We depleted either SDC-2 or DPY-27, both subunits of the DCC, using RNAi. Phenotypically, *sdc-2(RNAi)* has a strong effect, with most animals showing a Dumpy phenotype, while *dpy-27(RNAi)* is less penetrant (data not shown). Upon down-regulation of *sdc-2* or *dpy-27*, the *chr X lacO* insertion showed a 16% or 10% increase in the outermost zone 1 compared with control RNAi, respectively, while the same treatment did not change the position of the autosomal site (Fig. 1K). This implies that the DCC prevents the association of the *chr X* with the nuclear periphery.

Our results show that in rapidly cycling male embryonic blastomeres, the X chromosome is localized at the nuclear periphery. Such a conformation strongly suggests the existence of anchoring sequences on the X chromosome and anchor sites at the nuclear rim. A striking feature of the X chromosome is its enrichment for the *MEX* motif, a motif recognized by the DCC for loading (McDonel et al. 2006; Jans et al. 2009). We asked whether a single *MEX* motif would be able to direct an autosomal locus to the nuclear periphery in males specifically by creating strains with an ectopic autosomal insertion of a *MEX* motif (*rex-1*•33) (Fig. 2A; McDonel et al. 2006).

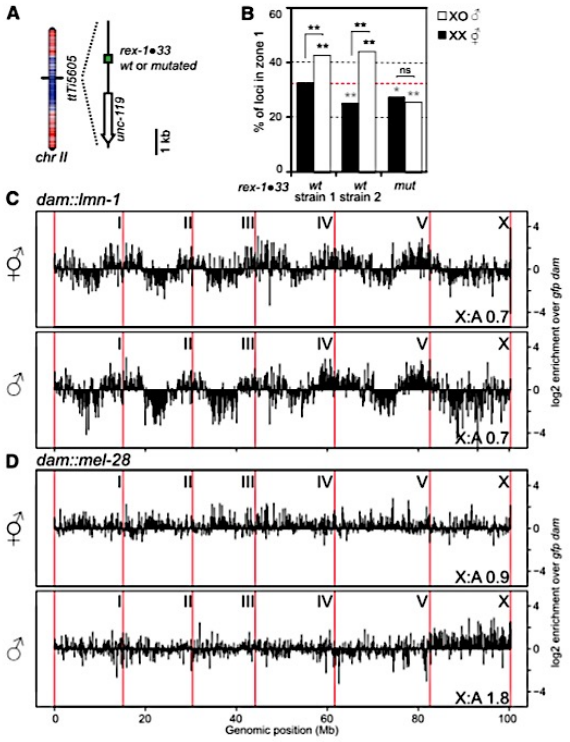

Figure 2. An ectopic *MEX* motif targets an autosomal locus to the nuclear periphery, and the male X chromosome shows widespread interaction with nuclear pores. (*A*) Location of the *MEX* motif insertion on *chr II*, with overlay of LEM-2 ChIP–chip profile (color as in Fig. 1B). (*B*) Zone 1 scorings for the insertion in *A* in two strains with a wild-type (WT) and one strain with a mutated *rex* site in male and hermaphrodite embryos. (*C*) DamID-seq profile of lamin interaction with the entire *C. elegans* genome in hermaphrodites and males. Chromosomes are separated by red vertical lines. The signal is averaged over 100-kb windows and normalized by free Dam-GFP control. (*D*) DamID profile as in *C* of nucleoporin MEL-28.

This locus was preferentially positioned internally in hermaphrodites, while in males, the same site showed significant enrichment in zone 1 (Fig. 2B). Insertion of a similar construct with a mutated *MEX* motif led to a slightly internal localization similar in both sexes. We conclude that in males, the *MEX* motif is sufficient for perinuclear targeting of an otherwise internal locus. As many *MEX* motifs are present on the X chromosome (Jans et al. 2009), *MEX* periphery interaction could position the entire X chromosome close to the nuclear rim in males.

The nuclear periphery is a contrasted environment with silent chromatin anchored at the nuclear lamina (Ikegami et al. 2010; Towbin et al. 2012; Gonzalez-Aguilera et al. 2014) and active domains located close to nuclear pores by transcription-dependent mechanisms (Ikegami and Lieb 2013; Rohner et al. 2013). We therefore asked which domain the X chromosome is interacting with using DNA adenine methyltransferase identification (DamID) followed by sequencing (DamID-seq). Male or hermaphrodite L4 animals expressing Dam fusions to either lamin (LMN-1) (Towbin et al. 2012), the nucleoporin MEL-28/ELYS (Fernandez and Piano 2006; Galy et al. 2006), or GFP (diffusible control) were used to map genomic regions in close proximity to these nuclear landmarks. For lamin DamID in hermaphrodites, we obtained profiles very similar to previously published data, showing the characteristic high interaction pattern of the autosomal arms (Fig. 2C; Gonzalez-Aguilera et al. 2014). In males, the lamin DamID profile was remarkably similar to hermaphrodites, except for the X chromosome, which showed slightly more interactions with the nuclear lamina (Fig. 2C). For MEL-28/ELYS DamID in hermaphrodites, the signal was very similar between autosomes and the X chromosome (Fig. 2D). A previous study found discrete interaction sites of chromatin with nucleoporins (Ikegami and Lieb 2013); however, the resolution of our low animal number DamID impairs such fine-scale analysis. In males, however, at the chromosome scale, the single X chromosome shows broad interactions with MEL-28 (Fig. 2D). This is highly reminiscent of *Drosophila* males, in which the activating DCC (MSL/MOF) coating the X chromosome contains Nup153 and TPR/Mtor, two nucleoporins that show widespread interaction with the X chromosome (Mendjan et al. 2006; Vaquerizas et al. 2010). Upon loading, the MSL/MOF complex changes the chromatin conformation of X, although this conformation was unaffected upon knockdown of Nup153 or TPR/Mtor (Grimaud and Becker 2009). The interaction of nucleoporins with chromatin has been shown in a variety of systems to increase transcriptional output (Casolari et al. 2004; Capelson et al. 2010; Kalverda et al. 2010; Liang et al. 2013). While in these studies, a significant proportion of interactions between nucleoporins and chromatin took place in the nuclear interior, our FISH data suggest that the interactions with MEL-28 observed by DamID to a large extent represent events at nuclear pores.

Together, this allows us to draw a model in which the X chromosome in males is targeted to the nuclear rim by *MEX* motifs. Targeting to nuclear pores may be achieved through Pol III transcribed noncoding RNA (ncRNA) sequences (Ikegami and Lieb 2013), which are particularly enriched on the X chromosome (ratios of annotated ncRNA to coding sequences of 1.2 for X and 0.3 for all autosomes [WormBase data; http://www.wormbase.org]). Nuclear pore-mediated interaction has been shown in yeast to depend on incorporation of the histone variant HTZ1 (H2A.Z) (Light et al. 2010). Interestingly, the same variant HTZ-1 is underrepresented on hermaphrodite X chromosomes (Whittle et al. 2008; Petty et al. 2011), suggesting a possible mechanism for pore-mediated activation of X-linked genes in males by histone exchange and promotion of HTZ-1 incorporation.

In hermaphrodites, one hypothesis for the mechanism of transcriptional down-regulation of X chromosomes is that the DCC and H4K20me1 increase chromosome compaction by physically entangling chromatin, thereby impairing access of the RNA polymerases to X-linked genes (Chuang et al. 1994; Vielle et al. 2012). In this model, a given genomic length on the X chromosome should be more compact in dosage-compensated hermaphrodites than in males and more compact than a similarly sized autosomal region. To evaluate the difference in chromatin compaction levels, we analyzed the physical distance between pairs of sites separated by a genomic distance of 1 or 4 Mb (Fig. 3A; Supplemental Fig. S1A,B). Using projections along the *Z*-axis, we measured the projected distances between these loci in male and hermaphrodite embryos after DC establishment. Distances between loci were normalized to the nuclear diameter to correct for size

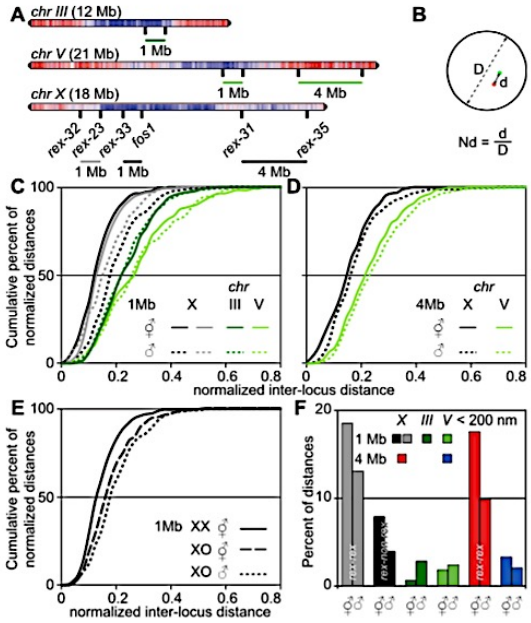

Figure 3. The X chromosome shows a higher degree of compaction compared with autosomes in males and hermaphrodites. (*A*) Probes used to assess chromatin compaction were *rex-31/rex-35* (4 Mb, X), *rex-32/rex-23* and *rex33/fos1* (1 Mb, X), and controls on *chr III* and *chr V* (1 and 4 Mb). (*B*) Interlocus distance normalization to the nuclear diameter. (*C*,*D*) Cumulative frequency plot of normalized interlocus distances for 1- and 4-Mb probe combinations described in *A*. (*E*) Cumulative frequency plot of normalized interlocus distances for *rex-33/fos1* in males, hermaphrodites, and non-dosage-compensated XO hermaphrodites. (*F*) Percentage of nonnormalized physical distances <200 nm measured in both sexes for all probe combinations. Statistical data are in Supplemental Table 1.

differences between nuclei (Fig. 3B). Data in Figure 3 are presented as a cumulative frequency distribution (the proportion of measurements [in the *Y*-axis] below a given threshold [on the *X*-axis]) (alternative box plot representation in Supplemental Fig. S3). Irrespective of the sex of the animal and for both 1- and 4-Mb distances, regions located on the X chromosome were more compact than similar distances measured on an autosome (Fig. 3C,D). For autosomes, no difference in the distance distribution could be observed between males and hermaphrodites, although compaction slightly varied between the two autosomal regions probed. Comparing X chromosome measurements between hermaphrodites and males showed a slightly higher compaction in hermaphrodites (Fig. 3C,D), while X compaction is similar between XO hermaphrodites and XO males (Fig. 3E). This strongly suggests that the higher hermaphrodite X compaction is due to the DCC. Our measurements also imply a DCC-independent mechanism that increases compaction of the X chromosome relative to autosomes in males. This may be due to a non-sex-specific loading of non-DCC condensins, which have a clear preference for loading at ncRNA genes (Kranz et al. 2013), particularly abundant on the X chromosome. Alternatively, nuclear pore anchoring might also lead to increased compaction of the X chromosome (see below). Altogether, it appears unlikely that the small increase in compaction is solely responsible for the restriction of RNA Pol II access and transcription down-regulation of X-linked genes in hermaphrodites.

How is X compaction achieved? Random or *rex* site-specific interactions between chromosomal sites could be mediated by the DCC in hermaphrodites or the *rex* anchor sites at the nuclear rim in males, leading to the formation of a "rosette"-type structure in which clustered *rex* sites make the center of the rosette, while inter-*rex* sequences loop out (Jans et al. 2009; Chow and Heard 2010). When measuring absolute distances between two *rex* sites (*rex-23/rex-32*) and a *rex* and a non-*rex* site (*rex-33/fos1*, both 1 Mb distance) (Fig. 3A), the proportions of distances <200 nm was smaller between *rex* sites than between *rex* and non-*rex* sites for both males and hermaphrodites (Fig. 3F). Moreover, these proportions were higher in hermaphrodites than in males, reflecting the higher compaction observed in hermaphrodites. In line with the difference in compaction between autosomes and X, very few measurements <200 nm were observed for a 1- and a 4-Mb genomic distance on *chr III* or *chr V* (Fig. 3F). Given the low frequency of spatially close *rex* sites, DC is unlikely to function by generalized clustering of *rex* sites, but as *rex* sites are abundant on the X chromosome, a loose rosette organization might arise with a subset of randomly interacting *rex* sites (Bohn and Heermann 2010). Therefore, the increased colocalization of *rex* sites compared with *rex*–non-*rex* sites in hermaphrodites might be due to inter-*rex* interactions. Alternatively, the higher proportion of very close sites could be the result of the DCC-dependent global increase of X chromosome compaction. In males, the increased proportions of spatially close sites might reflect clustering to the same anchor site at the nuclear periphery.

Our observation that the X chromosome is more compact than autosomes in both sexes is surprising. While in hermaphrodites, compaction of the X chromosome is likely achieved by the DCC, it remains unclear why this is the case in males. As the male X chromosome interacts with nucleoporins at the nuclear periphery, we asked whether anchoring could lead to compaction. We modeled the behavior of chromosomes as a bead spring polymer tethered at both telomeres to a surface representing the nuclear periphery (Fig. 4A; Supplemental Fig. S4; Kremer and Grest 1992). Using molecular dynamics simulations, we studied the time evolution of conformations (distance to the periphery [*z*] and size of the chromosome [R_g]) starting from a highly compact conformation: the mitotic chromosome (Fig. 4B). In the absence of interaction with the periphery (other than telomere tethering), higher self-affinity leads to more compact globular conformations (Fig. 4C, left, configurations 1 and 2; Doi and Edwards 1988). As condensins are known to cross-link chromatin fibers together, this could explain the observed compaction difference between autosomes and the hermaphrodite X chromosome. We then asked whether nuclear pore anchoring as in males would influence X compaction. In the absence of self-affinity, we introduced an affinity of the chromosome for anchor sites at the nuclear envelope. Unsurprisingly, this led to more peripheral conformations (Fig. 4C). When the chromosome was allowed to interact with any point on the surface, the interaction led to spreading (Fig. 4C, configuration 3; Metzger et al. 2003). In contrast, strong interaction with a limited number of anchor sites corresponding to the density of nuclear pores (about three pores per square micrometer) (Rohner et al. 2013) led to a limited spatial expansion of the chromosome compared with nonanchored chromosomes (Fig. 4C, right,

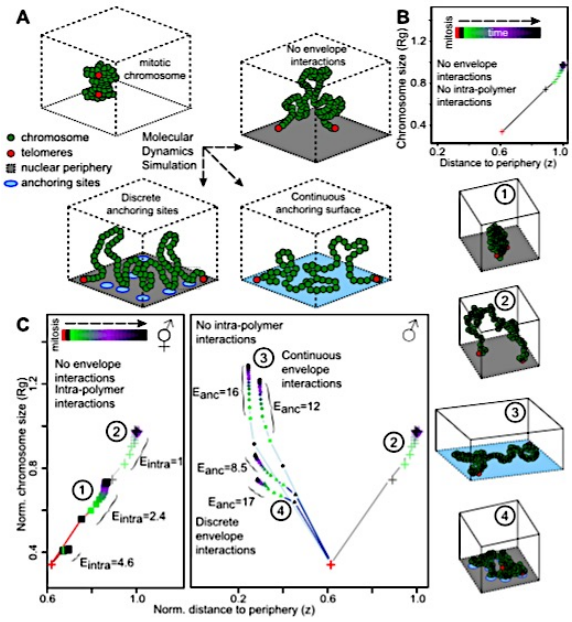

Figure 4. Theoretical modeling supports the competing roles of DCC loading and nuclear pore anchoring in X chromosome organization in males and hermaphrodites. (*A*) Bead spring polymeric model of chromosomes with intrachain attractive interactions and interactions with anchoring sites located at the nuclear envelope. Relaxation dynamics from an initial "mitotic-like" compact state were computed by molecular dynamics simulations. Chromosomal spatial organization is characterized by the typical size of the polymer, the radius of gyration (Rg), and the mean distance to the envelope (z). (*B*) Time evolution of $Rg(t)$ and $z(t)$ in the case of no anchoring and weak intrachain interactions. (*C*, *left*) Hermaphrodite situation: $Rg(t)$ versus $z(t)$ for different intrachain interactions: (+) $E = 1$; (■) $E = 2.4$ and 4.6. As a result of DCC loading ($E_{intra} > 1$), the X chromosome folds into a more compact structure than autosomes ($E_{intra} = 1$). (*Right*) Male situation: $Rg(t)$ versus $z(t)$ for different anchoring conditions and weak intrachain interactions ($E_{intra} = 1$): (+) no interaction; (▲) interactions with discrete anchors (three sites per square micrometer); (●) continuous interactions with highly dense anchors. Example configurations for the different situations (1–4) are pictured at the *right*.

configuration 4). The polymer is then stabilized in a compact conformation partly expanded from the dense mitotic state. As cells in embryos are rapidly dividing, steady state is not reached before the next cell division, and discrete anchoring of a chromosome to the nuclear pores entraps partially decondensed compact mitotic conformations. Modeling therefore indicates that strong chromosome anchoring to discrete sites is sufficient to explain the observed higher compaction of the X chromosome in males compared with autosomes.

A structural model for DC

Many hypotheses were put forward to mechanistically explain how a condensin-like DCC hinders RNA Pol II recruitment to X-linked genes. Here we show that loading of the DCC onto the X chromosome impairs its perinuclear localization and interaction with nuclear pore proteins. Based on our experiments, we suggest a structural model for DC. In males, the X chromosome interacts with nuclear pore components, which increases the transcriptional output of X-linked genes compared with autosomes, observed in two genome-wide studies (Deng et al. 2011; Kruesi et al. 2013) and similar to the up-regulation observed in male mammalian cells and *Drosophila* (Deng et al. 2011). In hermaphrodites, loading of the DCC on the X chromosome (Csankovszki et al. 2004; Ercan et al. 2009; Vielle et al. 2012) impairs its perinuclear localization by masking pore interaction sites, thereby inhibiting pore-mediated gene activation and reducing transcription levels on a global chromosomal scale. Similar subnuclear localization-induced gene regulation has been observed in yeast, in which relocation of the HXK1 gene away from nuclear pores decreases transcriptional output of the gene (Taddei et al. 2006). The validity of this location-induced gene regulation for an entire chromosome remains to be tested. Our DC model offers a simple explanation for the observation that in hermaphrodites carrying X:autosome fusions, the DCC and associated H4K20 methylation spread from the X onto the autosome for megabases, but little difference was observed for the transcriptional levels of the autosomal genes (Ercan et al. 2009; Pferdehirt et al. 2011; Vielle et al. 2012). As the autosomal part of the chromosome fusion is devoid of *rex* sites, it does not undergo pore-mediated up-regulation; therefore, DCC binding is expected to have little effect on transcriptional levels. Altogether, this study leads to an updated model for DC in *C. elegans*, with a mechanism much more similar to *Drosophila* DC. As DC has evolved independently in *Drosophila* and nematodes, it is noticeable that in both species, DC leads to changes of the tridimensional structure of the chromosome, providing a paradigm to study the link between the creation of nuclear subdomains and the coordinated fine-tuning of the expression of a large number of genes.

Materials and methods

Strains and culture conditions

Nematodes were grown on NG2 medium seeded with OP50 at 22.5°C unless otherwise stated.

Probe preparation, FISH, and microscopy

Probe preparation, FISH, and microscopy are detailed in the Supplemental Material.

DamID

L4 worms expressing fusions to *lmn-1*, *mel-28*, or *gfp*, grown at 25°C, were lysed and digested with DpnI. Fragments were ligated to double-stranded adapters before amplification and library preparation. Sequencing data can be accessed at Gene Expression Omnibus: GSE56270.

Polymer modeling

A chromosome was modeled by a self-avoiding bead and spring chain confined in a cubic box in which one face is the nuclear envelope. Two types of interactions were considered: intrachain nonspecific interactions between beads and specific interactions between beads and sites at the nuclear envelope.

Acknowledgments

We thank members of the Meister and Ochsenreiter laboratories for numerous discussions, Sonia Karaz and Julie Campos for expert technical help, Mylène Docquier and the iGE3 genomics platform of the University of Geneva for next-generation sequencing (NGS) and advice, and Iskra Katic and the Friedrich Miescher Institute (FMI) *C. elegans* laboratories for help

and discussions. Some strains were provided by the *Caenorhabditis* Genetics Center (CGC), which is funded by National Institutes of Health Office of Research Infrastructure Programs (P40 OD010440). Our laboratories are supported by the Swiss National Science Foundation (SNF assistant professor grant PP00P3_133744), the Swiss Foundation for Muscle Diseases Research, and the University of Bern (to P.M.); the French Centre National de la Recherche Scientifique and the Ecole Normale Supérieure de Lyon (to C.V. and D.J.); the Spanish Ministry of Economy and Competitiveness (BFU2010-15478), the European Regional Development Fund (to P.A.); Nederlandse Organisatie voor Wetenschappelijk Onderzoek (NWO)-Aard en Levenswetenschappen (ALW) Veni (to J.K.); and ZonMW (Medische wetenschappen)-TOP (to B.v.S.). D.J. and C.V. acknowledge the Pôle Scientifique de Modélisation Numérique for computing resources

References

Askjaer P, Ercan S, Meister P. 2014. Modern techniques for the analysis of chromatin and nuclear organization in *C. elegans*. In *WormBook* (ed. The *C. elegans* Research Community) *WormBook*, doi: 10.1895/wormbook.1.169.1. http://www.wormbook.org.

Bohn M, Heermann DW. 2010. Diffusion-driven looping provides a consistent framework for chromatin organization. *PLoS ONE* **5:** e12218.

Capelson M, Liang Y, Schulte R, Mair W, Wagner U, Hetzer MW. 2010. Chromatin-bound nuclear pore components regulate gene expression in higher eukaryotes. *Cell* **140:** 372–383.

Casolari JM, Brown CR, Komili S, West J, Hieronymus H, Silver PA. 2004. Genome-wide localization of the nuclear transport machinery couples transcriptional status and nuclear organization. *Cell* **117:** 427–439.

Chow JC, Heard E. 2010. Nuclear organization and dosage compensation. *Cold Spring Harb Perspect Biol* **2:** a000604.

Chuang PT, Albertson DG, Meyer BJ. 1994. DPY-27: a chromosome condensation protein homolog that regulates *C. elegans* dosage compensation through association with the X chromosome. *Cell* **79:** 459–474.

Csankovszki G, McDonel P, Meyer BJ. 2004. Recruitment and spreading of the *C. elegans* dosage compensation complex along X chromosomes. *Science* **303:** 1182–1185.

Csankovszki G, Collette K, Spahl K, Carey J, Snyder M, Petty E, Patel U, Tabuchi T, Liu H, McLeod I, et al. 2009. Three distinct condensin complexes control *C. elegans* chromosome dynamics. *Curr Biol* **19:** 9–19.

Dawes HE, Berlin DS, Lapidus DM, Nusbaum C, Davis TL, Meyer BJ. 1999. Dosage compensation proteins targeted to X chromosomes by a determinant of hermaphrodite fate. *Science* **284:** 1800–1804.

Deng X, Hiatt JB, Nguyen DK, Ercan S, Sturgill D, Hillier LW, Schlesinger F, Davis CA, Reinke VJ, Gingeras TR, et al. 2011. Evidence for compensatory upregulation of expressed X-linked genes in mammals, *Caenorhabditis elegans* and *Drosophila melanogaster*. *Nat Genet* **43:** 1179–1185.

Doi M, Edwards SF, ed. 1988. *The theory of polymer dynamics*. Oxford University Press, Oxford.

Ercan S, Dick LL, Lieb JD. 2009. The *C. elegans* dosage compensation complex propagates dynamically and independently of X chromosome sequence. *Curr Biol* **19:** 1777–1787.

Fernandez AG, Piano F. 2006. MEL-28 is downstream of the Ran cycle and is required for nuclear-envelope function and chromatin maintenance. *Curr Biol* **16:** 1757–1763.

Ferrari F, Alekseyenko AA, Park PJ, Kuroda MI. 2014. Transcriptional control of a whole chromosome: emerging models for dosage compensation. *Nat Struct Mol Biol* **21:** 118–125.

Ferreira HC, Towbin BD, Jegou T, Gasser SM. 2013. The shelterin protein POT-1 anchors *Caenorhabditis elegans* telomeres through SUN-1 at the nuclear periphery. *J Cell Biol* **203:** 727–735.

Galy V, Askjaer P, Franz C, Lopez-Iglesias C, Mattaj IW. 2006. MEL-28, a novel nuclear-envelope and kinetochore protein essential for zygotic nuclear-envelope assembly in *C. elegans*. *Curr Biol* **16:** 1748–1756.

Gonzalez-Aguilera C, Ikegami K, Ayuso C, de Luis A, Iniguez M, Cabello J, Lieb JD, Askjaer P. 2014. Genome-wide analysis links emerin to neuromuscular junction activity in *Caenorhabditis elegans*. *Genome Biol* **15:** R21.

Grimaud C, Becker PB. 2009. The dosage compensation complex shapes the conformation of the X chromosome in *Drosophila*. *Genes Dev* **23:** 2490–2495.

Ikegami K, Lieb JD. 2013. Integral nuclear pore proteins bind to Pol III-transcribed genes and are required for Pol III transcript processing in *C. elegans*. *Mol Cell* **51:** 840–849.

Ikegami K, Egelhofer TA, Strome S, Lieb JD. 2010. *Caenorhabditis elegans* chromosome arms are anchored to the nuclear membrane via discontinuous association with LEM-2. *Genome Biol* **11:** R120.

Jans J, Gladden JM, Ralston EJ, Pickle CS, Michel AH, Pferdehirt RR, Eisen MB, Meyer BJ. 2009. A condensin-like dosage compensation complex acts at a distance to control expression throughout the genome. *Genes Dev* **23:** 602–618.

Kalverda B, Pickersgill H, Shloma VV, Fornerod M. 2010. Nucleoporins directly stimulate expression of developmental and cell-cycle genes inside the nucleoplasm. *Cell* **140:** 360–371.

Kranz AL, Jiao CY, Winterkorn LH, Albritton SE, Kramer M, Ercan S. 2013. Genome-wide analysis of condensin binding in *Caenorhabditis elegans*. *Genome Biol* **14:** R112.

Kremer K, Grest GS. 1992. Simulations for structural and dynamic properties of dense polymer systems. *J Chem Soc, Faraday Trans* **88:** 1707–1717.

Kruesi WS, Core LJ, Waters CT, Lis JT, Meyer BJ. 2013. Condensin controls recruitment of RNA polymerase II to achieve nematode X-chromosome dosage compensation. *eLife* **2:** e00808.

Liang Y, Franks TM, Marchetto MC, Gage FH, Hetzer MW. 2013. Dynamic association of NUP98 with the human genome. *PLoS Genet* **9:** e1003308.

Light WH, Brickner DG, Brand VR, Brickner JH. 2010. Interaction of a DNA zip code with the nuclear pore complex promotes H2A.Z incorporation and INO1 transcriptional memory. *Mol Cell* **40:** 112–125.

McDonel P, Jans J, Peterson BK, Meyer BJ. 2006. Clustered DNA motifs mark X chromosomes for repression by a dosage compensation complex. *Nature* **444:** 614–618.

Mendjan S, Taipale M, Kind J, Holz H, Gebhardt P, Schelder M, Vermeulen M, Buscaino A, Duncan K, Mueller J, et al. 2006. Nuclear pore components are involved in the transcriptional regulation of dosage compensation in *Drosophila*. *Mol Cell* **21:** 811–823.

Metzger S, Muller M, Binder K, Baschnagel J. 2003. Surface excess in dilute polymer solutions and the adsorption transition versus wetting phenomena. *J Chem Phys* **118:** 8489–8499.

Petty E, Laughlin E, Csankovszki G. 2011. Regulation of DCC localization by HTZ-1/H2A.Z and DPY-30 does not correlate with H3K4 methylation levels. *PLoS ONE* **6:** e25973.

Pferdehirt RR, Kruesi WS, Meyer BJ. 2011. An MLL/COMPASS subunit functions in the *C. elegans* dosage compensation complex to target X chromosomes for transcriptional regulation of gene expression. *Genes Dev* **25:** 499–515.

Rohner S, Kalck V, Wang X, Ikegami K, Lieb JD, Gasser SM, Meister P. 2013. Promoter- and RNA polymerase II-dependent hsp-16 gene association with nuclear pores in *Caenorhabditis elegans*. *J Cell Biol* **200:** 589–604.

Strome S, Kelly WG, Ercan S, Lieb JD. 2014. Regulation of the X chromosomes in *Caenorhabditis elegans*. *Cold Spring Harb Perspect Biol* **6:** a018366.

Taddei A, Van Houwe G, Hediger F, Kalck V, Cubizolles F, Schober H, Gasser SM. 2006. Nuclear pore association confers optimal expression levels for an inducible yeast gene. *Nature* **441:** 774–778.

Towbin BD, Gonzalez-Aguilera C, Sack R, Gaidatzis D, Kalck V, Meister P, Askjaer P, Gasser SM. 2012. Step-wise methylation of histone H3K9 positions heterochromatin at the nuclear periphery. *Cell* **150:** 934–947.

Vaquerizas JM, Suyama R, Kind J, Miura K, Luscombe NM, Akhtar A. 2010. Nuclear pore proteins nup153 and megator define transcriptionally active regions in the *Drosophila* genome. *PLoS Genet* **6:** e1000846.

Vielle A, Lang J, Dong Y, Ercan S, Kotwaliwale C, Rechtsteiner A, Appert A, Chen QB, Dose A, Egelhofer T, et al. 2012. H4K20me1 contributes to downregulation of X-linked genes for *C. elegans* dosage compensation. *PLoS Genet* **8:** e1002933.

Wells MB, Snyder MJ, Custer LM, Csankovszki G. 2012. *Caenorhabditis elegans* dosage compensation regulates histone H4 chromatin state on X chromosomes. *Mol Cell Biol* **32:** 1710–1719.

Whittle CM, McClinic KN, Ercan S, Zhang X, Green RD, Kelly WG, Lieb JD. 2008. The genomic distribution and function of histone variant HTZ-1 during *C. elegans* embryogenesis. *PLoS Genet* **4:** e1000187.

Appendix II

Programs

Scripts Review in Chapter V

(See description in Table 5.3 in Chapter V)

Loop_MACS2.sh

```
#!/bin/bash

FILES=/your_path/*.bed
for filename in $FILES
do
  echo "Processing $filename file...";
MACS2 bdgpeakcall -i "$filename" -o "${filename%.bed}_c0.6_g81_PEAKS.bed" -c 0.6 -g
81 --outdir PEAKS_MACS2_c0.6_g81;
done


FILES=/your_path/*_PEAKS.bed
for filename in $FILES
do
echo "Processing $filename file...";
wc -l "$filename";
done
```

Usage:

```
$ bash Loop_MACS2.sh > number_peaks.txt
```

Loop_cut_peaks.sh

```
#!/bin/bash

FILES=/your_path/*_PEAKS.bed
for filename in $FILES
do
  echo "Processing $filename file...";
awk 'BEGIN { OFS = "\t" }{print $1, $2, $3}' "$filename" > "${filename%.bed}_STAD.bed";

echo "Processing $filename file...";
awk 'BEGIN { OFS = "\t" }{print $1, $2, $3, $5}' "$filename" >
"${filename%.bed}_SCORE.bed";
done
```

Usage:

```
$ bash Loop_cut_peaks.sh
```

Loop_stadistic.sh

```
#!/bin/bash

FILES=/your_path/*_STAD.bed
for filename in $FILES
do
  echo "Processing $filename file...";
grep -v "t" "$filename" > "${filename%.bed}2.bed";
done
```

Usage:

```
$ bash Loop_stadistic.sh
```

Loop_peak_size.sh

```
#!/bin/bash

FILES=/your_path /*_STAD2.bed
for filename in $FILES
do
  echo "Processing $filename file...";
awk 'BEGIN { OFS = "\t" }{ $4 = $3 - $2 } 1' "$filename" >
"${filename%.bed}_peakSIZE.bed";



echo "Processing $filename file...";
awk 'BEGIN { OFS = "\t" }{ $4 = $3 - $2 } 1 {print $4}' "$filename" >
"${filename%.bed}_SIZE.txt";
done
```

Usage:

```
$ bash Loop_peak_size.sh
```

Loop_intersect_wID.sh

```
#!/bin/bash

FILES=/your_path/*_PEAKS.bed
for filename in $FILES
do
/path/bedtools2/bin/intersectBed -a /path/WormID.bed -b "$filename" -f 0.5 -wo > "${filename%.bed}_wID_GOfull.bed";
done


FILES=/your_path/*_wID_GOfull.bed
for filename in $FILES
do
echo "Processing $filename file...";
wc -l "$filename";
done
```

Usage:

```
$ bash Loop_intersect_wID.sh > number_genes.txt
```

Loop_GO.sh

```
#!/bin/bash

FILES=/Users/Georgina/Desktop/bed/test/*_GOfull.bed
for filename in $FILES
do
  echo "Processing $filename file...";
awk '{print $4}' "$filename" > "${filename%.bed}_end.txt";
done
```

Usage:

```
$ bash Loop_GO.sh
```

Acknowledgements

Por fin ha llegado el día, estoy muy cerca de cumplir este objetivo y casi no lo puedo creer. En estos 6 años, que se han hecho tan cortos y tan largos a la vez, he vivido muchas experiencias las cuales me han ayudado a crecer personal y profesionalmente.

Esta aventura no hubiera sido posible sin una persona, la cual admiro profundamente y respeto en el ámbito profesional y personal, mi mentor, Dr. Peter Askjaer. Cuando digo que esta tesis no hubiera llegado a su fin sin tu ayuda, paciencia, motivación y comprensión, no lo digo en broma. Todo el mundo sabe que si hoy estoy aquí es gracias a ti. Espero algún día ser por lo menos la mitad del gran jefe que eres.

Otra pieza importante de esta tesis es la colaboración con otros grupos de investigación de los cuales he aprendido mucho. Gracias al Dr. Peter Meister por recibirme en su laboratorio y enseñarme bioinformática, y a la Dra. Anita Fernández por los cientos de email y amenas charlas que hemos intercambiado.

Aunque el último año fue un poco sufrido y me hizo tambalear algunas veces, en general ha sido una experiencia maravillosa, y eso es gracias al estupendo equipo de trabajo que Peter a formado. Nada hubiera sido igual sin el gran recibimiento que me dieron Cristina G, Adela, Aga, Cristina A. y Machupi. De verdad nunca me he sentido sola, el worm corner formado junto con los grupos de los Drs. Antonio Miranda, Manolo Muñoz y Martha Artal se ha convertido en una segunda familia para mi. Todos los gusaneros tienen un lugar especial en mi corazón, espero no olvidar a nadie gracias a Fran, Briseida, Nando, Ana, María, Mercedes, Carlos, Ann, Roxani, Tony, Eduardo, Ana María, Curro. Así como a Kathy de microscopia, y todos los estudiantes y PI de CABD.

Miembros más recientes han hecho que mis últimos años estén llenos de recuerdos inolvidables. Gracias a Celia, Blanca, Patri y Artur. Con ustedes las jornadas de 12 horas han sido un abrir y cerrar de ojos… Bueno… no es cierto, han sido pesadas pero divertidas.

Por último gracias a mi Familia, estar lejos de ustedes a sido un sacrificio enorme. Pero su amor, risas, lagrimas, llamadas, skypes, whatsapp, etc. me daban energía todos los días. Los Amo y los extraño millones. Gracias Daniel por estar a mi lado siempre y no dejarme caer. Gracias a todos.

title: "Good results" - originally published 10/13/2010